LUDWIG-MAXIMILIAN-UNIVERSITY OF MUNICH

FACULTY OF PHYSICS

DNA Origami Meets Silica: Enhanced Methods and Functional Customization for Nanotechnological Innovation

Lea Marie Wassermann

München 2024

Erstgutachter: Prof. Dr. Tim Liedl

Zweitgutachter: Prof. Dr. Amelie Heuer-Jungemann

Tag der Einreichung: 18.12.2024

Tag der mündlichen Prüfung: 10.02.2025

DNA Origami Meets Silica: Enhanced Methods and Functional Customization for Nanotechnological Innovation

DNA-Origami trifft auf Silica: Verbesserte Methoden und funktionale Anpassung für nanotechnologische Innovationen

Dissertation

an der Fakultät für Physik

der Ludwig-Maximilians-Universität

München

vorgelegt von

Lea Marie Wassermann

aus Hattingen

München, 18.12.2024

List of peer-reviewed publications

Scheckenbach M[*], Brüggenthies GA, Schröder T, Betuker K, Wassermann LM, Tinnefeld P, Heuer-Jungemann A, Glembockyte V°*

Monitoring the Coating of Single DNA Origami Nanostructures with a Molecular Fluorescence Lifetime Sensor

ACS Nano (just submitted), bioRxiv: doi: 10.1101/2024.10.28.620667

Wassermann LM, Scheckenbach M*, Baptist AV, Glembockyte V°, Heuer-Jungemann A°*

Full Site-Specific Addressability in DNA Origami-Templated Silica Nanostructures.

Adv Mater. 2023 Jun;35(23):e2212024. doi: 10.1002/adma.202212024.

Awards:

1. Center for Nanoscience Publication Award – Best Junior Scientist Publication,
2. MPIB Junior Scientist Publication Award

Ober MF, Baptist A, Wassermann LM, Heuer-Jungemann A°, Nickel B°

In situ small-angle X-ray scattering reveals strong condensation of DNA origami during silicification.

Nat Commun. 2022 Sep 27;13(1):5668. doi: 10.1038/s41467-022-33083-5.

Award:

1. Center for Nanoscience Publication Award – Best Interdisciplinary Publication

*= These authors contributed equally to this work.; °= Corresponding author.

Dedication

In tribute to the unanticipated discoveries,

And the intricate pathways that gave us new theories.

To the cherished companions, both near and far,

Who graced our path like a shimmering star.

Abstract

DNA, the molecule of life, has become a versatile tool in nanotechnology due to its programmability, precise base-pairing, and ability to self-assemble into complex nanostructures. DNA origami, a method that folds long single-stranded DNA into predefined shapes using short complementary staples, has revolutionized nanoscale architecture. These structures hold great potential for materials science and biomedicine, including molecular diagnostics, drug delivery, and the creation of hybrid nanomaterials. However, DNA's fragility and susceptibility to denaturation under physiological conditions pose challenges that limit its utility. This thesis focuses on stabilizing and functionalizing DNA origami through innovative silicification techniques.

The work develops an accelerated silicification process that reduces processing time from days to hours while maintaining structural integrity. A rotation-based method ensures uniform coating without aggregation, enabling scalable production of silica-coated DNA origami.

Additionally, the thesis investigates whether DNA origami retains functional addressability post-silicification. My studies confirm that site-specific modifications remain feasible, preserving adaptability—a critical factor for integration into biosensing systems.

To further extend the utility of DNA origami, customizable silica coatings were developed. Fluorescent silica enables real-time imaging, while dissolvable silica introduces controlled degradation in response to environmental stimuli. These innovations provide tools for dynamic and responsive nanostructures.

By addressing challenges in stability, functionality, and adaptability, this work lays the foundation for the development of multifunctional hybrid materials and positions DNA origami as a cornerstone of future nanotechnological advancements.

Zusammenfassung

DNA, das Molekül des Lebens, hat sich durch seine Programmierbarkeit, präzise Basenpaarung und Fähigkeit zur Selbstorganisation in komplexe Nanostrukturen zu einem vielseitigen Werkzeug der Nanotechnologie entwickelt. DNA-Origami, eine Methode, bei der ein langes einzelsträngiges DNA-Molekül mithilfe kurzer, komplementärer „Staples“ in vorgegebene Formen gefaltet wird, hat die Konstruktion nanoskaliger Architekturen revolutioniert. Diese Strukturen bieten großes Potenzial für Anwendungen in Materialwissenschaften und Biomedizin, etwa in der Molekulardiagnostik, Arzneimittelabgabe und beim Aufbau hybrider Nanomaterialien. Dennoch stellen die Fragilität und Anfälligkeit für Denaturierung von DNA unter physiologischen Bedingungen Herausforderungen dar, die ihre Nutzung einschränken. Diese Arbeit konzentriert sich auf die Stabilisierung und Funktionalisierung von DNA-Origami durch innovative Silifizierungsverfahren.

Diese Arbeit entwickelt einen beschleunigten Silifizierungsprozess, der die Verarbeitungszeit von Tagen auf Stunden verkürzt, ohne die Integrität der Struktur zu beeinträchtigen. Eine rotationsbasierte Methode ermöglicht eine gleichmäßige Beschichtung ohne Aggregation. Diese Fortschritte eröffnen neue Möglichkeiten für eine skalierbare Produktion von DNA-Origami mit Silikabeschichtung. Zusätzlich wird untersucht, ob die funktionelle Adressierbarkeit von DNA-Origami nach der Silifizierung erhalten bleibt. Meine Studien zeigen, dass ortsspezifische Modifikationen möglich bleiben, wodurch die Anpassungsfähigkeit beibehalten wird. Dies ist entscheidend für die Integration in Biosensorsysteme.

Um die Anwendbarkeit von DNA-Origami zu erweitern, wurden anpassbare Silikabeschichtungen entwickelt. Fluoreszierendes Silica ermöglicht Echtzeit-Bildgebung, während lösliches Silica eine kontrollierte Degradation einführt. Diese Innovationen schaffen Werkzeuge für reaktionsfähige Nanostrukturen. Durch die Bewältigung dieser Herausforderungen legt die Arbeit die Grundlage für die Entwicklung multifunktionaler Hybridmaterialien und positioniert DNA-Origami als Schlüsseltechnologie zukünftiger nanotechnologischer Entwicklungen.

Acknowledgements

I had the extraordinary opportunity to perform my PhD thesis in the Emmy-Noether-Research Group for DNA Hybridnanomaterials of Dr. Amelie Heuer-Jungemann at the Max-Planck-Institute for Biochemistry. Under her mentorship, I was immersed in a dynamic and innovative research environment, where the boundaries of DNA nanotechnology were pushed to new frontiers. Dr. Heuer-Jungemann's expertise and passion for the field inspired me to approach scientific challenges with creativity and precision. The collaborative spirit of the group, coupled with the cutting-edge research projects, provided a fertile ground for intellectual growth and hands-on exploration. It was within this vibrant setting that I honed my skills, tackled complex scientific questions, and contributed to groundbreaking advancements in the realm of DNA-based nanomaterials.

During this enriching period, I had the privilege of engaging with a diverse and talented group of individuals who played an integral role in the culmination of the work presented in this thesis. Their collaborative spirit and collective effort not only contributed to the scientific endeavors but also fostered a supportive and constructive atmosphere in the lab. This experience was not only professionally gratifying but also personally rewarding, as it afforded me the chance to acquire invaluable insights and expertise. As such, I am eager to extend my heartfelt gratitude to each and every person involved for their instrumental contributions to this journey.

First and foremost, I would like to express my deepest gratitude to my supervisor and group leader, Dr. Amelie Heuer-Jungemann, for her invaluable guidance, unwavering support, and for providing me with the opportunity to be a part of her research team. Her mentorship and dedication have been instrumental in shaping my academic journey.

I am also indebted to Professor Tim Liedl at the LMU Munich for suggesting that I work with Dr. Heuer-Jungemann, and his then very generous support, both financially and academically. His contributions have greatly enriched my research experience.

A special thanks to my lab mates, especially Anna Baptist and Manar ElNagar, for the stimulating lunchtime discussions and unwavering friendships. Your insights and camaraderie have been a source of inspiration throughout this journey. Manar, you also give the best hugs! I would also like to acknowledge the steadfastness and support of Moritz Weck, especially during the initial phases of the lab, when we just moved and the generous IT support he provided.

A heartfelt appreciation goes out to my nine dedicated students, who have tirelessly contributed in big and small ways to the progress of my projects. Your hard work and commitment have been instrumental in our collective success and I hope you have learned as much from me as supervising you taught me. Among these students, Lily Göldel's exceptional dedication and intellectual prowess stood out prominently. Her contributions have been invaluable to the success of my research endeavors. Beyond the lab, Lily has also become a cherished friend, and I am grateful for her unwavering support and camaraderie.

A special mention goes to my collaborators, Michael Scheckenbach and Viktorija Glembockyte from Prof. Tinnefeld's Lab, whose unwavering dedication and support were invaluable in our joint research endeavors. I would also like to thank Nicholaas and Noah from the Seidel Lab, and Philipp Mauker from the Thorn-Seshold Group, for their insightful contributions that furthered my understanding of nanoscience.

I would like to express my profound gratitude to Ludwig Maximilian University of Munich (LMU) for providing the academic foundation upon which my entire scientific journey has been built. It was at LMU that I completed my Bachelor's in Physics, followed by an enriching Master's program in Physics/Biophysics, and ultimately pursued my PhD. The resources, mentorship, and scholarly environment at LMU have been invaluable in shaping my intellectual growth and research pursuits.

Additionally, I extend my heartfelt thanks to the Max Planck Institute for Biochemistry for providing a dynamic and collaborative research setting during the course of my PhD. The institute's commitment to excellence in scientific inquiry and its vibrant research community have greatly enriched my academic experience.

Here, I would also like to express my gratitude to Prof. Fässler for generously allowing us to use his facilities and to his team for their warm welcome and assistance. Especially Ines Lach-Kusevic and Klaus Weber, who organized a lot of things for us.

I would like to extend a special acknowledgment to my therapist, Julia Pickert, whose unwavering support and guidance were instrumental in helping me navigate the challenges and emotional hurdles that accompanied the pursuit of my PhD. Her expertise and compassionate care provided me with the strength and resilience needed to overcome moments of adversity and self-doubt. I am profoundly grateful for her invaluable contribution to my well-being and overall journey.

I am deeply grateful to my friends Pauline Kolbeck and Evangeline Heck for their unwavering support and encouragement throughout this journey. Your friendship has been a source of strength and inspiration.

To Emmanouil Koutsangelas, your unwavering, selfless support, understanding, and encouragement have been my rock. Your love and belief in me has been a constant source of strength. I wouldn’t be the same without you.

The last lines are dedicated to my family, and particularly my mother. Through all my life you were the person I knew I could always count on, no matter how difficult times were. You raised me with so much dedication and love, and continue to support me in all my decisions, both spiritually and materially. No words can describe how thankful I am for that. I love you.

Table of Contents

List of Abbreviations

Abbreviation	Designation
A	Ampere
AFM	Atomic force microscopy
AGE	Agarose gel electrophoresis
AuNP	Gold - Nanoparticles
bp	Base pairs
BTDS	Bis(triethoxysilylpropyl) disulfide
BTSPTS	Bis-[3-(triethoxysilyl)-propyl]-tetrasulfid
CAS	Chemical abstract service
CEM	Cryogenic transmission electron microcopy
Cy5	Cyanine 5
°C	Degree Celsius
DNA	Deoxyribonucleic acid
DON	DNA Origami Nanostructure
dsDNA	Double-stranded DNA
EDTA	Ethylenediamine tetraacetate
EDX	Energy dispersive X-Ray
GER	Germany
HeLa	Henrietta Lacks (immortal ovarian cancer cell line)
Hz	Hertz
IDT	Integrated DNA Technologies® company
kb	Kilobase
MD	Molecular dynamics
n.d.	Not defined
NEB	New England BioLabs® Inc.
nt	Nucleotides
PCR	Polymerase chain reaction
PEG	Polyethylene glycol

PNA	Peptide nucleic acid
pH	Negative common logarithm of concentration of protons
rcf	Relative centrifugal force
RNA	Ribonucleic acid
rpm	Revolutions per minute
RT	Room temperature (25 °C)
SAXS	Small angle electron microscopy
SiO_2	Silica
ssDNA	Single stranded DNA
TAE	Tris-Acetat-EDTA
TEM	Transmission electron microscopy
TEOS	Tetraethyl orthosilicate
TMAPS	Trimethyl((3-trimethoxysilyl)propyl)ammonium chloride
Tris	Tris(hydroxymethyl)aminomethane
U	Enzyme unit (µmol/min)
UFO	Uranyl formate
UK	United Kingdom
UPW	Ultrapure water (H_2O)
US	United States of America
UV	Ultraviolet
V	Volt
w/o	without
w/	with
1LS	One-layer sheet
18HB	18 helix bundle
18HBB	18 helix bundle bent
24HB	24 helix bundle
2D	Two dimensional
3D	Three dimensional
4LB	4 layer block

Chapter 1 - Introduction

The Nanoworld - a vast yet tiny realm full of potential. The integration of nanotechnology with biological systems has led to significant advancements in the interdisciplinary field of bionanotechnology[1]. This emerging area of research explores the utilization of nanoscale materials for applications in biology and medicine, particularly focusing on the development of inorganic nanomaterials for various biomedical implementations[2]. Inorganic nanoparticles, with their unique chemical and physical properties, have revolutionized many aspects of biomedical research, including imaging, sensing, and therapeutic applications, offering distinct advantages over traditional methods[3, 4].

Over the past two decades, considerable attention has been given to the functionalization of inorganic nanomaterials with biomolecules, including proteins, peptides, and nucleic acids[5]. The specificity and programmability of nucleic acids, in particular, have facilitated the assembly of nanomaterials into well-defined structures[6], which have demonstrated promising applications in materials science and biomedicine. DNA origami, a method of folding long single-stranded DNA into complex, predefined shapes with the help of short staple strands, has emerged as a powerful tool for constructing nanoscale architectures[7]. These DNA-based nanostructures have been explored for their potential in drug delivery, biosensing, and the creation of functional hybrid materials[8].

The research presented in this thesis builds upon these foundational concepts and aims to expand the applications of DNA origami nanostructures (DON) through the process of silicification. Silica-coated DNA origami offers enhanced mechanical stability and protection, making them suitable for a wide range of practical applications[9]. However, the traditional process of silicification is time-consuming, requiring several days to achieve full mineralization[9]. This thesis explores a novel approach to accelerate the silicification process and to integrate customized fluorescent and dissolvable silica coatings, without unwanted clustering or compromising the structural integrity and functionality of the DNA origami. Additionally, the thesis investigates the addressability of silicified DNA origami.

Chapter 4 of this thesis focuses on the development of an accelerated method for silicifying DONs. By implementing a rotation-based technique, where the DNA origami-silica solution is gently rotated for several hours, the silica coating process has been significantly expedited. This approach offers a stark contrast to the traditional static method, which typically requires up to seven days for completion. Notably, unlike shaking, which tends to cause clustering, this rotation method prevents aggregation while ensuring uniform silicification. This method was discovered through experiments involving Small-Angle X-ray Scattering (SAXS), which were conducted to explore and understand the mechanics underlying the silicification process. Moreover, the stability of silicified DONs in various storage places is explored.

Chapter 5 systematically investigates the extent to which silicified DNA origami retains its ability to be selectively functionalized. The addressability of DNA origami in both solution and surface-bound configurations is explored, as well as dynamic DONs.

Finally, chapter 6 delves into the customization of silicified DONs through the incorporation of additional functionalities into the silica coating. Specifically, fluorescent silica and dissolvable silica are integrated to enhance the versatility of these nanostructures. This chapter presents methods for tailoring the properties of the silica shell to meet specific application requirements. The addition of fluorescent labels allows for easier visualization and tracking of the nanostructures, while the development of dissolvable silica introduces the capability to control the degradation and removal of the silica coating under certain conditions. This chapter systematically presents these techniques, highlighting their potential for expanding the utility and functionality of silicified DNA origami.

This thesis aims to contribute to the growing body of knowledge in the field of DNA origami and biomineralization, with a particular focus on enhancing the practicality and functionality of DONs for real-world applications. The findings presented here pave the way for future research and development in the design and use of DNA-silica hybrid materials in various scientific and technological domains.

Chapter 2 - Theoretical Background

This chapter aims to provide a comprehensive overview of the theoretical principles underlying the various techniques and concepts employed in the study of DNA origami, their biomineralization, and the analytical methods used to characterize these structures.

To give a brief overview, I will first discuss DNA and DNA-based nanostructures, with a focus on DNA origami. The unique properties of DNA, including its ability to self-assemble into well-defined structures, make it an ideal candidate for creating nanoscale materials with precise control over their geometry and function and so serve as the fundamental building block in many nanotechnological applications.

Next, I will discuss the stabilization of DNA nanostructures focusing on silicification. These processes mimic natural biomineralization, enabling the fabrication of hybrid materials that combine the biological specificity of DNA with the mechanical robustness of minerals. I will discuss the mechanisms and techniques used to achieve these biomineralizations, highlighting the challenges and solutions in the field.

Additionally, this chapter will delve into the role of fluorophores in enhancing the visualization and functional analysis of DONS. The discussion will include various fluorescence-based techniques that allow for the detailed study of molecular interactions and dynamics within DNA origami, further enriching our understanding of these complex nanomaterials.

This chapter aims to provide a solid theoretical background that will inform and support the experimental investigations discussed in subsequent chapters.

2.1 DNA and DNA Based Nanostructures

2.1.1 DNA

DNA, or deoxyribonucleic acid, is a molecule that carries the genetic instructions for the development, functioning, growth, and reproduction of all living organisms. It is often referred to as the "building block of life" because it contains the information needed to create and sustain life.

DNA has a double-stranded helical structure, resembling a twisted ladder or a spiral staircase. Each strand of DNA is made up of nucleotides[10], which consist of three components: a sugar molecule (deoxyribose), a phosphate group, and a nitrogenous base. The four nitrogenous bases found in DNA are adenine (A), thymine (T), cytosine (C), and guanine (G). The two strands of DNA are held together by hydrogen bonds between complementary base pairs: A with T, and C with G[11], a discovery made by Watson and Crick in the 1950s (**Figure 2.1**a) and based on results of Rosalind Franklin. They proposed a double helical right-handed structure of two antiparallel chains as the natural structure of DNA (**Figure 2.1**.b, c & d), partly based on X-ray diffraction data (**Figure 2.1**.e) provided by Rosalind Franklin[12]. In this model the bases are on the inside, while the sugar-phosphate backbone is on the outside of the double helix (**Figure 2.1**.f), making the phosphate molecules easily accessible by cations, such as magnesium (Mg^{2+}) or calcium (Ca^{2+}). Since the two base pairs exhibit the same overall size (**Figure 2.1**.g), the double helix retains its shape, despite variations in base sequence[10].

The sequence of the bases along the DNA strands encodes the genetic information[13]. Genes, which are specific segments of DNA, contain the instructions for building proteins[14], which are the functional molecules that carry out various biological processes in cells. The arrangement of the nucleotide bases in a gene determines the order of amino acids in a protein, which, in turn, influences its structure and function. The discovery of the structure of DNA and its role in genetics was a significant breakthrough in the field of molecular biology. It provided the foundation for understanding inheritance, evolution, and the mechanisms of genetic diseases. Today, DNA analysis and manipulation techniques are used in a wide range of applications, including forensic investigations[15], medical diagnostics[16], genetic engineering[17], and evolutionary studies[18].

DNA synthesis plays a crucial role in biological research, biotechnology, and synthetic biology. In nature, DNA is synthesized through the process of replication[19], where DNA polymerases catalyze the addition of nucleotides to a growing DNA strand using an existing strand as a template. This extension proceeds from the 5' to 3' direction, with new nucleotides being added to the 3' hydroxyl group of the preceding nucleotide. The inherent specificity of base pairing (adenine with thymine, and guanine with cytosine) ensures the accurate transmission of genetic information.

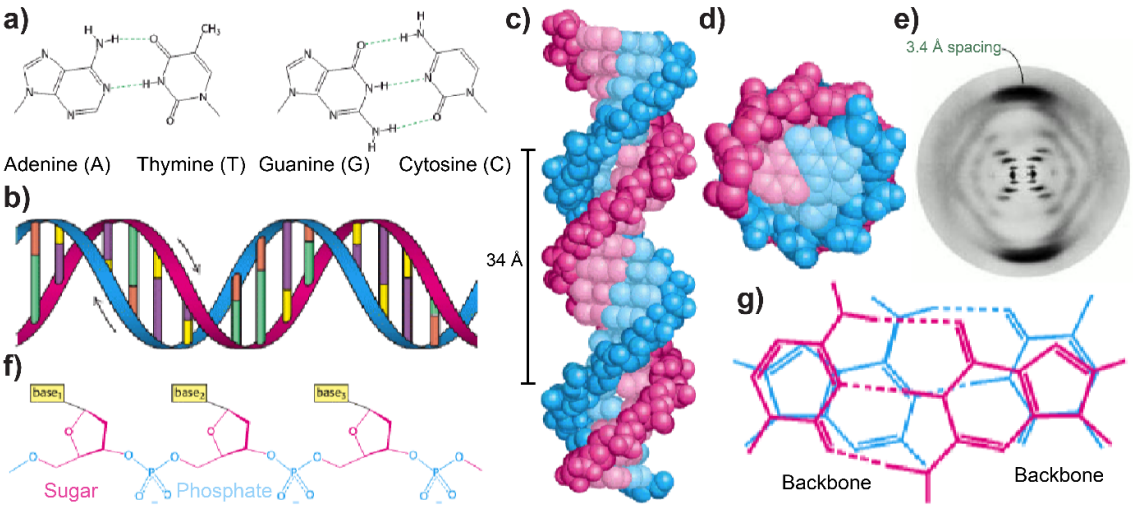

Figure 2.1: Schematic illustration of the structure of the DNA. a) Watson-Crick base pairing of Adenine (A) and Thymine (T), and Guanosine (G) and Cytosine (C). The blue dots indicate hydrogen bonds. b) Double helix formed by two antiparallel DNA strand (blue, magenta) bound by complementary Watson-Crick base pairing (orange, green, yellow, violet). c) Axial view of the Watson-Crick double helical model of the DNA structure. d) Radial view of the Watson-Crick double helical model of the DNA structure. One DNA backbone is shown in dark blue and the other one in dark magenta, while the bases are coloured in light blue and light magenta. e) X-ray diffraction photograph of a hydrated DNA fiber by Rosalind Franklin. 3.4 Å spacing is marked with a black arrow and is highlighted in blue. f) Linear polymer of nucleotides, where the deoxyribose is depicted in magenta, the phosphate in cyan and the base in yellow. g) Comparison of size and shape of the two complementary base pairs (A-T (cyan), G-C (magenta)). Since they have the same overall size, they are able to form a uniform double helix. This illustration is taken with permission from Berg, Tymoczko, Stryer, 2003[10].

In contrast, artificial DNA synthesis, is performed by solid phase synthesis and allows for the custom design and production of DNA sequences. This is typically done using the phosphoramidite method[20], which synthesizes DNA strands in the 3' to 5' direction, contrary to natural DNA synthesis. Each nucleotide is added sequentially, and the process involves several steps, including deprotection, coupling, capping, and oxidation. Synthetic DNA permits the incorporation of a variety of chemical modifications, which can be introduced at the 5' end, the 3' end, or internally within the DNA strand. Common modifications include the addition of functional groups such as thiols[21], biotin[22], or fluorophores[23], which are

primarily used for conjugation, immobilization, or detection, respectively, though they can serve other purposes as well. For example, a thiol group introduced at either the 5' or 3' end, allows for the covalent attachment of the DNA to surfaces or other molecules through maleimide-thiol chemistry[24]. Similarly, biotinylation at either end or internally enables DNA immobilization or purification using streptavidin-biotin interactions[25-27].

Beyond traditional DNA, significant advancements have been made with analogs such as Peptide Nucleic Acids (PNAs)[28], and other synthetic alternatives collectively referred to as Xeno Nucleic Acids (XNAs)[29], which make internal modifications to the nucleic acid backbone. PNAs are of particular interest due to their unique backbone composed of N-(2-aminoethyl)-glycine units, which are structurally distinct from the phosphodiester backbone of DNA and RNA. This modification confers PNAs with enhanced stability against enzymatic degradation and stronger binding affinity to complementary nucleic acids due to the neutral charge of the backbone, which eliminates electrostatic repulsion[27, 30, 31].

With all these unique characteristics, natural and artificial, DNA plays a crucial role in nano(bio)technology, offering unique properties that enable a wide range of applications. One of the primary roles of DNA in this field is its ability to form highly specific base-pairing interactions, making it an excellent tool for molecular recognition. This specificity is harnessed in applications like biosensors and diagnostics. In biosensors, specially designed DNA sequences can detect specific nucleic acid sequences, proteins, or small molecules, enabling highly sensitive and specific biosensing applications. In medical diagnostics, DNA probes are used to identify genetic disorders, infectious diseases, and cancer biomarkers.

DNA's dense information storage capacity and stability also make it an attractive medium for data storage. It can store digital information in a highly compact and durable form, potentially storing vast amounts of data in a small physical space. Furthermore, DNA can functionalize surfaces and materials, enabling the precise arrangement of molecules and nanoparticles. DNA strands attached to surfaces create functionalized interfaces for biosensing, cell culture, and biomolecular assembly. DNA-mediated hybridization links nanoparticles, proteins, or other molecules in a controlled manner, enabling the construction of complex assemblies and materials.

2.1.2 DNA Origami

The field of DNA origami was pioneered by Paul Rothemund in 2006, building on foundational concepts established by Nadrian Seeman in the early 1980s. Seeman, often regarded as the founder of structural DNA nanotechnology, first proposed the idea of using DNA to construct nanoscale objects through predictable base-pairing interactions[32]. Seeman's initial work involved the creation of DNA junctions and branched structures (**Figure 2.2**a & b), which laid the groundwork for the more complex architectures that DNA origami would later enable.

The first DNA nanostructures were DNA tiles. They are typically planar and modular, designed to self-assemble into larger arrays or lattices. Each tile is composed of several DNA strands that hybridize to form a specific shape, such as a triangle or square, which can then tessellate to create extended structures. DNA tiles are valuable in creating patterned surfaces for nanofabrication or templating the assembly of other materials, allowing for the precise spatial arrangement of functional groups or nanoparticles on a surface (**Figure 2.2**a & b)[33-37].

Rothemund expanded on these ideas by introducing the concept of folding a long single-stranded DNA scaffold, typically a circular one, into specific shapes using short synthetic oligonucleotides, known as staple strands[7]. These staples bind to complementary regions of the scaffold, directing its folding into a desired two- or three-dimensional structure with nanometer precision. This has since become a popular method for creating a wide variety of nanoscale structures, from simple shapes like squares and triangles to more complex designs such as nanorobots and DNA-based machines (**Figure 2.2**c, d & e).

Initially, the design and arrangement of staple strands were done manually, requiring extensive planning and trial-and-error experimentation on paper[7]. This process was both time-consuming and error-prone, as the precise positioning of hundreds of staples had to be carefully orchestrated to achieve the desired structural outcome. However, advances in computational tools have since revolutionized the design process, allowing for the rapid and automated generation of staple strand sequences through software such as caDNAno and others. These tools enable the visualization and optimization of complex DONs, significantly

reducing the time and expertise required to design new shapes and expanding the accessibility of the technique to a broader range of research[33, 38].

The scaffold strand is typically derived from bacteriophage sources, with the M13mp18 single stranded DNA (ssDNA) being the most commonly employed scaffold, but other sources such as Lambda Phage, synthetic long DNA strands or those derived from other sources, such as customized plasmids or PCR amplification of specific sequences have been also reported[39, 40]. M13 bacteriophage is a filamentous virus that infects *Escherichia coli* (E. coli) and can be easily propagated in large quantities. The genome of M13mp18, approximately 7,249 nucleotides long, serves as an ideal scaffold due to its well-characterized sequence and availability in sufficient quantities for large-scale production. It also is particularly advantageous due to its stability and predictable folding behavior when combined with complementary staple strands. The genome can be extended to a maximum of 9000 bases. To increase the versatility orthogonal scaffolds[41, 42] to these were developed to enable larger DONs designs, where multiple scaffolds are needed, but the possibility of cross-hybridisation, between either the two scaffolds or the staple strands of either, needs to be avoided.

Full DONs are dense, solid assemblies formed by tightly folding the DNA scaffold into compact 2D or 3D shapes, such as rectangles, cubes, or more intricate forms like nanoboxes. These structures are characterized by their high mechanical stability and precision (**Figure 2.2**b)[7, 33]. Full DONs come in various lattice designs, such as square lattices or honeycomb, to optimize packing and stability. The square lattice, typically employed in two-dimensional designs, offers a straightforward geometry that is particularly suitable for creating flat, rigid panels and surfaces ideal for scaffolding applications. Conversely, the honeycomb lattice, often utilized in three-dimensional origami designs, allows for a highly efficient use of space and material by arranging helices in a hexagonal pattern. This arrangement not only provides structural integrity but also maximizes the internal volume, which is advantageous for encapsulation tasks.

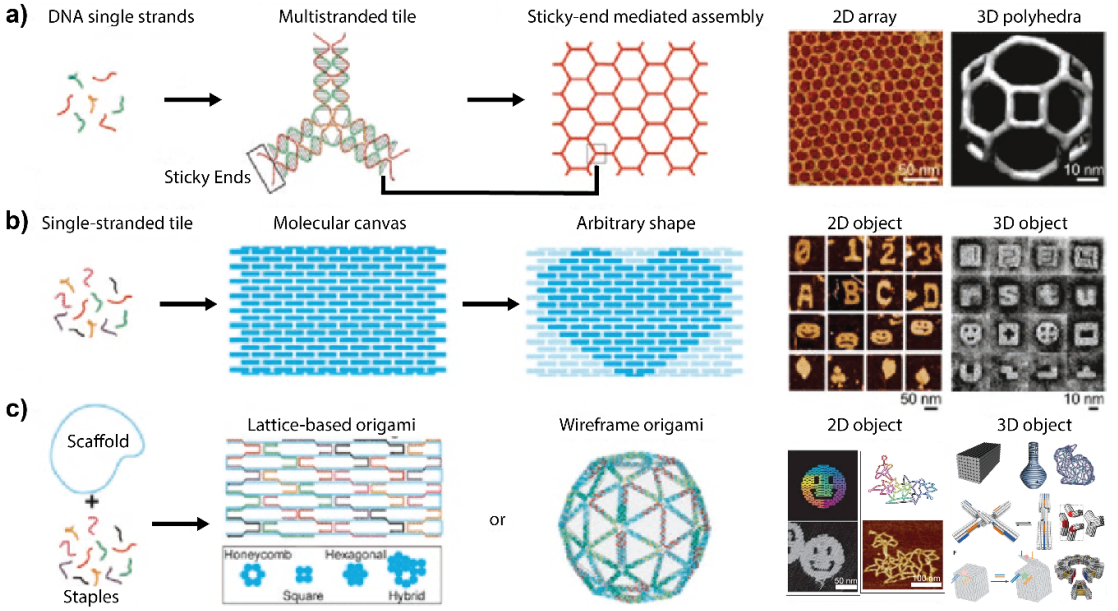

Figure 2.2: Examples of DNA nanostructures. a) Multistranded DNA tile. Each tile is composed of several short DNA strands. Strands of different colors have different sequences. Sticky-end mediated cohesion between tiles leads to the assembly of larger structures such as 2D arrays or 3D polyhedra[34]. b) ssDNA tile. A number of ssDNAs with unique sequences assemble into prescribed objects, which can serve as 2D and 3D canvases to construct arbitrary objects[36, 37]. c) Scaffolded DNA origami. A long ssDNA template serves as a scaffold that is folded by a number of shorter ssDNAs (staples) into both delicate 2D and 3D objects. DNA duplexes can be organized using parallel lattices[7, 33] or wireframe structures[43-45]. Figure taken and changed with permission from Wang et al.[35]

Each lattice type influences the DNA origami's mechanical properties and functional capabilities. For instance, the rectangular lattice provides a stable platform for the precise and orderly arrangement of functional groups, nanoparticles, proteins or fluorophores, enabling the creation of highly ordered composite materials. On the other hand, the honeycomb lattice can enhance the structural resilience and flexibility of the origami.

Lastly, wireframe DONs are more open and less dense, consisting of interconnected edges that form polygonal or polyhedral shapes. These wireframe designs resemble the skeletal framework of a structure, with minimal use of DNA, which reduces cost and increases structural flexibility. The reduced DNA usage also allows for the construction of larger and more complex shapes than would be feasible with full DNA origami (**Figure 2.2**c)[43-45].

The development and construction of these various DONs have been greatly facilitated by the advancement of specialized software tools that enable the design, visualization, and simulation of their structures with high precision. One of the most widely used software tools in this field is caDNAno[46], which provides a user-friendly interface for designing both

2D and 3D DONs. CaDNAno allows the visualization of the routing of the scaffold strand through the desired shape and to generate the corresponding staple strand sequences, significantly simplifying the design process[46]. There is also an browser-based version of this tool called scaDNAno[47].

Another important software tool is CanDo (Computational DNA Origami)[48], which simulates the mechanical properties and stability of DONs. CanDo is often used in conjunction with CaDNAno, allowing users to predict the folding behavior, thermal stability, and mechanical response of their designs. This capability is crucial for optimizing designs before experimental assembly, ensuring that the structures will fold correctly and maintain their intended shapes under various conditions. It is important to note, however, that CanDo does not provide an absolute scale for its simulations; the stability indicators such as color coding from blue (most stable) to red (least stable) are always relative to the specific origami being simulated. This relative scale helps identify potential instability areas within each individual structure, rather than providing a universal measure across different designs.

For more advanced modeling and simulation, OxDNA[49, 50] offers a coarse-grained molecular dynamics approach that models DNA at the nucleotide level, providing detailed insights into the folding process and the dynamic behavior of DONs. This tool is valuable for studying the kinetics of DNA folding and the stability of structures in different environments.

Lastly, NuPack[51, 52], short for Nucleic Acid Package, is a software suite designed to facilitate the analysis and design of nucleic acid structures, including DNA and RNA. In the context of DNA origami, NuPack is particularly valuable for predicting the secondary structure of DNA strands and designing sequences that minimize unintended folding or hybridization, which can affect the efficiency and accuracy of DNA origami assembly. By providing tools for sequence design, secondary structure prediction, and thermodynamic analysis, NuPack helps to create more reliable and stable DONs, ensuring that the staple strands bind correctly to the scaffold strand to form the desired 2D or 3D nanostructures.

There are certainly further design tools available for DNA origami (like Tiamat[53] or vHelix[54]), but the ones mentioned here were the ones utilized throughout the course of this thesis.

The steps to actually create a functioning DON are as follows. First the shape of the DON is determined. With the help of caDNAno this is then translated onto a scaffold with complementary staples added in. The most crucial approach is optimizing the design of staple strands. Staples are pivotal in stabilizing a DON, and by carefully designing their sequences and optimizing their lengths and positions, stability can be significantly enhanced. This includes maximizing staple crossovers, reducing unwanted interactions between staple strands, and optimizing the distribution of stabilizing motifs along the scaffold strand. This should be done in the design stage of the process to get a stable origami.

After the DON is designed *in silico*, the staple strands can be ordered and are custom-synthesized separately. To fold the structure the scaffold and staple strands are mixed in a buffer solution. The mixture is then subjected to a precise heating and gradual cooling regimen. Heating the solution to temperatures near the DNA melting point ensures that the DNA strands are fully denatured, meaning that eventual double-stranded DNA (dsDNA) regions are separated into single strands, allowing the scaffold and staples to become completely flexible and unpaired. Subsequently, the solution is slowly cooled, typically over several hours up to several days, permitting the staple strands to anneal to their complementary regions on the scaffold strand at controlled rates. This gradual cooling is critical as it allows the formation of correct base pairs incrementally, fostering the intended folding pathways to form the desired structure without trapping the system in misfolded configurations.

Some DONs can be folded isothermally at a constant temperature due to the inherent stability of their design and the robustness of interactions among their specific sequences. Isothermal folding is particularly advantageous for structures that are designed to be stable under a narrower range of thermal conditions and can fold correctly without the need for a wide temperature gradient, simplifying the experimental setup and potentially increasing the yield of correctly folded structures[55, 56].

During the assembly, the type and concentration of cations in the buffer solution are also critical influences. Cations such as magnesium ions (Mg^{2+}) stabilize the DNA double helix, improving the overall structural integrity of the DON, but too much can cause aggregation[57].

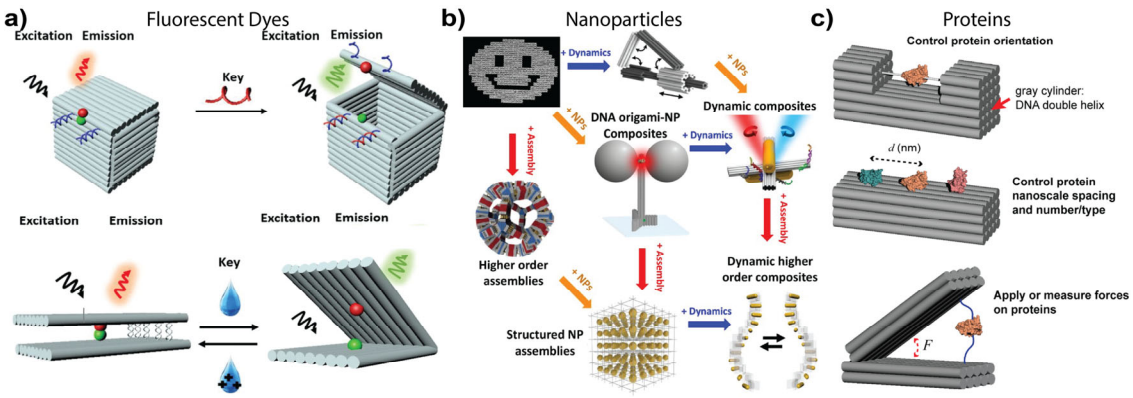

Figure 2.3: Schematic illustration of the customization variability of DONs. a) Fluorescent Dyes: Illustration of DONs functionalized with fluorescent dyes. The excitation of these particles leads to emission, which can be utilized for biosensing and imaging applications. Different configurations demonstrate the flexibility in design, allowing specific placement and control of fluorescence properties[58]. b) Nanoparticles: DNA origami used to create nanoparticle composites. Dynamic composites and higher-order assemblies showcase the ability to integrate nanoparticles with DNA origami, enabling complex structures and dynamic behaviors. The images depict various potential configurations, including dynamic interactions and structured assemblies, highlighting the versatility of DNA origami in nanotechnology[59]. c) Proteins: DNA origami for protein manipulation. These structures can control protein orientation, spacing, and types at the nanoscale. The figure shows how DNA origami can be used to apply or measure forces on proteins, providing precise control for biochemical and biophysical studies. The capability to fine-tune protein interactions demonstrates the potential for advanced biomolecular engineering and synthetic biology applications[60]. Figure taken and changed with permission from the references given.

Optimizing these conditions can significantly enhance stability, and is usually done as the first thing before further research is done with a new DON.

The resulting DNA origami structure can be used for a variety of applications, such as drug delivery, biosensing, and nanoelectronics. DONs can also be functionalized with other molecules, such as fluorescent dyes (**Figure 2.3**a)[58], nanoparticles like gold or silver (**Figure 2.3**b)[59] or proteins (**Figure 2.3**c)[60], to create hybrid materials with novel properties and functions, for example deliver drugs and therapeutic agents with high precision.

Guest molecules such as fluorophores, proteins, or nanoparticles can be functionalized onto DNA origami by incorporating functional groups like biotin, thiols, or azide/alkyne groups into the DNA strands. Biotin-streptavidin interactions are widely employed due to their high specificity[61], while click chemistry is utilized to enable efficient covalent binding under mild conditions[62]. Gold nanoparticles are commonly attached using thiol-modified oligonucleotides, and fluorophores or proteins are conjugated through reactive groups such as amines or maleimides[63]. These methods are designed to provide versatile and robust strategies for anchoring guest molecules without disrupting the origami structure.

2.2 Enhancing DNA Origami Stability

DNA and DNA origami structures exhibit remarkable stability under specific conditions, primarily determined by environmental factors such as pH, temperature, ionic strength, and the absence of nucleases. Typically, these structures are stable in buffered solutions with a neutral pH and temperatures below room temperature (RT). However, their structural integrity becomes compromised under extreme pH conditions, elevated temperatures, missing cations and in the presence of organic solvents or DNases[64].

To enhance the stability and durability of DNA and DNA origami, several strategies can be employed. Coating with stabilizing agents such as PEG (polyethylene glycol)-poly Lysine or other copolymers offers a protective layer that shields the DNA from enzymatic degradation and adverse environmental conditions[65, 66]. Another innovative approach involves the use of UV-induced cross-linking to form thymine dimers within the DNA strands, thereby enhancing their resistance to thermal and enzymatic breakdown[67].

In addition to these methods, biomineralization offers a promising approach to stabilize DONs. Biomineralization in contrast to mineralization is a usually biologically mediated process. Examples of biomineralization include the formation of bones and teeth in vertebrates, shells in mollusks, and exoskeletons in certain algae and invertebrates. Biomineralization is normally highly controlled and occurs in specific biological environments, involving organic molecules like proteins and polysaccharides that regulate the nucleation, growth, and organization of the minerals. This process results in complex and functional materials with unique mechanical properties, often surpassing those of purely inorganic minerals due to the precise biological control over mineral deposition. Mineralization refers to the process by which inorganic minerals are deposited in an organized matrix, often occurring in nature through geological processes such as precipitation from water. This can include the formation of various minerals in the Earth's crust, where conditions such as temperature, pressure, and chemical environment dictate the type and extent of mineral deposition[68] (**Figure 2.4**).

With DNA origami biomineralization involves the incorporation of minerals into the DNA origami backbone, enhancing mechanical properties and overall stability. This technique is

inspired by natural processes, such as those seen in bones and teeth, where minerals like calcium phosphate are deposited to provide strength and durability.

Silica plays significant roles in various biological systems. It is used as a composite material in the cell walls of diatoms[69] and serves as a defense mechanism in certain grass species against herbivores[70]. This ceramic material, with its high melting point, offers excellent protection and barrier properties[71], making it particularly suitable for the stabilization of DNA-based nanostructures[72]. However, the negatively charged nature of some silica precursors and reaction intermediates, similar to the phosphate groups in the DNA backbone, creates electrostatic repulsion that hinders successful silicification with DNA molecules. Various methods have been developed to address this challenge[9, 72, 73].

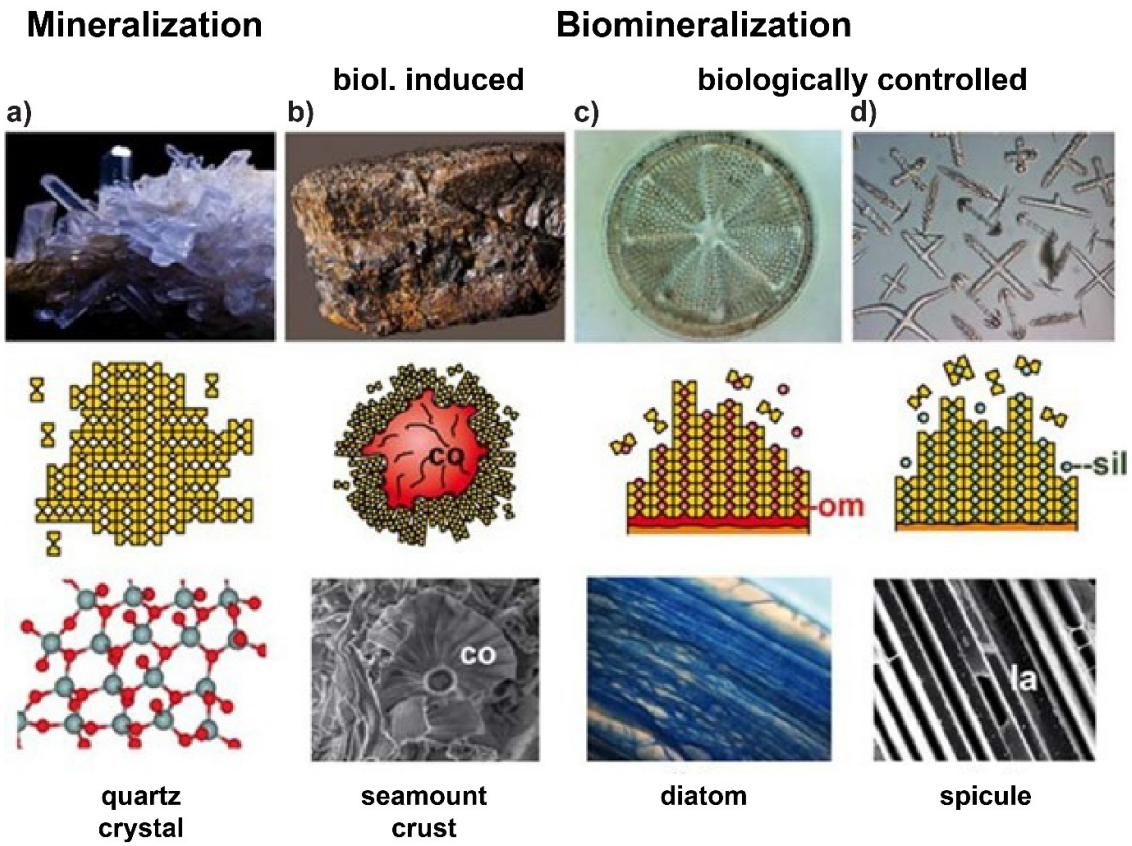

Figure 2.4: Mineralization versus biomineralization. a) Mineralization process: example, quartz crystal formation. Inorganic monomers of silicic acid form crystals with defined chemical compositions and physical structures in a hydrothermal environment and under high pressure. b) Biologically induced mineralization: example, ferromanganese crust formation in the deep sea. Coccospheres (co) of biogenic origin serve as organic template for mineral deposition. c) Biologically controlled mineralization: example, frustule formation in the diatom. d) Unique form of biologically controlled mineralization: example, spicule formation in the hexactinellid Hyalonema mirabile. Figure taken with permission from Müller et al.[68]

In 2013, Panescu et al. demonstrated that DNA could be adsorbed, hermetically sealed, and subsequently released from silica particles[71]. DNA is first adsorbed onto positively charged particles, after which a thin silica layer is grown on top through polycondensation. This process involves the silicification reagents tetraethyl orthosilicate (TEOS), a neutral silanol derivative, and N-[3-(trimethoxysilyl)propyl]-N,N,N-trimethylammonium chloride (TMAPS), an ammonium salt with a positively charged quaternary ammonium head group. TMAPS serves as a positively charged co-structure directing agent, electrostatically binding to the DNA's phosphate backbone and templating the silica shell formation by polycondensation with TEOS.

The templating of silica nanomaterials with DNA origami was first demonstrated by Chunhai Fan and his team in 2018[72, 74]. The electrostatic potential barrier was overcome by slightly modifying the Stöber process, a sol-gel process commonly used to produce uniform spherical silica nanoparticles, and using pre-hydrolyzed clusters of TMAPS and TEOS, which were able to bind to DNA origami and 2D origami lattices that had been pre-adsorbed onto a surface, such as a Transmission Electron Microscopy (TEM) grid or mica (**Figure 2.5**c)[74] for atomic force microcopy (AFM). This was achieved by placing the immobilized DNA origami upside down in a magnesium acetate buffer and applying a pre-hydrolyzed solution of TMAPS and TEOS. This process typically takes up to seven days in a static environment, during which the TEM grids may begin to dissolve partially. In 2023, my colleagues and I adapted this method for DNA-PAINT applications, where DNA origami is immobilized on a glass surface, which cannot be inverted into a solution, requiring modification of the original technique[75].

DONs can be silicified not only on surfaces but also in solution. In 2019, Nguyen et al. successfully demonstrated the silicification of DNA nano-objects in solution, combining the controllable self-assembly of DNA with the stability and inertness of silica to create nanostructured silica objects with high precision and robustness[9]. Unlike previous methods, the use of pre-hydrolyzed clusters was unnecessary because DNA origami maintained their structural integrity even at very low cation concentrations in EDTA-free buffers[76]. The basis of their method is also a modified Stöber reaction, (**Figure 2.5**a & d)[77].

The Stöber process is divided into two parts[9]. First: acid or base-catalyzed hydrolysis of alkoxy silanes ($Si(OR)_4$) in multiple steps forms orthosilicic acid ($Si(OH)_4$).

$$Si(OR)_4+H2O \rightarrow Si(OR)_3OH+ROH \rightarrow\rightarrow\rightarrow Si(OH)_4 \quad \text{(Eq. 2.2.1)}$$

Second, the resulting orthosilicic acid condenses either by water (Eq. 2.2.2) or alcohol (Eq. 2.2.3) condensation to form connective siloxane bridges (Si-O-Si).

$$2\ Si(OR)_3OH \rightarrow Si(OR)_3{-}O{-}Si(OR)_3{+}H_2O \quad \text{(Eq. 2.2.2)}$$

$$Si(OR)_4{+}Si(OR)_3OH \rightarrow Si(OR)_3{-}O{-}Si(OR)_3{+}ROH \quad \text{(Eq. 2.2.3)}$$

Nguyen et al. also discovered that shaking the solution during synthesis disrupts the encapsulation process[9]. Consequently, samples were shaken for 15 min and then left undisturbed for up to 7 days. The thickness of the silica layer could be adjusted by varying the concentration of reactants, reaction time, and temperature.

During the course of this thesis it was discovered that slowly rotating the sample at a constant speed for 4 to 6 h in a tube revolver rotator produced a silicified sample comparable to one left undisturbed 5 days, but within 24 h[75, 78]. The thickness of the silica layer could similarly be adjusted by concentration of the reactants and time on the rotator.

Another study, by Anton Kuzyks Group[79], describes a two-step silicification process for coating DONs with an ultrathin layer of silica, aimed at enhancing their stability in various environments. The first step involves applying a primary silica coating using coupling agents like TMAPS or (3-Aminopropyl)triethoxysilane (APTES), which bind to the DNA's phosphate backbone, followed by the addition of TEOS to form the silica layer. The second step involves reinforcing this coating with a secondary silica layer in an isopropanol-water mixture at a higher pH, ensuring a denser and uniform silica shell (**Figure 2.5**e).

In 2020 Baoqan Ding's Group discovered that silica would adhere to dsDNA before it would silicify a larger origami[80]. In their study protruding dsDNA strands on origami templates guided silica to only form at desired locations (**Figure 2.5**b & f). The question what happens to single stranded protruding DNA was answered in 2023 and is part of this thesis[75].

In 2022 Nayan Agarwal and Ashwin Gopinath used a polyplex micellization strategy[65, 66] to create DNA nanostructures (brick and ring-shaped DONs) using the standard Stöber process that can withstand salt-free, buffer-free, alcohol-water mixtures, enabling them to control

the material growth conditions while maintaining the monodispersity and organization of nanoelements[81].

In 2023, Jing et al. used Cryo-Electron Microscopy (CEM) to study the dynamics of amorphous silica mineralization templated by DNA nanostructures[82]. Their work revealed a process of "adaptive templating," where both DNA frameworks and silica cluster morphologies cooperatively adjust, offering new insights for the rational design of silica-based materials.

Also in 2023, Jonggang Ke's group investigated how site-specific polynucleotide brushes influence the silicification of DNA origami, using experiments and molecular dynamics simulations[83]. They found that long DNA brushes suppress DNA origami aggregation and that double-stranded brushes selectively promote silica growth, providing insights for creating novel DNA-based hybrid nanomaterials.

The different approaches and settings for the different styles of silicification used in this thesis are detailed in Appendix B section B.2.4.

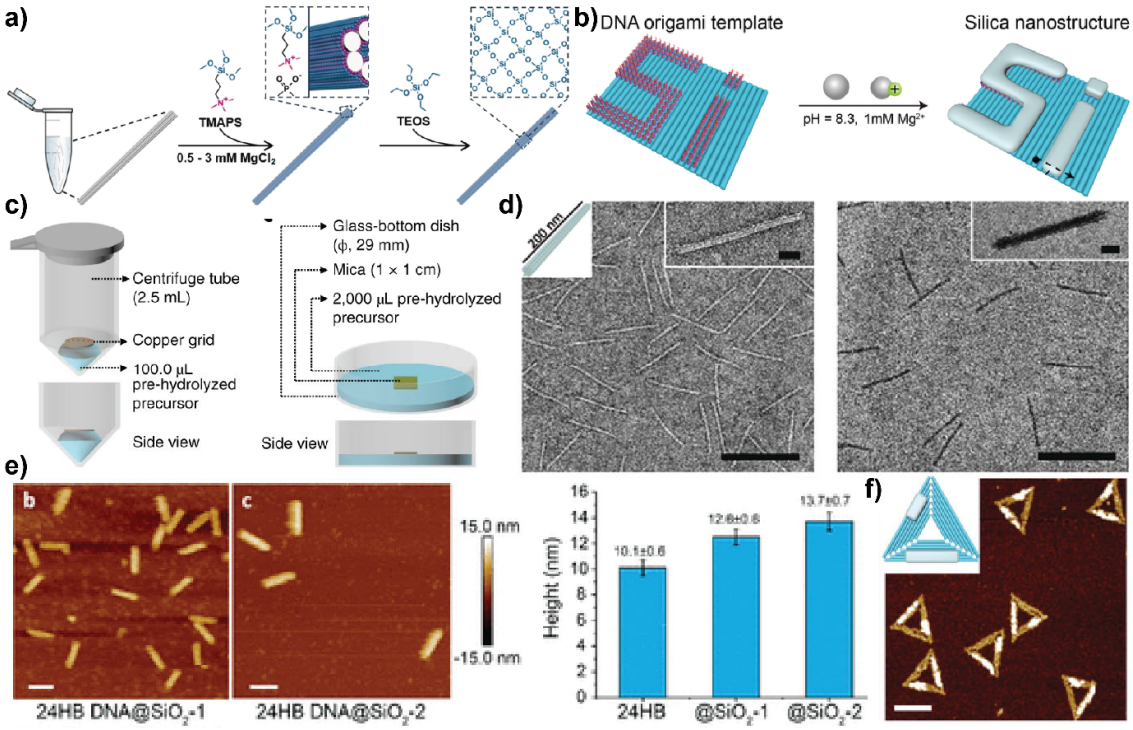

Figure 2.5: Silicification Process of DONs. a) Schematic representation of the silicification process[9]. b) The DNA origami template is designed to incorporate specific features and patterns, allowing for precise control over the silica coating[80]. c) Experimental setup for silicification on different surfaces, including a centrifuge tube setup for TEM grids and a glass-bottom dish setup for mica substrates[74]. d) TEM images illustrating the morphology of a 14HB before and after silicification. The images show that the silica coating preserves the overall structure of the DNA origami[9]. e) AFM images and corresponding height profiles of DNA origami before and after silica coating, demonstrating the uniformity and thickness of the silica layer[79]. f) AFM image of triangular DONs after silica coating, highlighting the ability for precise control over the silica deposition[80]. Scale bars are 100 nM as indicated in the images. Images taken from the indicated references and changed with permission.

2.3 Fluorophores

Fluorophores, molecules capable of re-emitting light upon excitation, have been pivotal in molecular biology and biochemistry for visualizing, tracking, and measuring biological processes at the molecular level since their discovery. The phenomenon of fluorescence was first described by Sir George Gabriel Stokes in 1852[84], and the first synthetic fluorophore, fluorescein, was created by Adolf von Baeyer in 1871[85]. Since then, the development of fluorophores has advanced significantly[86], particularly with the introduction of fluorescein derivatives like rhodamine in the late 19th century[87]. These early developments set the stage for the modern use of fluorophores in biological imaging.

Fluorophores typically consist of several combined aromatic groups, or planar or cyclic molecules with several π bonds[88], allowing them to absorb light at specific wavelengths (EX) and emit light at longer wavelengths (EM) (**Figure 2.6**a & b). To describe fluorescence of molecules the Jablonski diagram (**Figure 2.6**c) was developed by Aleksander Jabłoński in 1933[89]. It illustrates the electronic states of a fluorescent molecule and the transitions between these states, including absorption, fluorescence, and non-radiative decay[90].

In DNA and DNA origami studies, fluorophores are extensively used to tag specific sequences or structures, thus allowing visualization of the DNA's location[91], movement[92], and interactions[93, 94], either within cells[95, 96] or on surfaces[97, 98]. Tagging is usually accomplished by directly attaching the fluorophores to nucleotides during DNA synthesis for precise placement[99, 100] in a DNA Origami[101, 102]. Various fluorescence microscopy techniques (like Total Internal Reflection Fluorescence (TIRF)[103] and Single-Molecule Localization Microscopy (SMLM)[104,105] exploit these fluorophores to enhance DNA origami studies by utilizing different aspects of fluorescence and light to surpass the diffraction limit of light (**Figure 2.6**d & e).

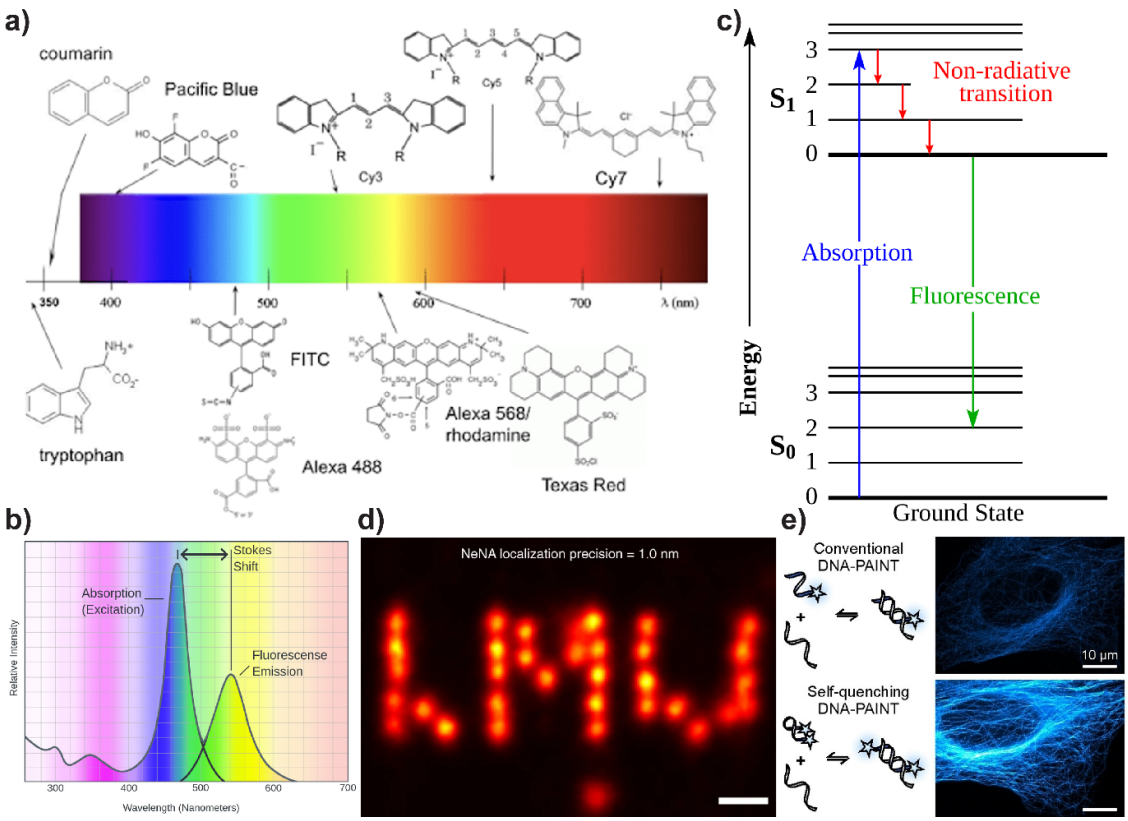

Figure 2.6: Fluorophores and DNA-PAINT. a) A range of commonly used fluorophores across the visible spectrum, illustrating their chemical structures and corresponding excitation-emission profiles. From left to right: coumarin, tryptophan, FITC, Alexa 488, rhodamine, Texas Red, Pacific Blue, Cy3, Cy5, and Cy7[106]. b) Typical absorption and fluorescence emission spectrum demonstrating the Stokes shift, where the emission peak is at a longer wavelength than the excitation peak[107]. c) The Jablonski diagram, depicting the transitions between the ground state (S0) and excited state (S1) of a fluorophore, including absorption, fluorescence emission, and non-radiative transitions. d) A high-resolution fluorescent image of DNA strands labeled with a fluorophore, demonstrating the application of these molecules in nanoscale biological imaging. 'Ultra-resolution' with DNA-PAINT[105]. e) Comparison of conventional DNA-PAINT versus self-quenching DNA-PAINT techniques, illustrating the enhanced resolution and contrast achievable with advanced fluorescence imaging methods. Also showing how fluorophores are usually attached to DNA strands at the end[97]. Images taken from the indicated references and changed with permission.

Chapter 3 - Methods

This chapter aims to provide a comprehensive overview of the theoretical principles underlying the various analytical methods used to characterize DONs.

To give a brief overview, I will first discuss the microscopy techniques essential for visualizing and characterizing nanoscale materials. TEM, CEM, AFM, and DNA-PAINT provide different modes of imaging and analyzing the structural details of DNA nanostructures and their mineralized forms. Each technique has its strengths and limitations, which will be discussed to provide an understanding of their applications.

Following microscopy, I examine two scattering techniques, SAXS and Dynamic Light Scattering (DLS), which can be used to understand the size, shape, and distribution of nanoparticles in solution. These techniques offer complementary information to microscopy, enabling a more comprehensive characterization of nanoscale materials.

Gel electrophoresis, specifically agarose (AGE) and polyacrylamide (PAGE), is another essential analytical method covered in this chapter. These techniques allow for the separation and analysis of DNA and protein samples based on their size and charge, providing insights into their purity and composition.

This chapter aims to provide a solid foundation of the methods that will inform and support the experimental investigations discussed in subsequent chapters.

3.1 Microscopy Techniques

3.1.1 Transmission Electron Microscopy

TEM is a powerful technique initially demonstrated by Max Knoll and Ernst Ruska in 1931[108]. The first electron microscope was invented in the 1930s, with the first commercially available model produced by Siemens in 1939[109]. This method uses accelerated electrons to image thin samples, typically ranging in thickness from 10 nm to 1 µm[110], and can achieve magnifications from 10^3 to 10^6, allowing for atomic-level resolution.

TEM exploits the wave-particle duality of electrons, which, like photons, exhibit both wave-like and particle-like characteristics[111]. An electron beam emitted from an electron source can be focused by magnetic fields[112]. The wavelength λ of this beam, known as the de Broglie wavelength[110], is given by:

$$\lambda = \mathrm{hp} = \mathrm{hm} \times \mathrm{v} \qquad \textbf{Eq. 3.1}$$

where h indicates the Planck constant, p the momentum, m the mass and v the velocity of an electron. Since the wavelength of electrons is significantly smaller than that of light, and because the maximum resolution d of microscopic imaging is limited by the wavelength λ of the image-forming wave, electron microscopes achieve a resolution limit that is 1000 times smaller than that of light microscopes[112]. The resolution d is calculated by:

$$\mathrm{d} = 2\lambda \mathrm{n} \times \sin\alpha \qquad \textbf{Eq. 3.2}$$

where λ represents the wavelength of the image forming wave, n the refractive index of the medium in which in the microscope is working and α the maximum half angle of the beam that can enter the lens.

A conventional TEM[113] consists of an electron source, various electromagnetic lenses, a specimen holder, and a detector screen (**Figure 3.1**a)[110]. The electron source, typically a tungsten cathode, is induced by a high voltage source to emit electrons into a vacuum to prevent collisions with gas molecules, which could alter the electrons' direction or energy (**Figure 3.1**a). These electrons are accelerated by an anode and focused by the condenser lens system (**Figure 3.1**a). The focused electrons then pass through the specimen, which is mounted on a holder and inserted into the microscope through an airlock (**Figure 3.1**a).

As the electron beam transmits through the specimen, electrons interact with its molecules, resulting in various scattering behaviors (**Figure 3.1**b). Some electrons pass through the sample without interaction, while others are elastically (**Figure 3.1**b) or inelastically (**Figure 3.1**b) scattered. Inelastic scattering involves a fast electron interacting with an atomic electron, causing the incoming electron to lose energy. Elastically scattered electrons result from interactions between a fast electron and an atomic nucleus. These scattered electrons carry information about the sample's characteristics.

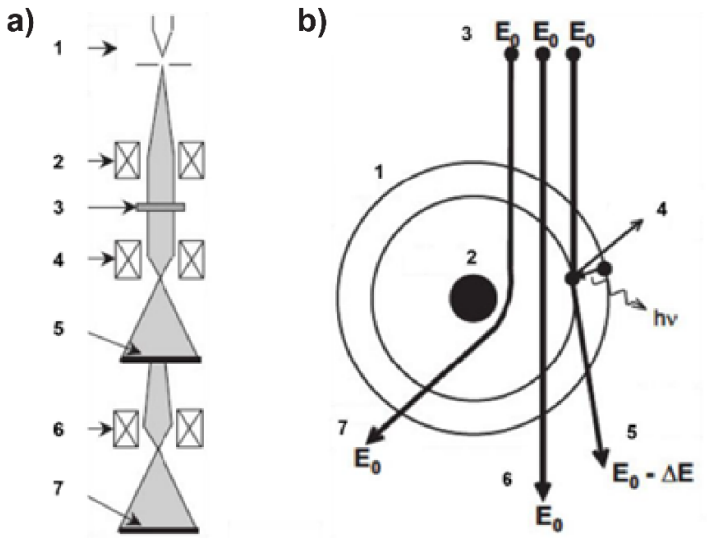

Figure 3.1: Overview of TEM. a) Schematic illustration of the construction of a TEM and the beam path. 1) Electron source 2) Condenser lens 3) Specimen 4) Objective lens 5) Single stage magnified intermediate image of the specimen 6) Projector lens 7) Fluorescent detector screen. The electron beam is depicted in light grey, the specimen in dark grey and the image and the detector in black. b) Schematic illustration of the interactions of the accelerated electrons from the electron source of the microscope with the atoms of the specimen. 1) Electron shell 2) Atomic nucleus 3) Accelerated electrons 4) Ejected electron of the specimen 5) Inelastically scattered electron 6) Transmitting electron 7) Elastically scattered electron. E0 indicates the energy of the electrons, ΔE the energy difference, h the Planck constant and v the frequency of the photon. The illustration is taken and adapted with permission from images of Prof. Dr. G. H. Michler[114].

After passing through the specimen, the electrons are magnified by objective lenses and further focused by projector lenses to produce an image on the detector screen. This screen is used for focusing the TEM image, with binoculars attached outside the viewing port for precise adjustment. Images can be captured using photographic film or electronic image-recording devices like charge-coupled device (CCD) cameras[110].

Biological samples, mainly composed of elements with low atomic numbers, scatter fewer incoming electrons and appear nearly featureless. To enhance contrast, specimens are

stained with heavy metals such as lead citrate or uranyl formate, which tend to accumulate in biological material and strongly scatter incoming electrons due to their high atomic numbers, resulting in darker images[110].

3.1.2 Cryogenic Electron Microscopy

CEM allows observation of samples in solution in a more native state. Therefore, this method is widely used for the determination of 3D structural information of proteins[115]. In the preparation procedure, a thin film of liquid residues remains on the grid. This cryo-grid then gets rapidly frozen in liquid ethane and kept at around < -150 °C until the sample is imaged. This procedure builds up an ice layer in which the sample gets immobilized in a biologically native state (**Figure 3.2**)[116]. This ice layer also protects the sample from the electron beam to a certain degree[117]. Therefore, a higher acceleration voltage, up to 300 kV, can be applied. Standard TEM operates at an acceleration voltage up to 120 kV. Depending on the specimen (thickness and atomic number) and the acceleration voltage, a resolution up to 0.45 Å15 can be achieved using TEM.

CEM is a cutting-edge imaging technique used to study the structure of biological macromolecules at near-atomic resolution. Unlike traditional electron microscopy, which may require extensive sample preparation that can alter the specimen's natural state, CEM involves rapidly freezing the sample to preserve its native structure and hydration state.

The core principle of CEM involves cooling the sample to cryogenic temperatures, typically using liquid nitrogen or liquid ethane. This rapid freezing process, known as vitrification, prevents the formation of ice crystals that can damage the sample and distort the imaging results. Instead, the water in the sample forms a glass-like, amorphous solid, preserving the specimen in a near-native state. An electron beam is directed through the sample, and electrons interact with the sample, with the transmitted or scattered electrons being detected to form an image. Multiple images are taken from different angles or positions to capture the three-dimensional structure of the sample. The collected images are computationally processed to correct for any distortions or noise and then used to reconstruct a model in 3D.

CEM has revolutionized structural biology by enabling the visualization of biological macromolecules, such as proteins, nucleic acids, and complex assemblies, at near-atomic

resolution. Key applications include determining the structure of large protein complexes and molecular machines, studying the architecture of viruses and their interactions with host cells, and investigating the structural basis of diseases and aiding drug discovery by revealing the precise binding sites of potential therapeutic compounds.

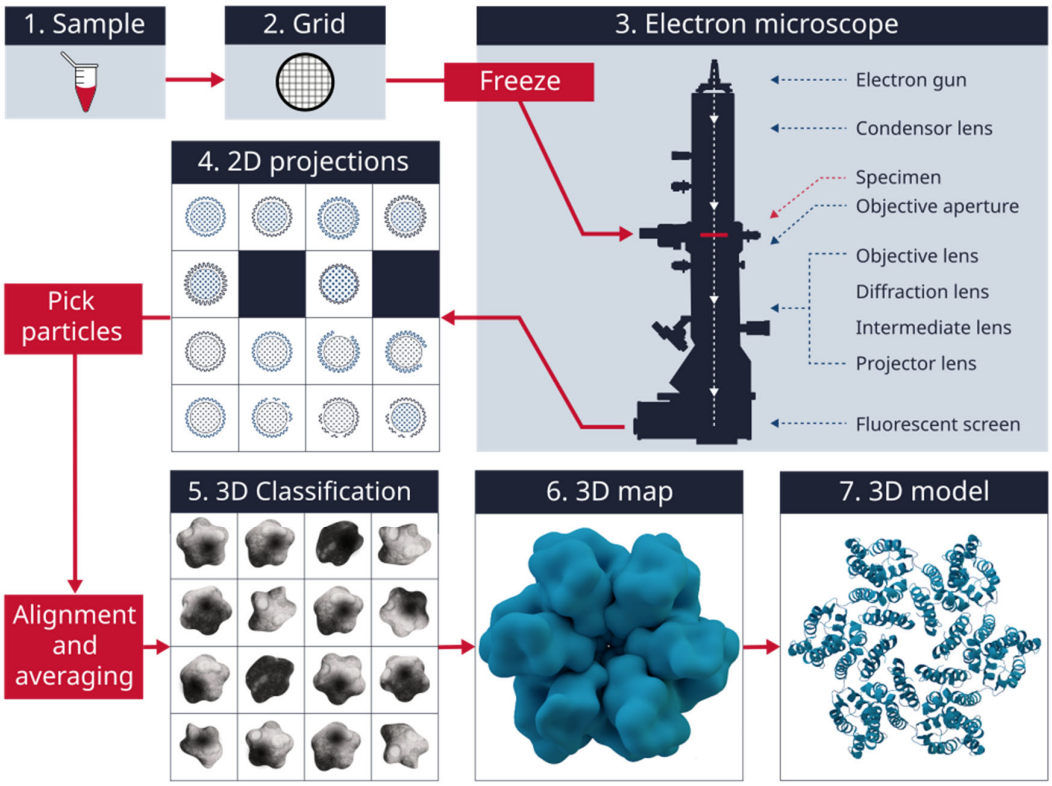

Figure 3.2: Workflow of CEM: (1) Prepare the sample. (2) Apply the sample to a grid and freeze it. (3) Image the sample using an electron microscope. (4) Obtain 2D projections of the sample. (5) Pick particles from the projections, followed by alignment and averaging. Perform 3D classification. (6) Generate a 3D map from the classified images. (7) Construct a 3D model from the 3D map. Image used with permission[118].

3.1.3 Atomic Force Microscopy

AFM is a high-resolution imaging technique used to visualize and characterize surfaces at the nanoscale[119, 120]. Unlike optical microscopy, which relies on light, AFM operates by scanning a sharp probe over the surface of a sample, providing detailed information about its topography, roughness, and mechanical properties. The basic principle of AFM involves the interaction between a probe and the surface of the sample. The probe consists of a sharp tip attached to a cantilever, which acts as a tiny mechanical spring[121]. As the probe scans across the surface, the interaction forces between the tip and the sample cause the cantilever to bend. These deflections are measured by a laser beam reflected off the back of the cantilever onto a position-sensitive detector, allowing for precise tracking of the probe's movement (**Figure 3.3**).

AFM can operate in several different modes, depending on the specific application and the information desired[120]. The most common mode is contact mode, where the probe is in constant contact with the sample surface. In this mode, the deflections of the cantilever are used to create a topographic image of the surface. Another mode is tapping mode (also known as intermittent contact mode), where the probe oscillates close to the surface, periodically tapping the surface. This mode reduces the lateral forces between the probe and the surface, minimizing damage to the sample and improving image quality. Tapping mode is particularly useful for imaging soft or delicate samples. In addition to imaging topography, AFM can provide information about various other sample properties. For instance, force spectroscopy can be performed to measure the mechanical properties of the sample, such as stiffness or adhesion forces. This is achieved by applying controlled forces to the cantilever and recording the resulting deflections[119].

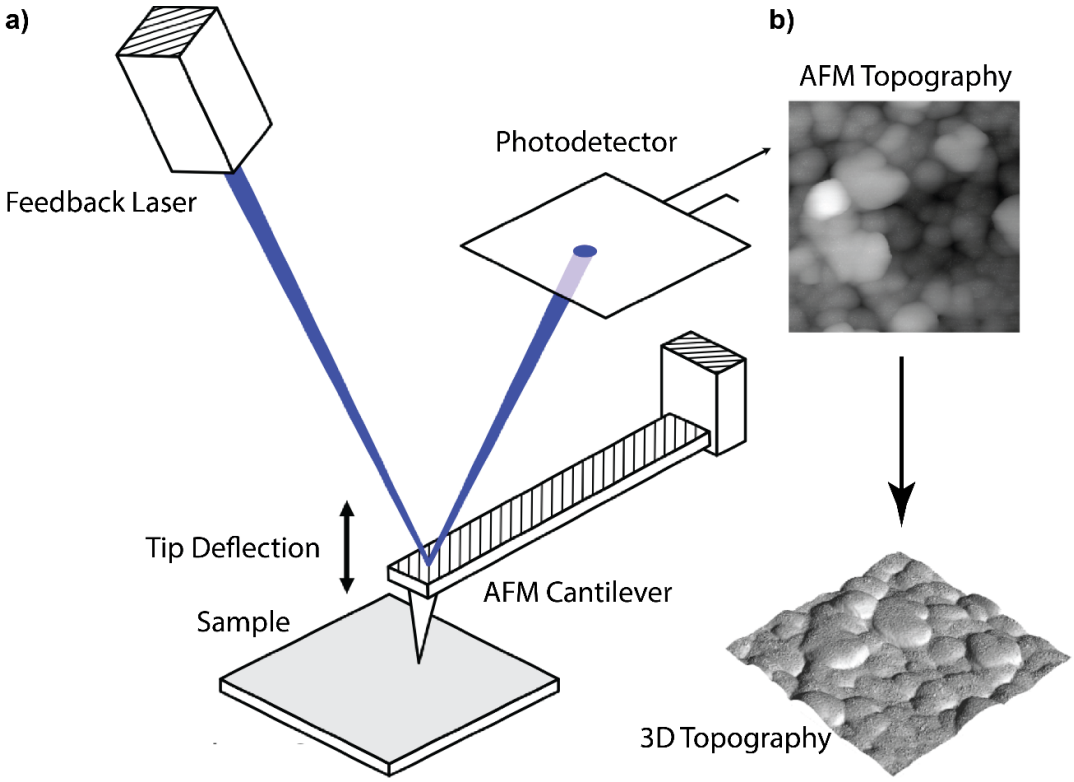

Figure 3.3: Schematic diagram of an AFM. a) The AFM operates by scanning a sharp probe attached to a cantilever over the sample surface. A laser beam is focused on the cantilever and reflected onto a photodetector, which measures deflections of the cantilever as the tip interacts with the sample. The feedback system adjusts the tip's height to maintain a constant force, b) enabling the reconstruction of the sample's topography with high resolution. Images taken and changed from An Introduction to AFM-IR[122].

3.1.4 DNA-PAINT

DNA-PAINT is a super-resolution microscopy technique, developed by Jungmann et al. in 2010[123], that enhances the imaging resolution beyond the diffraction limit of light. This technique is an evolution of the PAINT method initially conceived by Sharonov et al. in 2006 for cellular applications[124]. The principle underlying DNA-PAINT is based on the transient binding of short, fluorescently labeled DNA strands (imagers) to complementary DNA sequences (docking sites) tethered to the target of interest (**Figure 3.4**a)[123, 125]. This approach provides an elevated level of specificity and control within the imaging process, enabling detailed visualization at a molecular level.

In DNA-PAINT, the target molecule or structure is labeled with DNA oligonucleotides that serve as docking sites. These docking strands are typically integrated into the structure of interest using bioconjugation techniques. The complementary imagers are tagged with a

fluorescent dye and are introduced into the sample at a low concentration. Due to their transient and reversible interaction with the docking sites, the imagers bind and unbind repeatedly, causing stochastic blinking of the fluorescence signal (**Figure 3.4**a)[105].

This blinking behavior is central to DNA-PAINT and is exploited to achieve super-resolution imaging. Each binding event localizes the fluorescent imager to a precise location, and through repeated localization of many such binding events over time, a high-resolution image of the target structure is reconstructed. The temporal separation of the fluorescence signals allows for the resolution of structures that are closer together than the diffraction limit of light[105].

The resolution of DNA-PAINT can be tuned by adjusting the length and sequence of the DNA strands, as well as the imaging conditions, such as the concentration of imagers and the ionic strength of the solution. Typically, shorter docking and imager strands result in faster binding kinetics, which can decrease imaging time but may also affect the stability and specificity of the binding events. Furthermore, TIRF[103] microscopy is always employed in DNA-PAINT experiments to enhance the signal-to-noise ratio. TIRF generates an evanescent field that selectively excites fluorophores within a thin region (~100-200 nm) adjacent to the glass-water interface, where the sample is located[126]. This selective excitation further reduces background fluorescence from regions farther away from the interface. DNA-PAINT also offers the advantage of multiplexing[127], where different sets of imager and docking strand pairs, each with distinct sequences and fluorescent labels, are used simultaneously. This enables the simultaneous imaging of multiple targets within the same sample.

DONs are particularly well-suited for use in DNA-PAINT[128]. By incorporating specific docking sites into the DNA origami design, these nanostructures can serve as highly customizable platforms for the precise localization of fluorophores. This approach enables the high-resolution imaging of complex nanostructures, offering insights into their spatial arrangement and functional interactions. The integration of DNA origami with DNA-PAINT thus represents a powerful synergy in the field of super-resolution microscopy, allowing for the detailed visualization of nanoscale architectures with unprecedented accuracy[128].

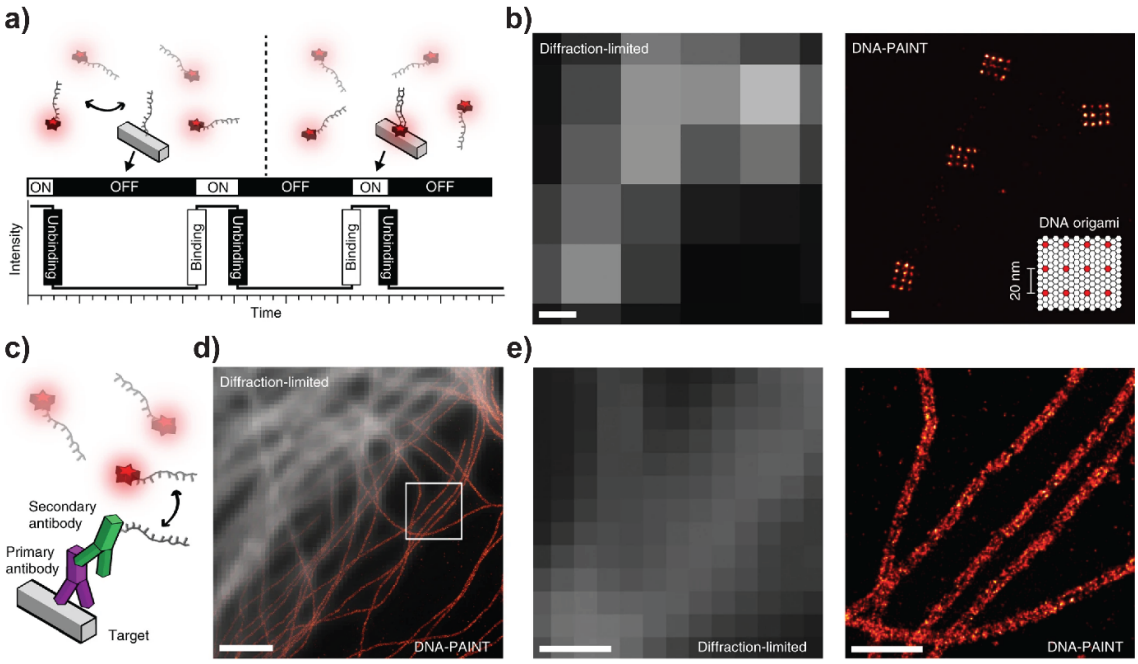

Figure 3.4: Overview of DNA-PAINT. a) DNA-PAINT concept. Transient binding of dye-labeled DNA strands (imagers) to their complementary target sequence (docking site) attached to a molecule of interest. The transient binding of imager strands is detected as 'blinking', illustrated by the intensity versus time trace. b) Diffraction-limited (left) and super-resolved DNA-PAINT images (right) of DONs. Each structure consists of 12 docking strands that are arranged in a 20-nm grid (scheme in lower right corner). c) *In situ* protein-labeling strategy for DNA-PAINT using primary and DNA-conjugated secondary antibodies. d) Overlay of a diffraction-limited α-tubulin image (top left) with a super-resolved DNA-PAINT image (bottom right). e) Close-ups of the highlighted area in d, comparing diffraction-limited image (left) with DNA-PAINT super-resolved image (right). Scale bars, 100 nm (b), 2 µm (d), 500 nm (e). Image taken with permission from Schnitzbauer et al.[105].

3.2 Scattering Techniques

3.2.1 Small-angle X-ray scattering

SAXS is a technique used in structural biology and materials science to investigate the three-dimensional structure of macromolecules or materials at the nanometer scale[129, 130].

In SAXS, a beam of X-rays is directed towards the sample, and the scattered X-rays are detected by a detector (**Figure 3.5**a). The scattering pattern obtained is then analyzed to obtain information about the size, shape, and arrangement of the sample. The intensity of the scattered X-rays is plotted against the angle of scattering to produce a scattering profile, which contains information about the spatial distribution of electron density in the sample (**Figure 3.5**b)[131, 132].

SAXS can be used to study a wide range of samples, including proteins[133], nucleic acids[134], lipids[135], and polymers[136, 137]. The technique is particularly useful for studying samples in solution, as it can provide information about the conformational changes that occur when a macromolecule interacts with ligands or undergoes structural transitions[138].

One of the advantages of SAXS is that it is a technique that can be used to study samples under a wide range of conditions, including at different temperatures, pH values, and in the presence of different solvents or ligands. Additionally, SAXS can be used in combination with other techniques such as X-ray crystallography[139], nuclear magnetic resonance spectroscopy (NMR)[140], and electron microscopy[141] to provide complementary information about the structure and dynamics of macromolecules.

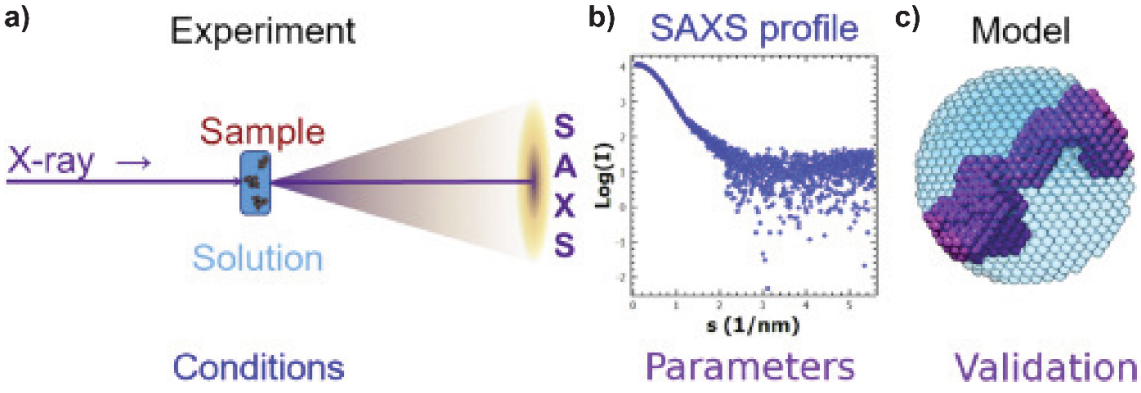

Figure 3.5: Schematic illustration of SAXS. a) A collimated X-ray beam is directed at a sample. As the X-rays interact with the sample, they are scattered at small angles. The scattered X-rays are then detected by a 2D detector placed behind the sample. b) The resulting scattering pattern provides information about the size,

shape, and internal structure of the sample at the nanoscale. c) A model of the sample can then be worked out with previously set parameters. Image used with permission from Da Vela et al.[142].

3.2.2 Dynamic Light Scattering

DLS is a powerful analytical technique utilized to determine the size distribution of small particles in suspension or polymers in solution[143]. It operates on the principle of scattering light from a laser beam that interacts with particles undergoing Brownian motion[144]. The fluctuation in the intensity of the scattered light is analyzed to determine the velocity of the particles, from which the hydrodynamic radius (size) is calculated using the Stokes-Einstein equation[143]:

$$D = \frac{k_B T}{6\pi\eta r} \qquad \textbf{Eq. 3.3}$$

where D is the diffusion coefficient of the particle, kB is the Boltzmann constant (1.38×10−23 J/K)[145], T is the absolute temperature of the system in Kelvin, η is the dynamic viscosity of the fluid and r is the radius of the spherical particle.

DLS is highly sensitive, allowing for the detection of particle sizes ranging from sub-nanometers to micrometers, making it particularly valuable in characterizing nanoparticles, colloids, proteins, and polymers.

To measure the zeta potential of particles DLS is integrated with electrophoretic light scattering (ELS), an electric field is applied to the sample, causing charged particles to move and creating a Doppler shift in the scattered light[146]. Zeta potential is a critical parameter that indicates the stability of colloidal systems. A higher zeta potential (either positive or negative) typically implies greater electrostatic repulsion between particles, leading to increased stability of the suspension, whereas low zeta potential values suggest a tendency for aggregation or flocculation. The combination of DLS and ELS in a Zetasizer enables comprehensive analysis of both particle size and surface charge, providing insights into the behavior, stability, and interactions of colloidal systems in various environments[147].

3.3 Gel Electrophoresis

Since the 1960s, gel electrophoresis has been a fundamental analytical technique in molecular biology, enabling the separation of nucleic acids and proteins by size and charge as they move through a matrix under the influence of an electric field[148]. AGE is frequently utilized in the context of DNA origami to assess the size of the nanostructures, verify successful folding, and evaluate the efficacy of purification methods such as ultrafiltration or PEG purification[149, 150]. The porous nature of agarose gels makes them particularly suitable for resolving large DNA molecules, including complex DONs. This technique is also instrumental in confirming the attachment of functional groups or nanoparticles, such as fluorophores or gold nanoparticles, to the DNA origami, serving both analytical and purification purposes[151].

On the other hand, polyacrylamide gel electrophoresis provides a higher resolution compared to agarose and is beneficial for analyzing smaller DNA fragments, such as staple strands. This makes it exceptionally useful for confirming whether staple strands, especially those designed as handle staples, have properly annealed to each other. Polyacrylamide gels are valuable for detailed examinations of DNA origami components, ensuring the correct assembly and integrity of the nanostructures at a molecular level[152].

Both types of gel electrophoresis play critical roles in the characterization and refinement of DNA origami techniques, allowing to verify the structural fidelity and functionality of these intricate nanostructures. The selection between AGE and PAGE depends on the specific requirements of the analysis, with each offering distinct advantages in terms of resolution and applicable molecular size range.

Chapter 4 - Results and Discussion on Finding a Faster Solution to DNA Origami Nanostructure Biomineralization

The organizational complexity of biominerals has long fascinated scientists seeking to understand biological programming and implement new developments in biomimetic materials chemistry[68, 153, 154]. Recent years have seen significant advancements in the field of DONs, particularly in biomineralization, where inorganic materials are integrated with DNA-based constructs to enhance their stability and functionality[155].

Silicification, the process of coating DNA origami with silica[9], has been a focal point due to its ability to improve the mechanical strength and thermal stability of these nanostructures. However, the conventional silicification process typically requires an extended incubation period of 5 to 7 days[9], which is impractical for high-throughput applications and delays experimental workflows. Therefore, finding a faster and equally effective method for DNA origami biomineralization became a crucial goal of my research.

In this chapter, the efforts to develop a rapid silicification method for DONs are presented. A novel approach that significantly reduces the biomineralization time from several days to just 4 h is introduced, without compromising the structural integrity or functionality of the nanostructures. The necessity of this expedited process cannot be overstated, as it

addresses a critical bottleneck in the production and application of biomineralized DNA nanostructures.

First, I will detail the structural properties of different DNA origami designs, showing *in silico* simulations, and comparing their configurations before and after the silicification process. TEM, AGE and zeta potential measurements were utilized to show the differences between unsilicified/bare and silicified samples, demonstrating that there is no significant change, thereby confirming the preservation of surface charge properties. Furthermore, I assess the stability of the biomineralized DNA nanostructures against DNase degradation, providing insights into their enhanced durability.

Then, I will discuss the SAXS measurements that led to the development of the new method. These experiments, conducted on the 24-helix bundle (24HB) and the four-layer block (4LB), show that the new rotating method achieves results comparable to the traditional undisturbed approach. Indeed, it seems that the rotating method is superior as it minimizes aggregate formation by preventing sedimentation of the DNA origami.

Afterwards, I will examine the long-term stability and storage conditions of silicified DNA origami, which is crucial for their practical application.

Through these comprehensive analyses, the new rapid silicification method is established as a viable and superior alternative, paving the way for more efficient and scalable production of robust DONs.

Parts of this chapter were published in Nature Communications under the title: In situ small-angle X-ray scattering reveals strong condensation of DNA origami during silicification[78].

4.1 Characterization of the used DNA Origami Nanostructures

4.1.1 Simulations of DNA Origami

I will now detail the characterization and comparison of the structural and functional attributes of several bare DONs, which are central to the subsequent discussions in this work. The structures under examination include the 24HB, 4LB, and the 18-helix bundle (18HB). A graphical size comparison of these DNA origamis, created using 3ds Max, can be found in **Appendix A.1, Figure A.1**. Prior to the synthesis of staples and folding of the DNA origamis, both CanDo[48] and oxDNA[49, 50] analyses were conducted to assess their structural integrity (**Figure 4.1**). These simulations provide insights into the structural flexibility and identify potential areas of instability, which are depicted through a color gradient from blue (indicating high stability) to red (signifying potential weak points) in the MD simulations. This evaluation, even in its relativity, is crucial for detecting structural weaknesses and assists in refining the origami designs. Instability typically appears at the helix ends, as expected, but occasionally other unforeseen vulnerabilities may also be revealed, necessitating design adjustments[156].

The initial DNA origami nanostructure investigated in this thesis is the rod-like 24HB, which is approximately 108 nm long with a diameter of 16 nm (**Figure 4.1**a). This structure was selected for detailed study to evaluate various silicification methods and their impact on structural stability and resistance to degradation. Prior to experimental folding, CanDo modelling (**Figure 4.1**a) and oxDNA MD simulations (**Figure 4.1**b) analyses were conducted to assess the stability and molecular interactions of the bare 24HB structure. Although slight instabilities were noted at the helix-ends and occasionally in the central region of the structure, they are not observable in the oxDNA simulations. So, despite these minor issues, the 24HB maintains substantial structural integrity.

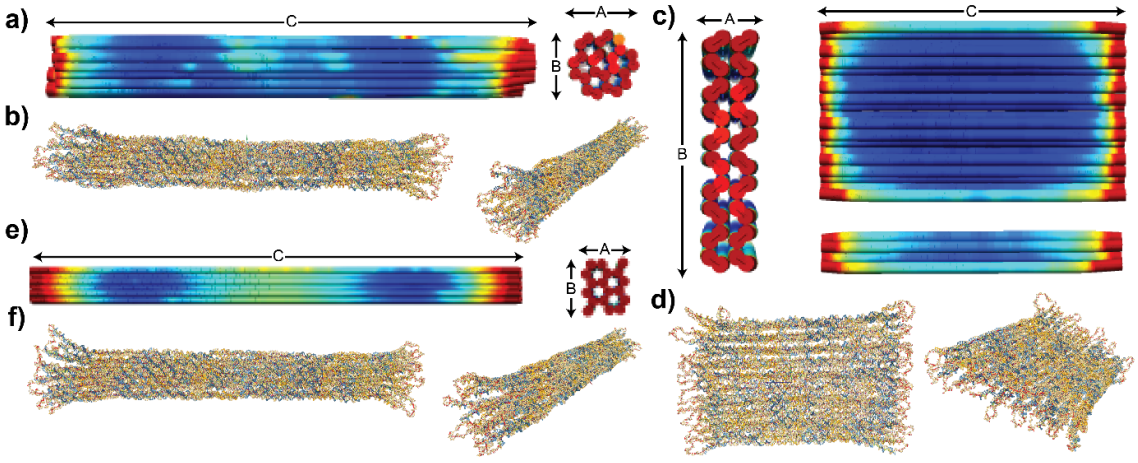

Figure 4.1: Structural Analysis of DONs. a) CanDo simulation of the 24HB, approximately A and B = 16 nm and C = 108 nm, illustrating stability variations across the structure. b) oxDNA simulation for the 24HB, highlighting the helical stability and potential weak points. c) CanDo simulation[38, 48] of the 4LB DNA origami, showcasing its dimensions of approximately A = 7 nm, B = 33 nm 67 nm in length and 33 nm in width. d) oxDNA[50] simulation of the same 4LB structure, emphasizing potential areas of structural concern. e) CanDo simulation of the 18HB, measuring A = 10.8 nm, B = 12.7 nm and C = 162 nm, showing its robustness and structural nuances. f) oxDNA simulation of the 18HB, providing detailed insights into the molecular interactions and flexibility.

The second DNA origami structure examined is the brick-shaped 4LB, measuring approximately 67 nm in length, 33 nm in width, and 7 nm in height. It was utilized alongside the 24HB to demonstrate that structural variations do not influence the effectiveness of silicification processes. Pre-fabrication simulations of the 4LB using both CanDo (**Figure 4.1**c) and oxDNA (**Figure 4.1**d) affirmed its overall stability. These simulations indicated that despite some minor instability and fraying at the helix-ends, the 4LB generally exhibits robust stability.

The third primary DNA origami structure utilized in this thesis is the 18HB, with dimensions of approximately 162 nm length by 12.7 nm height and 10.8 nm in width. The unique square-rod shape of the 18HB provides a distinctive model for testing. Simulation results (**Figure 4.1**e,f) once again confirmed the expected mechanical behaviors: some fraying at the ends and potential flexibility in the central region due to its extended length relative to its persistence length[157-161], suggesting a tendency for slight bending. This characteristic underscores the inherent challenges in maintaining rigidity in longer, thinner origami structures.

4.1.2 TEM and AGE Analysis of DNA Origami

Following synthesis and folding, TEM was utilized to visualize morphological differences in the DONs, and AGE was employed to assess their purity and size distribution. Additionally, DNase I assays were conducted to evaluate their resistance to enzymatic degradation. Detailed methodologies applied in this section can be found in **Chapter 3.2**.

TEM analysis of the 24HB (**Figure 4.2**a), stained with uranyl formate, verified the precise folding of the structure, displaying its characteristic cylindrical form (**Figure 4.2**a, inset). These images indicated no significant aggregation, likely attributable to the scaffold loops preserved at the helix termini (**Appendix C.9, Figure C.3**). Despite its structural robustness under TEM, DNase I assays revealed rapid degradation within 20 min (**Figure 4.2**d), exposing its susceptibility to enzymatic activity and indicating a need for additional protective measures.

Similarly, the 4LB was imaged via TEM (**Figure 4.2**b), affirming its correct assembly into a stable brick-like shape. The images demonstrated no significant aggregation in the unsilicified form, attributed to the scaffold loops preserved at the helix ends (**Appendix C.9**, **Figure C.4**). However, akin to the 24HB, the 4LB rapidly succumbed to enzymatic degradation, disintegrating within 30 min as shown in DNase I assays (**Figure 4.2**e).

TEM also confirmed the integrity of the 18HB (**Figure 4.2**c), exhibiting a rod-like shape with no notable aggregation, a result of omitting end staples during its assembly (**Appendix C.9, Figure C.5**). However, DNase I assays (**Figure 4.2**f) demonstrated that it degraded completely within 30 min, echoing the vulnerabilities observed in the other DNA origami constructs when exposed to DNase I.

The rapid degradation observed in the DNase I assays underscores the inherent challenges in deploying DNA origami in biological environments without adequate protective strategies. This vulnerability emphasizes the importance of exploring silicification or other stabilization techniques to enhance the durability and functionality of DONs in potential medical or technological applications.

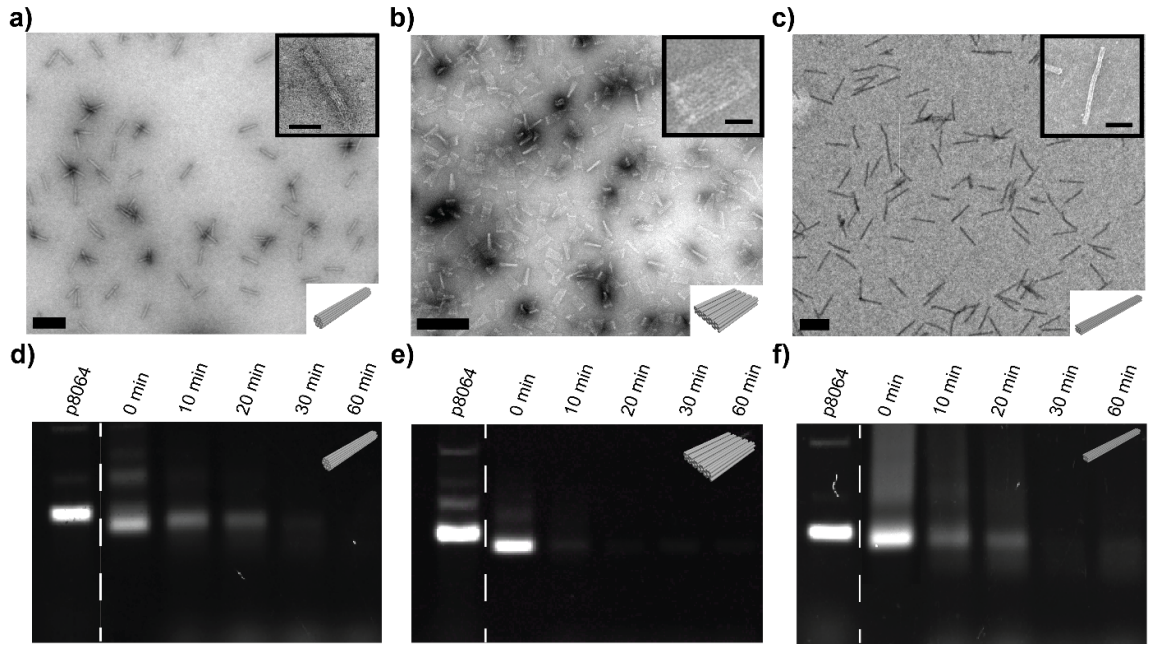

Figure 4.2: TEM Imaging and DNase I Stability Tests of Bare DNA Origami. a) TEM image of the 4LB, confirming the precise assembly and clear visibility of its brick-like structure. b) TEM image of the 24HB DNA origami, displaying its long cylindrical shape with well-defined edges. c) TEM image of the 18HB DNA origami, illustrating its square-rod-like configuration with noticeable structural integrity. d) DNase I assay for the 4LB, showing rapid degradation within 20 min. e) DNase I assay for the 24HB, with the structure degrading completely by 30 min. f) DNase I assay for the 18HB, also showing total degradation by 30 min, underscoring the need for protective strategies in biological applications. Scalebars are 200 nm for the large image and 20 nm for the inset in a) and 50 nm for the inset in b) and c).

4.2 Analysis of Silicification

SAXS measurements were carried out in collaboration with the group of Bert Nickel at the LMU. DNA origami samples were provided by me, SAXS analysis was done by Martina Ober. Electron microscopy and DNase I tests were done by me[78].

The traditional method of silicifying DNA origami, while effective in enhancing structural robustness, typically requires extended reaction times, up to seven days[9], during which DNA origami may sediment due to gravity, leading to inhomogeneous samples unsuitable for some analytical techniques like SAXS. To overcome these limitations, a novel method involving the dynamic rotation of the sample during the silicification process was developed and a specialized cell was constructed, enabling sample tumbling at about one rotation per second, ensuring well-dispersed DNA origami solutions throughout the measurement (see **Appendix C.4**, **Figure C.1** for photograph of custom-build tumbler for SAXS measurements). This approach not only ensures a more homogeneous distribution of the silica reagents across the DNA origami but also significantly accelerates the silicification process to just 4-6 h.

4.2.1 Structural Analysis Using SAXS

This study utilized an X-ray lab source with Mo characteristic radiation, chosen for its lower radiation dose compared to Cu radiation of the same intensity[162, 163]. This choice allowed for prolonged in situ SAXS experiments with reduced radiation damage to the sample. Mo radiation also enables larger absorption lengths along the beam (10 mm vs. ~ 1.5 mm), providing more practical geometric constraints for SAXS samples.

The silicification reaction was continuously monitored by SAXS, with measurements binned in time to optimize the signal-to-noise ratio. A binning time of one hour proved sufficient to closely follow the reaction with reliable X-ray statistics. A reference measurement of the purified origami was taken prior to silicification (**Figure 4.3**a). The SAXS intensity distribution for the bare 24HBs exhibited distinct intensity oscillations, characteristic of their cylindrical shape, and was modeled as a homogeneous cylinder with a radius of 80.1±0.2 Å. The interhelical distance was determined to be 26.2±0.3 Å, consistent with previously reported values for this type of origami. These profiles capture the intricate details of silica growth,

depicted through the intensity changes and peak shifts in the SAXS patterns. The Lorentzian peak modifications are particularly notable, as they provide insights into the internal structural changes occurring within the origami as silicification progresses.

Structural changes during silicification were monitored over a period of up to 80 h. Silica growth was initiated by the addition of TMAPS, followed by the injection of TEOS. The time dependence of the Porod invariant Q was evaluated to determine the time required for silicification to reach completion. The Porod invariant Q, a measure of the total scattering contrast, increased as a function of time and saturated after approximately 24 h, indicating that the reaction had finished (**Figure 4.3**c). This was significantly shorter than previously reported reaction times[9, 72, 79, 164]. One possible explanation is that in previous studies, the silicification reaction mixture was left undisturbed at temperatures slightly below RT, whereas in this case, gentle tumbling was applied at RT during the measurement to prevent sedimentation. Since silicification reaction kinetics are strongly influenced by factors such as movement, pH, and temperature, the tumbling at RT likely inadvertently accelerated the reaction[165].

The temporal intensity changes of the Lorentzian peak, sensitive to the inner structure of the DNA origami, were analyzed. The peak vanished shortly after the reaction started but recovered in intensity after more than 4 h of silicification, surpassing the initial intensity level and showing a second-order peak. This phenomenon, known as contrast matching, occurs when the scattering length densities of the object and its matrix are equal.

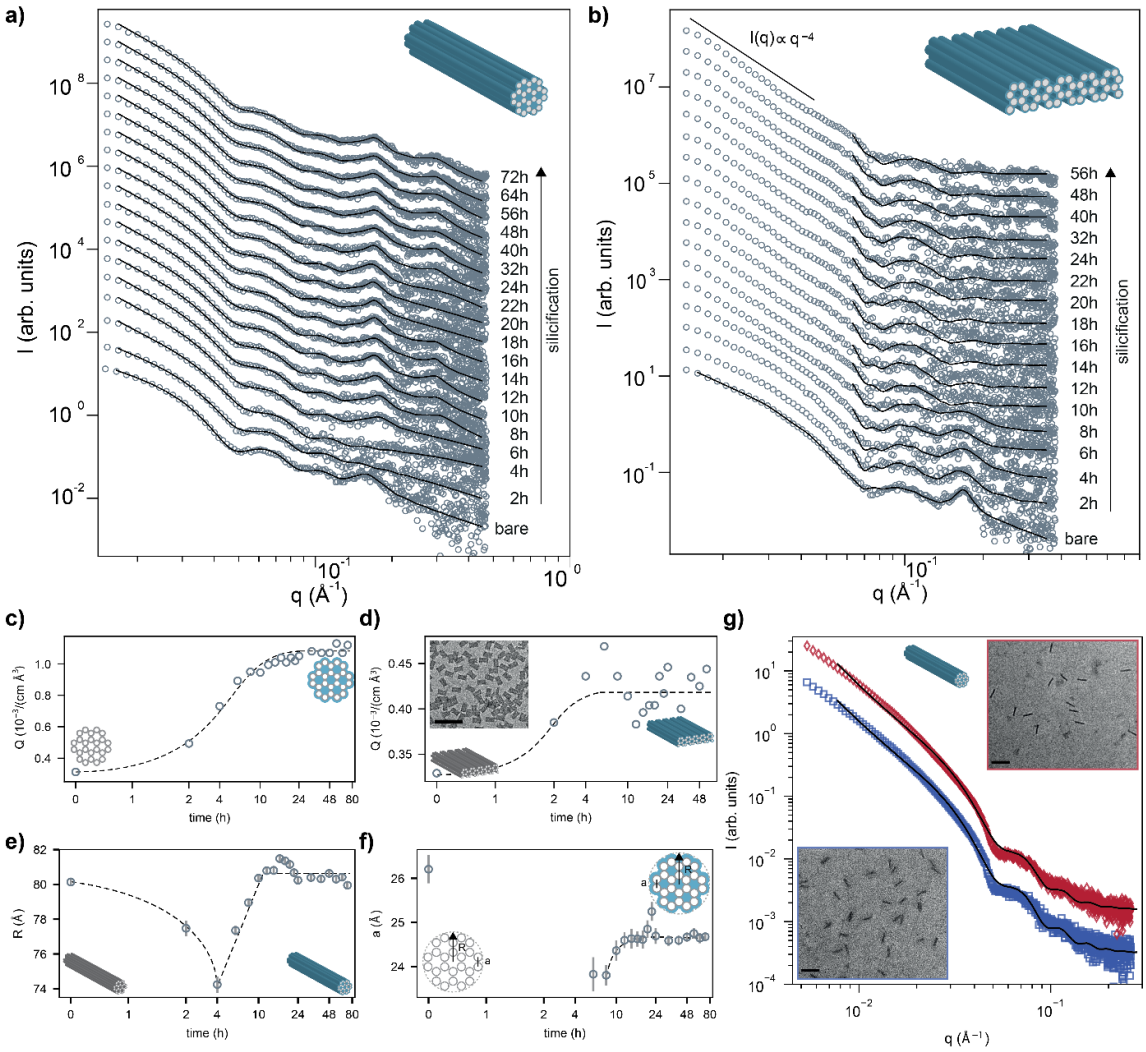

Figure 4.3: Structural analysis of DNA origami 24HB and 4LB during in situ silicification monitored by SAXS. a) and b) show the SAXS data of the 24HB and 4LB structures, respectively, with both bare and silicified states included, scaled for clarity. The dashed lines highlight Lorentzian peaks accounting for the inner honeycomb lattice arrangement. The growth of the silica layer over time is monitored. c) and d) illustrate the Porod invariant Q, serving as a measure of overall scattering contrast for both 24HB and 4LB during silicification, along with normalized interhelical peak intensities I_{Lor}. TEM images provide visual confirmation of the structures post-silicification (insets). e) and f) display the radii and interhelical distances extracted from SAXS data over time during TMAPS and TEOS-induced silicification. g) shows the temperature stability of silicified 24HBs using SAXS and TEM. SAXS data is recorded before and after heating the structures to 60 °C for 30 min, with TEM images confirming structural integrity post-heating. Figure used with permission from Ober et al.[78].

As an alternative, cuboid, brick-shaped origami (4LB) were also studied, exhibiting a tendency towards aggregation during silicification. The SAXS intensity for the 4LBs before silicification indicated distinct oscillations, characteristic of their cuboid shape (**Figure 4.3**b). After initiating silicification, the Porod invariant Q saturated much earlier than for the 24HBs (**Figure 4.3**d). The brick thickness condensed but did not reverse, indicating limited silica uptake and increased aggregation tendency.

Our study revealed that silica forms within the double helix arrangement of the origami structure, verified by evaluating the origami cylinder radius (R) and the interhelical distance (a). The interaction of the DNA phosphate backbone with TMAPS condensed the outer radius and the DNA-double helix spacing. When TEOS was added, condensation occurred even faster, suggesting hydrophobic effects within the origami in response to early silica formation **Figure 4.3**e & f). A comparison of the radius before and after silicification suggested a sub-nanometer outer silica shell. To ensure complete coverage after silicification using the new rotating method, the thermal stability of the silicified 24HB was also determined. SAXS measurements conducted before and after heating it to 60 °C for 30 min (**Figure 4.3**g), a temperature significantly higher than the melting point of bare 24HBs, illustrate that the structure not only retains its overall shape but also its scattering characteristics, suggesting that the silica layer effectively protects the DNA origami from thermal denaturation. The TEM images taken post-heating (**Figure 4.3**g, insets) further confirm that the structural integrity is preserved, indicating the robustness of the silica shell.

Overall, cylindrical origami showed more efficient silica uptake and greater stability compared to brick-shaped origami, with significant implications for the design and application of DONs in various fields.

The Porod invariant Q serves as a model-free indicator for the kinetics and yield associated with DNA origami silicification. The process of DNA origami silicification is relatively slow, characterized by a pronounced condensation during the initial phase of silica incorporation. This phenomenon is observed not only in origami structures based on honeycomb lattice arrangements, such as the 24HBs and 4-LBs, but also in those based on square lattice designs, including three-layered blocks (3-LBs), as detailed in the paper[78].

In general, silicification under similar conditions exhibits two reaction phases. Initially, TMAPS primes the silica polymerization reaction, which then consumes TEOS to yield "primary silica particles," or short silica chains averaging 3-4 units (1 TMAPS + 2-3 TEOS = 3-4 silica units). These primary silica particles should form within minutes, significantly faster than the silicification reaction kinetics observed here, which take hours. It is suggested that the silicification reaction of the DNA origami is driven by the second phase of the general silicification reaction: aggregation of primary silica particles and their condensation into silica networks. This scenario implies the diffusion of primary silica particles (silica chains) into the DNA origami and subsequent electrostatic binding of cationic TMAPS-TEOS precursors to anionic DNA.

The binding of these less polar chains to the internal surfaces of DNA helices induces hydrophobic effects, resulting in the initial condensation of all studied origami structures. Additionally, binding to the outer surfaces promotes strong aggregation of brick-shaped origami, even with ultrathin silica shells.

4.2.2 Analysis of the silicification in the TEM

Further TEM analysis provided direct visual evidence of the effects of silicification on the DONs. For the 24HB and 4LB, post-silicification TEM images (**Figure 4.4**a & b) reveal that the origami retains its intended shape with no significant aggregation or morphological distortions. This observation is critical as it confirms that the dynamic silicification process does not compromise the structural fidelity of the origami designs. Further TEM analysis with another DNA origami, the 18HB - not used in the initial study with SAXS - shows a similar preservation of morphology (**Figure 4.4**c). The images display the origami as rod-like structures with a uniform silica coating, highlighting the method's effectiveness across different origami shapes.

Zeta potential measurements were then conducted to assess any changes in the surface charge characteristics of the origami following silicification (**Figure 4.4**d, e & f). The results indicate minimal changes in the zeta potential profiles between the bare and silicified states for all three types of origami.

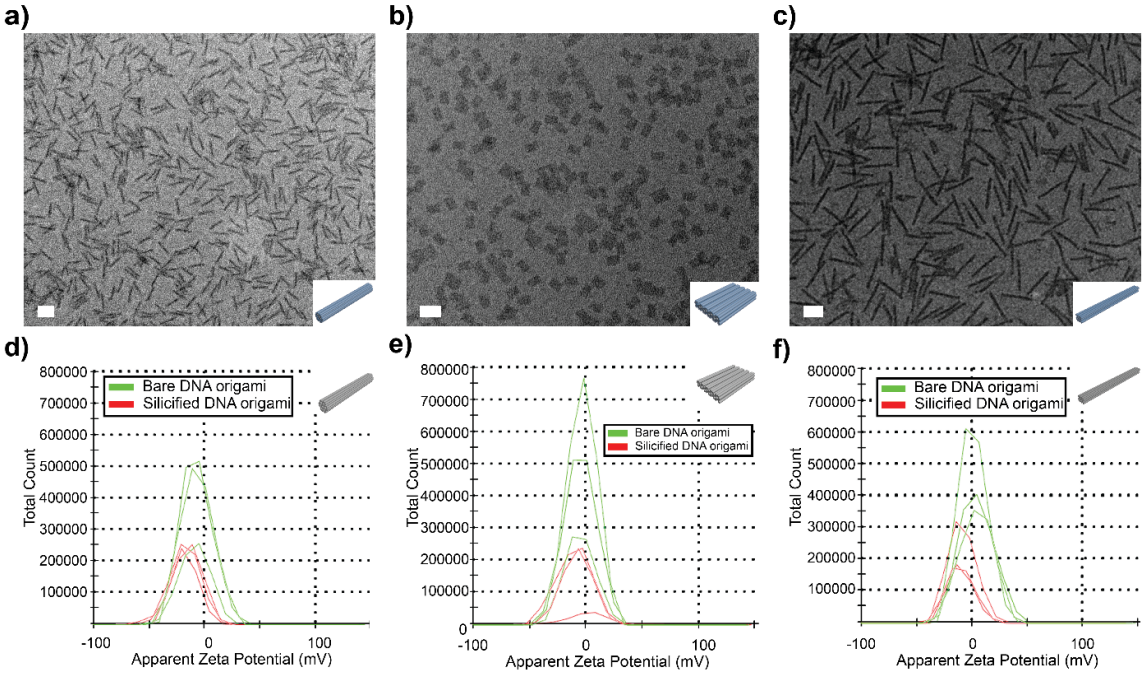

Figure 4.4: TEM and Zetapotential Analysis of Silicified DNA Origami. a) TEM image of the silicified 24HB showing a robust cylindrical form with no significant aggregation. b) TEM image of the silicified 4LB displaying minimal morphological changes post-silicification. c) TEM image of the silicified 18HB retaining its structural integrity with a dense appearance due to the silica layer. d, e, & f) Zeta potential distributions of the silicified 24HB, 4LB, and 18HB, respectively. Each plot shows little deviation from the bare origami, indicating the preservation of surface charge properties after silicification. Scalebars are 100 nm. Figure used with permission from Wassermann et al.[75].

4.2.3 Enhanced Durability Assessed by DNase I Degradation Tests

To corroborate the findings of the heat test, that this silicification method preserves structural integrity and gives a robust silica shell, the resistance of silicified origami to enzymatic degradation was evaluated on the three DNA origami using DNase I assays (**Figure 4.5**a, b & c). The assays show a remarkable improvement in the structural integrity of the silicified origami compared to their bare counterparts (**Figure 4.2**d, e & f). For instance, the bare 24HB disintegrates within minutes when exposed to DNase I, whereas the silicified version withstands enzymatic attack for several hours (**Figure 4.5**a). Similar results are observed for the 4LB and 18HB, where the silicified structures exhibit significantly prolonged resistance to enzymatic degradation. This enhanced durability is visually confirmed through post-assay TEM images (**Figure 4.5**d, e & f), which show the silicified origami maintaining their structural integrity even after extended exposure to DNase I.

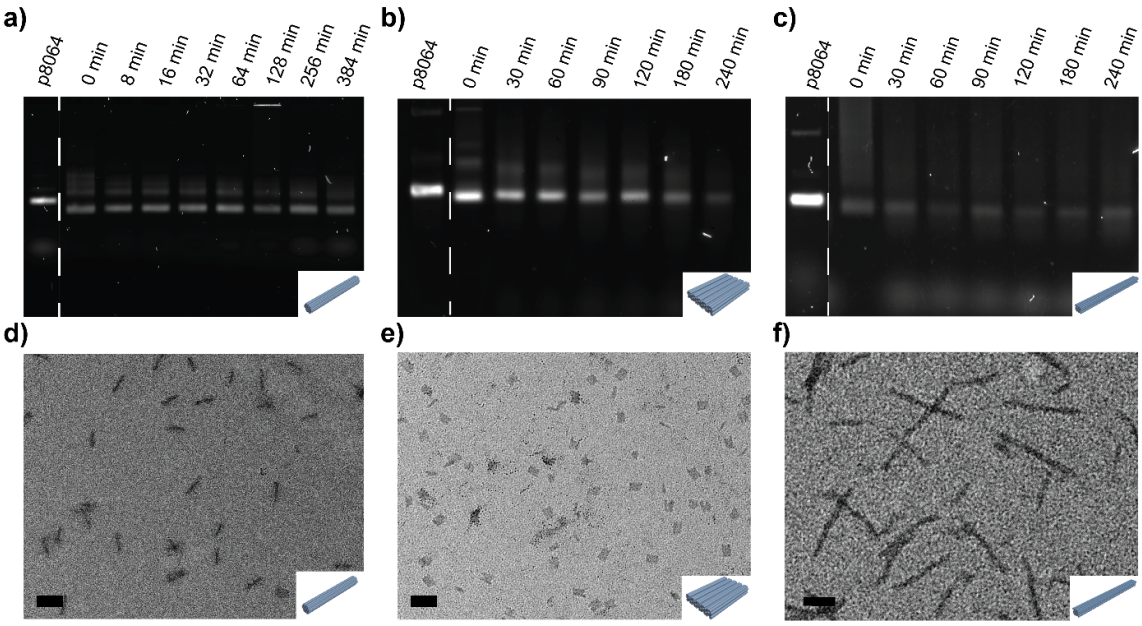

Figure 4.5: DNase I Degradation Tests and TEM Validation**.** a, b, & c) AGE images of 24HB, 4LB, and 18HB subjected to DNase I over time. Each gel demonstrates the enhanced resistance of silicified structures to enzymatic degradation. d, e, & f) Corresponding TEM images post-DNase I treatment confirming the maintenance of structural integrity despite exposure to degrading enzymes. Figure used and changed with permission from Wassermann et al.[75].

A cuboid DNA Origami had been included in this study to explore its potential as a template for silicification; however, the results revealed unexpected challenges that could not be resolved within the scope of this thesis. Despite using established silicification techniques, the Cube exhibited significant deformation, transitioning into a more rectangular shape rather than retaining its intended cubic geometry. This behavior, possibly linked to condensation effects or unintended stacking during silicification, suggests the need for further optimization of the process. Details of these findings, along with preliminary analysis and recommendations for future work, are provided in **Appendix A.2**.

4.3 Storage of Silica-DNA Origami Hybrid Materials

Storing Silica-DNA Origami Hybrid Materials properly is crucial for preserving their structural integrity and functionality over extended periods, facilitating their use in various experimental and practical applications without necessitating the silicification of new batches each time[166]. To identify optimal storage conditions, I conducted a series of experiments in triplicates over a three-month period to assess the stability of the hybrid materials under different environmental conditions.

Three distinct storage conditions were tested. The first condition was storage on the bench as the easiest storage solution. This involves fluctuating temperatures, humidities and UV exposure according to daily cycles and laboratory activities, thereby challenging the robustness of the storage conditions. The second condition was storage at a stable room temperature of 21 °C, providing a convenient and energy-efficient option, assuming the integrity of the hybrid materials is maintained. The third condition involved refrigeration at 4 °C, which typically minimizes the degradation of biological samples and should slow down any potential chemical reactions that could compromise the silica-DNA hybrid structures.

The storage protocols included three different approaches. Standard storage involved storing samples in 20 µL aliquots at a concentration of 10 nM, representing a typical storage scenario with a lower concentration. High volume/concentration storage was tested by storing samples in larger volumes of 50 µL at a higher concentration of 50 nM, to examine the effects of increased sample concentration on stability. Finally, disturbance storage started with 50 µL at 50 nM, with an appropriate part taken out at each time point for measurements, thereby decreasing the volume over time. This method was used to evaluate the impact of repeated handling and volume reduction on sample integrity.

Throughout the three months, periodic assessments were conducted to monitor the aggregation behaviour of the Silica-DNA Origami Hybrid Materials (see **Appendix A.3, Figure A.4**). These assessments included evaluating potential aggregation via AGE and structural integrity via TEM. The goal was to determine the most effective storage condition and approach to ensure the long-term preservation of the hybrid materials. This analysis provides valuable insights for both research and practical applications, highlighting the

importance of proper storage conditions in maintaining the quality and functionality of Silica-DNA Origami Hybrid Materials over extended periods.

Regarding storage location, samples kept in a stable room temperature (21 °C) showed the best performance, with minimal aggregation and well-preserved structures as seen in **Figure 4.6**a and c. The samples stored in the fridge (4 °C) exhibited the most aggregation, likely due to condensation or other environmental factors that might encourage aggregation. Storage at a stable room temperature likely maintains a more consistent environment, reducing the risk of aggregation and preserving the integrity of the structures.

The AGE and TEM images also indicate that the storage conditions significantly impact the aggregation of silicified 24HB DONs over three months (**Figure 4.6**a & b to d upper row). Under "Standard" storage approach, there is noticeable aggregation, as shown by aggregation in the wells and smearing in the bands on the gel and clustering in the TEM images. This suggests that while the silica coating offers protection of the DNA origami, these conditions might not be optimal for preventing aggregation, potentially due to the small volume and low concentration that might be more susceptible to environmental fluctuations.

In contrast, both the "Volume" and "Disturbance" storage approaches resulted in minimal aggregation, evidenced by distinct bands and no aggregation in the wells on the gel and well-dispersed structures in the TEM images (**Figure 4.6**a & b to d lower row). The larger initial volume and concentration might provide a more stable environment for the DNA origami, possibly reducing the effects of minor concentration fluctuations and mitigating the impact of sample handling. Interestingly, the "Disturbance" approach seems to show the least aggregation overall, which might be due to the frequent mixing or handling of the samples. This could prevent the DNA origami from settling or forming aggregates by keeping the sample evenly suspended in solution.

These findings suggest that a combination of stable room temperature storage, higher volume and concentration, and some minimal disturbances to avoid settling might be most conducive to maintaining the stability of silicified DNA origami over extended periods. The settling of the structures and thus the increase in local concentration in undisturbed

samples, in conjunction with only partially reacted silanol groups, which may still react in water and when close to other silica groups, are the main reasons leading to aggregation.

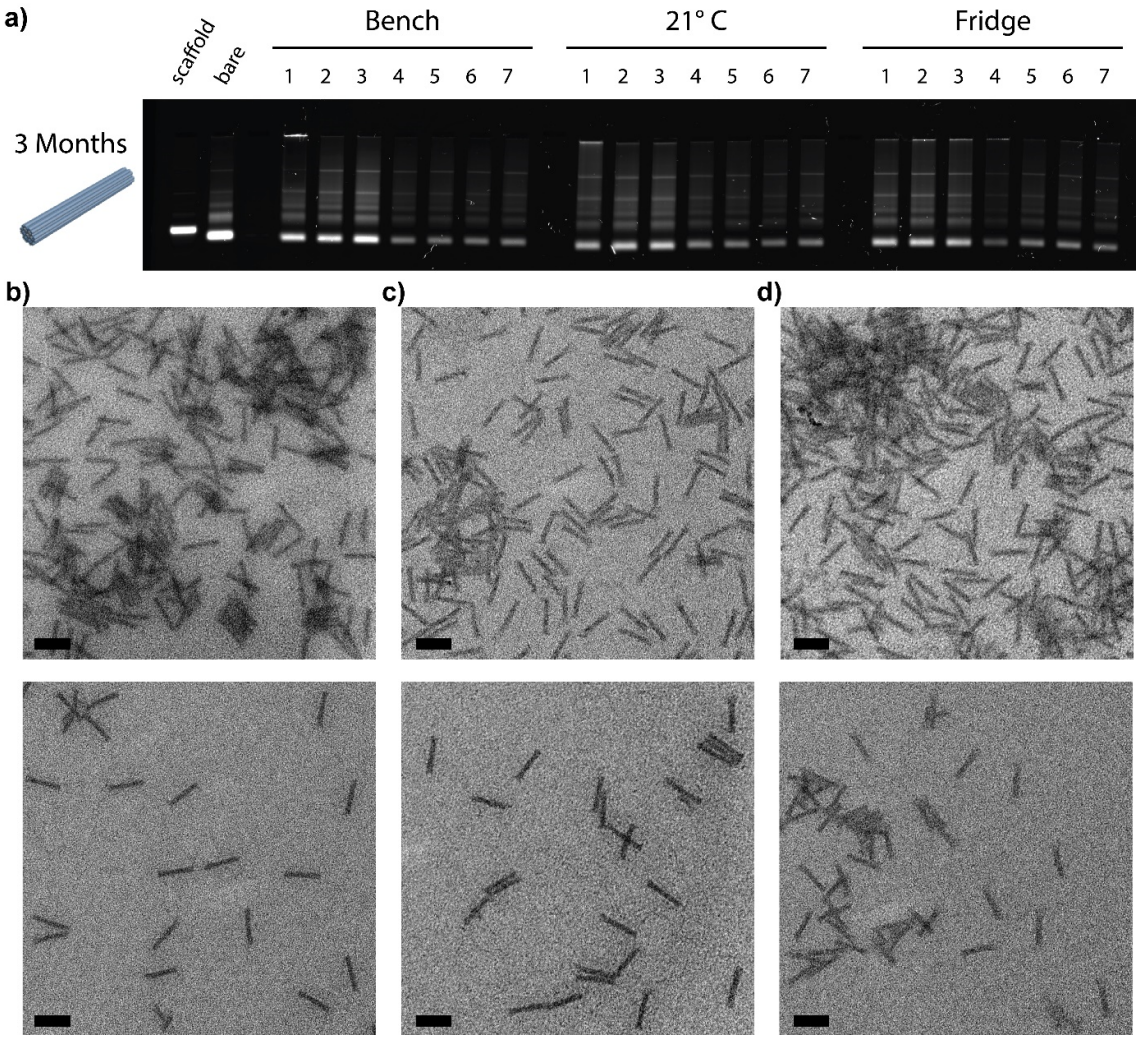

Figure 4.6: Storage of DNA Origami Silica Structures after three months. a) AGE image of silicified 24HB samples stored for 3 months under three different storage conditions: on the bench (varying temperature), at room temperature (21 °C), and in the fridge (4 °C). Rows 1 to 3 represent the standard storage approach (10 µL and 10 nM), row 4 represents the volume condition, and rows 5 to 7 represent the disturbance condition. The AGE results suggest that the 24HB samples show different degrees of aggregation depending on the storage conditions, with the fridge samples showing more pronounced aggregation. b) to d) TEM images of the stored samples for each storage condition: b) bench, c) room temperature (21 °C), and d) fridge. The upper row of images corresponds to the standard storage approach, while the lower row corresponds to the disturbance condition. The TEM images further support the aggregation observed in the AGE analysis, particularly under the fridge storage condition. Scale bars: 200 nm.

Chapter 5 - Results and Discussion on the Addressability of Silicified DNA Origami Nanostructures

The results of this chapter were published in Advanced Materials under the title: Full Site-Specific Addressability in DNA Origami-Templated Silica Nanostructures[75]. DNA-PAINT and AFM measurement were carried out by Michael Scheckenbach from the Tinnefeld group at the LMU. Silicification, AGE, electron microscopy and DNase I tests were done by me.

Initial hybridization experiments with fluorescently labeled oligonucleotides or DNA-coated AuNPs for structures silicified in solution (thin silica shell, as discussed in Chapter 4), followed by DNA-PAINT super-resolution microscopy analysis[123, 167] of structures silicified on a surface (thick silica shell)[74], demonstrated that, independent of the silicification method or thickness of the silica layer, structures remain fully site-specifically addressable. Further experiments showed that not only handles protruding from a structure remain accessible, but also ssDNA segments of the scaffold within a nanostructure, allowing for dynamic changes in the shape of an 18HB after silicification in solution.

5.1 Samples silicified in solution

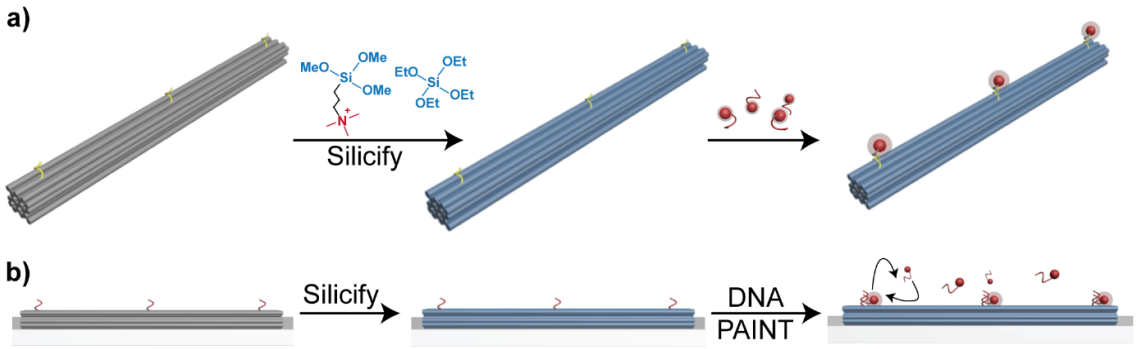

Scheme 5.1: Schematic illustration displaying the assessment of ssDNA handle accessibility on DNA origami after silicification in solution (a) and on a surface (b). Samples silicified in solution are in or near the maximally condensed state (see Chapter 4) and contain a set of ssDNA handles. If these remain unsilicified, a fluorophore-labelled anti-handle will be able to hybridize to the structure. Samples silicified on a surface with silica shell thicknesses of a few nm contain a set of 8 nucleotide (nt) long docking sites to which fluorescently-labelled imager strands bind transiently (DNA-PAINT super-resolution microscopy). Image taken with permission from Wassermann et al.[75].

Given that the interaction between DNA and TMAPS/TEOS relies on electrostatic interactions between the anionic phosphate backbone of DNA and the cationic TMAPS, we initially hypothesized that PNA[168], with its net neutral charge due to a peptide backbone, could serve as an effective alternative to DNA handles for maintaining addressability in silicified DNA nanostructures. Since TMAPS and the peptide backbone in PNA cannot electrostatically associate, PNA should remain unsilicified and thus available for post-silicification hybridization.

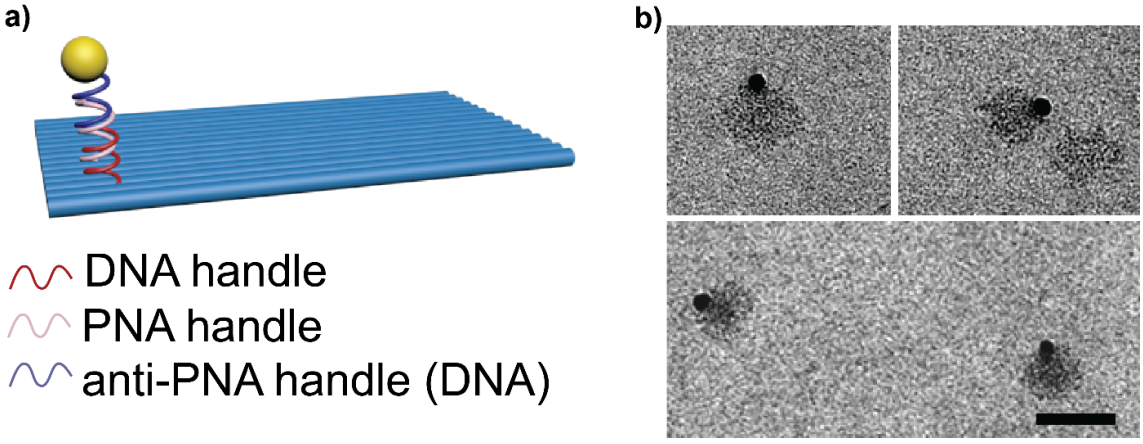

Figure 5.1: Schematic illustration (a) and TEM images (b) of silicified 1LS designed with protruding PNA handles, hybridized to 15 nm AuNPs. Scale bar is 100 nm. Structures were not stained. Image taken from Wassermann et al. with permission[75].

Initial studies employing a three-strand DNA handle:PNA:anti-PNA handle system (see **Figure 5.1**a) were promising, demonstrating that PNA remained accessible for hybridization with anti-PNA coated AuNPs (**Figure 5.1**b). However, due to the high cost of PNA, I also explored more sustainable alternatives. Inspired by the work of Ding and colleagues[80], which indicated that TMAPS-TEOS precursors preferentially accumulated on dsDNA compared to the closely packed dsDNA in a DNA origami nanostructure, we considered whether ssDNA might exhibit less silica precursor accumulation.

We hypothesized that ssDNA, with its comparatively fewer phosphate groups relative to dsDNA, would attract fewer TMAPS molecules. Additionally, given the significantly shorter persistence length of ssDNA compared to dsDNA (~2 nm[158] vs ~35-50 nm[169]), we anticipated that TMAPS accumulation could be minimized, resulting in largely unsilicified strands of ssDNA.

To test whether ssDNA remains unsilicified and accessible, I utilized two distinct DONs: the 24HB and the 4LB, previously discussed in Chapter 4, both displaying ssDNA A_{15}-handles or handles with a random sequence (random handles) protruding from the structure. I silicified them following the established protocol using a rotator (see **Appendix B.2.4** for protocol & **Chapter 4, Figure 4.4**). After approximately 4 h, the reaction was halted, resulting in structures with sub-nanometer silica deposition that displayed enhanced stability against DNase I degradation compared to non-silicified structures (**Figure 4.5**b, d & e). The silicified structures were then incubated with Cy5-labeled T_{19}-anti-handles and analyzed by gel electrophoresis.

The silicified DNA structures entered the agarose gel and exhibited electrophoretic mobilities similar to the non-silicified structures (**Figure 5.2**a, b (each on the left), & c). This result is consistent with expectations, as the sub-nanometer silica deposition in the maximally condensed state does not significantly impact electrophoretic mobility. A fluorescent band in the Cy5 fluorescence channel was clearly observed for both the 24HB and the 4LB displaying the A15-handle, indicating successful hybridization with the Cy5-labeled T_{19}-anti-handle, for the bare as well as the silicified structures. To ensure that this signal resulted from specific hybridization rather than non-specific interactions between the

Cy5 anti-handle and the silica, I also tested the same origami structures without the A_{15}-handle. As shown in **Figure 5.2**, no fluorescent band was observed for these structures, even though they were incubated with the Cy5 anti-handle. This confirmed that the fluorescence was due to specific hybridization to the ssDNA handles.

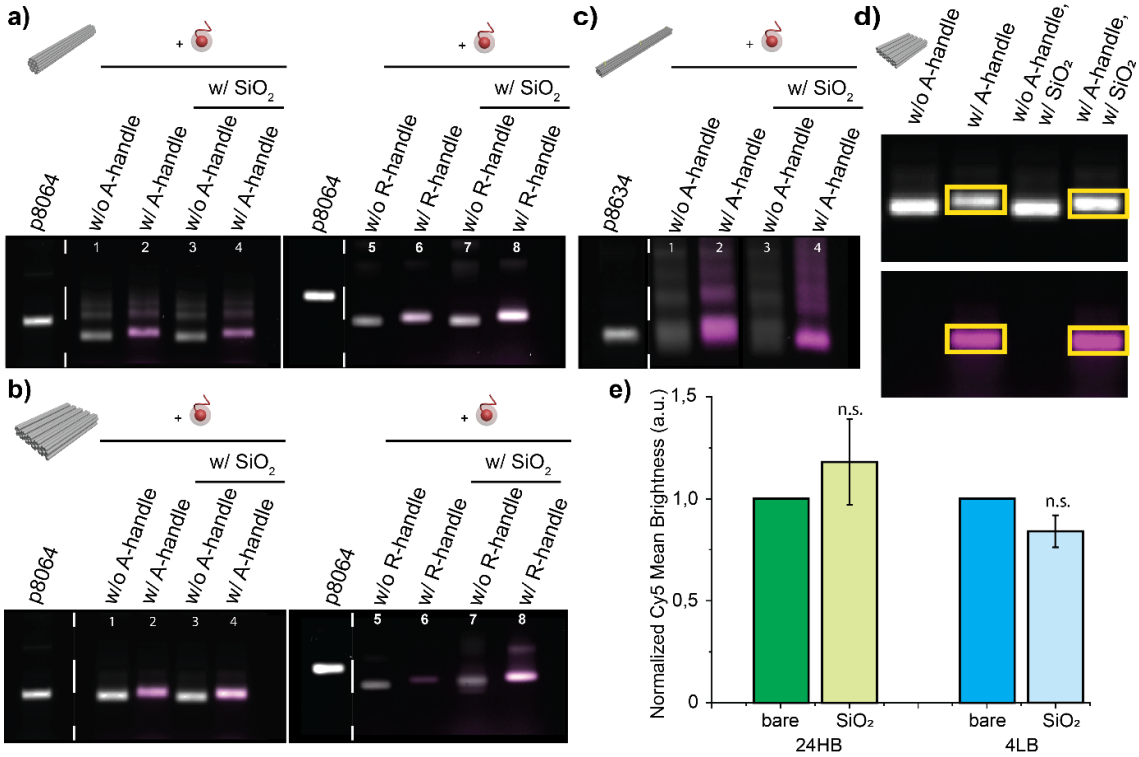

Figure 5.2: AGE image of the (a) 24HB, (b) 4LB and (c) 18HB before (lanes 1, 2, 5 and 6) and after silicification (lanes 3, 4, 7 and 8) and addition of the (poly-T_{19} or random) Cy5-anti-handles. Signal in the Cy5 channel is only observed in the presence of handles, suggesting that the Cy5 anti-handle does not bind to the silica non-specifically and that random handles also remain accessible after hybridization. (d) SYBRSafe channel and Cy5 channel images of a representative gel of a 4LB. Brightness analysis was performed on regions of interest indicated by the yellow boxes. (e) Normalized Cy5 mean brightness histograms for bare and silicified 24HB (left) and 4LB (right). Each bar represents a sample size of six gels, with dark colors representing bare and lighter colors representing silicified structures. Error bars denote the standard error of the mean. (N.B.: Due to normalization of the silica sample to the bare samples, no error bars are shown for bare samples). T-tests showed values of $p > 0,1$ for both silicified structures (n=6). Image taken and modified from Wassermann et al. with permission[75].

I then qualitatively assessed whether handle accessibility might be reduced in silicified samples, which could indicate partial silicification of the handle strand. By comparing the relative brightness of the Cy5 signal in the gel for both bare and silicified structures (**Figure 5.2**d & e), I found no significant reduction in handle accessibility due to silicification. To further confirm that retained accessibility was not specific to polyA-polyT hybridization, I designed a handle with a random sequence and observed consistent results (**Figure 5.2**a &

b right side). These observations confirm that the Cy5 anti-handles successfully hybridized to the ssDNA handles on the origami, the ssDNA handles remain accessible for hybridization, and thus are mostly unsilicified, and there is no non-specific interaction between the silicified structures and the Cy5 oligonucleotide.

However, given that these solution-silicified structures only display sub-nanometer silica deposition, it could be argued that the retained addressability is not surprising and does not necessarily indicate that ssDNA handles remain accessible if structures are coated with a thicker silica layer. As reported by Liu et al., structures silicified on a surface generally exhibit silica layers several nanometers thick. Therefore, I next investigated the accessibility of ssDNA handles on DONs immobilized and silicified on a surface.

5.2 Samples silicified on surface

To assess the addressability of DNA nanostructures immobilized and silicified on glass and mica surfaces, my collaborator Michael Scheckenbach from the Tinnefeld Group employed DNA-PAINT super-resolution imaging. This method allows for single-particle level analysis of DONs. Here we used one-layer sheets (1LS) and 12 helix bundles (12HB). In DNA-PAINT, ssDNA docking sites on the nanostructure transiently bind short, fluorescently-labeled imager strands, facilitating sub-nanometer localization precision[123, 167].

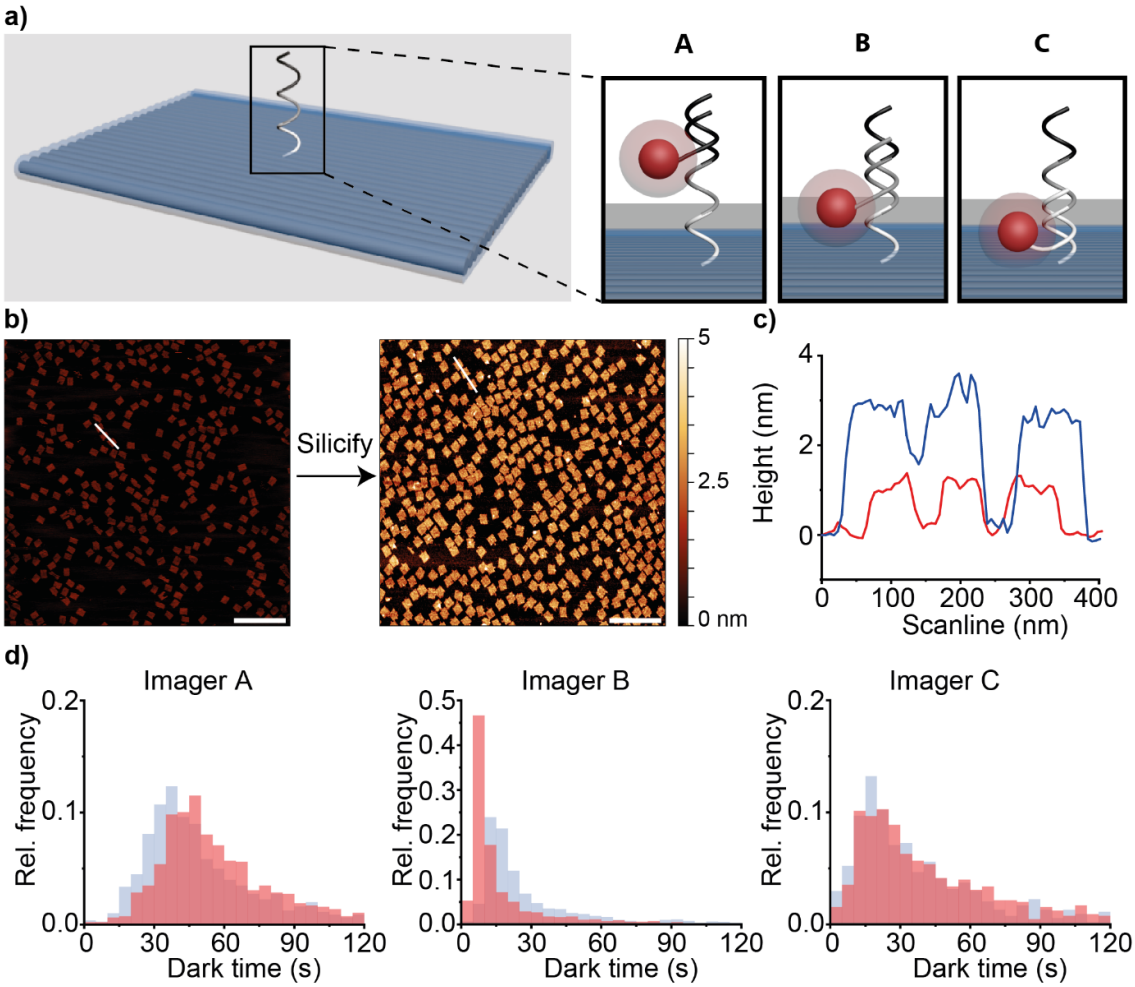

Figure 5.3: Investigation of 1LS DONs immobilized and silicified on a surface. a) Schematic illustration of 1LS DNA origami nanostructure containing a single-stranded concatenated sequence for DNA-PAINT able to bind three different imager strands (A, B, and C) at different distances from the DNA origami surface. b) AFM images of 1LS immobilized on a mica surface before (left panel) and after (right panel) silicification (scale bar: 500 nm). c) Height profile of silicified (blue) and bare (red) 1LS nanostructures obtained from AFM images (white lines in b) indicate the line scan). d) Extracted distributions of spot integrated dark times for different positions (A-C) on the DNA-PAINT docking site. At least 537 spots were analysed in each experiment. Image taken from Wassermann et al., with permission[75].

To investigate whether ssDNA handles protruding from DNA origami remain accessible under a silica shell several nanometers thick, a 1LS DNA origami was designed containing a single-stranded concatenated docking sequence for DNA-PAINT. This sequence is capable of binding three different imager strands (A, B, and C) at varying distances from the DNA origami surface (**Figure 5.3**a, **Table C.22** in **Appendix C**). Initially, the silica shell thickness on 1LS structures, which were immobilized on mica surfaces and silicified for four days, was quantified. AFM analysis revealed a homogeneous height increase of approximately 2 nm (**Figure 5.3**b & c).

Contrary to DNA nanostructures silicified in solution with sub-nm silica deposition, the observed 2 nm thick silica coating on immobilized 1LS could potentially affect ssDNA docking site accessibility. To explore this possibility, DNA-PAINT studies were conducted, imaging all three 8-nt sub-sequences (A, B, and C) on the concatenated docking site. The DONs were immobilized on BSA-biotin-streptavidin-coated glass coverslips via biotinylated DNA staple strands and silicified as before.

Single-molecule binding kinetics of both silicified and non-silicified 1LS nanostructures were further analyzed to extract average dark times for each labeling spot (**Figure 5.3**d). The dark time, which indicates the diffusion and hybridization time of an imager strand to a docking site, indirectly probes docking site accessibility. Comparable dark times were observed for all docking site parts between silicified and non-silicified structures, suggesting that ssDNA on 1LS remains accessible (**Figure 5.3**d). Surprisingly, even the docking site closest to the DNA origami surface remained accessible, despite being theoretically partially embedded in the ~2 nm silica coating.

This accessibility is hypothesized to result from pore-like structures within the silica shell around the ssDNA docking site. Fluorescence colocalization experiments with complementary green fluorescence labels confirmed that the number of addressable docking sites remained nearly unchanged post-silicification. Encouraged by these findings, more complex structures were investigated, specifically 12HB DONs used as super-resolution microscopy standards (**Figure 5.4**a & b)[170, 171].

AFM imaging of bare and silicified 12HB nanostructures indicated a silica layer thickness of ~4-6 nm after four days of silicification (**Figure 5.4**c & d). The 12HB design included 18 docking sites arranged in three positions (six per position) to enhance binding probability and spot brightness (**Figure 5.4**a). DNA-PAINT imaging of bare 12HB structures displayed the expected triple spot pattern (**Figure 5.4**e, left panel), and silicified 12HB structures also exhibited well-resolved triple spots, indicating retained docking site accessibility despite the thicker silica layer (**Figure 5.4**e, right panel).

However, the dark time distribution for silicified 12HB structures was broader and shifted to longer times compared to bare 12HB (from 15.2 ± 5.7 s to 26.9 ± 15.4 s), suggesting either slowed diffusion kinetics or partial inaccessibility of some docking sites (**Figure 5.4**e). Further investigation involved preparing 12HB nanostructures with a single docking site per spot at the top of the 12HB. Here, only a slight shift in dark time was observed, similar to the 1LS, indicating no significant change in accessibility post-silicification (**Figure 5.4**f).

Stability of silicified structures in degrading buffer conditions was also assessed. Both silicified and non-silicified 12HB nanostructures were incubated in 1× Tris-Acetat-EDTA (TAE) buffer for 2 h. While bare 12HB structures collapsed due to the absence of Mg^{2+} (**Figure 5.4**g, left panel)[172], silicified 12HB structures retained their triple-spot pattern, confirming the stabilizing properties of the silica shell (**Figure 5.4**g, right panel). This suggests that silicification can extend the utility of DNA nanostructures to applications limited by DNA origami stability. Finally, tests were conducted to determine if ssDNA inside a DNA origami structure could remain accessible for hybridization, potentially enabling flexible, shape-changing structures.

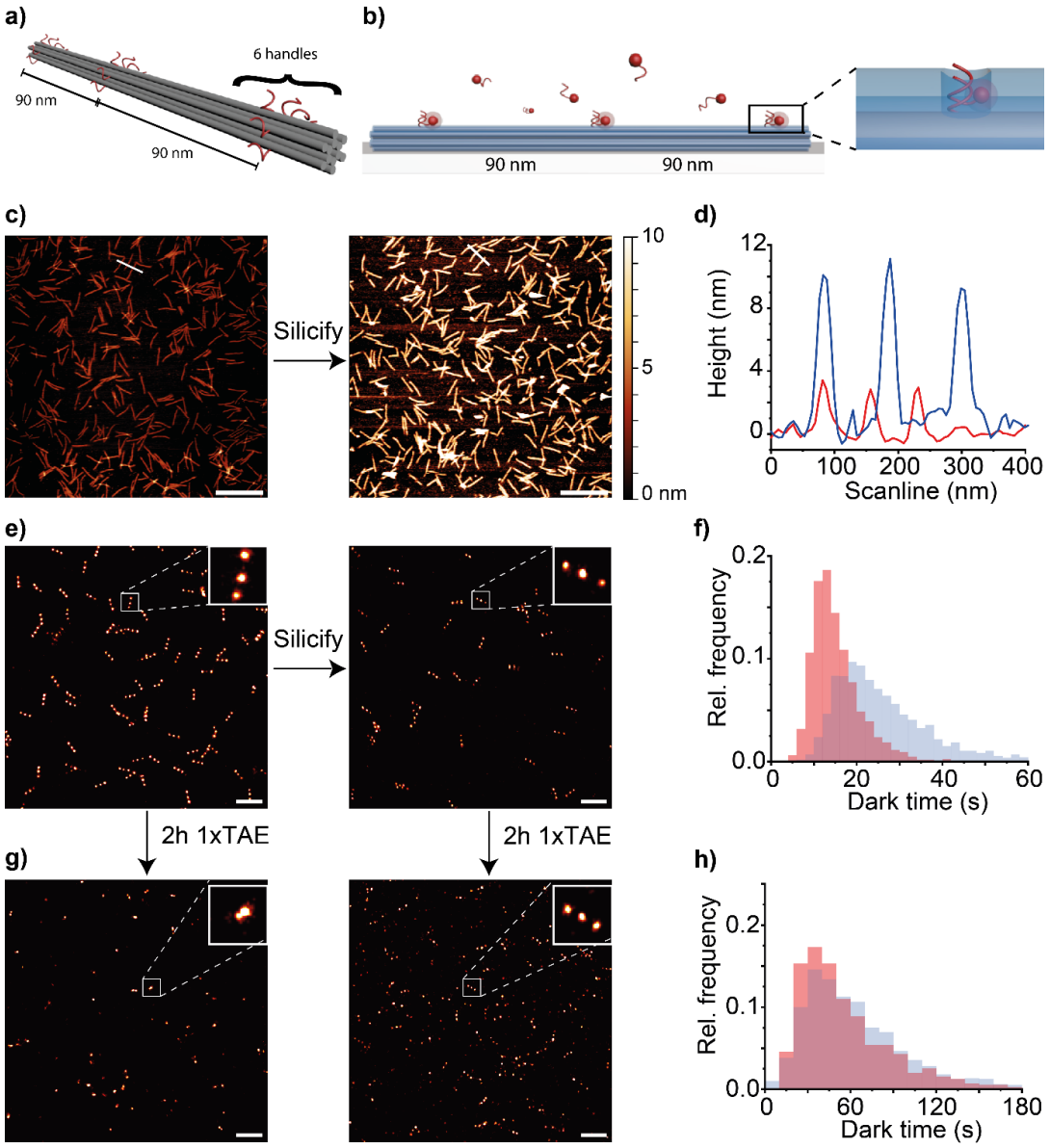

Figure 5.4: Investigation of 12HB DONs immobilized and silicified on a surface. a) Side view schematic 3×6 12HB showing three labeling spots in 90 nm distance each consisting of 6 docking sites. b) Schematic illustration of 12HB DNA origami nanostructure used for DNA-PAINT measurements and illustration of the docking site placement. Inset shows the unsilicified docking site surrounded by silica (blue). c) AFM images of 12HB immobilized on a mica surface before (left panel) and after (right panel) silicification (scale bar: 500 nm). d) Height profile of silicified (blue) and bare (red) 12HB nanostructures obtained from AFM images (white lines in c) indicate the line scan). e) Super-resolution DNA-PAINT images of 12HB nanostructures before (left panel) and after (right panel) silicification using an Atto655-labelled imager strand (the expected triple spot pattern is shown in the zoomed in images in the insets). Scale bars are 500 nm. f) Extracted distributions of spot integrated dark times for bare (red) and silicified (blue) 12HB nanostructures. At least 1653 spots were analyzed per condition. g) DNA-PAINT images of the reference (left) and silicified (right) 3×1 12HB and h) corresponding extracted dark time histograms of the bare (red) and the silicified 12HB (blue) after 2h incubation in 1×TAE buffer. Scale bars are 500 nm Image taken and modified from Wassermann et al. with permission[75].

5.3 Dynamic DNA origami

To create a dynamic and flexible DNA origami with shape-changing properties, I modified an 18HB by omitting a set of staples from its middle section, leaving only the scaffold to connect the two halves (see **Figure 5.5**a). This omission resulted in a flexible structure that appeared significantly bent when deposited on a TEM grid (**Figure 5.5**b, left panel). The observed bending angles ranged from 15 to 180 °, with the majority of structures displaying angles between 120 and 150 ° (**Figure 5.5**b, left panel).

To assess whether this bending could be reversed, I added the missing middle staples, referred to as "straightening staples," and incubated the structures at 36 °C. This addition resulted in a distinct shift in bending angles (**Figure 5.5**b, right panel), with most structures straightening out, as evidenced by TEM analysis (**Figure 5.5**b, right panel). This effect has also been observed previously in 12HB structures.

Having confirmed that bent 18HBs can be straightened by adding the straightening staples, I next tested whether this property was retained after silicification. Bent 18HB structures were silicified for 4 h using a solution-based approach. TEM analysis revealed that the silicified structures also appeared bent, confirming their retained flexibility (**Figure 5.5**c, left panel). These structures displayed a similar range of bending angles, with most being between 135 and 180 ° (**Figure 5.5**c, right panel). However, silicified structures tended to exhibit slightly larger bending angles on average, likely due to the increased stiffness imparted by the silica.

To determine if the ssDNA scaffold sections in the middle remained accessible for further hybridization, I reintroduced the straightening staples to the silicified structures. This resulted in a significant shift towards 180 ° angles, indicating that the ssDNA scaffold segments within the DNA origami remained largely accessible (**Figure 5.5**c, right panel). However, the proportion of fully straight structures was slightly lower for silicified samples compared to non-silicified ones (41% vs. 60%) (**Figure 5.5**d).

We hypothesize that this difference is partly due to the increased flexibility of dsDNA compared to inorganic silica. In these hybrid structures, the ends are likely stiffer and heavier due to silicification, while the middle remains more flexible as it consists only of

dsDNA (**Figure 5.5**a). This could lead to more observable fluctuations in bending angles. Additionally, the diffusion of staples into the silicified nanostructure might be partially obstructed, as staples need to hybridize to both freely accessible scaffold segments and sections partially embedded in silica. We further showed that DNA origami single crystals could be formed from pre-silicified monomers, leaving the single-stranded connector regions unsilicified. These structures showed strongly enhanced stability in vacuum.

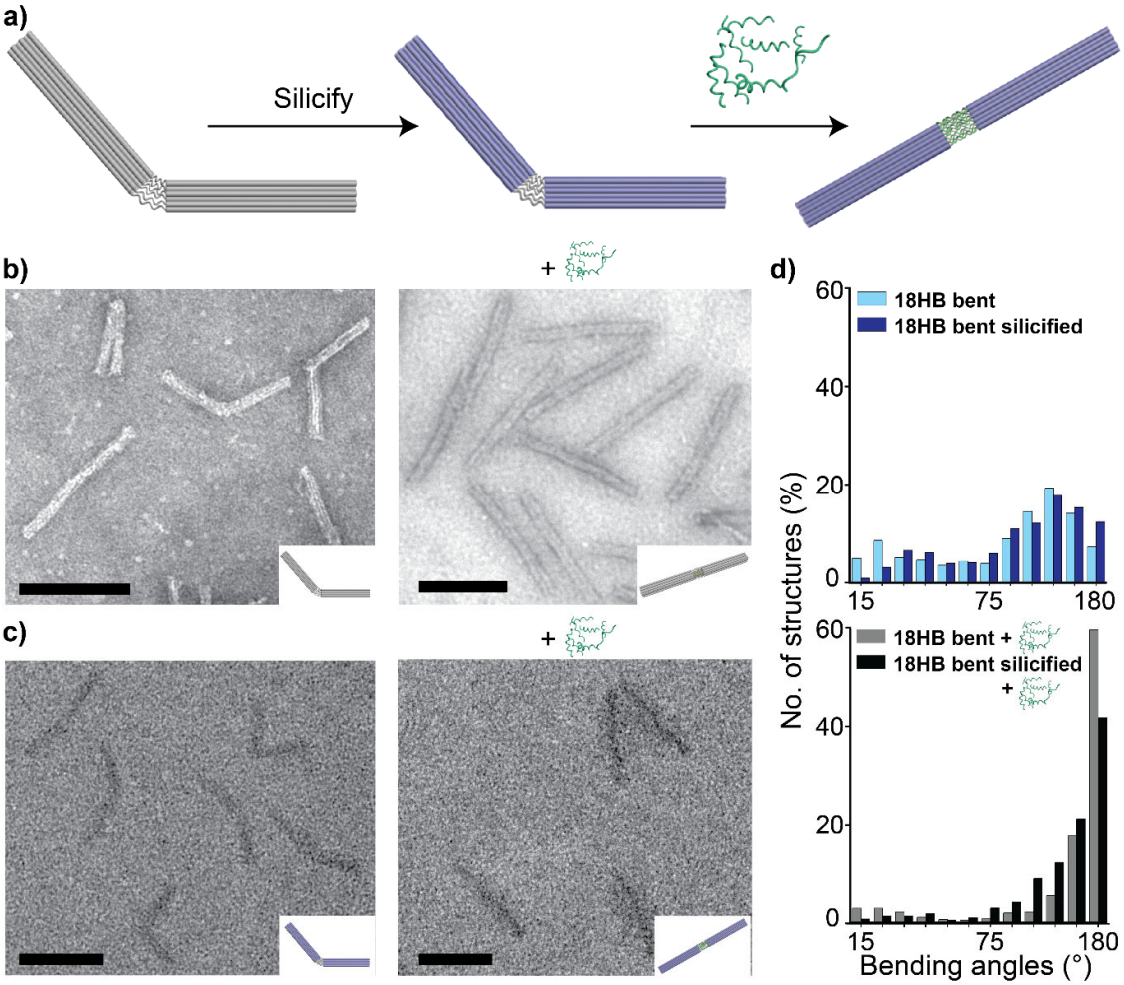

Figure 5.5: 18HB dynamic. a) Schematic illustration of a bent 18HB with missing middle staples. After silicification (blue structure) and subsequent addition of the corresponding straightening staples (green), structures straighten out. b) Bare and c) silicified 18HB before and after addition of the corresponding straightening staples. Bare structures were stained with uranyl formate, while silicified structures were not stained. Scale bars are 100 nm. d) Histograms of bending angle before (left) and after addition of straightening staples (right). More than 480 structures were analyzed for each condition. (Angle distributions were collated in 15 ° bins). Image taken and modified from Wassermann et al. with permission[75].

Despite these challenges, this study strongly suggests that forming dynamic, flexible, shape-changeable silica-DNA hybrid nanostructures is feasible. This opens up new possibilities for applications in biosensing, materials science, and nanorobotics.

Chapter 6 - Results and Discussion on Customizing Silica for DNA Origami Applications

The focus of this chapter is the customization of the silica surrounding DONs, a critical aspect that enhances their functionality and application potential. The results of this chapter are currently being prepared for publication.

Customizing silica allows for greater uniqueness and versatility in the behavior of DNA origami, facilitating the development of advanced nanostructures tailored for specific applications, such as drug delivery, biosensing, and imaging. The ability to modify the silica coating opens avenues for improving stability, altering degradation rates, and enabling specific interactions with biological environments.

Two primary customizations of silica will be discussed in detail: dissolvable silica and fluorescent silica. The use of Bis(triethoxysilyl)disulfide (BTDS)[173] and Bis-[3-(triethoxysilyl)-propyl]-tetrasulfide (BTSPTS)[174] was explored for creating dissolvable silica structures. Unlike TEOS (**Scheme 6.1**a), which forms a permanent and inert silica coating, both BTDS (**Scheme 6.1**b) and BTSPTS (**Scheme 6.1**c) introduce a disulfide bond that imparts environmental sensitivity, allowing for responsive degradation under specific conditions. BTDS was preferred over BTSPTS due to its smaller size and simpler structure, which features a single disulfide bridge. This simplicity facilitates easier integration into the silica network and minimizes potential disruptions compared to BTSPTS. The latter, with its three disulfide bridges, is hypothesized to cause larger disruptions due to its increased size. However, these additional disulfide bridges could theoretically enhance its dissolvability by providing more cleavage points in reducing environments.

The incorporation of fluorescent silica represents another significant customization. Fluorescein and rhodamine modified silane precursors[175] were synthesized in collaboration

with Philip Mauker from the Thorn-Seshold Lab. Following unsuccessful initial attempts to incorporate these fluorescent silanes during the silicification process, we hypothesized that their size was creating holes in the silica shell, necessitating a shift in strategy. The decision was made to add the fluorescent components post-silicification. However, this approach presented challenges in purifying the silicified origami due to the residual fluorescence. This issue was mitigated through the passivation of pluronic F-127 in Amicon filters, allowing for effective separation of excess fluorophores.

While this chapter will concentrate on these two key customizations, it is worth noting that other avenues for silica modification could be explored in future research. For instance, the incorporation of targeting ligands into or on top of the silica matrix could enhance the specificity of the DNA origami in biological applications. Additionally, the exploration of silica with varied porosity or functionalization with reactive groups may offer improved interactions with cellular environments or facilitate the attachment of other biomolecules. The ongoing customization of silica for DNA origami applications holds the promise of developing sophisticated nanostructures that can respond to specific stimuli and fulfill diverse roles in biomedicine and materials science.

6.1 Dissolvable Silica

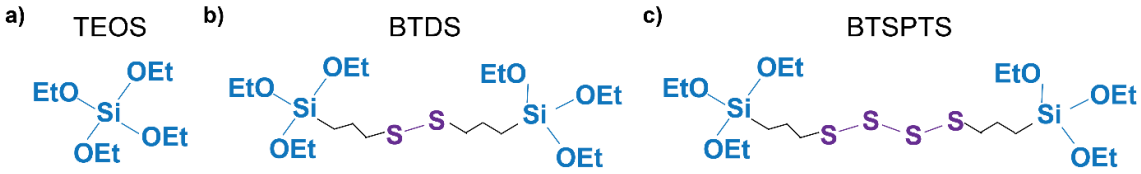

Scheme 6.1: Structural comparison of silica precursors: TEOS, BTDS, and BTSPTS. a) shows the structure of TEOS the simplest molecule, with four ethoxy groups attached to a silicon atom. b) illustrates BTDS, which consists of two TEOS units connected by a single disulfide bridge. c) shows BTSPTS, featuring three disulfide bridges connecting two TEOS units, making it the largest molecule in the set. These disulfide bridges in BTDS and BTSPTS introduce additional reactivity and degradation pathways, potentially enhancing the functional capabilities of the silica materials formed from these precursors.

In the context of protecting DNA origami from degradation, silicification using conventional methods such as TEOS has proven highly effective, as can be seen in Chapter 4. TEOS forms a solid and protective silica shell around DNA origami, providing excellent defense against enzymatic degradation, as also demonstrated in the top gel of **Figure 6.1**b. Here, the 24HB DNA origami, fully silicified with TEOS, remained entirely intact even after exposure to DNase I for 24 h. This high level of protection is crucial in scenarios where the stability of nanostructures must be preserved for long periods, such as during storage or transport in biological systems. TEOS, being a small, simple molecule, hydrolyzes to produce silanol groups that condense into a uniform silica network, creating a robust and enduring coating.

In contrast, BTDS offers unique chemical properties that go beyond simple protection. While BTDS can also form a silica shell through its siloxyl groups, its disulfide bridge (-S-S-) (**Scheme 6.1**) introduces the additional possibility of controlled degradation in the presence of reducing agents like glutathione (**Figure 6.1**a, lower pathway). This feature is particularly significant because it allows for the targeted release of encapsulated molecules or the triggered disassembly of the structure under specific environmental conditions. The ability to precisely control the degradation of silica shells opens up innovative applications in drug delivery, where the silica-encapsulated therapeutics can be released directly at the site of interest, such as tumor cells rich in glutathione[176, 177]. Moreover, the controlled degradation of silica can prevent the accumulation of nanoparticles in organs, which could otherwise lead to potential toxicity and adverse effects[178, 179]. This aspect is crucial in nanomedicine,

where minimizing side effects and enhancing biocompatibility are paramount for successful therapeutic outcomes.

As shown in the lower gels of **Figure 6.1**b, DNA origami silicified with 100% BTDS exhibited significant degradation when treated with glutathione, while a structure with a 50/50 mixture of TEOS and BTDS showed partial degradation. These results indicate that BTDS-based silica coatings provide a mechanism for programmed degradation, allowing the DNA origami or its cargo to be released in response to specific environmental cues. This functionality is particularly appealing for drug delivery applications, where a protective shell may dissolve at a specific target site, such as inside a cell where glutathione is present in higher concentrations.

A potential alternative to BTDS is BTSPTS, which contains two additional disulfide bridges compared to BTDS. This theoretically increases its degradability, but the larger size of BTSPTS molecules could potentially complicate the coating process or affect the uniformity of the silica layer. Due to these uncertainties, I opted to begin experimentation with the smaller BTDS. However, future research could explore the use of BTSPTS for applications where a more precise or rapid degradation profile is required. The balance between protective stability and triggered degradability presents exciting possibilities for dynamic and responsive DNA-silica nanostructures.

As illustrated by the data in the supplementary appendix, BTDS alone forms a stable protective layer in the absence of glutathione (GSH), much like TEOS (**Appendix A, Figure A.5**). This property enables DNA origami to circulate or exist in environments without immediate degradation yet be susceptible to breakdown once glutathione is introduced. Since glutathione is present in higher concentrations inside cells than in extracellular spaces, BTDS coatings could provide intracellular delivery mechanisms that degrade specifically within targeted cells, allowing for precise control of therapeutic release or material function.

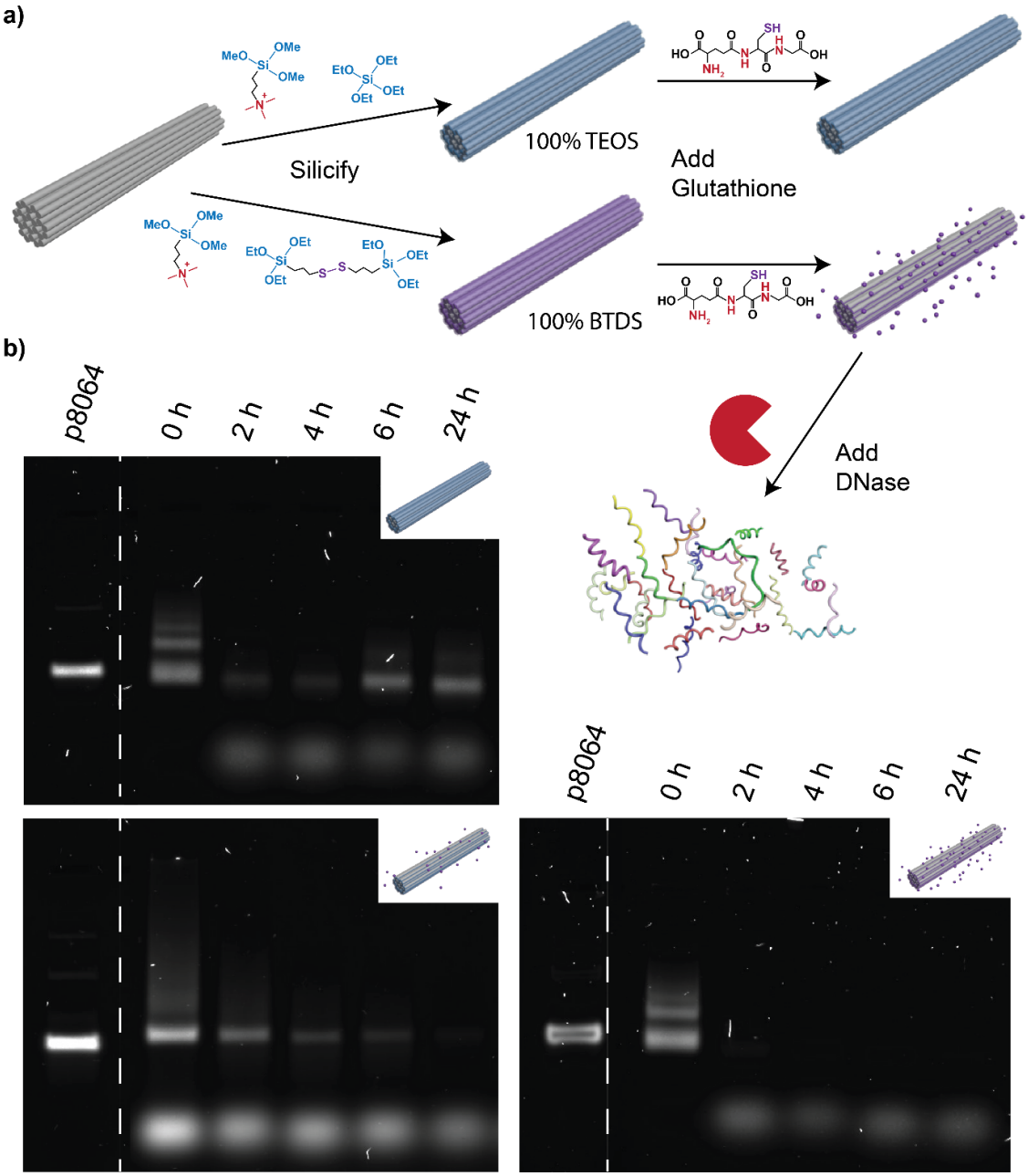

Figure 6.1: Comparison between TEOS and BTDS silicification. a) Schematic illustration of two silicification pathways on the 24HB structure using TEOS (upper pathway) and BTDS (lower pathway). Addition of glutathione, does not change the structure of the TEOS silicified structure, but degrades the BTDS silica shell around the 24HB. b) AGE results showing DNase I degradation tests of the silicified 24HB structures with different amounts of TEOS and BTDS as well as treatment with glutathione. The top gel (100% TEOS) shows no degradation, while the bottom left gel (50% TEOS + 50% BTDS) reveals partial degradation, and the bottom right gel (100% BTDS) displays significant degradation. The data highlight the customizable degradability of the silica shell based on the composition of TEOS and BTDS. Lanes are labeled according to the incubation times of the samples with DNase I (0h, 2h, 4h, 6h, and 24h).

Furthermore, this ability to tune the degradation profile by adjusting the ratio of TEOS and BTDS introduces significant flexibility. By modulating the composition, the degradation rate of the DNA origami can be fine-tuned according to the specific application requirements—ranging from slow, gradual breakdown to rapid dissolution upon exposure to a reducing agent (**Figure 6.1**b).

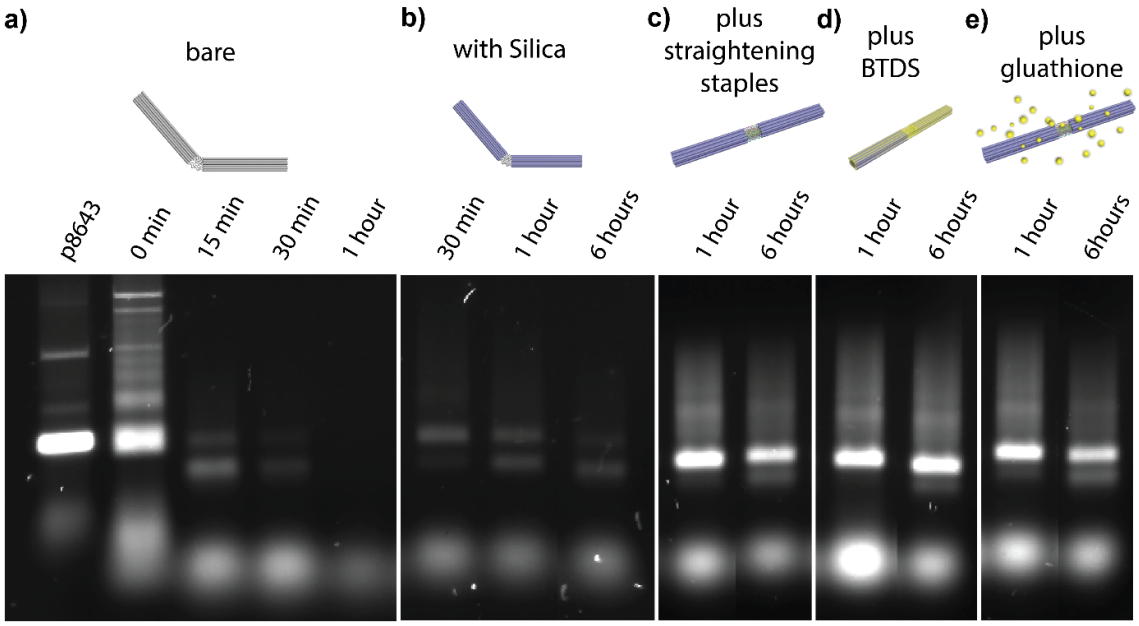

Figure 6.2: DNase I digestion assay of various 18HB bent. a) displays the bare bent 18HB subjected to DNase I for different time points (0 min, 15 min, 30 min, 1 h). b) shows the bent 18HB silicified with TEOS silica for 30 min, 1 h, and 6 h. c) represents the same structure with the addition of straightening staples (1 h, 4 h, and 6 h). d) shows the addition of BTDS silica to the straightened 18HB, with digestion time points of 1 h and 6 h. e) shows the addition of glutathione, which causes the silica to vanish at the bend. The gel displays that each modification increasingly enhances the stability of the DNA origami against DNase digestion and glutathione makes it more vulnerable again.

Next, I wanted to show that BTDS can be used to only make certain spots of the silicified DNA origami dissolvable. For this I utilized the bent 18HB structure that was introduced in Chapter 4. DNase I was again used in this test. In the next presented DNase I assay, the dynamic DNA origami, based on the bent 18HB structure (**Chapter 5.4**), was subjected to several treatments to assess its stability against enzymatic degradation (**Figure 6.2**). Initially, the bent 18HB was silicified, following the standard silicification protocol. The results of DNase I testing after silicification show two distinct bands (**Figure 6.2**b): one corresponding to the intact 18HB (upper band) and the other representing a "broken" (lower band) form of the origami where the bent spot was degraded by DNase I, splitting the structure into

two separate fragments. A similar, albeit less pronounced, splitting can be observed in the unsilicified structure (**Figure 6.2**a), as well as in the silicified structure that already has middle staples added (**Figure 6.2**c), highlighting the fragility of the bent configuration.

The second stage of stabilization involved the introduction of BTDS (**Figure 6.2**d). The results indicate that BTDS stabilizes the DNA origami, significantly reducing the impact of DNase I digestion and the degradation in the bent region. When glutathione is introduced to the BTDS-treated 18HB origami (**Figure 6.2**e), it selectively breaks down the silica at the bent region, effectively reverting the structure to a state similar to that seen in **Figure 6.2**c, where middle staples are present without BTDS treatment. To assess that this is really the case as the bands in **Figure 6.2**c, d & e look very similar, I did a quantitative study (protocol in **Appendix B.2.7**) to compare the brightness of the bands representing intact versus broken forms of the various silicified 18HB bent post-treatment with DNase for 6 h (**Figure 6.3**). This preliminary study, conducted with a single gel, suggests that while the 18HB bent with straightening staples and the one after treatment with GSH have about the same percentage (ca 30%) of broken 18HB, while the one with BTDS has only 15% broken 18HB. This finding highlights the potential for selective degradation is, although further experiments are required to optimize the controlled exposure of specific sites on the DNA origami and enabling further experimental manipulations or the triggered release of payloads encapsulated within these sites.

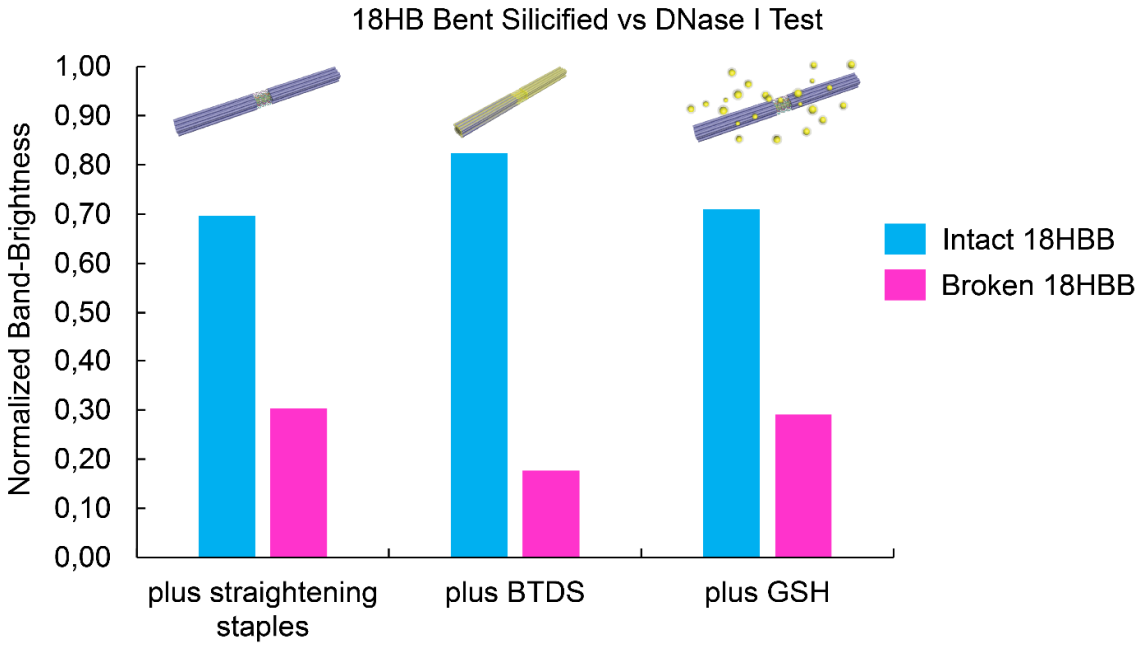

Figure 6.3: Quantitative analysis of DNase I resistance in silicified 18HB bent. This histogram compares the intensity of bands representing intact (full) and broken 18HB structures after 6 h of DNase I treatment, as shown in the gel images from **Figure 6.2**c, d & e. The y-axis represents the normalized brightness, with the overall intensity set to 1 each. The 'plus Middle' indicates the 18HB with straightening staples only, 'plus BTDS' refers to the addition of BTDS silica, and 'plus GSH' shows the effect of glutathione on dissolving the silica and reducing structural integrity. This data was only done on one gel, but demonstrates the protective effect of BTDS and the vulnerability introduced by glutathione treatment.

6.2 Fluorescent Silica

Beyond controlling degradation, customized silica coatings also offer the opportunity to incorporate functional elements such as fluorescent dyes. In her master thesis conducted under my guidance, Lilian Göldel[180] utilized Cy5-modified Brick DONs for studies in HeLa cells, tracking their uptake and localization through Cy5 fluorescence. However, this method crucially depends on the fluorescent dye remaining bonded to the DNA origami; a similar study by Lacroix et al.[181] noted that cleaved fluorescent dyes could misleadingly appear to be associated with the DNA structures. Addressing this issue, together with Philip Mauker from the Thorn-Seshold group, we developed a fluorescent silane, where one ethyl group of the typical silicification agent TEOS is replaced with a modified fluorescein or rhodamine dye (**Figure 6.4**a and **Figure 6.6**a). This modification ensures more reliable tracking of structures by integrating the fluorescent marker directly into the silica matrix. By embedding fluorescent molecules like fluorescein into the silica matrix, it becomes possible to monitor the behavior and localization of the nanostructures in real time without compromising the protective stability of the silica shell.

6.2.1 DNA Origami with Fluorescein-Silane

Fluorescein has a high quantum yield and distinct excitation/emission peaks at 490 nm and 517 nm (bright green fluorescence)[182], respectively. Its ability to undergo various chemical modifications[86, 183] allows for tailored spectral properties and enhanced environmental sensitivity. However, its integration into silica coatings presents challenges, primarily due to its size. In this work the fluorescent silane was incorporated into the silica shell of DONs post-silicification (**Figure 6.4**b). The adoption of a two-stage silicification process - initial formation of a complete silica shell with standard TEOS followed by a secondary application/ incorporation of dye-functionalized silane - addressed the critical issue of maintaining structural integrity while embedding the functional dye.

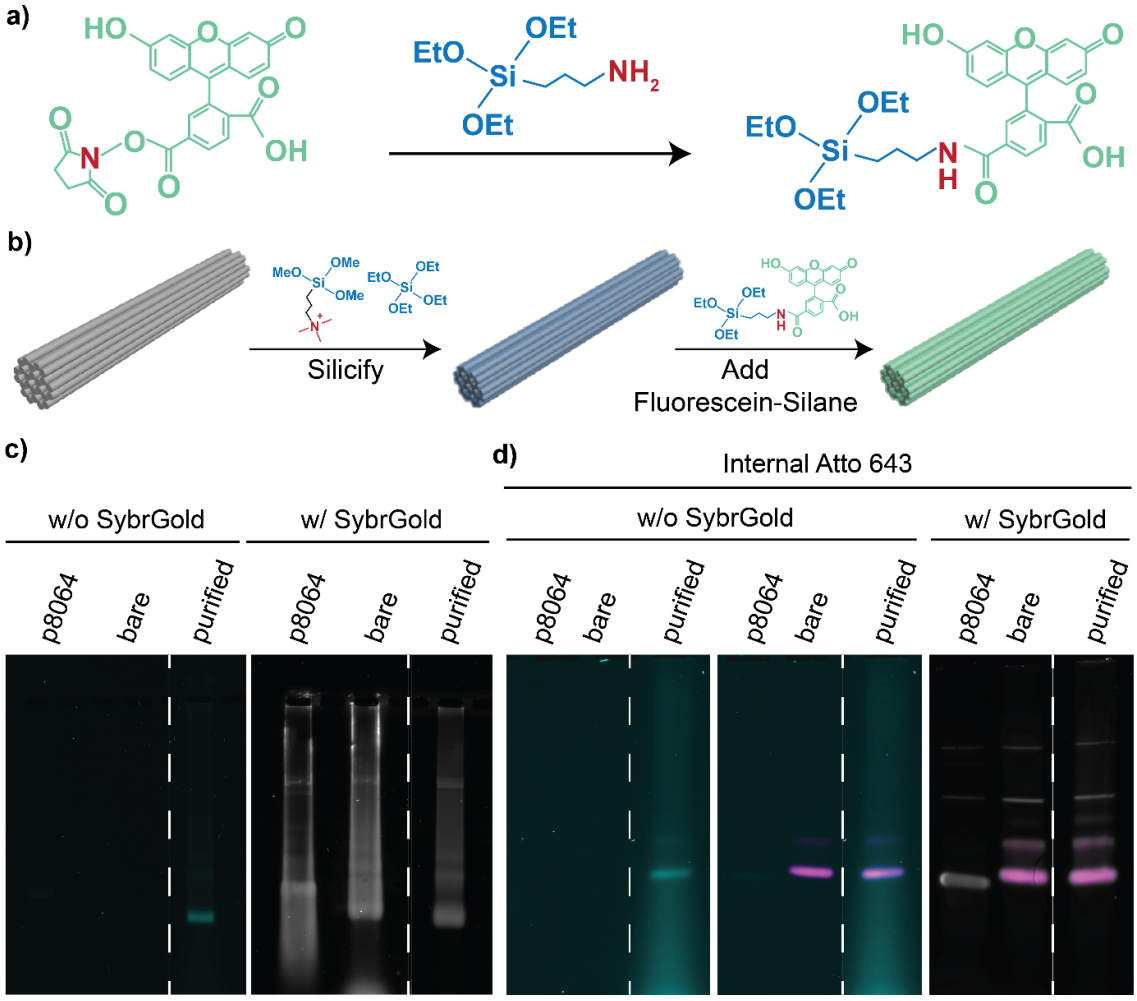

Figure 6.4: Fluorescein-Silane addition to 24HB. a) Schematic of the synthesis of a fluorescein-silane conjugate: the fluorescein dye was functionalized with a triethoxysilyl moiety for subsequent incorporation into silica structures. b) Schematic representation of the (post-)silicification process, where fluorescein-silane is added to previously silicified DONs, enhancing their fluorescence without compromising structural integrity. c) AGE of bare and fluorescently silicified DONs before and after staining with SybrGold. Post-staining differentiates the fluorescence signal from the fluorescein labeling (grey) and the SybrGold-stained DNA. d) AGE images of 24HB DNA origami with internal Atto 643 visualized under two different excitation wavelengths: left (473 nm) highlighting fluorescein fluorescence (cyan), and right (overlay of 473 nm and 635 nm) showing Atto 643 fluorescence (magenta). The far-right image shows the gel post-staining with SybrGold (grey), illustrating the DNA backbone alongside the fluorescence labels.

Subsequent purification was essential to remove unbound fluorescein. Despite trying numerous purification methods with the assistance of my master student Marius Blackholm[184], significant enhancements in purification efficiency were only achieved with the introduction of pluronic F-127 passivated filters[185], as detailed in **Appendix A, Figure A.6**. This process involves treating the filters with 5% pluronic F-127 solutions, which coat the filter surfaces and prevent the nonspecific binding and loss of nanostructures (see

Appendix B.2.4 for protocol). Our comparative studies, one detailed in **Table 6.1**, demonstrate that passivated filters significantly improve the yield and quality of purified samples. Without pacification, repeated purification attempts lead to substantial losses, as the nanostructures adhere to the filter membranes. This approach not only retained the structural and fluorescent properties of the DNA origami but also prevented the loss of material typically associated with non-passivated purification systems.

Table 6.1: Retention and loss percentages of a DNA origami sample after undergoing purification with and without passivated filters. Starting conditions for all samples were 50 µL at a concentration of 50 nM. The percentage lost is calculated based on the difference in volume from the expected final volume (calculated based on Eq.B.1), reflecting the efficiency of the purification process under different conditions.

Sample	*Final concentration [nM]*	*Final volume [µL]*	*Percentage Lost [%]*
Not passivated	11	60	74
	12	43	79
	31	56	31
	24	46	56
Passivated	54	45	3
	63	35	12
	56	44	0
	95	25	5

In **Figure 6.4**, parts c and d demonstrate the complementary utility of combining internal and external fluorescence markers. **Figure 6.4**c showcases an AGE analysis where the purified DNA origami samples, labeled with fluorescein-silane, exhibit a clear and distinct band under UV light, indicative of successful purification. The fluorescence signal aligns with the expected position of the DNA origami (**Figure 6.4** right gel), suggesting effective incorporation of the fluorophore within the silica shell. However, due to the similar excitation wavelengths of fluorescein and the commonly used SybrSafe for DNA visualization, SybrGold staining is employed instead, necessitating the removal of the gel from the gel imager. This change precludes a direct overlay with previous images, making precise localization challenging.

Incorporating DNA origami-internal fluorescence markers in conjunction with the external fluorescent labeling of the fluorescein-silane, provides a robust dual-labeling system that enhances the tracking and validation of nanostructures in complex environments. As shown in Chapter 5, handles provide a good source to attach fluorophores to an origami. However, directly linking a fluorophore to an internal staple within the structure provides a more reliable indicator of its integrity and localization. This is because internal markers are less vulnerable to environmental disturbances such as enzymatic cleavage by DNase I. It is important to note, however, that if the origami structure itself is compromised—for example, if the silicification process fails—the internal markers will also be destroyed along with the structure. Although internal labeling is costlier—requiring multiple fluorophore-labeled staples—it ensures greater stability and accuracy in intact structures. In contrast, external handles marked with fluorophores present a more economical option. A single fluorophore-labeled staple can be used across various origami designs as long as they contain compatible handles, offering a versatile and cost-effective solution, but they risk detachment and are more prone to enzymatic cleavage.

For further experiments I chose to incorporate Atto 643 as a DNA origami marker, by labelling three staples with it (see **Appendix C.10.3** for exact staples), providing a consistent reference point that can be measured before and after SybrGold staining (**Figure 6.4**d). The leftmost gel images, observed under a single excitation wavelength (473 nm), highlight the fluorescence from the fluorescein-silane, primarily illuminating the external silica shell. The central gel images represent an overlay of two excitation wavelengths (473 nm for fluorescein and 635 nm for Atto 643), revealing both the silica shell and the internal fluorescence of the DNA origami. This overlay confirms that the fluorescent signals correspond to the actual locations of the nanostructures, not merely free-floating or detached fluorophores. The rightmost gel, after treatment with SybrGold, further validates the presence and integrity of the DNA within the silica shell by staining the DNA itself, shown in grey, which aligns with the fluorescence signals from both internal and external labels. This dual-fluorescence approach confirms that the observed external fluorescence is not due to free-floating or detached dyes but is directly associated with the DNA origami. The ability to measure and overlay these signals before and after staining provides an invaluable

tool for verifying the precise localization and structural integrity of the nanostructures in various assays.

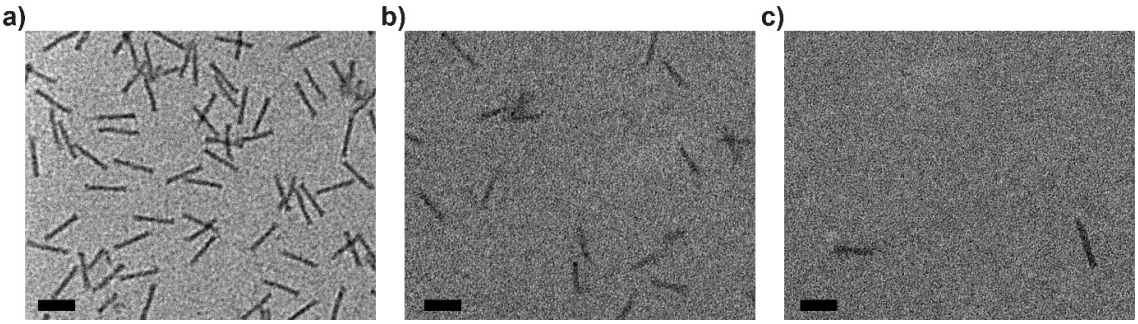

Figure 6.5: TEM analysis of fluorescent silicified 24HB. a) Normal silicified 24HB showing typical structural integrity. b) 24HB silicified with the addition of fluorescent silane, illustrating comparable structural features to the non-fluorescent variant. c) Fluorescently silicified 24HB after exposure to DNase I for 6 h, demonstrating no enzymatic degradation. Scale bars: 100 nm.

In the TEM images shown in **Figure 6.5**, the structural integrity and appearance of the 24HB were compared across the two different silicification conditions. The images reveal no discernible differences in the structural morphology between the normally silicified 24HB (**Figure 6.5**a) and the 24HB treated with fluorescent silane (**Figure 6.5**b), suggesting that the addition of fluorescein-silane to the silicification process does not adversely impact the physical structure of the DNA origami. This is crucial for ensuring that the fluorescence labeling does not compromise the nanostructure's utility in potential applications.

However, while the TEM images indicate structural preservation, the stability and integrity of these fluorescently modified structures under biological conditions remain to be fully assessed. **Figure 6.5**c shows the fluorescently silicified 24HB after a 6 h exposure to DNase I, serving as an initial exploration into the enzymatic resistance of these structures. Comprehensive DNase I testing is essential to verify whether the inclusion of fluorescent tags affects the protective properties of the silica shell or the DNA's inherent structural stability. Such verification is paramount for future biomedical applications where both the durability and the functional precision of the DNA origami are critical. This testing will help confirm if the novel fluorescent silicification approach can be reliably used in dynamic biological environments without compromising the integrity and functionality of the DNA nanostructures.

6.2.2 DNA Origami with Rhodamine-Silane

Similar to fluorescein, Rhodamine has a notable history and functional characteristics that make it a valuable tool in biochemical applications. Rhodamine was first synthesized in the late 19th century, quickly becoming prominent in scientific and medical fields due to its intense fluorescence. Rhodamine has an excitation peak around 540 nm and emits light at about 625 nm[186], which makes it distinctly visible under specific filters, contrasting sharply with the green fluorescence of fluorescein.

Rhodamine is known for its excellent photostability and high fluorescence quantum yield, characteristics that are highly valued in fluorescence microscopy and other imaging techniques. Its chemical structure allows for various substitutions, making it adaptable for different conjugation strategies to proteins, nucleic acids, and other biomolecules. This versatility has facilitated its widespread use in cell biology to trace cell organelles and structures, label proteins, and monitor dynamic biological processes *in vivo*.

Moreover, the stability and brightness of rhodamine make it suitable for long-term studies, as it resists photobleaching better than many other dyes, such as fluorescein. This property is particularly beneficial for experiments requiring prolonged illumination and observation.

Exploring rhodamine-silane as an alternative (**Figure 6.6**) highlighted the differences in charge properties and fluorescence behavior compared to fluorescein. Rhodamine's positive charge and red fluorescence offer distinct advantages, especially for multi-color applications. However, the similar migration patterns of rhodamine-silane and DNA origami in gel electrophoresis underscored challenges in confirming covalent attachment, as free dye could mimic the localization of modified origami.

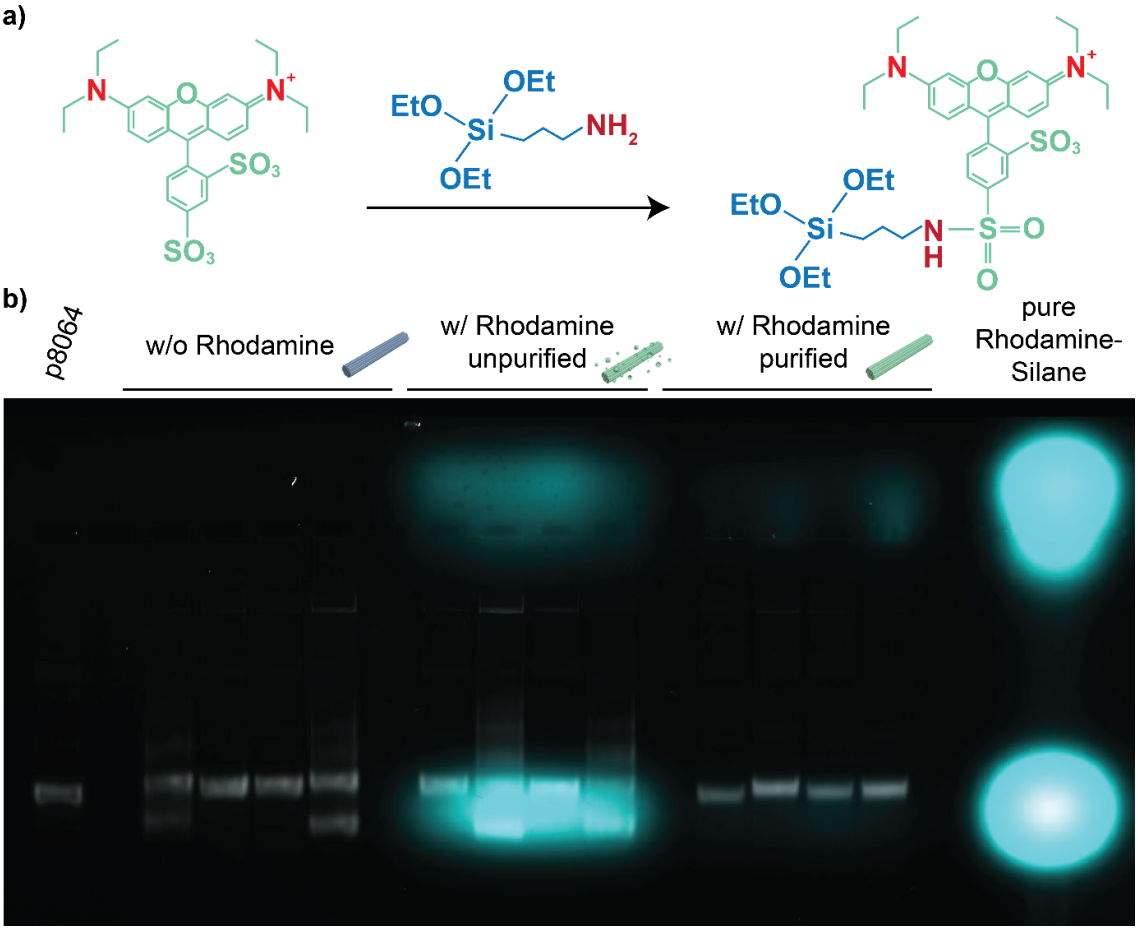

Figure 6.6: Rhodamine-Silane. a) Schematic of the synthesis of a rhodamine-silane conjugate: the disulfide rhodamine B dye was functionalized with a triethoxysilyl moiety for subsequent incorporation into silica structures. b) Overlay of AGE under excitation for SybrSafe (grey) and rhodamine-silane (cyan), showing the co-migration of pure rhodamine-silane and silicified 24HB. This suggests the challenges in ensuring that fluorescence observed in DNA origami bands is due solely to bound rhodamine-silane, as unbound dye may co-localize.

Chapter 7 - Summary and Future Outlook

In recent decades, the field of bionanotechnology has advanced rapidly, particularly in the use of DNA as a versatile building material. Numerous DNA-based assembly techniques have been developed, and their integration with biomineralization has enabled the formation of nanomaterials into well-defined structures. These innovations have demonstrated significant potential for applications in materials science and biomedicine. The overarching aim of this thesis was to advance the practical utility and functional versatility of DONs through innovations in silicification techniques, exploration of addressability post-silicification, and customization of silica coatings for enhanced functionality. Chapters 4, 5, and 6 collectively reveal the success of these efforts, demonstrating accelerated processes, retained addressability, and customizable functionalities that significantly enhance the scope and applicability of silicified DNA origami.

7.1 Summary of Results

Chapter 4 focused on addressing the time-intensive nature of traditional silicification methods. Generally, achieving a uniform silica coating required up to a week of static incubation, limiting scalability and application feasibility. By employing a rotation-based silicification process, the required time was significantly reduced to just 4–6 h, without compromising the structural integrity or uniformity of the silica layer. SAXS and TEM analyses confirmed the consistency and quality of the silica coatings achieved through this novel approach. The enhanced durability of the silicified DNA origami was validated through DNase I degradation assays. These studies confirmed that the silica layer provides robust protection against enzymatic degradation, a critical requirement for biomedical applications such as drug delivery and biosensing. Furthermore, the storage stability of these structures was explored under various conditions, revealing that silica coatings

bestow extended shelf life to DNA origami, ensuring their readiness for long-term use in diverse environments.

Chapter 5 explored a critical question: Does silicification preserve the addressability of DONs? Addressability, or the ability to selectively functionalize specific sites on the nanostructure, is a cornerstone of DNA nanotechnology. In this chapter I systematically investigated the addressability of silicified DNA origami under various conditions, including silicification in solution, on surfaces, and within dynamic configurations. Results revealed that the functional addressability of silicified DNA origami remains largely intact, whether silicification occurs in solution or on a surface. Notably, dynamic DONs, which undergo conformational changes, also retained their functional sites post-silicification.

The findings in chapter 6 expand the functionality of silicified DNA origami by introducing dissolvable and fluorescent silica coatings. The development of dissolvable silica coatings introduces a dynamic dimension to these structures, enabling the selective degradation of the silica layer in response to environmental stimuli, such as the presence of glutathione. This capability allows for controlled release of encapsulated molecules or the degradation of the nanostructure, which is particularly relevant for applications in targeted drug delivery, where precise control over cargo release is essential. These dissolvable coatings not only enhance the functional versatility of silicified DNA origami but also align with the broader trend in nanotechnology toward responsive and adaptive materials. In addition to dissolvable coatings, fluorescent labeling enhances the utility of these nanostructures in imaging and tracking applications, particularly in biological systems. For example, dual-labeling techniques—such as Atto 665 on a staple for stability verification and fluorescein-silane for external tracking—enable simultaneous monitoring of nanostructure integrity and location. These advancements represent a significant step forward in integrating DNA origami into live-cell environments.

7.2 Outlook to the future

The future of DNA origami biomineralization and functionalization is rich with possibilities, driven by advancements in silica customization, live-cell applications, and novel analytical techniques. In this thesis some projects were started that can provide a lot of insight and progress for this field if continued. Among the promising avenues, the use of CEM to study not only bare DNA origami but also silicified ones represents a critical step toward understanding the molecular intricacies of this process. By capturing high-resolution images of DNA origami during different stages of silicification, CEM could illuminate the dynamics of silica layer formation and identify key structural features that influence stability and functionality. Such insights would not only refine existing methodologies but also inform the design of more robust and efficient silicification protocols[82].

Experimental and systematic quantitative studies of the way handles (placement and form) impact the aggregation during silicification will shed light on how sequence variations and positional adjustments impact silica clustering and structural integrity, providing a foundation for designing more precise and versatile nanostructures.

The versatility of customizable silica coatings further enhances the potential applications of DNA origami in nanotechnology. Beyond the use of TEOS and BTDS, exploring alternative silica precursors like tetramethyl orthosilicate (TMOS) or BTSPTS could yield unique properties, such as responsiveness to environmental cues like pH, temperature or specific biomolecules. Hybrid systems combining silica with organic or inorganic components could lead to nanostructures with enhanced functionality, such as catalytic activity, biosensing capabilities or molecular assembly. This approach could also pave the way for programmable, multifunctional coatings, enabling DNA nanostructures to be both stable and dynamic, adapting to their environment as needed.

Fluorescent silica coatings open a new dimension for tracking and analyzing DNA origami in biological environments. The dual labeling approach—using internal Atto 665 for structural integrity verification and fluorescein-silane for external tracking—demonstrates the potential of multifunctional fluorescence strategies. Expanding on this foundation, multiplexed imaging with multiple dyes could enhance the resolution and functionality of these nanostructures, enabling their use in complex biological systems. Biological

applications of silica-coated DNA origami hold immense promise, particularly in live-cell imaging and therapeutic delivery. The successful internalization and localization of standard silica-coated DNA origami into cells, underscores the potential of fluorescein-silica-coated DNA origami as tools for studying intracellular processes, trafficking, and nanostructure stability in real time. Customizable coatings, such as those incorporating BTDS, could further enhance these capabilities by allowing controlled interactions with the cellular environment, enabling both imaging and targeted delivery.

Looking ahead, the field of DNA origami and biomineralization is ripe for further exploration and innovation. The integration of advanced techniques, such as CEM, with innovations in silica chemistry and functionalization strategies will propel DNA origami research into new frontiers. These efforts will not only enhance our understanding of biomineralization processes but also unlock unprecedented opportunities for the practical application of DNA-silica hybrids in biology, medicine, and beyond. As the field continues to evolve, the vision of creating intelligent, multifunctional nanoscale materials is steadily becoming a reality.

Appendix A - Supplementary Figures

A.1 DNA Origami Size Comparison

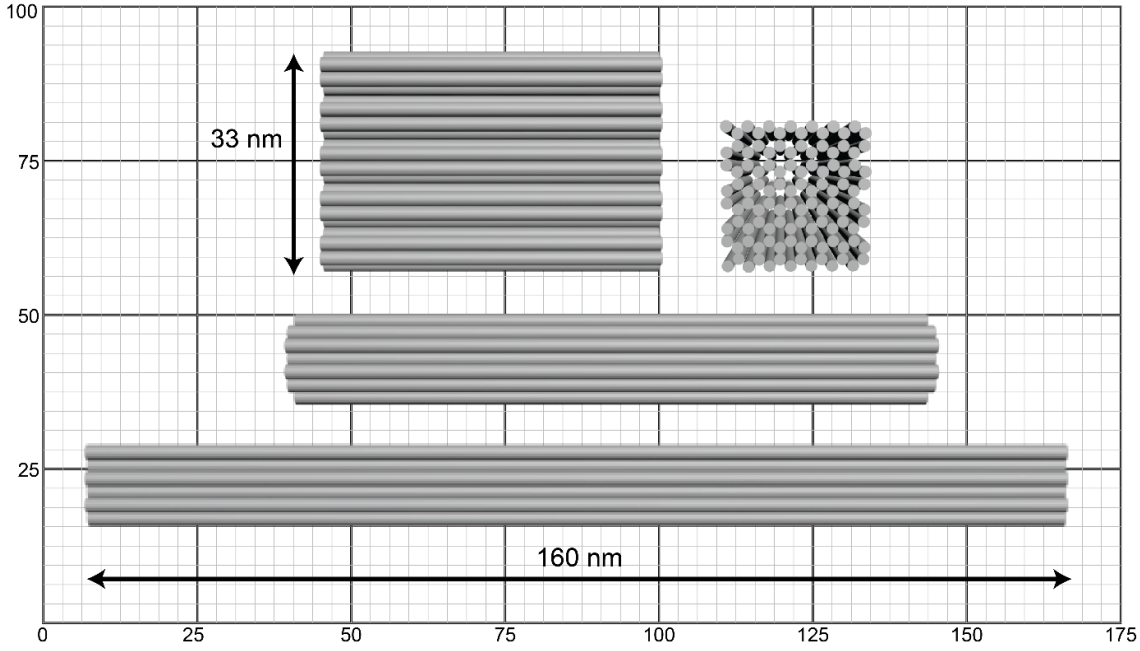

Figure A.1: Size Comparison between the most used Origami. The 4LB measures approximately 67 nm in length, 33 nm in width, and 7 nm in height, depicted at the top. Directly below is the 24HB, which is about 108 nm long and 16 nm in diameter. The 18HB is shown next, stretching to a length of 160 nm and a diameter of about 10 nm. Finally, the Cube, which appears on the right, is modeled with dimensions of approximately 25 nm on each side. This visual scale provides a clear perspective on the relative sizes and geometries of these structures, essential for understanding their applications and behaviors in nanotechnology.

A.2 Analysis of the DNA Origami Cube

The DNA origami Cube, uniquely designed and nearly completely cubical, is the final structure used in this study and measures approximately 25 x 25 x 26 nm. The Cube, like the 18HB, showcases a distinct shape entirely conceptualized and developed for this thesis. Simulations using CanDo and oxDNA (**Figure A.2**a &b, respectively) demonstrate the Cube's stability. Unlike the other DNA origamis discussed previously, the Cube exhibits only very minimal instability at the helix ends and some at the edges, confirming it as a fundamentally stable structure.

TEM analysis of the Cube (**Figure A.2**a), stained with uranyl formate, confirmed the accurate folding of the structure. The TEM images illustrate precise lattice and helical alignment (see **Figure A.2**c, inset), and indicated no significant aggregation. This likely results from the deliberate design variations at the helical ends—some helices are intentionally lengthened or shortened to prevent end-to-end stacking, as detailed in **Appendix C.9, Figure C.6**. Additionally, the strategic inclusion of four thymine bases in some staples helps avoid helix-helix stacking (refer to **Appendix C.10**, **Table C.1**).

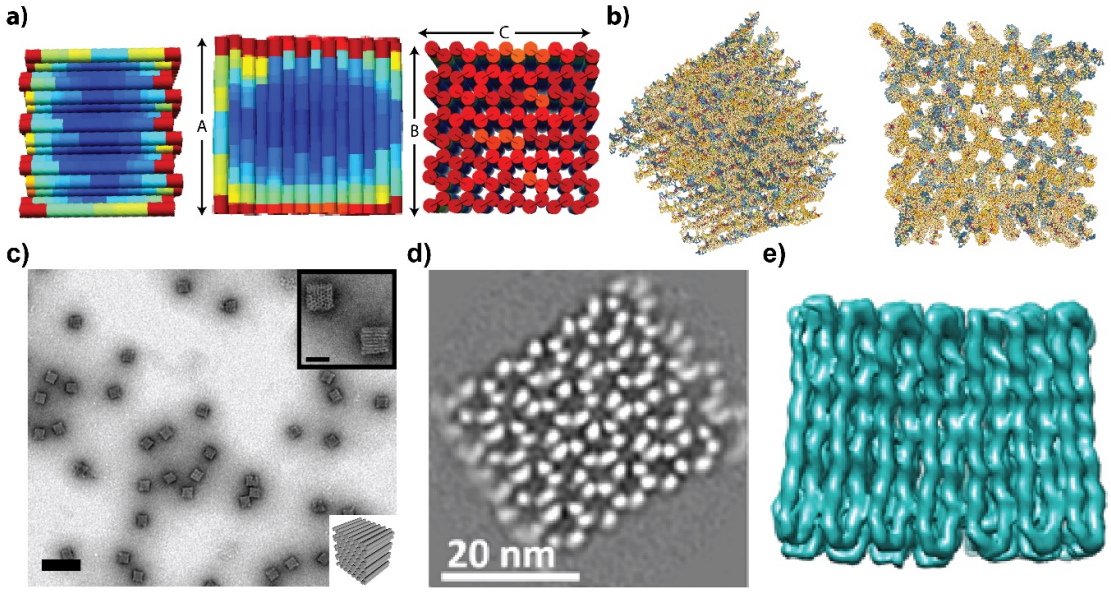

Figure A.2: Comprehensive Characterization of the Bare DNA Origami Cube. a) MD simulation of the Cube highlighting stability zones with red at the ends, some yellow on the edges, and mostly dark blue in the middle, indicative of varying stability, with dimensions A = 26.4 nm, B = 25.2 nm, C = 25.8 nm. b) oxDNA simulation of the Cube showing minimal fraying and robust structural integrity. c) TEM image showcasing the Cube with insets detailing views from the side and top, revealing lattice holes and helix orientations. d) High-resolution

CEM image of the bare Cube. e) 3D CEM simulation offering a detailed structural representation of the Cube. Scale bars: TEM images, 100 nm; CEM images, 20 nm.

CEM analysis, conducted by Bachelor student Alexander Ullrich, provided a high-resolution view of the Cube (**Figure A.2**d). This analysis distinctly displayed all 112 helices, offering deeper insight into the Cube's configuration. Further structural details were captured in a comprehensive 3D CEM simulation (**Figure A.2**e), which, along with the high-resolution CEM image, revealed some distortion along the direction of the helices. These discrepancies likely arise from the sample preparation methods used in Cryo-EM, where the absence of stabilizing factors during blotting or plunge-freezing can cause structural changes. This highlights the need for meticulous attention to detail in the handling and analysis of such intricate nanostructures.

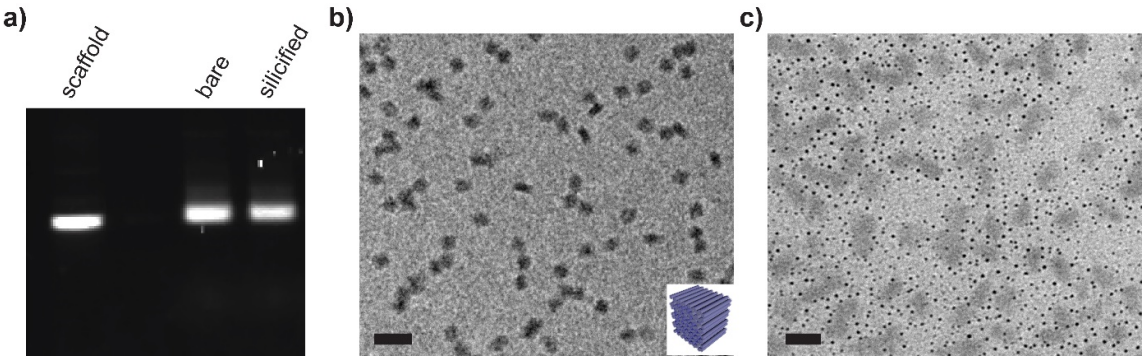

Figure A.3: Analysis of the Cube post-silicification and DNase I testing. a) AGE results showing lanes for scaffold, bare Cube, and silicified Cube, indicating similar migration patterns, suggestive of minimal impact on size or charge. b) TEM image displaying the Cube post-silicification, demonstrating preservation of sharp corners and edges. c) TEM image after a 4-h DNase I digestion test conducted directly on the TEM grid, displaying the durability of the silicified Cube against enzymatic degradation, confirming the preservation of structural details. Scale bars in TEM images represent 100 nm.

The unique geometry of the DNA Origami Cube was meticulously analyzed through its silicification process. Unlike the previously discussed origami structures, the Cube was studied in a separate context due to its distinct shape and the challenges associated with maintaining its form during silicification.

The pre-silicification TEM images (**Figure A.2**c) revealed a uniform distribution of the Cube, with each maintaining its precise cuboidal geometry, indicative of successful initial folding and structural integrity. This baseline imaging was crucial for comparing post-silicification changes. The silicification process of the DNA Origami Cube revealed challenges in maintaining its cubic geometry. Post-silicification analysis using agarose gel electrophoresis

(AGE) indicated that bare and silicified Cubes migrated similarly, suggesting that silica deposition did not significantly affect the overall size or charge density of the Cube (**Figure A.3**a). However, TEM imaging revealed discrepancies, highlighting potential structural differences not apparent from AGE analysis (**Figure A.3**b). While still seemingly well dispersed, some cubes appeared to deform into elongated rectangular 3D shapes rather than retaining their original cubic form (**Figure A.3**b). This deformation might result from condensation behaviors observed in DNA origami (**Chapter 4**) during silicification. Another possible cause could be unintended stacking of the cubes, either end-to-end or top-to-top, despite the addition of extra Ts (4 nt long) to the outer staples to minimize such interactions. These findings indicate that the silicification process requires further fine-tuning to ensure the Cube retains its cubic shape after silica deposition.

Interestingly, the corners and edges of the cubes remained sharp, even in the deformed structures, highlighting partial success in preserving some aspects of the geometry. SAXS could be instrumental in pinpointing the exact timepoint when the deformation occurs during silicification. Similarly, TEM or CEM could be employed at different stages of the silicification process to monitor these changes and refine the conditions accordingly to achieve better control over the silicification process [82].

A DNase I test was conducted to evaluate the durability of the silicified Cube against enzymatic degradation (**Figure A.3**c). Conducted directly on the TEM grid over a 4-hour period, the test revealed that the Cube retained its structural integrity, preserving the more rectangular shape induced by silicification rather than the original cuboid form of the bare DNA origami. A comprehensive DNase I assay is recommended to gain deeper insights into the structural stability of the silicified Cube, both in its current deformed state and under conditions that preserve a proper cuboid geometry.

A.3 Storage of DNA Origami

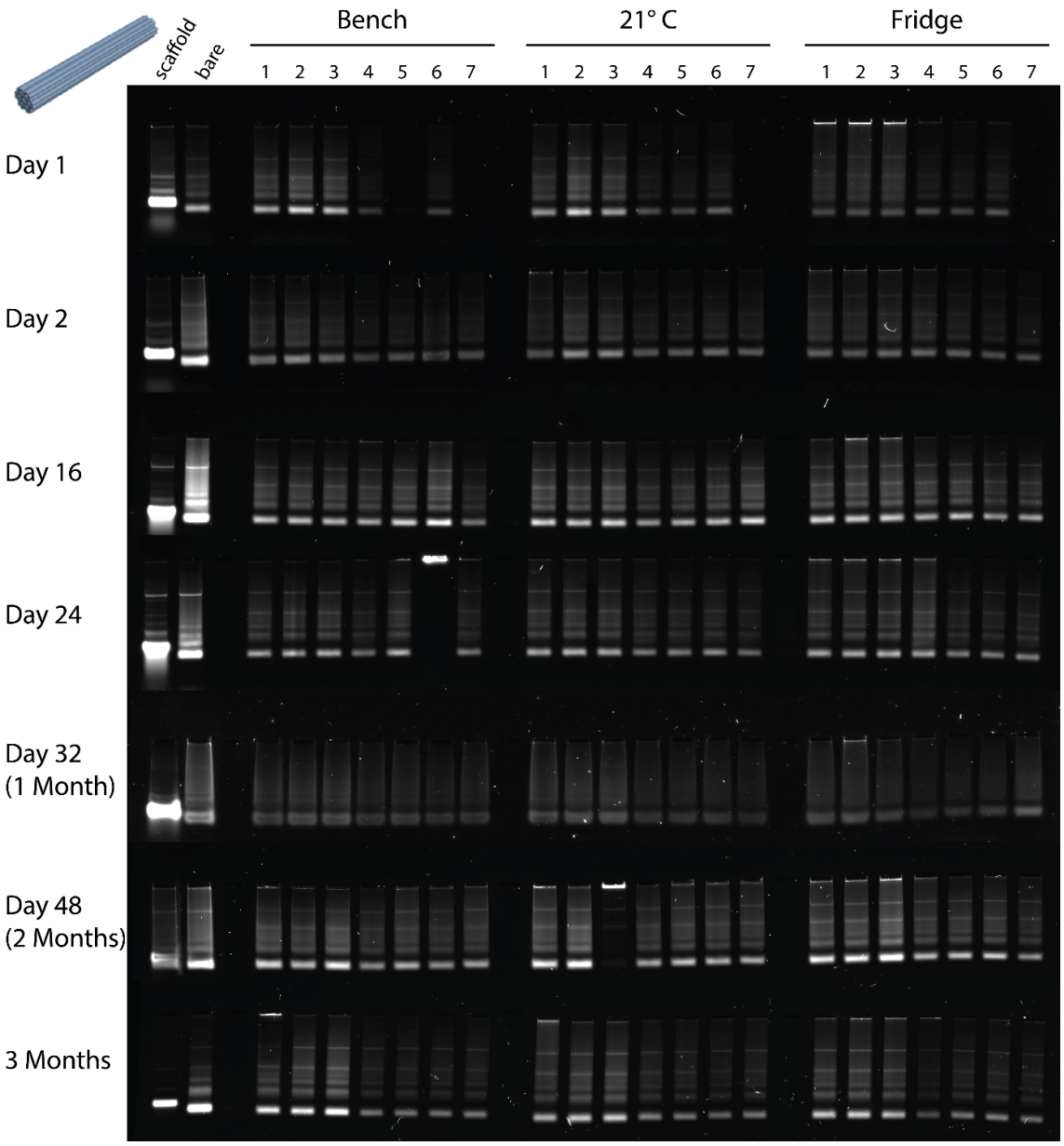

Figure A.4: AGE results from the extended storage experiment of silicified 24HB DNA origami over a period of 3 months under different storage conditions. Rows indicate different time points: Day 1, Day 2, Day 16, Day 24, Day 32 (1 Month), Day 48 (2 Months), and 3 Months. Columns show storage locations (Bench, 21 °C, Fridge) and sample approaches (1-3: standard approach, 10 µL at 10 nM; 4-6: volume approach for Day 1, 50 µL at 50 nM; 7: does not exist on Day 1 due to no disturbance). From Day 2 onwards, rows 5-7 represent disturbance samples (50 µL at 50 nM, steadily used throughout the experiment). The gel compares the migration patterns of the 24HB scaffold, bare origami, and the silicified 24HB under these conditions.

A.4 Designing of Handle Positioning for their Effect on Silicification

During my research of the addressability of handles after silicification, I observed that DONs equipped with multiple handles often resulted in the formation of large, silicified aggregates rather than individual silicified origami when processed in solution. These handles, rich in phosphate groups, could potentially act as nucleation sites for silica condensation, thus leading to a denser silicification than intended. This intriguing phenomenon prompted the start of a systematic investigation to discern the influence of handle density, arrangement and sequence on silicification outcomes.

Clustering of silicified DONs can be problematic for several reasons, particularly when precision and uniformity are crucial for specific applications. In contexts such as drug delivery, biosensing, and nanoelectronics, the individual DONs are often designed to function as discrete and uniformly distributed entities. Clustering can lead to significant variations in the size and shape of silicified constructs, potentially affecting their functionality and reliability. For instance, in drug delivery applications, non-uniform particle sizes can result in inconsistent release rates and bioavailability of therapeutic agents. Similarly, in biosensing applications, clustering might impede the accessibility of functional sites on the origami, reducing the sensitivity and specificity of the sensors. Moreover, in the realm of nanoelectronics, aggregated structures could lead to unpredictable electrical properties and connectivity issues. Therefore, preventing clustering is essential to ensure that the precise engineering of DNA origami translates effectively into their intended applications, maintaining the integrity and performance of the nanoscale designs.

To address these objectives, I designed a series of experiments, including variations in handle placement, number and sequence. Additionally, I modified the design of some handles so that they fold into a hairpin shape instead of protruding straight out from the DNA origami. The hypothesis is that this modification might reduce aggregation by effectively eliminating the presence of single-stranded handles during the silicification process. The hairpin handles, however, retain their functionality and can unfold when exposed to the appropriate anti-handle sequence, thus allowing for further functionalization if the ds stem region of the hairpin is kept short enough to prevent full silicification[80].

The main goals of this study were as follows: understanding the mechanics of the aggregation process through experiments involving gel electrophoresis and TEM. In this context, aggregation observed in gel electrophoresis would manifest as the sample being stuck in the well, while aggregation in TEM would appear as clusters of DONs. By systematically evaluating these factors, I aimed to develop strategies to prevent aggregation and ensure the production of well-defined, uniformly silicified DONs.

I designed an experimental setup, where the 24HB origami was modified to include handles in distinct configurations: arranged in rows (with each row containing 9, 9, and 10 handles) (**Scheme A.1**a), clustered in groups of six (**Scheme A.1**b), at the elongated end staples (**Scheme A.1**c) and randomly placed across the origami structure(**Scheme A.1**d). For exact placement of the handles see Appendix C, **Table C.28** - **Table C.31**. The specific handle placements on the DNA origami—random placement, clustered placement, elongated end staples, and one row to three rows—were chosen to investigate how different spatial configurations affect the silicification process and the resulting properties of the DONs.

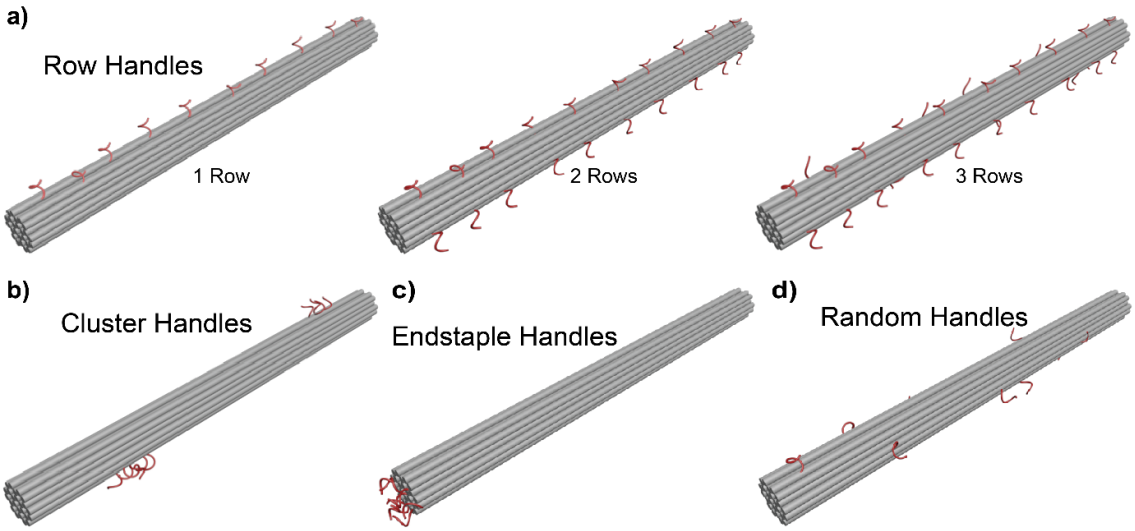

Scheme A.1: Various configurations of handle positioning on a 24HB. a) Row Handles: Single-stranded DNA handles are arranged in one, two, or three parallel rows along the length of the origami structure. b) Cluster Handles: Handles are grouped together in a tight cluster at a specific location on the origami. c) Endstaple Handles: Handles are positioned at the ends of the DNA origami, attached to the end staples. d) Random Handles: Handles are distributed randomly across the entire structure. These handle configurations were used to investigate how different positions and densities of handles influence the aggregation behavior during silicification.

In exploring the silicification of DNA origami, various handle placement strategies were tested to understand their impact on silica deposition, aggregation tendencies, and

structural integrity. Random handle placement served as a control, providing insights into the baseline behavior of silicification without any specific design constraints, helping to gauge how unpredictability in handle positioning might affect the process. Clustered handle placement, where handles are positioned closely together in specific regions, was investigated to assess the effects of localized high concentrations on silicification. The placement of elongated end staples, positioning handles at the extremities of the DNA origami, was designed to explore the effects of handle location on silicification at the structural edges. Finally, the configurations of one to three rows of handles along the length of the DNA origami were tested to examine how a linear and organized distribution affects the silicification process.

Additionally, different handle sequences were tested: poly-A sequences (**Scheme A.2**a), random nucleotide sequences (**Scheme A.2**b), and hairpins with double-stranded stem regions of 8 (**Scheme A.2**c) and 12 (**Scheme A.2**d) base pairs in length.

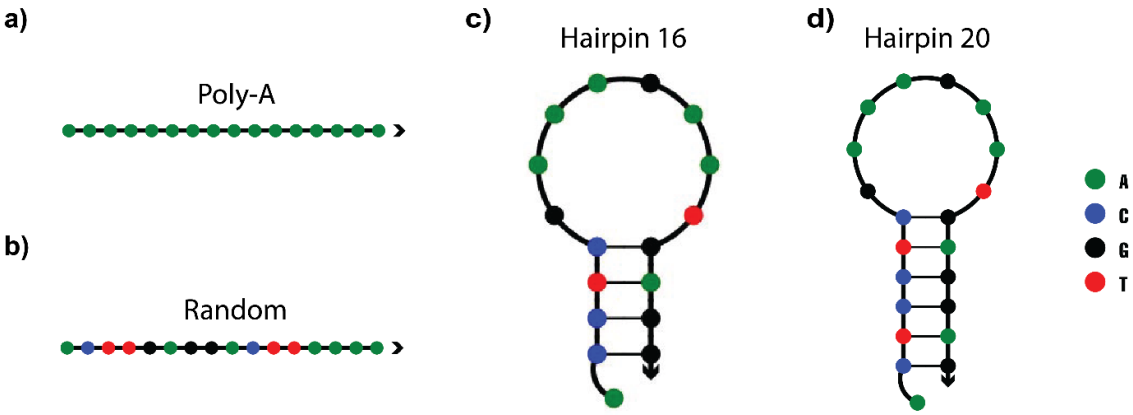

Scheme A.2: Schematic representation of different handle designs used in DNA origami experiments. a) Poly-A handle composed entirely of adenine (A) nucleotides. b) Random sequence handle composed of a mixture of all four nucleotides (A, C, G, T). c) Hairpin structure with an 8-nucleotide loop forming a stable double-stranded stem 8 long. d) Hairpin structure with an 8-nucleotide loop and a stable double-stranded stem 12bp long. Scheme made with NuPack[51, 52].

Poly-A Handles: Poly-A handles (AAAAAAAAAAAAAAA) consist of a sequence of adenine nucleotides, which tend to form single-stranded DNA (ssDNA) structures. The uniformity of the poly-A sequence allows for a controlled study of how a homopolymeric ssDNA interacts with the silicification process.

Random Sequence Handles: Random sequence handles (ACTTGAGGACTTAAAA), composed of a mix of nucleotides in no particular order, introduce variability in the handle structure.

This randomness can affect the handle's ability to hybridize and its electrostatic interaction with other DNA origami or their handles. The heterogeneity of random sequences provides a contrasting model to the poly A handles, offering insights into how sequence complexity and variability influence the aggregation during the silicification process.

Hairpin Handles: Hairpin handles are designed to fold back on themselves to form a double-stranded stem with a loop, creating a more rigid and structured domain. The hypothesis is that this modification might reduce aggregation by effectively eliminating the presence of single-stranded handles during the silicification process. The hairpin handles, however, retain their functionality and can unfold when exposed to the appropriate anti-handle sequence, thus allowing for further functionalization. The length of the double-stranded region is particularly relevant because previous studies suggest that dsDNA longer than 6 base pairs is more readily silicified than shorter or single-stranded DNA[80]. I therefore employed hairpin handles of different lengths (e.g., 16 nt (4 bp, ACTCCTCGAAAGAATGAGGAG) and 20 nt (8 bp, ACCCTCCTCGAAAGAATGAGGAGGG)). The difference in hairpin lengths allows the comparison of shorter and longer dsDNA regions, potentially revealing a threshold length that significantly affects aggregation during silicification.

A plausible hypothesis is that the spatial congregation of negative charges on the handles creates electrostatic conditions favorable for the nucleation and growth of silica nanoparticles. As these particles form, they may bridge between adjacent handles, particularly in configurations where handles are densely packed or in close proximity, such as in clusters or rows. This bridging could lead to the formation of larger silica aggregates rather than uniform coating, particularly under dynamic conditions where the diffusion of silicification agents is not uniformly controlled.

As another potential way to mitigate this clustering effect, the use of PNA[168] handles could be explored. PNA could reduce the local concentration of negative charges, thereby decreasing the electrostatic-driven aggregation of silica precursors. PNA's neutrality might lead to a more uniform silicification process, avoiding the dense clustering associated with DNA handles. Additionally, PNAs are known for their enhanced stability and specificity in binding, which could further contribute to the precision of origami folding and

functionalization in the presence of silicifying agents. However, it is important to note that PNAs are significantly more expensive than traditional DNA, which could limit their widespread use. Moreover, the synthesis of PNA is more complex and time-consuming, which might present practical challenges in large-scale applications.

These investigations are pivotal for refining the silicification techniques for DNA origami, ensuring that the functionalization capacity via handles is preserved without compromising the structural fidelity of the nanostructures. This research not only enhances the understanding of DNA-silica interactions but also improves the reliability of using silicified DNA origami in diverse applications, from nanoelectronics to biomedicine.

A.5 Dissolving Silica

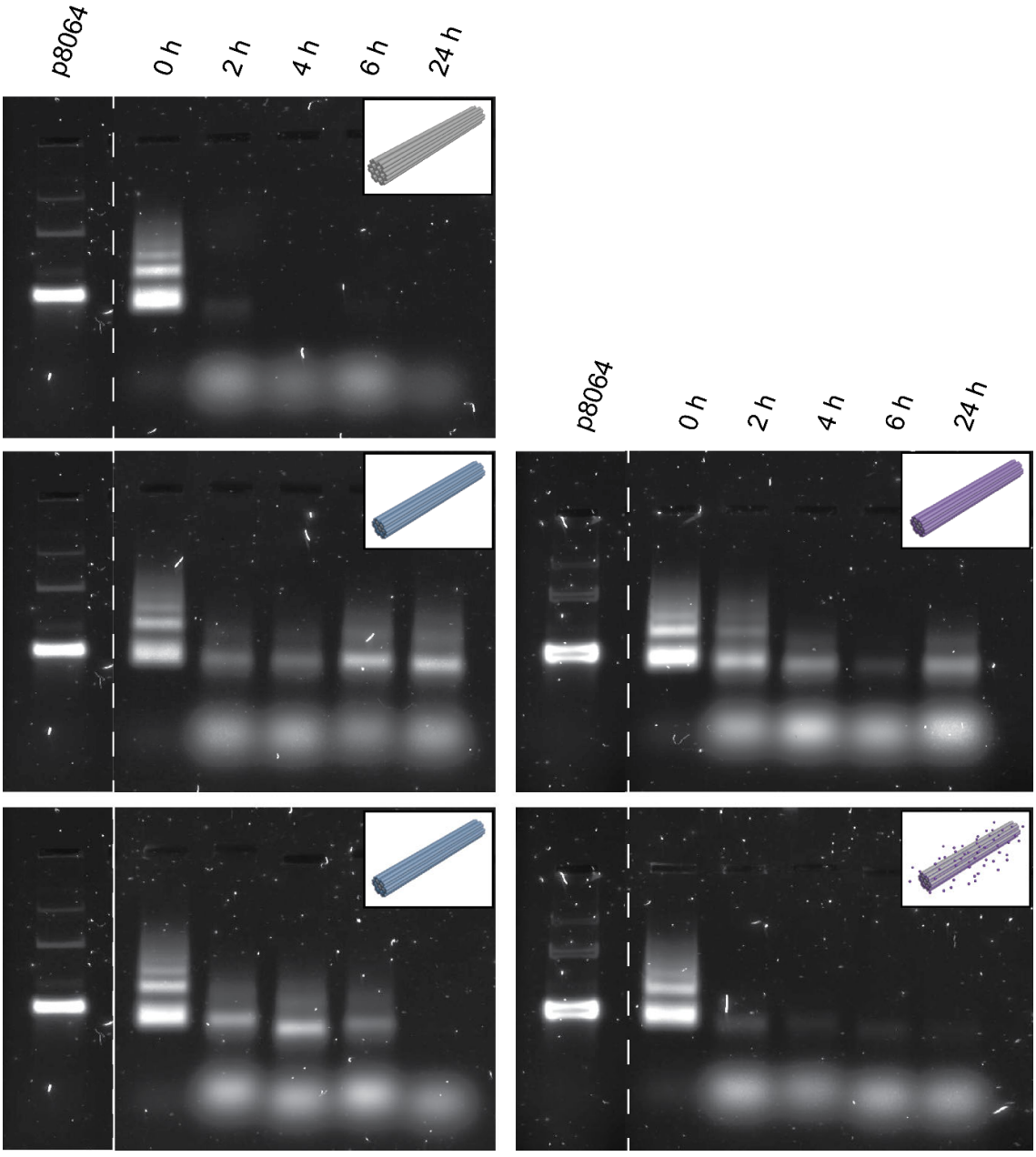

Figure A.5: Comparative DNase I degradation profiles of 24HB DNA origami under various conditions. A series of gel electrophoresis images capturing the stability of the DNA origami over time (0h, 2h, 4h, 6h, 24h) under different experimental setups: (1) bare 24HB DNA origami, (2) 24HB with a standard silica coating, (3) 24HB with standard silica post-glutathione treatment for 2 h, (4) 24HB fully silicified with BTDS silica, and (5) 24HB with BTDS silica post-glutathione treatment for 2 h.

A.6 Fluorescent Silica

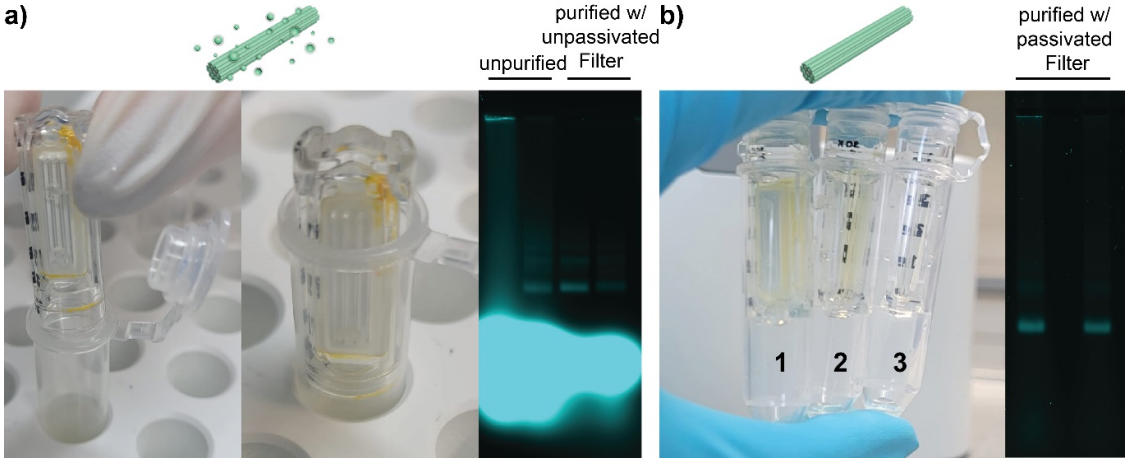

Figure A.6: Fluorescein-silane and 24HB passivation comparison. a) Visualization of non-passivated filter usage showing visible retention (yellow) of fluorescein-silane within the filter, accompanied by an AGE image illustrating inefficient purification of 24HB with an unpassivated filter. b) Sequential images of Amicon tubes during the purification process of 24HB silicified with fluorescein-silane, using passivated filters. The progression from before the first (1) to after multiple (2,3) purification steps illustrates the effectiveness of passivated filters in maintaining sample integrity and decreasing (yellow) fluorescence visibility (at least by eye), confirmed by an AGE image after extensive purification (10 steps).

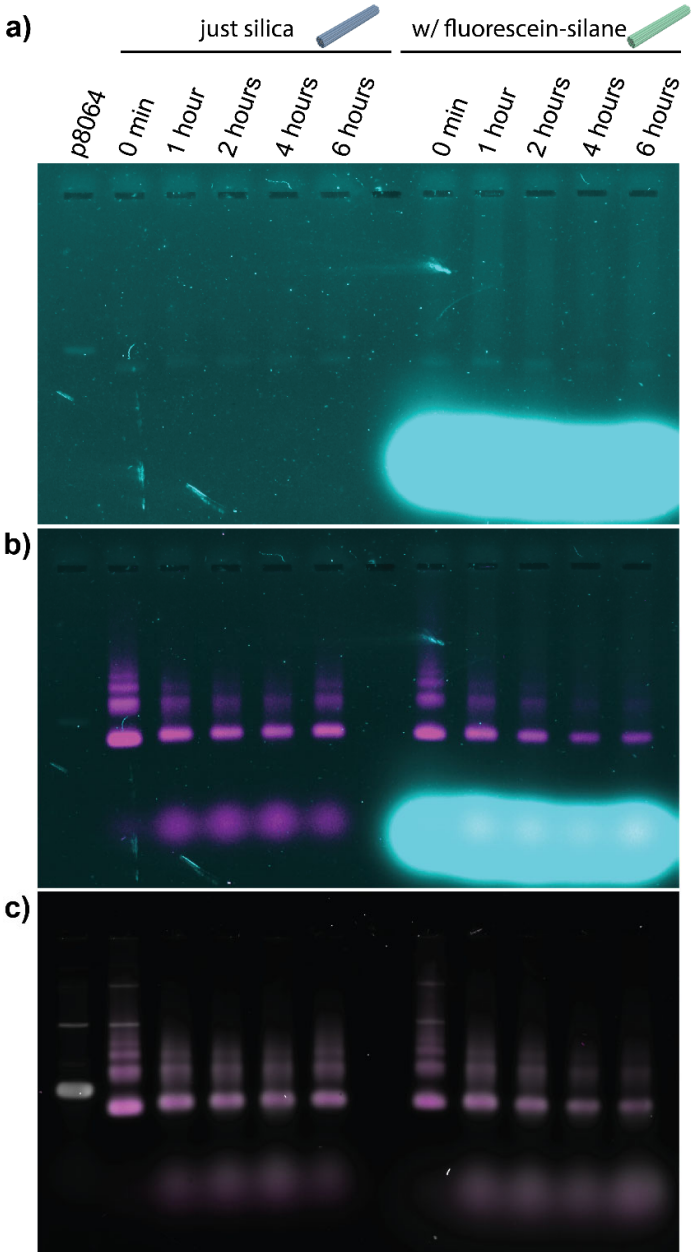

Figure A.7: Gel images displaying DNase I stability test over time (0 min, 1 h, 2 h, 4 h, 6 h) for 24HB DNA origami silicified with fluorescein-silane. a) show the fluorescein channel, b) the overlay of Atto 643 and fluorescein channels confirming the co-localization of fluorescence with the DNA structure, and c) the same gel post-SybrGold staining, verifying the integrity and position of DNA origami.

Appendix B - Experimental Procedures

This chapter provides a detailed account of the experimental procedures employed throughout this research. A comprehensive list of materials used in this thesis, including, chemicals, biological materials, consumables, instruments, software, and buffer compositions, can be found in the appendix (**Appendix C**).

The methods detailed herein encompass a wide range of techniques, some of which were performed by my students or collaborators. These collaborative efforts are clearly indicated. An overview of and protocol for each of these techniques is presented nevertheless to facilitate a thorough understanding of the research procedures used to investigate DONs and their biomineralization processes.

Production of DONs

The production of DONs includes three primary steps: design, folding, and purification. The design of DONs was carried out using the caDNAno software. Once designed, the DNA origami was folded by mixing scaffold strands with a set of staple strands, following a thermal annealing protocol. Purification of the folded structures was achieved through gel electrophoresis to ensure the removal of excess staple strands and other impurities.

Quantification and Quality Control of DONs

A variety of techniques were employed to quantify and assess the quality of the DONs. A Nanodrop spectrophotometer was used to measure DNA concentration. AGE provided a method for visualizing the integrity and size distribution of the DNA origami. To evaluate the hybridization of the handles on the DONs to the complementary fluorescently labelled oligonucleotides, PAGE was employed. TEM and CEM, were used to observe the detailed structural features at high resolution. Energy Dispersive X-ray Spectroscopy (EDX) and SAXS offered further insights into the elemental composition and structural properties. The Zetasizer was utilized to determine the size and zeta potential of the nanostructures,

providing insights into their stability and aggregation behavior. Atomic Force Microscopy (AFM) was used to obtain high-resolution images of the DONs. This technique provided detailed topographical information and allowed for the visualization of individual DONs on a substrate.

Stability Tests

DNase and heat stability tests were conducted to assess the resistance of the DONs to enzymatic degradation. These tests involved exposing the nanostructures to DNase enzymes or high temperatures and analyzing their structural integrity over time.

DNA-PAINT

DNA-PAINT was utilized for super-resolution imaging of the DONs. This technique involved preparation of glass surfaces to facilitate the immobilization and imaging of DONs and the use of fluorescently labeled oligonucleotides that transiently bind to specific sites on the nanostructures, allowing for high-resolution visualization of their spatial organization. These preparations involved cleaning and functionalizing the glass surfaces to enhance their compatibility with the nanostructures.

Production of Biomineralized DNA Origami Hybrid Nanostructures

The production of biomineralized DNA origami hybrid nanostructures is a key aspect of this research and included both calcification and silicification processes. Calcification involved the deposition of calcium phosphate onto the DNA origami, while silicification was carried out under various conditions (normal silicification, dissolvable silica, fluorescent silica) to create silica-coated structures. These hybrid structures were analyzed for their enhanced stability and potential applications in biomedical and materials science fields.

In summary, this chapter details the extensive and meticulous procedures undertaken to produce, analyze, and optimize the DONs, providing a foundation for the subsequent experimental results and discussions.

B.1 Materials

B.1.1 Biological Material

DNA and DNase were bought and used as received. A detailed list of the used biological materials (**Table C.1**) is shown in **Appendix C**.

B.1.2 Buffers and Solutions

All buffers were mixed by me and were used as stated. A detailed list of the used buffers (**Table C.2**) and solutions (**Table C.3**) is shown in **Appendix C**.

B.1.3 Chemicals

Unless stated otherwise, all chemicals were used as received. A detailed list of the used chemicals (**Table C.4**) is shown in **Appendix C**.

B.1.4 Devices

A detailed list of the used devices (**Table C.5**) is shown in **Appendix C**.

B.1.5 Materials

Unless stated otherwise, all materials were used as received. A detailed list of the used materials (**Table C.6**) is shown in **Appendix C**.

B.1.6 Software

The program caDNAno was utilized for DNA origami design, while imaging processes were conducted using Image Lab, LAS-X, and GMS. Data analysis was performed using Fiji, MS Office, NanoDrop Software, and Zetasizer Software. 3D models of the DNA origami were simulated with CanDo and oxDNA and modelled using 3DS Max, and Adobe Illustrator was employed to generate coherent figures. Further references and details regarding these software tools are outlined in **Appendix C** (**Table C.7**).

B.2 Methods

B.2.1 Production of DNA Origami Nanostructures

B.2.1.1 Design of DNA origami nanostructures

All DNA nanostructures were designed using the lattice-based design software caDNAno[46] and simulated with CanDo[38, 48] and oxDNA[49, 50] before ordering. A variety of DON designs were used in this thesis (listed alphabetically):

The 1 Layer Sheet (1LS) has a square lattice-based design and consists of 24 helices, which incorporate 184 staples and the p8064 scaffold. Dimensions are a width, height and length of 57.6 nm, 2.4 nm, and 87 nm respectively.

The 12 helix bundle (12HB) is a thin, long star-shaped rodlike honeycomb lattice based DON with 12 helices formed by 272 staple oligonucleotides and the p8064 scaffold. Dimensions are a width, height and length of 7.2 nm, 12 nm, and 231 nm respectively. It was used in silica-addressability experiments with DNA-PAINT analysis and thus has three handles for the attachment of fluorescent oligonucleotides on one side and biotin anchors on the other.

The 18 helix bundle (18HB) is a square, rod-like honeycomb lattice-based DON with 18 helices formed by formed by 187 staple oligonucleotides and the p8634 scaffold. Dimensions are a width, height and length of 10.8 nm, 12.7 nm, and 162 nm respectively. The 18HB was used in silica-addressability experiments and has three handles for the attachment of fluorescent oligonucleotides on one side and biotin anchors on the other. Furthermore, for some experiments 25 staples in the middle of the DON were removed to make a flexible origami (called 18HB bent or 18HBB).

The 24 helix bundle (24HB) is a short, rod-like honeycomb lattice-based DON with 24 helices formed by 190 staple oligonucleotides and the p8064 scaffold. Dimensions are a width, height and length of 15.4 nm, 13.2 nm and 108 nm respectively. The 24HB was used in a variety of experiments and thus has an assortment of modifications that can be used. Modifications include various handle configurations and internal oligonucleotides with fluorophores.

The 4 Layer Block (4LB) uses a honeycomb lattice design and consists of 40 helices, which incorporate 221 staples using the p8064 scaffold. Dimensions are a width, height and length of 36 nm, 7 nm, and 57 nm respectively.

The Cube is a compact honeycomb lattice-based DNA origami with 112 helices, which incorporates 263 staples and the p8064 scaffold. Dimensions are a width, height and length of 25.2 nm, 26.4 nm, and 25.8 nm respectively. The Cube was mainly used in CEM Experiments and thus does not have any modifications.

The associated sequences and caDNAno designs are listed in the appendices (**Figure C.3** - **Figure C.9**). Width, height and length were calculated with a base-length of 0.34 nm and a base-width of 2.4 nm.

B.2.1.2 Fluorescent Labelling of DNA origami nanostructures

To detect addressability after silicification or later the location of the nanostructures within cells as well as in cell culture media, the DNA origami were fluorescently labelled with Cy5. Therefore, three different strategies were implemented:

The first strategy contains three sequential steps. First, staples on the outside of the DON were elongated on the 3' end with a 15-28 nucleotide sequence (refer to **Appendix C, Table C.12** - **Table C.17**). This sequence was designed to complement various different oligonucleotides, which are equipped with a fluorophore at their 5' end (see **Appendix C**, **Table C.25**). Subsequently, the DONs were assembled using a staple mixture solution containing these three specific staples, following the folding process outlined in the respective section below. In the final step, one of the fluorescent oligonucleotides was introduced after purification (and optional silicification) of the DON in a 10-fold molar excess and hybridized to the elongated staples at 36 °C for 16 h, thereby fluorescently labelling the DONs. Detailed information regarding the modified staples can be found in Appendix C, **Table C.18** - **Table C.23**.

In contrast, the second approach involves only two distinct steps. Firstly, staples located on the periphery of the DONs were elongated, similarly to the first strategy, but on the 5' side

and then directly modified with a fluorophore at this end. Subsequently, the nanostructures were folded using a staple mixture solution containing these specific staples, following the folding protocol outlined in the relevant section below. Consequently, the DONs were directly labeled with a fluorophore via covalent bonds. Additional information pertaining to the fluorophore-linked staples is provided in **Appendix C**, **Table C.25**.

The third method, similarly comprising two steps, adopts a different approach. Instead of targeting staples on the exterior of the origami structures, internal oligonucleotides were chosen and directly modified with a fluorophore at their 5' termini. The DONs were folded using a staple mixture solution containing these specific internal staples, as described in the folding process section. Consequently, the DONs were directly labeled with a fluorophore via covalent bonds. Further details concerning the fluorophore-linked staples are available in **Appendix C**, **Table C.26**.

B.2.1.3 Folding of DNA origami nanostructures

All volumes for applications were calculated by using the dilution equation:

$$c_i \times V_i = c_f \times V_f \qquad \textbf{Eq. B.1}$$

With c_i the initial concentration, V_i the initial volume, c_f the final concentration and V_f the final volume.

1 Layer Sheet (1LS), 4 Layer Block (4LB): The 1LS and 4LB were each folded using 10 nM of the scaffold p8064, 100 nM of each staple strand in buffer containing 1× TAE and 20 mM $MgCl_2$. The mixture was heated to 65 °C and held at this temperature for 30 min, then cooled down to 4 °C over a period of 16 h. All additional handle staples were incorporated during folding. (see **Appendix C**, **Table C.16** and **Table C.12** for specific sequences)

12 Helix Bundle (12HB): The 12HB DNA origami was folded using 20 nM of the scaffold p8064, 200 nM of each unmodified staple strand and 600 nM of each modified staple strand (biotinylated and DNA PAINT staple strands) in buffer containing 50 mM Tris, 20 mM acetic acid, 1 mM EDTA (pH = 8) and 16 mM $MgCl_2$. The mixture was heated to 65 °C and then cooled down to 4 °C over a period of 25 h with a non-linear thermal annealing ramp adapted

from ref.[187]. All additional handle staples were incorporated during folding. (see **Appendix C**, **Table C.17** for specific sequences)

18 Helix bundle (18HB): The 18HB DNA origami structure was folded using 10 nM of the scaffold p8634, 100 nM of each staple strand in buffer containing 1× TAE and 18 mM $MgCl_2$. The mixture was heated to 65 °C and held at this temperature for 30 min, then slowly cooled down to 4 °C over a period of 16 h. To achieve the bent structure in the 18HB, 25 staples from the middle of the 18HB were not included in the folding procedure (see **Appendix C**, **Table C.14** for omitted staples). This results in a 18HB with a single-stranded (scaffold-only) part in its middle where the two fully folded parts can move independently from each other, giving the structure the appearance of being bent. The missing staples were added in a 10-fold molar excess after silicification to straighten the 18HB back out and the mixture was kept at 36 °C for 16 h to guarantee incorporation.

24 Helix Bundle (24HB): The 24HB was folded using 10 nM of the scaffold p8064, 100 nM of each staple strand in buffer containing 1× TAE and 18 mM $MgCl_2$. The mixture was heated to 65 °C and held at this temperature for 30 min, then cooled down to 4 °C over a period of 16 h. All additional handle staples were incorporated during folding. (see **Appendix C**, **Table C.13** for specific sequences)

Cube: The Cube was folded using 10 nM of the scaffold p8064, 100 nM of each staple strand in buffer containing 1× TAE and 20 mM $MgCl_2$. The mixture was heated to 65 °C and held at this temperature for 30 min, then cooled down to 4 °C over a period of 54 h. All additional handle staples were incorporated during folding. (see **Appendix C**, **Table C.15** for specific sequences)

B.2.1.4 Purification of DNA origami nanostructures

To purify the folded DONs from excess staple strands, ultrafiltration was performed. Initially, the folding mixture, usually 2 mL in volume, was evenly distributed between two Amicon Ultra filters (0.5 mL each, 100 K, Millipore, USA), which had been pre-wetted with 500 µL of storage buffer. These filters were then centrifuged at 6,000 rcf for 4 min. Depending on the volume folded, the folding mixture might need to be distributed over

several centrifugation steps, as each filter can only hold 500 µL. This centrifugation process was repeated 10 times and fresh storage buffer (1×TAE, 6 mM $MgCl_2$) was added at each step. Finally, the DNA origami were eluted by inverting the filter, placing it in a new tube and centrifuging the new tube for 3 min at 5000 rpm. The successful folding of structures was confirmed by TEM or AGE analysis as described in the sections below. DNA origami solutions were stored at -20 °C until further use.

To purify silicified samples the sample was added to an Amicon Ultra filter (0.5 mL each, 30 K) which had been pre-wetted with 500 µL of storage buffer. The filter was then centrifuged at 5,000 rcf for 4 min. The silicified DNA origami was eluted right after by inverting the filter, placing it in a new tube and centrifuging the new tube for 3 min at 5000 rpm. It is crucial to note that silica samples should be filtered only once to prevent the silica from getting stuck in the filter. The successful silicification of structures was confirmed by TEM or AGE analysis as described in the sections below. Silicified samples were stored at RT until further use.

B.2.2 Quantification and Quality Control of DONs

B.2.2.1 Nanodrop Spectrophotometer

To measure the concentration of DONs in solution using a Nanodrop spectrophotometer, the following procedure was followed. First, 2 µL of the blanking solution, always the buffer the sample was stored in, was pipetted onto the measurement pedestal, the sample arm was closed, and the “Blank” button in the software was clicked to perform a blank measurement. After the blank measurement, the pedestal and sample arm were wiped clean with a lint-free lab wipe. Subsequently, 2 µL of the sample was pipetted onto the pedestal, the sample arm was lowered, and the “Measure” button in the software was clicked. The concentration in the mass concentration form c[ng/µL] was recorded. The pedestal and sample arm were wiped clean after each measurement. This process was repeated for each sample, beginning with a blank measurement if necessary. Afterwards the concentration was converted from mass concentration form c[ng/µL] to molar concentration form c[nM] with

$$c[M] = \frac{c[{}^{g}/_{L}]}{\langle M_W(bp)\rangle[Da] \times \#bp \times 2} \qquad \textbf{Eq. B.2}$$

Where c[M] is the concentration in molar (mol per liter), c[g/L] is the concentration in grams per liter, $\langle M_W(bp)\rangle[Da]$ is the mean molecular weight of oligonucleotide in Dalton, which is 649 Da for DNA base pairs and #bp is the number of DNA base pairs in the DON.

B.2.2.2 Agarose Gel Electrophoresis

DNA origami samples (10 µL, diluted to 10 nM in 1× TAE buffer with 6 mM $MgCl_2$) were combined with a loading buffer containing orange G and Ficoll. The mixture was then loaded onto a 0.85% agarose gel prepared with 1× TAE and 11 mM $MgCl_2$, and usually stained with 1× SYBR Safe. A reference in the form of the scaffold (10 nM, 10 µL) used for the particular origami was always added in the first well of the gel. Depending on the size of the Gel the electrophoresis was conducted on ice for 90 min at 75 V (for small gels) or 90 V (for large gels) using 1× TAE with 11 mM $MgCl_2$ as the running buffer. Gel imaging was performed using the respective channels of the Typhoon FLA-9000 (GE Healthcare) corresponding to SYBR Safe and the various fluorophores used. Gels that were not stained with SYBR Safe before electrophoresis were post-stained with 1× SYBR Gold in MilliQ for 20 min and usually imaged before and after staining. Analysis of gel images was done using the ImageJ software FIJI.

B.3.2.3 Polyacrylamide Gel Electrophoresis

To determine whether the handles and the complementary fluorescently labelled oligonucleotides would hybridize, Polyacrylamide Gel Electrophoresis was performed. Oligonucleotides (2 mM, 100 µL) were hybridized by maintaining them at 36 °C for 16 h. Subsequently, 10 µL of the hybridized DNA oligos were loaded into a gel prepared with 1× TBE buffer, 12% acrylamide, TEMED, and 0.05% APS. The gel was run at 75 V for 2 h. Post-staining was performed with 1× SYBR Gold in MilliQ water for 30 min. Gel imaging was conducted using the respective channels of the Typhoon FLA-9000 (GE Healthcare) corresponding to SYBR Safe and the various fluorophores used. Analysis of the gel images was completed using the ImageJ software FIJI.

B.2.2.4 Transmission Electron Microscopy

A DNA origami sample (10 nM, 10 µL) was applied to a carbon-coated copper grid that had been plasma-cleaned for 30 s. Bare DNA origami samples were incubated for 90 s, and the

remaining solution was removed with filter paper. The samples were then stained with a 2% uranyl formate solution (5 µL) for 30 s. Silicified DNA origami samples were incubated on the grid for 10 min before the remaining solution was removed using filter paper. The grid was subsequently washed once with MilliQ water and dried in air before imaging. Images were obtained on a Jeol-JEM-1230 TEM operating at an acceleration voltage of 80 kV and were analyzed using the ImageJ software FIJI[188].

B.2.2.5 Cryogenic Electron Microscopy

To investigate the structures via CEM, the DNA origami had to be immobilized on cryo-grids. Similar to TEM grids, cryo-grids require plasma-cleaning to remove hydrocarbon contaminants and render the grid hydrophilic. The Vitrobot was set to 4°C and 90% humidity with a blotting time of 3 s and a blotting force of 5. Ethane was liquefied and condensed for vitrification by cooling it with liquid nitrogen in a heat/cold conductive container.

For sample application, the plasma-cleaned cryo-grid was first attached to the Vitrobot using forceps and loaded with 4 µL of the folded DNA origami through the sample port. After the respective incubation period, which varied for each grid to test different conditions, the cryo-grid was blotted with filters, attached to the blotting pads, and plunge-frozen in the liquid ethane. The grids were then transferred into liquid nitrogen for storage.

Cryo-grids were imaged using either the Titan Halo with a Falcon 3EC camera or the Titan Krios with a Gatan K3 camera.

After CEM data collection, the dataset was processed using RELION for 3D reconstructions. Initially, the raw CEM movies were aligned and averaged into 2D micrographs. The contrast transfer function (CTF) was then estimated, and a few dozen particles were manually picked to calibrate the algorithm. These particles were extracted, averaged into 2D models, and representative 2D classes were selected as templates for auto-picking.

After auto-picking, the particles were extracted, sorted into new 2D classes, and representative classes were selected for the initial 3D model. The initial spherical 3D model was refined using selected 2D classes to create 3D classes. Further refinement and masking focused on relevant areas, increasing the resolution. The final 3D model was post-processed to improve definition.

This work was done completely by BSc student Alexander Ullrich under my supervision.

B.2.2.6 SAXS Analysis

The X-ray data were primarily acquired utilizing an in-house Mo X-ray SAXS setup. Measurements were conducted at an X-ray energy of 17.4 keV, with the X-ray beam focused to a size of 1.0 × 1.0 mm² at the sample position. The sample-to-detector distance was set to 1 meter. Data collection employed a Dectris Pilatus 3 R 300 K CMOS Detector, comprising 487 × 619 pixels with dimensions of (172 × 172) µm² each. Calibration of the sample-to-detector distance and beam center position was performed using silver behenate powder.

This work was done by my collaborator Martina Ober of the Nickel Lab at the LMU.

B.2.2.7 Zetasizer Analysis

The DON sample was prepared by diluting it to 1 mL and at least 1 nM and ensuring proper dispersion by turning the sample on its head a few times. The instrument was initialized, and the measurement parameters were set up as: Material – Protein, Dispersant – 6 mM $MgCl_2$, Temperature – 25 °C, Equilibration Time – 300 s, runs per sample – 3 measurements with 20 runs a 20 s. The sample was loaded into the disposable folded capillary cell, and the measurement process was started. An electric field is applied to the sample by the EDX/ Zetasizer, and the electrophoretic mobility of the particles was measured to calculate the zeta potential. The results provided by the instrument's software interface were analyzed with the same software.

B.2.2.8 Atomic Force Microscopy

AFM scans in aqueous solution (AFM buffer: 40 mM Tris, 2 mM EDTA, 12.5 mM Mg(OAc)2·4 H2O) were performed using a NanoWizard® 3 ultra AFM (JPK Instruments AG). For sample immobilization, a freshly cleaved mica surface (Quality V1, Plano GmbH) was incubated with a 10 mM solution of NiCl2 for 3 min. The mica was then washed three times with ultrapure water to remove unbound Ni2+ ions and blow-dried with air. The dried mica surface was incubated with a 1 nM sample solution for 3 min and subsequently washed three times with AFM buffer. Measurements were conducted in AC mode over a scan area of 3 × 3 µm using a BioLeverMini cantilever (vres = 110 kHz in air / 25 kHz in fluid, kspring = 0.1 N/m, Bruker

AFM Probes). Leveling, background correction, and extraction of height histograms of the obtained AFM images were performed using the Gwyddion software (version 2.60).

This work was done by my collaborator Michael Scheckenbach of the Tinnefeld Lab at the LMU.

B.2.2.9 DNase Stability Tests

DNase stability tests were conducted according to established literature protocols[189]. Briefly, (silicified) DNA origami (10 nM, 45 µL in 1× TAE buffer containing 3 mM $MgCl_2$) were mixed with 10× DNase I buffer (5 µL, NEB) and then evenly divided into 1.5 mL tubes, and added to a thermo mixer (Eppendorf) at 37 °C. The lid was kept closed unless DNase I was added. DNase I (1 µL, 0.1 U/µL, NEB) was then added consequentially to one tube each to react for predetermined amounts of time (15 min, 30 min, 60 min, 240 min, etc.). As a reference, 1 µL nuclease free water instead of DNase I was added to the last tube (0 min reaction time). Reactions were subsequently quenched by putting the tubes on ice. Samples were then analyzed by AGE and TEM.

B.2.3 DNA PAINT

B.2.3.1 Glass surface preparation

For the optical microscopy experiments, the DNA origami sample was immobilized on Nunc™ LabTek™ II chambers (Thermo Fisher, USA). The chambers were first cleaned with 500 µL of 1% HellmanexIII™ solution (Sigma Aldrich, USA) overnight and washed thoroughly with water, then three times with 1× PBS buffer. Then the surfaces were passivated with 100 µL BSA-biotin (0.5 mg/mL in PBS, Sigma Aldrich, USA) for 15 min and washed three times with 1× PBS buffer. The passivated surfaces were incubated with 100 µL streptavidin (0.25 mg mL-1 in PBS, S4762, Sigma Aldrich, USA) for 15 min and washed three times with 1× PBS buffer. The sample solution with DNA origami featuring several staple strands with biotin modifications on the base was diluted to approximately 200 pM in 2× PBS buffer containing 500 mM NaCl and incubated in the chambers for 5 to 15 min. Sufficient surface density was probed with a TIRF microscope.

B.2.3.2 Measurements

DNA PAINT measurements were performed using a custom-built total internal reflection fluorescence (TIRF) microscope. The setup included an inverted microscope (IX71, Olympus) with an actively stabilized optical table (TS-300, JRS Scientific Instruments) and a nosepiece (IX2-NPS, Olympus) for drift suppression. The sample was excited at 644 nm using a 150 mW laser (iBeam smart, Toptica Photonics), and the fluorescence light was filtered with an emission filter (ET 700/75, Chroma). Image stacks were recorded by an electron multiplying charge-coupled device camera (Ixon X3 DU-897, Andor) controlled by Micro-Manager 1.4.

Measurements were conducted at approximately 1.8 kW/cm² at 640 nm in TIRF illumination, with an exposure time of 100 ms and 18,000 frames taken over 30 min. Imaging used a 2× PBS buffer with 500 mM NaCl and 0.05% Tween20®, and an imager concentration of 10 nM. The 8 nt imager oligonucleotide, labeled with Atto655 at the 3'-end, was obtained from Eurofins Genomics GmbH

DNA PAINT raw data were analyzed using the Picasso software package. The TIF-movies were first processed with the "localize" software to fit the centroid positions of single point spread functions (PSF) using maximum likelihood estimation (MLE). The minimal net gradient was set to 5000 with a box size of 5 pixels. The localizations were further processed with the "render" software, and x-y-drift corrections were applied using RCC drift correction.

This work was done by my collaborator Michael Scheckenbach of the Tinnefeld Lab at the LMU.

B.2.4 Production of biomineralized DNA Origami hybrid nanostructures

B.2.4.1 Equations

First a few equations that are needed to accurately mix the ingredients for silicification. Calculation of the concentration of the phosphate in the DNA backbone in a given solution by

$$c_{PO_4^{3-}} = c_{DNA-bases} = c_{origami} \times \#bp \times 2 \qquad \textbf{Eq. B.3}$$

Where $c_{PO_4^{3-}}$ is the concentration of phosphate, $c_{DNA-bases}$ is the concentration of the DNA bases, $c_{origami}$ is the concentration of the DON, which can be measured with a nanodrop, and #bp is the number of basepairs the DON consists of, also readable as the length of the scaffold.

Calculation of the needed volume of TMAPS:

$$V_{TMAPS} = \frac{c_{PO_4^{3-}} \times V_{Origami}}{c_{TMAPS}} \times a \qquad \textbf{Eq. B.4}$$

Where V_{TMAPS} is the volume of TMAPS needed in the silicification, $c_{PO_4^{3-}}$ is the concentration of the phosphate groups as calculated in Eq. B.3, $V_{Origami}$ is the volume of DON solution used in the silicification, c_{TMAPS} is the concentration of TMAPS, which is 3.6 M in undiluted form, but was normally adapted via dilution in MeOH, if the resulting TMAPS volume was not large enough for pipetting, and a is the desired ratio of TMAPS molecules to the phosphate groups, usually a molar ratio of 1:5 (phosphate groups:TMAPS) was used.

Calculation of the needed volume of TEOS:

$$V_{TEOS} = \frac{c_{PO_4^{3-}} \times V_{Origami}}{c_{TEOS}} \times b \qquad \textbf{Eq. B.5}$$

Where V_{TEOS} is the volume of TEOS needed in the silicification, $c_{PO_4^{3-}}$ is the concentration of the phosphate groups as calculated in Eq. B.3, $V_{Origami}$ is the volume of DON solution used in the silicification, c_{TMAPS} is the concentration of TEOS, which is 4.48 M in undiluted form, but was normally adapted via dilution in MeOH, if the resulting TEOS volume was not large enough for pipetting, and b is the desired ratio of TEOS molecules to the phosphate groups, usually a molar ratio of 1:12.5 (phosphate groups:TEOS) was used.

Calculation of the needed volume of BTDS:

$$V_{BTDS} = \frac{c_{PO_4^{3-}} \times V_{Origami}}{c_{BTDS}} \times c \qquad \textbf{Eq. B.6}$$

Where V_{BTDS} is the volume of BTDS needed in the silicification, $c_{PO_4^{3-}}$ is the concentration of the phosphate groups as calculated in Eq. B.3, $V_{Origami}$ is the volume of DON solution used in the silicification, c_{BTDS} is the concentration of BTDS, which is 2.16 M in undiluted form, but was normally adapted via dilution in MeOH, if the resulting BTDS volume was not large enough for pipetting, and c is the desired ratio of BTDS molecules to the phosphate groups, usually a molar ratio of 1:12.5 (phosphate groups:BTDS) was used.

B.2.4.2 Silicification in solution

Method 1 (3-7 days): Using the approach Nguyen[9] et al devised to silicifiy a sample of DNA Origami, a 80 µL, 20 nM solution of purified origami in 3 mM $MgCl_2$ was used. The sample was placed in a thermo-shaker set to 21°C. TMAPS (TCI, USA) (50% in methanol) was then added to the sample, diluted as necessary (according to Eq. B.4). The mixture was left in the thermo-shaker at 350 rpm for 1 minute. Subsequently, TEOS (Sigma Aldrich, USA) (50% in methanol) (volume according to Eq. B.5) was added, and the sample was shaken at 350 rpm for 15 min. The sample was then left at 21 °C for 3 to 7 days to allow the silica shell to grow.

Method 2 (SAXS): 110 µL of purified 24HBs (270 nM) were mixed with 0.67 µL of TMAPS and shaken at 350 rpm for 1 min in an Eppendorf tube. 2.67 µL of TEOS were added to the tube, followed by shaking for another 15 min. Finally, the solution was filled into a sample cell for SAXS, which tumbles slowly (50 rpm). This way, molar ratios of (1:5:12.5) of phosphate groups:TMAPS:TEOS, were achieved, respectively.

For the 4-LB structures, the TMAPS-only containing origami solution was filled into the SAXS tumbling chamber after shaking at 350 rpm for 1 min in an Eppendorf tube. Subsequently, TEOS (50% in methanol) was added 15 min later directly into the SAXS tumbling chamber and incubated directly in the sample chamber to reduce aggregation.

Method 3 (4-6 h): Adapting the protocol from method 2, unless stated otherwise, all DNA origami solutions used had a concentration of 50 to 200 nM and were dispersed in 1× TAE buffer containing 3 mM $MgCl_2$ (50 µL total reaction volume). The sample was placed on a thermo shaker and the first silica precursor TMAPS (TCI, diluted 1:19 in methanol) was added to the sample in 5-fold molar excess to the number of nucleobases (volume according

to Eq. B.4). After one minute of shaking at 300 rpm at 21 °C, TEOS or BTDS (Sigma Aldrich, diluted 1:9 in methanol) in 12.5-fold molar excess to the number of nucleobases was added to the solution (Volume according to Eq. B.5 or Eq. B.6). The sample was then transferred to a tube revolver rotator (Thermo Scientific) and rotated at 40 rpm at 21 °C for 4 h to 6 h to reach the "maximally condensed state"[78]. Following this, the silicified sample was purified once via ultrafiltration (Amicon filter, 30kDa).

B.2.4.3 Silicification on surface:

For surface silicification, the well-established literature protocol by Fan and co-workers was adapted[72, 74]. DNA origami samples were either immobilized on glass slides (see "Glass surface preparation") or on mica. Initially, a precursor solution was prepared by adding 1 mL of 1× TAE–Mg^{2+} buffer (40 mM Tris, 2mM EDTA-Na_2, 12.5 mM $MgAc_2$, pH=8.0) to a 10 mL glass bottle with a suitably-size magnet and then slowly adding 20 µL of TMAPS (50% (wt/wt) in methanol). This solution was then stirred vigorously for 20 min at room temperature. After that, 20 µL of TEOS were slowly added and the resulting solution was again stirred for 20 min at room temperature. Finally, 400 µL of the precursor solution were immediately transferred to the glass slide containing the immobilized DNA origami. Alternatively, mica slides containing adsorbed DNA origami were placed on top of a large precursor droplet on a small petri dish as described in detail in the literature[74]. The glass slide or petri dish was closed airtight and was then gently shaken for 60 min at 40 rpm at room temperature, the samples were left undisturbed for up to 5 days. Afterwards the samples were washed once with 400 µL 80% ethanol and once with 400 µL MilliQ water. Then the samples were stored with a sufficient amount of MilliQ to prevent drying and the samples were sealed airtight again until analysis.

B.2.4.4 Silica Customization:

Silicification with BTDS – Adapting the previous protocol (method 3), unless stated otherwise, all DNA origami solutions used had a concentration of 50 and were dispersed in 1× TAE buffer containing 3 mM $MgCl_2$ (50 µL total reaction volume). The sample was placed on a thermo shaker and the first silica precursor TMAPS was added to the sample in 5-fold molar excess to the number of nucleobases. After one minute of shaking at 300 rpm at 21

°C, BTDS in 12.5-fold molar excess to the number of nucleobases was added to the solution. The sample was then transferred to a tube revolver rotator (Thermo Scientific) and rotated at 40 rpm at 21 °C for 4 h to reach the "maximally condensed state"[78]. Following this, the silicified sample was purified once via ultrafiltration (Amicon filter, 30kDa). For this purpose, the silicified sample was loaded into a pre-washed filter unit and 400 µL of fresh MilliQ water were added. The filter was then centrifuged for 4 min at 5000 rpm. Finally, the DNA origami were eluted by inverting the filter, placing it in a new tube and centrifuging the new tube for 3 min at 5000 rpm.

Silicification with Fluorophores – The silicified DNA origami nanorods (25 nM) were added to a labeled 0.5 mL Eppendorf tube, which was then placed on a thermoshaker operating at 350 rpm at RT. Subsequently, fluorescent silane (10 mM) was added to the tube, and it was shaken for 15 min. The tube was left overnight on a rotator for 16 h. On the following day, the purification process was initiated by adding 500 µL of 5% pluronic F-127 (Sigma Aldrich, US) solution to a 30 kDa Amicon ultrafilter, which was then incubated for 30 min, to passivate it. The pluronic solution was discarded without centrifugation, and three washes were performed with 500 µL of buffer (1× TAE, 6 mM $MgCl_2$) for each cycle, without centrifugation. Subsequently, 500 µL of buffer was added to the ultrafilter, followed by centrifugation at 5000 rcf for 4 min. The supernatant was discarded, and this step was repeated with the sample, followed by 350 µL of buffer. The washing process was repeated a total of 15 times. For elution, the filter was inverted and placed in a new collection tube, followed by centrifugation. The purified sample was assessed by electrophoresis on a 0.85% agarose gel without the addition of SybrSafe, which was run for a minimum of 2 h at 90 V for a large gel or 75 V for a small gel. The gel was scanned using a Typhoon multi-mode laser imaging system. After gel scanning, the agarose gel was immersed in a 1× SybrGold solution (100 mL) for 30 min. The gel was then imaged once again using the Typhoon imaging system, and the obtained images were compared to assess the efficacy of the purification process.

B.2.5 DNA origami crystal formation

Octahedral DNA origami monomers were folded using 20 nM of the scaffold p7249 and 100 nM of each staple strand in a buffer containing 5 mM Tris, 1 mM EDTA (pH 8), and 12.5 mM

$MgCl_2$. Two mixtures with different end staples (type A or type B) were prepared, heated to 95 °C for 1 minute, and cooled to 20 °C over 20 h. The folded nanostructures were purified via ultrafiltration using Amicon centrifugal filter units with a 100 kDa cut-off, centrifuged at 2,000 rcf for 20 min, and repeated 5 times with fresh 1× TAE, 7.5 mM $MgCl_2$ buffer.

Silicification of the monomers was performed with 50 µL of DNA origami sample at 50 nM in 1× TAE, 7.5 mM $MgCl_2$ buffer for 4 h on a rotator, followed by ultrafiltration to remove excess silica. Polymerization into crystalline lattices involved mixing the two types (A and B) of silicified monomers in 1× TAE buffer with 20 mM $MgCl_2$, heating to 48 °C for one hour, and gradually cooling to 20 °C (-1 °C per 150 min).

For TEM grid preparation, 10 µL of the sample was taken from the bottom of the tube and applied to a grid that had been plasma-cleaned for 30 s. The sample was incubated on the grid for 45-55 min, excess solution was removed with filter paper, the grid was washed twice with 5 µL of MilliQ water each, and air-dried before imaging.

This work was completed by my colleague Anna Baptist of the Heuer-Jungemann Lab at the MPI of Biochemistry.

B.2.6 Statistical Analysis

B.2.6.1 Assessment of handle availability by gel image analysis:

To evaluate the availability of handles using AGE, the brightness of the bands corresponding to both bare and silicified DNA origami in the SybrSafe and Cy5 channels was analyzed. The bands in each channel were selected by drawing a region of interest around them using ImageJ software[188], and a brightness histogram for the selected area was generated. The mean brightness value from each histogram was extracted and normalized to the SybrSafe brightness value for both channels (s. Figure 3.1 for an idea how this analysis works). Subsequently, the normalized mean Cy5 brightness values were compared between the bare and silicified DNA origami, with the values normalized to the Cy5 brightness value of the bare DNA origami. The data was obtained by averaging the values from six gels, and the results were presented in a histogram, with the standard error of the mean represented as error bars. Each data point was based on six gels. Statistical significance was determined using a Student's t-test in Microsoft Excel.

B.2.6.2 DNA-PAINT kinetics on 1LS:

The acquired DNA-PAINT raw data were processed using the Picasso software package[105]. Initially, the TIF movies were analyzed using the "localize" tool within Picasso. Maximum likelihood estimation (MLE) was employed to fit the centroid positions of single point spread functions (PSFs) of individual imager strands, utilizing a minimal net gradient of 2500 and a box size of 7 for the 1LS measurements. The localized points were then further processed with the "render" tool, where X-Y drift correction was performed using the RCC drift correction method. For co-localization studies, the green labels on the 1LS origami were first localized, and the green localizations from the initial frame were converted into pick areas with a radius of 3 camera pixels using a custom Python script. After aligning the green and red localizations, the green pick areas were applied to the red localizations to ensure the selection of only co-localized binding events on the 1LS DNA origami. To exclude impurities and non-specific binding events, the red picks were filtered for a minimum number of localizations—10 for sequence A, and 25 for sequences B and C. The statistics from these pick regions were then exported for further analysis. The sample sizes of picked single docking sites on bare 1LS were as follows: sequence A had 947 in red vs. 1214 in green, sequence B had 970 in red vs. 1211 in green, and sequence C had 537 in red vs. 888 in green. For silicified 1LS, the sample sizes were: sequence A with 803 in red vs. 1089 in green, sequence B with 903 in red vs. 1216 in green, and sequence C with 652 in red vs. 1145 in green.

This work was done by my collaborator Michael Scheckenbach of the Tinnefeld Lab at the LMU.

B.2.6.3 DNA-PAINT kinetics on 3×6 12HB and 3×1 12HB:

The acquired DNA-PAINT raw data were processed using the Picasso software package[105]. Initially, the TIF movies were analyzed using the "localize" tool within Picasso. Maximum likelihood estimation (MLE) was employed to fit the centroid positions of single point spread functions (PSFs) of individual imager strands, utilizing a minimal net gradient of 2500 and a box size of 7 for the 12HB measurements. The localized points were then further processed with the "render" tool, where X-Y drift correction was performed using the RCC drift

correction method. Individual docking sites were identified, and the statistics for these pick regions were exported for further analysis. The sample sizes of selected single label spots were as follows: for bare 3×6 12HB, 3101 spots were picked (with 600 after 2 h incubation in 1× TAE), and for silicified 3×6 12HB, 1653 spots were picked (with 2859 after 2 h incubation in 1× TAE). For bare 3×1 12HB, 794 spots were picked (with 699 after 2 h incubation in 1× TAE), and for silicified 3×1 12HB, 1276 spots were picked (with 2024 after 2 h incubation in 1× TAE).

This work was done by my collaborator Michael Scheckenbach of the Tinnefeld Lab at the LMU.

B.2.6.4 18HB bending angle:

To analyze the bending angles of the 18HB, TEM images of bent and straightened DNA origami were examined using the Image J software[188]. The angle tool was used to measure the angle the structures, and a dataset of over 480 structures was collected for each configuration of the DNA origami. The angles were sorted into bins with a size of 15 °, and each bin was normalized to the total number of data points in the corresponding set.

B.2.6.5 18HB bent BTDS Glutathione Breaking Analysis:

To evaluate the percentage of aggregation in each gel, the brightness of the bands corresponding to the wells and the bands within each sample were analyzed. The bands and wells in each channel were selected by drawing a region of interest around them using ImageJ software[105], and a brightness histogram for the selected area was generated. The mean brightness value from each histogram was extracted (as illustrated in Figure 3.1) and the percentage of aggregation for each sample was calculated using the formula:

$$A = \frac{\mu_w}{\mu_w + \mu_B} \qquad \textbf{Eq. B.9}$$

where A stands for Aggregation percentage, μ_w represents the mean gray value of the well and μ_b represents the mean gray value of the band.

This process was meticulously repeated for every sample across all gels. The resulting data were then normalized to draw meaningful conclusions about the aggregation behavior of the silicified DONs.

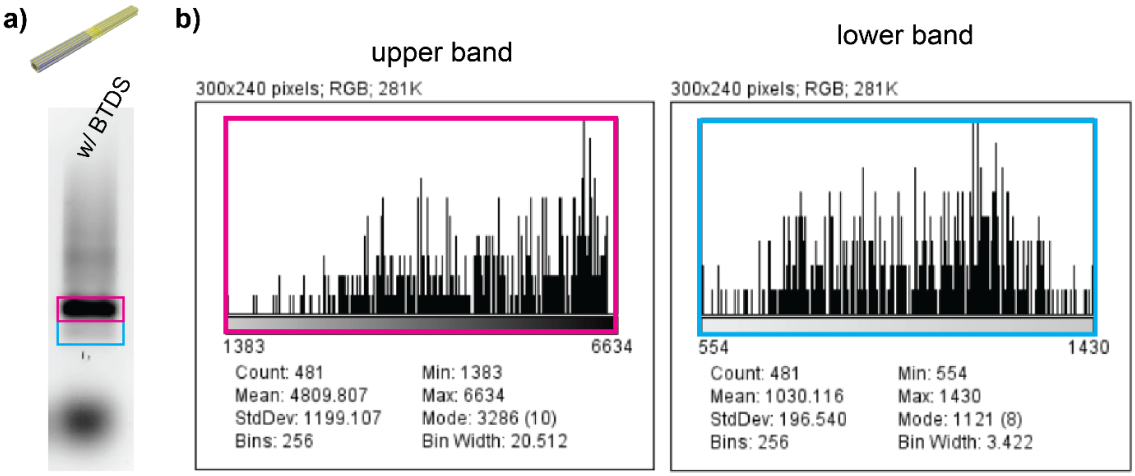

Figure B.1: Example-Analysis of 18HB bent silicified variations after DNase I testing for 6 h. a) Gel electrophoresis image showing the migration of silicified 18HB bent after silicification then adding the middle staples and then adding BTDS. b) Histograms corresponding to selected regions (highlighted in boxes) from the gel image. The histograms provide metrics such as mean gray value, standard deviation, and minimum/maximum values for quantifying the brightness of the bands, which correlate to the availability and aggregation of handles post-silicification.

Appendix C - Technical Data

C.1 Biological material

Table C.1: Biological materials used in this work including the Cat. Nr. and manufacturer.

Biological material	Cat. Nr.	Manufacturer
DNase 1	M0303S	NEB, Ipswich, US
Oligonucleotides (Staples)	-	IDT, Iowa, US
Oligonucleotides (Staples)	-	Eurofins Scientific, Luxembourg
ssDNA scaffold type p8064	M1-51	Tilibit nanosystems, Garching, GER

C.2 Reagents

C.2.1 Buffers

Table C.2: Buffers used in this work including the composition or CAS or Cat. Nr., pH-value, and the manufacturer.

Buffer	Composition/CAS/Cat Nr.	pH	Manufacturer
DNase 1 Reaction Buffer (10×)	B0303S	7,6	NEB, Ipswich, US
PEG Buffer (2×) (1 L)	150 g PEG 8000 20 mL 50x TAE 29,2 g NaCl UPW (fill up to 1 L)	-	AG Heuer-Jungemann According to Wagenbauer, et al.[190]
TAE Buffer (50×) (1 L)	242,28 g Tris 57,19 mL Acetic Acid 100 mL ETDA UPW (fill up to 1 L)	8,0	AG Heuer-Jungemann

C.2.2 Solutions

Table C.3: Solutions used in this work including the composition or CAS or Cat. Nr., pH-value, and the manufacturer.

Solution	stock / final concentration	pH	Manufacturer

DPBS (200 mL)	1 tablet PBS 20 mg $CaCl_2$ (- / 0,9 mM) 20 mg $MgCl_2*6H_2O$ (0,5 mM) UPW (fill up to 200 mL)	7,5	AG Fässler
$MgCl_2$ stock (1 M) (500 mL)	101,7 g $MgCl_2$ * $6H_2O$ UPW (fill up to 500 mL)	-	AG Heuer-Jungemann
PBS	1 tablet / 200 mL	7,6	Sigma-Aldrich, St. Louis, US
Trypan Blue	72-57-1	7,5	Sigma-Aldrich, St. Louis, US

C.3 Chemicals

Table C.4: Chemicals used in this work including the CAS or Cat. Nr. and manufacturer.

Chemical	CAS/Cat. Nr.	Manufacturer
Acetic acid	64-19-7	Thermo Fischer, Waltham, US
Agarose (UltraPure™)	15510-027	Thermo Fischer, Waltham, US
BTDS	56706-10-6	Abcr, Karlsruhe, GER
BTSPTS	40372-72-3	Sigma Aldrich, St. Louis, US
Calcium chloride	10043-52-4	Merck, Darmstadt, GER
EDTA	6381-92-6	Sigma-Aldrich, St. Louis, US
Ethanol (80%)	64-17-5	Sigma-Aldrich, St. Louis, US
Methanol	67-56-1	Thermo Fischer, Waltham, US
Orange G (6× Loading Dye)	0318.1	Carl Roth, Karlsruhe, GER
PBS	041M8227	Sigma-Aldrich, St. Louis, US
PEG 8000	25322-68-3	Carl Roth, Karlsruhe, GER
Pluronic F-127	9003-11-6	Sigma-Aldrich, St. Louis, US
Potassium dihydrogen phosphate	7778-77-0	Merck, Darmstadt, GER
Sodium chloride	7647-14-5	VWR Chemicals, Radnor, US
Sodium hydroxide	1310-73-2	Merck, Darmstadt, GER
SYBR Gold DNA gel stain	S11494	Thermo Fischer, Waltham, US
SYBR Safe DNA gel stain	S33102	Thermo Fischer, Waltham, US
TEOS	78-10-4	Sigma-Aldrich, St. Louis, US
TMAPS	35141-36-7	TCI, Tokyo, Japan
Tris	77-86-1	Merck, Darmstadt, GER
Ultrapure water (Milli-Q® quality)	-	Merck, Darmstadt, GER
UFO	16984-59-1	Science Services, Munich, GER
2-Propanol	33539	Thermo Fischer, Waltham, US

C.4 Devices

Table C.5: Devices used in this work including the type and the manufacturer.

Device	Type	Manufacturer
Centrifuge	Allegra X15R	Beckman Coulter, Brea, US
Centrifuge	Multifuge 1L-R	Heraeus, Hanau, GER
Confocal microscope	TCS SP5	Leica, Wetzlar, GER
CO_2 incubator	HERAcell 240i	Thermo Fischer, Waltham, US
GE power source	Basic Power Supply	Bio-Rad, Hercules, US
Freezer (-20 °C)	LGUex 1500 MediLine	Liebherr, Ochsenhausen, GER
Freezer (-80 °C)	HERAFreeze Basic	Thermo Fischer, Waltham, US
Gel documentation system	Gel Doc EZ Imager	Bio-Rad, Hercules, US
Ice machine	106262	Ziegra, Isernhagen, GER
Magnetic stirrer	Combimag Reo	IKA, Staufen, GER
Microwave	Kor63-D7	Daewoo, Seoul, South Korea
Mixer	Analog Vortex Mixer	VWR, Radnor, US
Nanoimager	S	ONI Ltd., UK
pH Meter	inoLab pH7110	WTW, Weilheim, GER
Phospho-imager	Tyhoon FLA 9000	GE Healthcare, Boston, US
Pipetting aid	accu-jet pro	Brand, Wertheim, GER
Pipetting aid	Pipetboy	Integra, Biebertal, GER
Pipetting aid	Pipetman	Gilson, Middleton, US
Pipetting aid	Xplorer plus	Eppendorf, Hamburg, GER
Plasma Cleaner	PDC-32G-2	Harrick Plasma, Ithaca, US
Precision scale	MSE225P-100-DU	Satorius, Göttingen, GER
Refrigerator (+4 °C)	KTL15NWFA	Bosch, Gerlingen, GER
Refrigerator (+4 °C)	profi line	Liebherr, Ochsenhausen, GER
Scale	LP3200D	Satorius, Göttingen, GER
Shaker	Mixer compact	Eppendorf, Hamburg, GER
Shaker	Skyline S4	Elmi, Newbury Park, US
Shaker	ThermoMixer C	Eppendorf, Hamburg, GER
Sonicator	Sonorex RK100	Bandelin, Berlin, GER
Spectrophotometer	NanoDrop ND-1000	Peqlab, Erlangen, GER
Tabletop centrifuge	5417C	Eppendorf, Hamburg, GER

Tabletop centrifuge	Mini star	VWR, Radnor, US
TEM	JEM-1230	Jeol, Tokyo, Japan
TEM camera	Orius SC 1000	Gatan, Inc., Pleasanton, US
Thermocycler	Biometra 43	Analytikjena, Jena, GER
Transilluminator	M-15V	UVP, Upland, Us
Vacuum centrifuge	Speed concentrator	Bachofer, Reuttlingen, GER
Vacuum pump	BVC 21	Vacuubrand, Olching, GER
Vortex Mixer	Analog Vortex Mixer	VWR International, Radnor, US
Water bath	Pura 22	Julabo, Seelbach, GER
Water purification system	Milli-Q Advantage	Merck, Darmstadt, GER

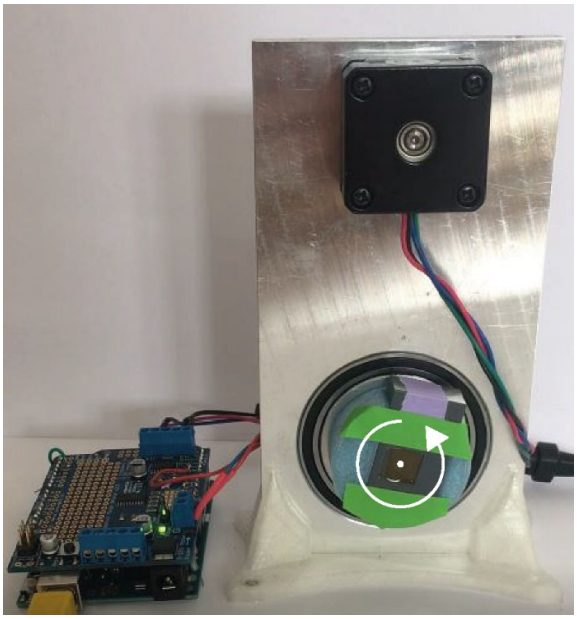

Figure C.1: Photograph of the custom-built sample tumbler for SAXS measurements, which rotates the sample with ~ 1 round/s around the X-ray beam axis to avoid sedimentation of origami with SiO_2[78].

C.5 Materials

Table C.6: Materials used in this work including the type and the manufacturer.

Material	Type	Manufacturer
AFM Mica	Quality V1	Plano GmbH, Wetzlar, DE
Centrifuge filter	Amicon Ultra Ultracel 100 K	Merck, Darmstadt, GER
Centrifuge tubes	15 and 50 mL	Corning, Corning, US
Counting chamber	Neubauer Improved 0,0025 mm^2	Marienfeld, Lauda, GER
Cryogenic vial	430489 (2 mL)	Corning, Corning, US
Filter (0.22 µm)	Millipak Express 40	Merck, Darmstadt, GER
Filter (0.2 µm)	Supor Membrane	PALL, New York, US
Filter (0.22 µm)	Ultrafree - MC - GV Durapore	Merck, Darmstadt, GER
GE system	Easycast B1A-BP	Thermo Fischer, Waltham, US
GE system	Owl Easycast B2	Thermo Fischer, Waltham, US
Gloves	Semper Guard Nitrile Powder Free	SATRA Technology Centre, Kettering, UK
Parafilm	PM-996	Starlab, Hamburg, GER
PCR Strips (Caps)	8 Domed Caps	Kuhnle GmbH, Karlsruhe, GER
PCR Strips (Tubes)	8 Thin Wall 0.2 mL, clear	Kuhnle GmbH, Karlsruhe, GER
Pipette tips	costar Stripette (5, 10, 25 mL)	Corning, Corning, US
Reaction tube	0.5, 1.5 and 2 mL	Eppendorf, Hamburg, GER
Syringe	10 mL, non-sterile	Thermo Fischer, Waltham, US
Syringe	1 mL, Omnifix F Solo Luer-Lock	B. Braun, Puchheim, GER
TEM grid	carbon, 300 mesh, Cu	TED Pella, Inc., Redding, US

C.6 Software

Table C.7: Software used in this work including the version and the manufacturer.

Software	Version	Manufacturer
Adobe Illustrator	2024	Adobe, San Jose, US
CaDNAno	v0.2.3	Douglas et al. 2009[46], Dana Farber Cancer Institute, US
CaDNAnoSQ	v0.2.4	Douglas et al. 2009[46], Dana Farber Cancer Institute, US
CaDNAno2	2.3.0	Wyss Institute, Havard University, US
FPbase	-	Lambert 2019[191], Harvard Medical School, Boston, MA, USA
GMS	3	Gatan, Inc., Pleasanton, US
ImageJ	Fiji	Schindelin et al. 2012[188], MPI-CBG, GER
Image Lab	6.0.1	Bio-Rad, Hercules, US
IMOD	4.63	Nokia Corporation, Espoo, FIN
LAS-X	3.7.4.23463	Leica, Wetzlar, GER
MS Office	2107	Microsoft Corporation, Redmond, US
Nanodrop Software	-	Thermo Fisher Scientific, Waltham, US
NUPACK	Cloud alpha	Pierce et al. 2022[51, 52], California Institute of Technology, US
oxDNA	-	Sulc et al. 2014[49, 50], Arizona State University, US
RELION	3.1.1	MRC Laboratory of Molecular Biology[192], Cambridge, UK
SerialEM	4.1	University of Colorado[193], Boulder, US
UCSF Chimera	1.3	University of California[194], US
UCSF Chimera	Alpha 1.12	University of California[195], US
VNC Viever	VE4.6.3	RealVNC Ltd., Cambridge, UK
Zetasizer Software	8.02	Malvern Panalytical[147, 196], Worcestershire, UK
3DS Max	2020	Autodesk, San Francisco, US

C.7 Thermocycler Programs

C.7.1 DNA Origami Folding

Table C.8: Folding programs used in this work including the steps, temperature, time, and repetition (h = hours, m = minutes, s = seconds).

Folding program	Step	Temperature (°C)	Time (hh:mm:ss)	Repetition w/ T drop - 1 °C
16HF65	1	65	00:00:50	
	2	64	00:01:35	
	3	63	00:01:35	
	4	62	00:01:35	
	5	61	00:01:35	
	6	60	00:09:00	
	7	59	00:09:00	
	8	58	00:19:00	
	9	57	00:29:00	
	10	56	00:39:00	
	11	55	00:49:00	
	12	54	00:59:00	9×
	13	44	00:49:00	
	14	43	00:39:00	
	15	42	00:29:00	
	16	41	00:19:00	2×
	17	38	00:09:00	
	18	37	00:09:00	
	19	36	00:04:50	6×
	20	29	00:00:50	8×
	21	20	forever	
54HF65	1	65	00:30:00	
	2	64	00:10:00	4×
	3	60	00:35:00	2×
	4	58	01:00:00	
	5	57	01:25:00	
	6	56	01:45:00	
	7	55	02:10:00	

8	54	02:35:00	13×
9	41	02:10:00	
10	40	01:45:00	
11	39	01:10:00	
12	38	01:00:00	
13	37	00:35:00	
14	36	00:25:00	7×
15	29	00:05:00	9×
16	20	forever	

C.7.2 Other Thermocycler Programs

Table C.9: Other Thermocycler programs used in this work including the steps, temperature and time (h = hours, m = minutes, s = seconds).

Folding program	Step	Temperature (°C)	Time (hh:mm:ss)
36Grad	1	36	forever

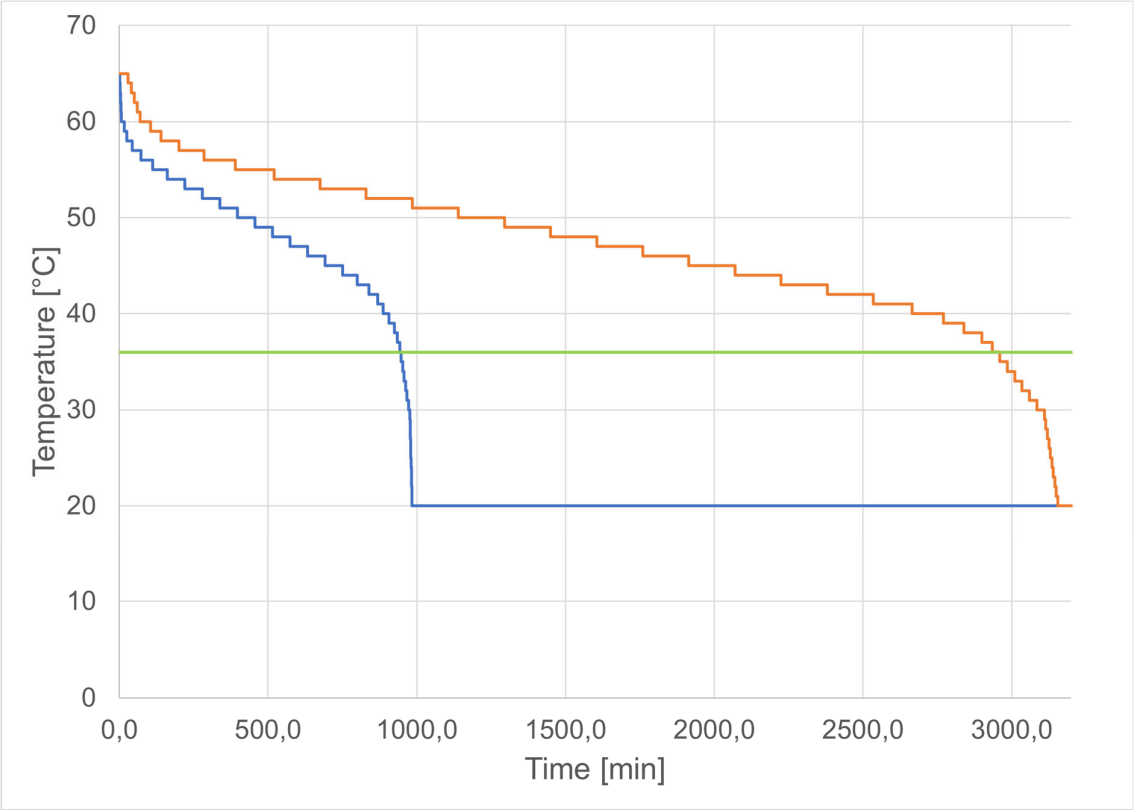

Figure C.2: Thermocylcer Programs Visual Representation

C.8 Fluorophores

Table C.10: Fluorophores used in this work including the peak of excitation and emission wavelength.

Fluorophore	Excitation peak (nm)	Emission peak (nm)
Atto 542	542	562
Atto 643	643	666
Atto 655	663	680
Atto 665	661	681
Cy5	628	670
Fluorescein Sodium	498	518
Hoechst 33342	357	447
mScarlet	569	594
Rhodamine 6G	526	648
SYBR Gold	496	539
SYBR Safe	509	525

C.9 DNA Origami Structure Designs

DNA origami structures were designed using the caDNAno software[46] (design schematics in **Figure C.3** to **Figure C.9**).

Table C.11: DNA origami dimensions by design. The values are calculated in nanometer assuming a base pair distance of 0.34 nm, an average interhelical distance of 2.6 nm and a radius of a DNA double helix of 1 nm.

DNA Origami	*A (nm)*	*B (nm)*	*C (nm)*	*R (nm)*	*L (nm)*	*#helices*
4LB	7.8	27	57.1	-	-	40
24HB	-	-	-	7.9	100	24
18HB	10.8	12.7	162	-	-	18
Cube	26.4	25.2	25.8	-	-	112
1LS	57.6	2.4	87	-	-	24
12HB	-	-	-	12	231	12

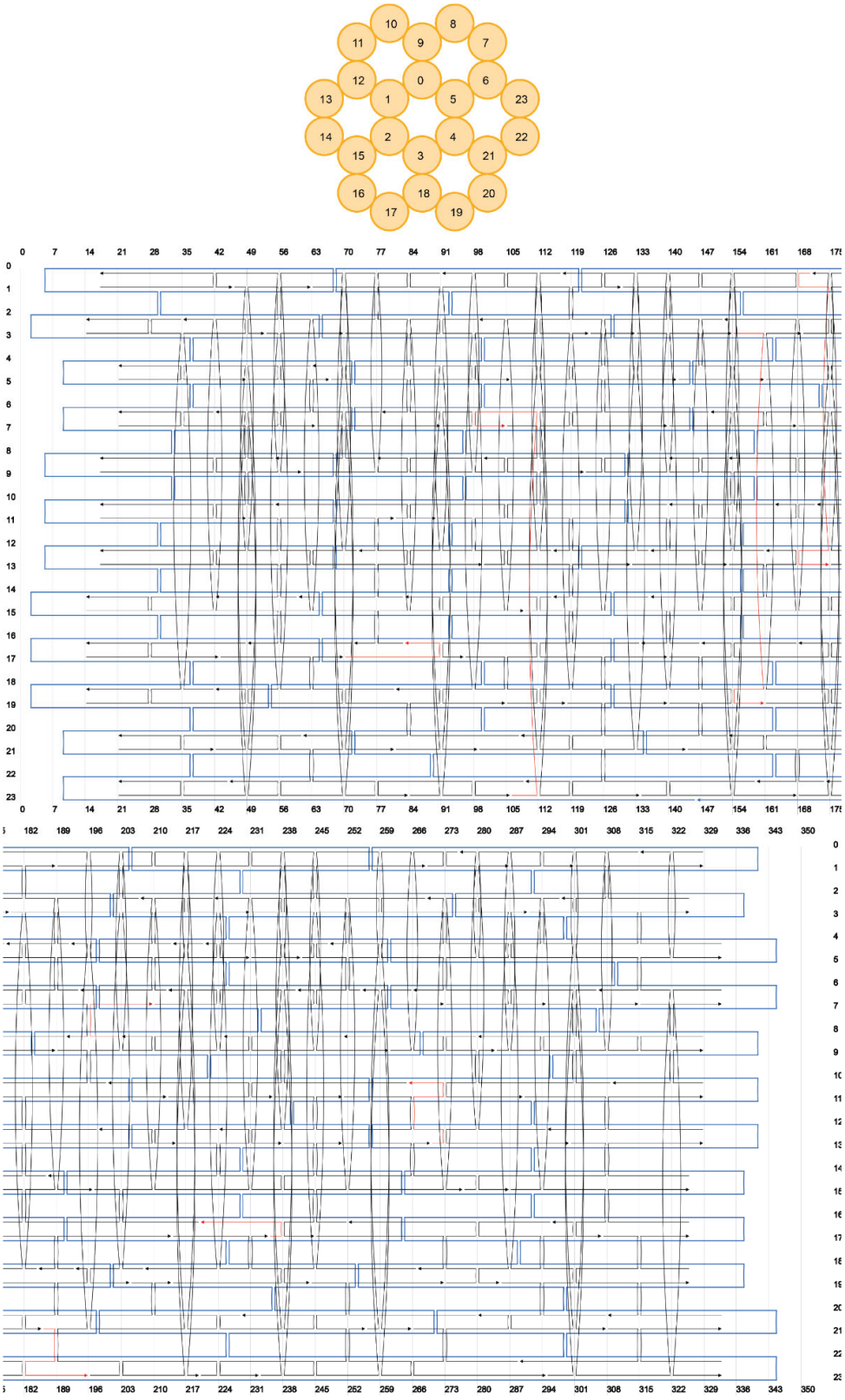

Figure C.3: CaDNAno scaffold (blue, p8064) and staple paths (black) of the 24 helix bundle (24HB) structure. The staples marked in red are extended handles (poly A or random sequence, extension at 5' end).

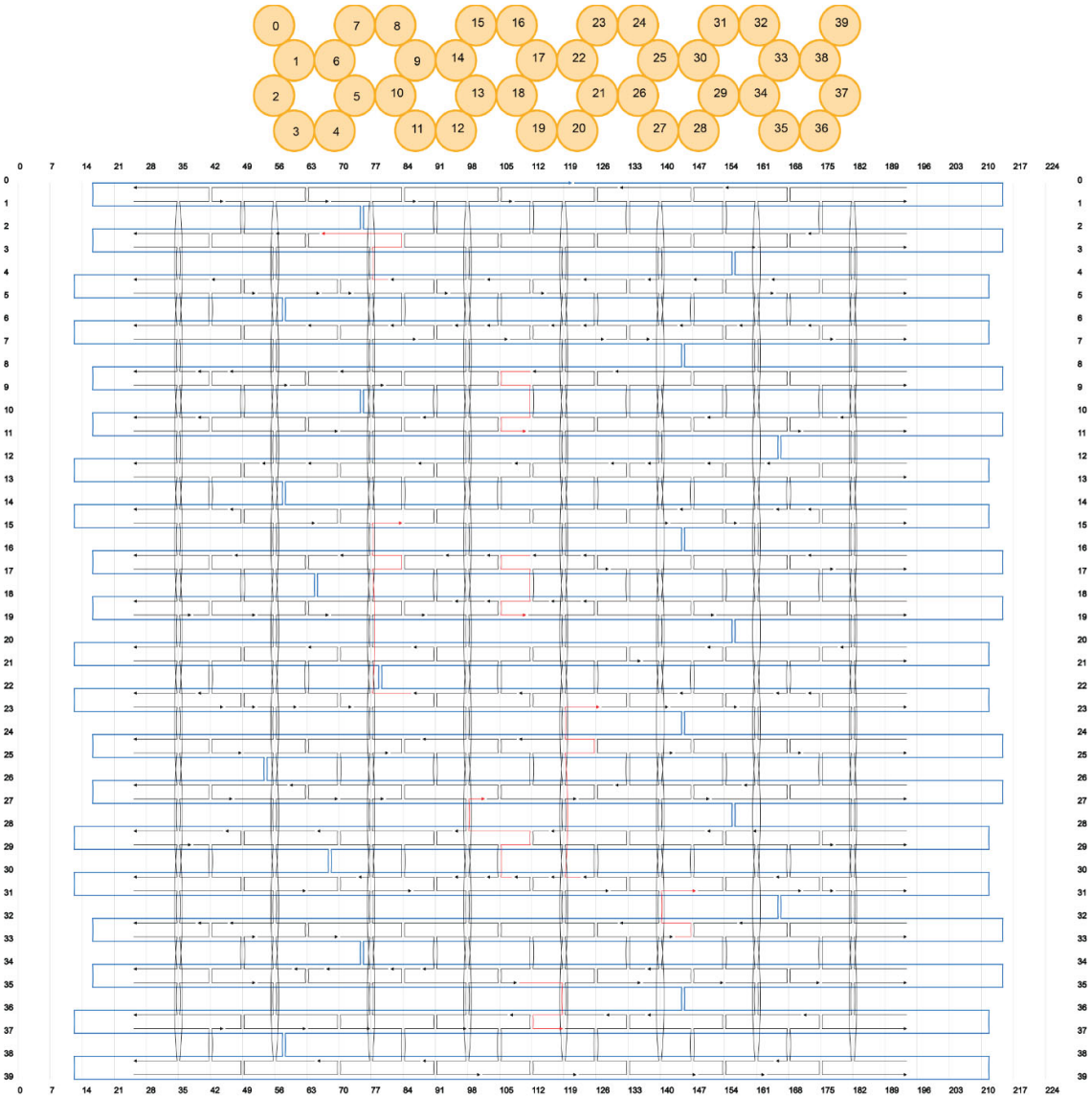

Figure C.4: CaDNAno scaffold (blue, p8064) and staple paths (black) of the four-layer block (4LB) structure. The staples marked in red are extended handles (poly A or random sequence, extension at 5' end).

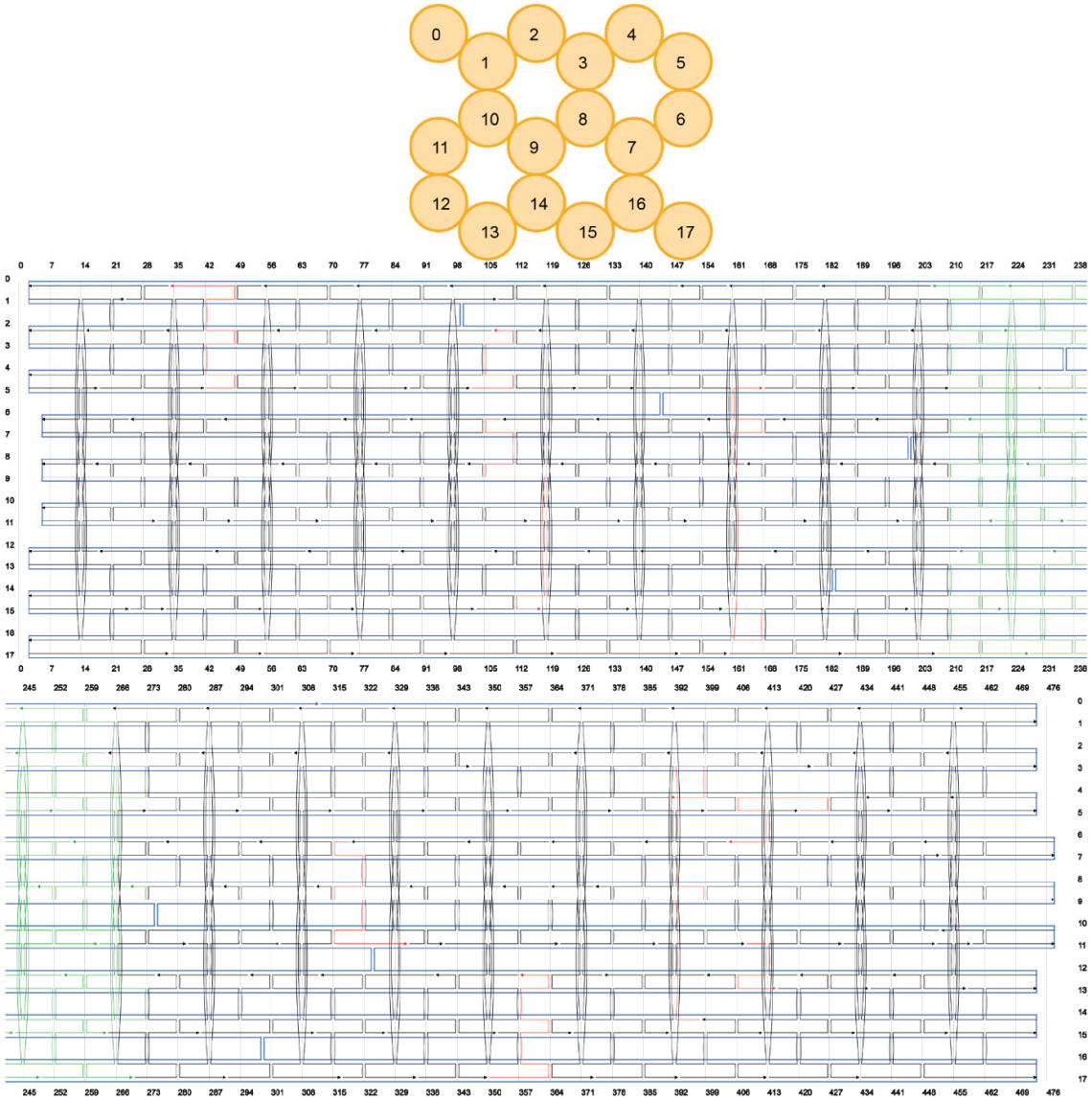

Figure C.5: CaDNAno scaffold (blue, p8634) and staple paths (black) of the 18 helix bundle (18HB) structure. The staples marked in red are A15-extended handles (extension at 5' end). The staples marked in green were omitted for the bent 18HB structure.

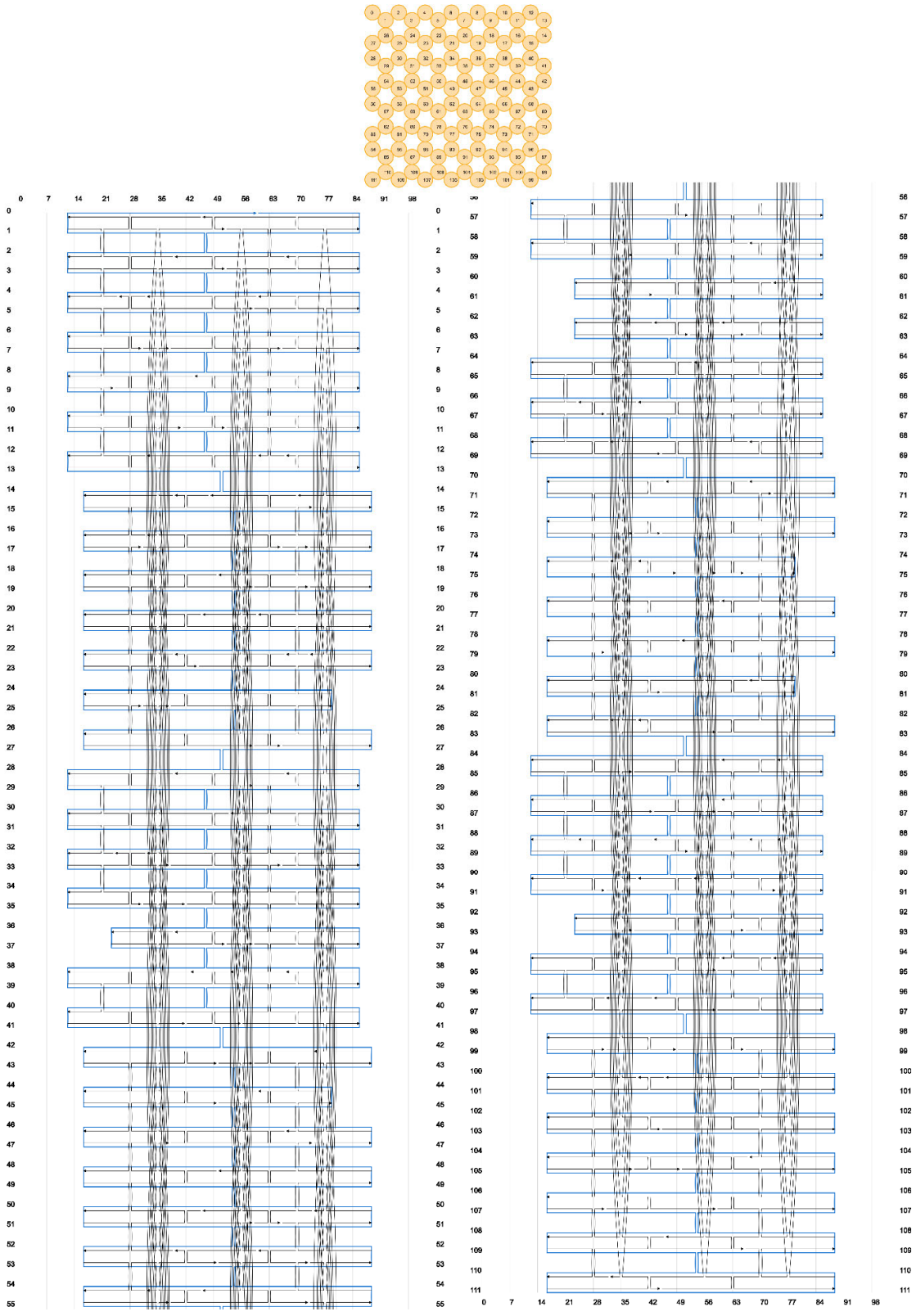

Figure C.6: CaDNAno scaffold (blue, p7249) and staple paths (black) of the Cube.

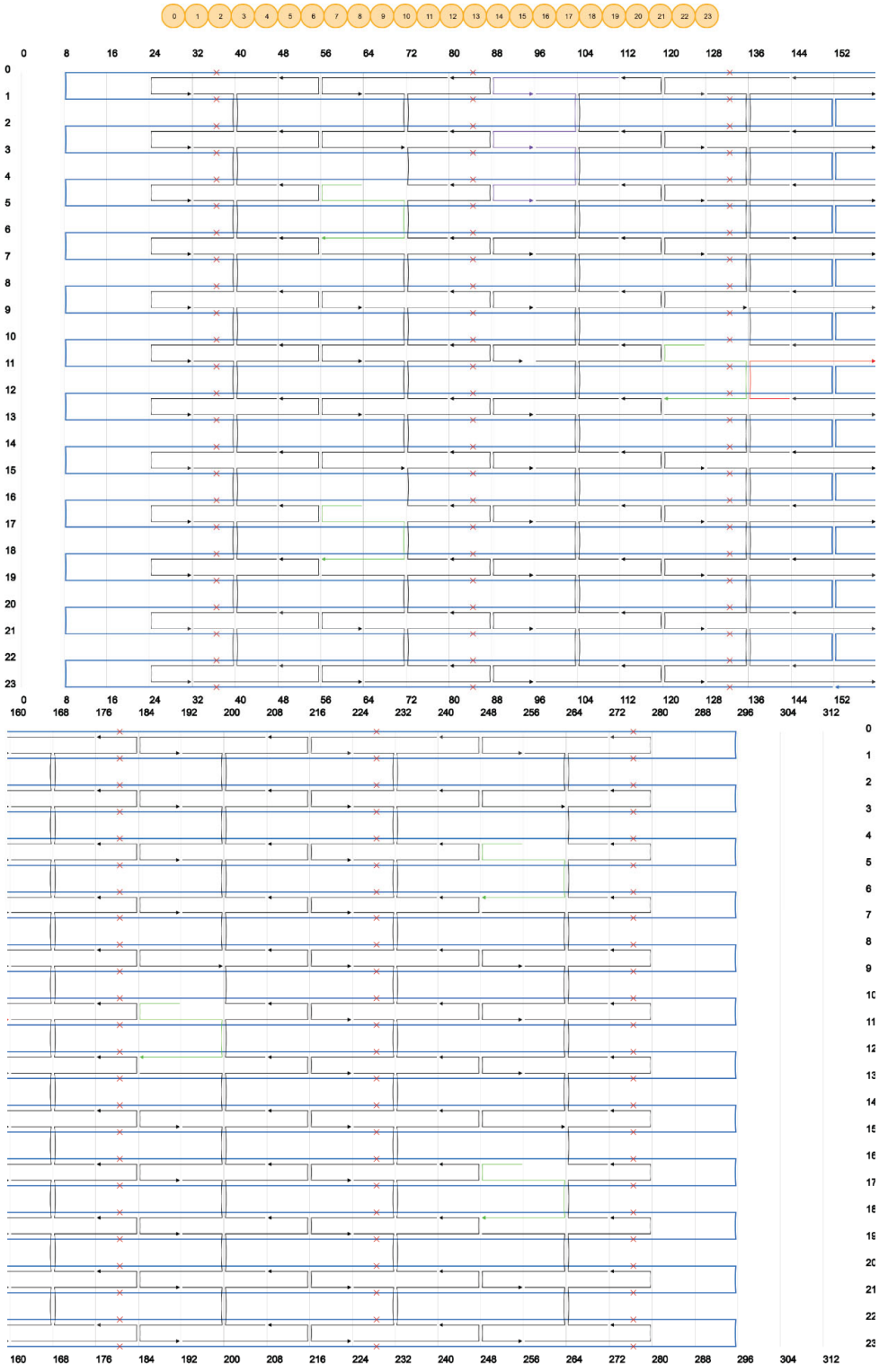

Figure C.7: CaDNAno scaffold (blue, p7249) and staple paths (black) of the one-layer sheet (1LS) structure. Green staples denote biotinylated staples for surface immobilization. The red staple represents DNA-PAINT staple with a docking site of the concatenated 24 bp binding sequence (sequence A + B + C) on the 3'-end. Purple staples represent staples with a 21 bp docking site for external labeling of DNA origami.

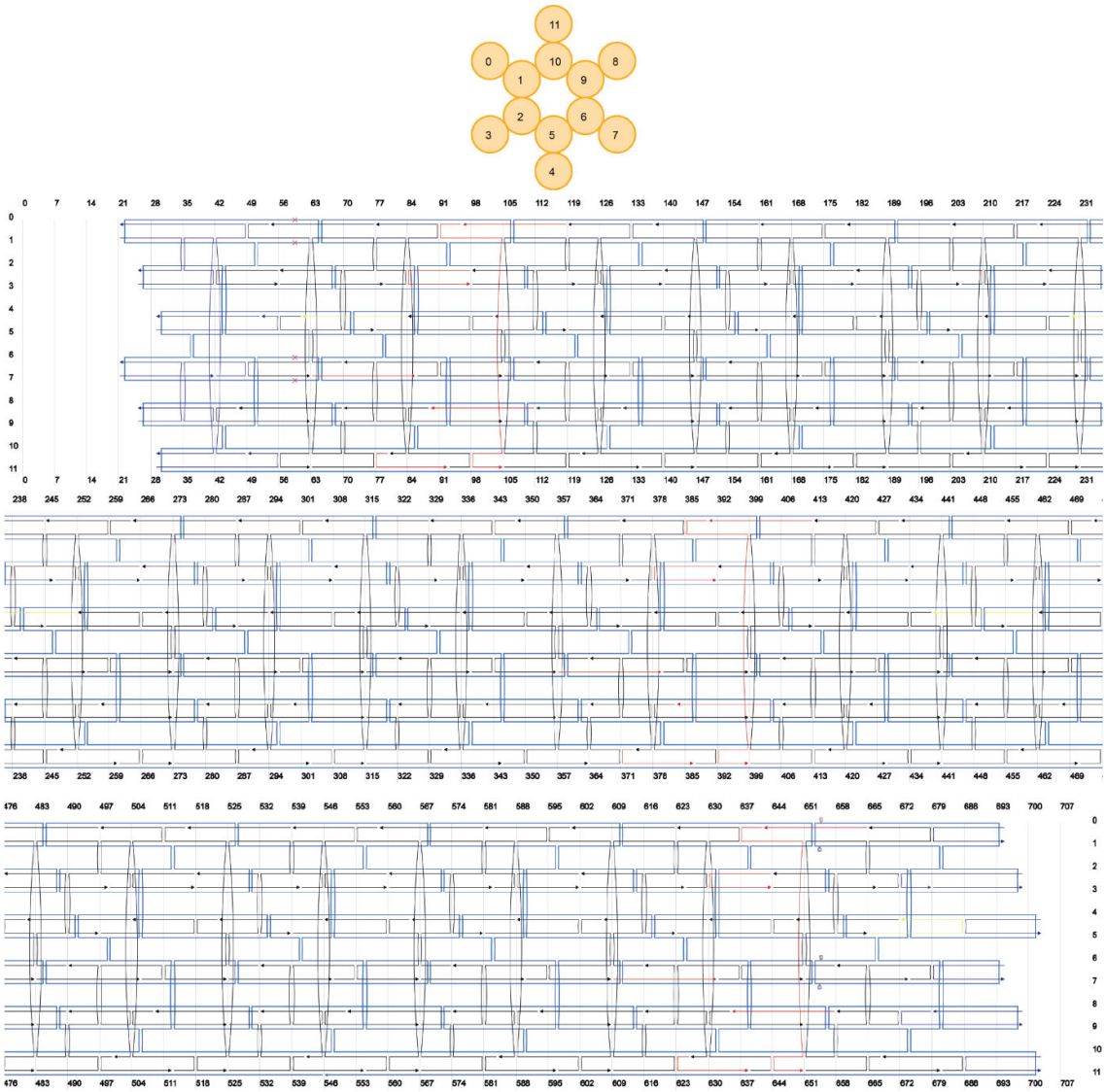

Figure C.8: CaDNAno scaffold (blue, p8064) and staple paths (black) of the 12 helix bundle (12HB) structure[197]. The red staples represent DNA-PAINT staples with docking sites of a 8 bp binding sequence on the 3'-end. Yellow staples denote biotinylated staples for surface immobilization.

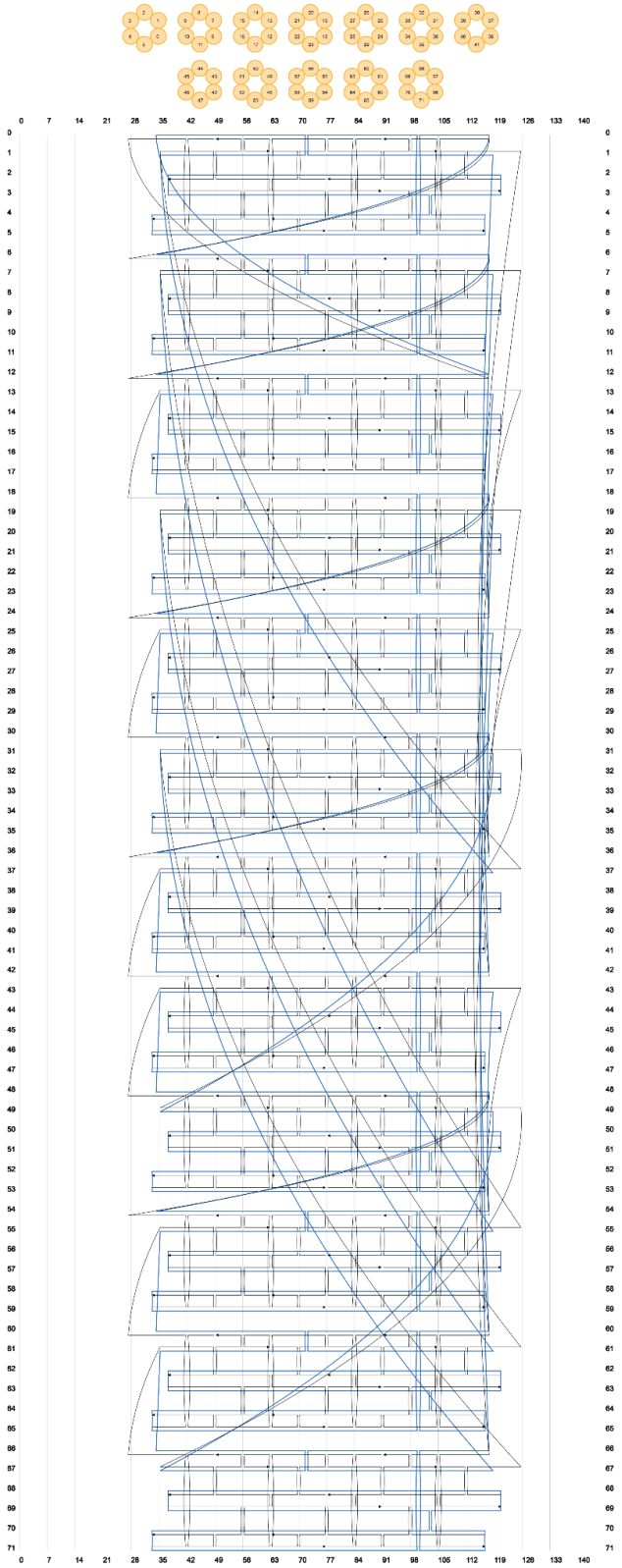

Figure C.9: CaDNAno scaffold (blue, p7249) and staple paths (black) of the octahedron. The design was created using TALOS[198] and caDNAno.

C.10 Sequences

C.10.1 Unmodified DNA Origami Staples

Table C.12: Staple sequences for folding the 4LB including the oligo number Staple sequences that are to be taken out for handles are marked in red.

Oligo Number	Sequence (5' → 3')
Oligo1	ATCCTGATTAAGCTTTGTCATTGTCAGCTCATTTGGGAAG
Oligo2	TCCAGGAGCCGTGAGAGATAATA
Oligo3	GAATTGTAAAAGCAAACATCGCATTGGTGGCATTATCCGGT
Oligo4	ATTGGTGTCTGGGCGCGAGATGACCCCCAA
Oligo5	TGCCAGCACGCTCCCGTACACATCCCGGAAACCTGTAAATC
Oligo6	GTCGATTGACCGACCGCTTCAGTGCCGTTT
Oligo7	GAACATGACCAGCAATAACATCCAATATTTAACGA
Oligo8	GTTTCATATTTGAGCATATTCAGAATTTAATTGCT
Oligo9	TAACACCAAGTACGCGAGTGCAAATTTACGAGTCA
Oligo10	AGGGTAAACAGAAGCTAATACTAATTATTTTGTTA
Oligo11	GTGTGCCTTTAAGCGTCCTACCTTTAGCTGCTTGG
Oligo12	TTTGTTTCAAATGATTGCCGAATTAAAGGTTACAA
Oligo13	CGGCGTAAAGTGGTCCGTCTGTTGGAACAGTATTAGA
Oligo14	TCATTTCTTCGCTATTACAAGG
Oligo15	GCGCACCAGCTTACGGCTACGTCAGGCAGTTGCTT
Oligo16	TAATACGTTAAAGTAGTAAGCAAATCCTCCCGACT
Oligo17	TGCCCGCCATTGCAAATGAAAAATCCAAACGCTAA
Oligo18	ATAACAACAGGGGCTTGCACCGACTTGAGCCGCAT
Oligo19	AGTAATAATACTATCTTTAAATCGCATTACATAATCATAGG
Oligo20	TGCGATCGCGTAACGAGAACCCTGAACAAAGTAAC
Oligo21	TCCTCATTAGCATACGTAGAACAACAGAAACACCG
Oligo22	TCAACTCATTGTATTATACCGAAGCCCTTTTTAGCG
Oligo23	ACACAACAGACGTCCGTGTGTACAGCCGGACTTCCGGCTAA
Oligo24	AGCACTCAAATAGTCTTTAATGCGCGCAGTGT
Oligo25	GAAGCCTTTTTTAATGGAGAAGGGCTGCAAGGTAAA
Oligo26	TGAGATATTGATAGCAAGGCCGGAACAAAGTACGA
Oligo27	CCAGAGAGCCGCCGCCAGTACAGGATAGAAAG
Oligo28	CCGTCGGTCCACGGAGAGGGCAAATTAACCGTTACT
Oligo29	AGAGAATACTGCGATAAAAACCAAATAAGAGCTGA
Oligo30	CACCTATGTTAGCAAATTTAAGC
Oligo31	CCAACCCCTCAAACCAGACCAGAACTAAAGGTCACCAGTAG
Oligo32	GAAGACCTAAGAACGCGAGGCGTTTCAAAGCGAAT
Oligo33	GAAGGGTTAGGAATTATCCGCACACGGGGGTATG
Oligo34	TCATGAGTAGTAAAACGATAATAAGAGCAAGACAG
Oligo35	CTCGCACAGGTAGATTAAACCCGCGACGCCCTCAAGCCACCAC
Oligo36	CATCCTGGCTCGAATTACTTAAGAGCAAGATTTTTCATCGT
Oligo37	TCAAAATTATAAGAAACATGAAGGGGGCCGTGCG

Oligo38	TAACCTTTACCAGACGACGGAATCCTTTTGCTAT
Oligo39	CACTGAAGCGCCGCGGGAAGAAAGCGAAAGGAGCGCCG
Oligo40	CACCAATCATCGTACGAAGAACAAATAAA
Oligo41	TTGGCGAGCTTTAGCGAACAGATATAGAAGGCTCA
Oligo42	GATTTAAAGGAATGGCTTTTGATGACATTGACACT
Oligo43	TTAACGATTGACAATGAAACCATCGGCGATTACTA
Oligo44	CGCCAAAGACGTAGAAAATACAAGCGGAACCCAGCGAACA
Oligo45	TTAAGACGCATTGTATATATGTAACACC
Oligo46	GCATGTTGGGTTGCGCAATTTTTCGGCCAGCAAAAAATACC
Oligo47	ATAATAAATGAATTCGCGAAAACGTCACGGGAGGGAAG
Oligo48	CGTTAAATATCGAGCCCCTGAACACCCTGAAAAAAGACTT
Oligo49	TGAACCCAGTCAGCGCCAGCCTCCGTGCAACAAGCAGAAGA
Oligo50	TTTCATTTTTTATTCTCCATAGGTCACGTTGGCAC
Oligo51	ACAGAAATAAACATTATTGCTGATGTGCTGCTCA
Oligo52	GACGAACAGCTGCGAACGTGGCGAGAAAGGAATACAG
Oligo53	CATAGATTGTAACGTAAAAGAAAAAGCCT
Oligo54	AAATGAATTATCACCGTCCCTGACGATTATTACAAG
Oligo55	AAATGAAGCCCAAAATCAAGACGGGAGAATTAATC
Oligo56	GGATTATACTTTATCAGAAAAAAAGTGCCTGGCA
Oligo57	GAGGTTTGAATGTCAGATGAATATAAAATCCTGAT
Oligo58	TTGAGTAAGAAATTAAAGGGGTGATAATCAGAAAGTAAGG
Oligo59	AAACAGGAGGTTGAGGCAGTCATACATTGCGA
Oligo60	ACCTAACCACCGTGCCACGCTGAGATCTCGTCTTT
Oligo61	TTCATTCAAATGGAGGTTCGCGCCCAATAGCAGCA
Oligo62	ACATCCCTGCAGGCCAGAAGAACAATAT
Oligo63	CATTGGTCTTTAAAAAGAATTAGCAAGGCA
Oligo64	TGGTCCACCGAGGGTGGTTTTTCTTCTTCACCCGG
Oligo65	AAGACGATTGGCCTTGATGAATTTAACGTTGA
Oligo66	CTCCAACGCAGGCGAATGAATTACTTCTTTTACGA
Oligo67	CCTCAGTAGTTAGAGCCTTTCTGAGGCTTAAGCCAGA
Oligo68	GTGCGCCTGGCAGAGCTTGACGGGGAAAGCCGGAT
Oligo69	GAACAGTTTTACTGAAACATGCGGA
Oligo70	AATGAAATCTACCTAAAACAACGGACCAGACGCGCCACCCTC
Oligo71	TTTTCAGTTAATTTTCAATAGATCGCGCCTG
Oligo72	ATTCATCGGTTTAATTGAGAATCGCAGTATCACGA
Oligo73	CAGAAGGAAAAAATAGCCCCAATCTGCAGAAAAA
Oligo74	TTACCAGTCAGGAATACATACCAAGTTCTGTACGTACTCAGG
Oligo75	CCGCTAACGTGTTTTAGACAGGAACAACGCTCACC
Oligo76	GTAAATGGTTTGGAAGAAAAATAGCAATAGCTACT
Oligo77	AGTGCACCAGAAGGAGCGAACCTACGGGTTTTCGG
Oligo78	TCTCCGTGGTGGAATTTGCCACGGGGAGATCTAGG
Oligo79	GGCGCGTGCATCCAGCGAACTGATCACCTT
Oligo80	AGCTTTGTAGAGGAGGTGCGCACTCAATCCGCATA
Oligo81	TCGGAACCAATACAAAGGGAGACAGTCAAATCAAT

Oligo82	CAATTCTAAAAATTTGAGTTGCCCGAACGTTAGTT
Oligo83	CGCCGCCAGAGAAAAAAGCATCATATTCCTGATCT
Oligo84	AAAATTGACAACTTAGCCCGGAATAGGTGTATCACTGG
Oligo85	TAAAGGCTCGGTCGAATTGTATCGGTTTACA
Oligo86	CTGACGGTGTACAGACCAATGTTACATGAGGAGCGGGAT
Oligo87	TTTCTATGCAACTAAAGTCAAACTCATATTCAGAGA
Oligo88	TGCCTTCACCATATAATCAGTGAGGAATATCCATG
Oligo89	AGTGAATCAAAGCCCCAAAAAAAAATAATTT
Oligo90	GACACTGCTCCGGCATTTGGGA
Oligo91	GCCTTATTAGCCCGCCTCGCCGCCACCA
Oligo92	TAAAAGCATCAGTTCTGCCTGAGTAGAAG
Oligo93	AAATAGAGAATTATGCGTTATACAATAGGGCTGTA
Oligo94	GGAATCATAGTAATTTAAATTAATAAATCAGAAAGACACT
Oligo95	CCAATATGTAAGAGACTAAGAAAACAAAATTAGCA
Oligo96	TATCCAATATTTTTGAATATTCTGGTCACACGATGGAAA
Oligo97	CCAGTAAGCGGTCAGAGGCAAAAGACGTTGAAT
Oligo98	ATAATCAGGATTTTTAAAATTCCATATAACAGTTA
Oligo99	GAATGAATAACCTTGCTTCAGGCAAACGACGTAATG
Oligo100	AAAAAAATTTTCGGCTATTAATTAATTTTCCCTTA
Oligo101	CAGGGAAAGAAAAGTTAAGAATTCACCGGAA
Oligo102	GCCACGTGGTGAAGATCGTGTAGATTAACAACCCG
Oligo103	TGTCGCATAAAGTGTAAATTATCCGTTGAGGAGCC
Oligo104	TAACATCGTAGCAACGGCCAACGCGCGGGCTGGTTGTTAACGCAGAG
Oligo105	AATTGAGTTATATCAGATTGAATCAAACATTCTG
Oligo106	CCTCATTTTCAGGCATTCCATCAGCTCATA
Oligo107	AGGAATACAGGCAAGGCGACAGGAAGTGA
Oligo108	TCGATACAATTTTATCCTAAAATAA
Oligo109	GAACGGCAGCCATTTCACGTCGGCCTTGC
Oligo110	TTATAGTTGCTATTTTGCTTGCATCCTATTATATAAAAA
Oligo111	GCAGTCTCTATTCACAGCACCAACGTTAATAAA
Oligo112	TATTACGGGGTCAGTGCCCCTCAGACCTCAGATTA
Oligo113	CTCTCCCTTATGTTTGATTAAAGAACGTGGA
Oligo114	GCTAGGGAGAAAGGTAAAGATTCAAAAGGGAGTGTAATAGTC
Oligo115	AGCAAGCCGTATCCCAGATAAGTAGTAATA
Oligo116	GAACAACTTGCTAAACCCCCAATAGCAGGGGCGACAT
Oligo117	TACCGTGTTTTGTGAGACGGACTAT
Oligo118	GGTGCGCTTTTCCAGCATCAGCGGGGAACGTTCGA
Oligo119	CATATGATGGCAATTCATCAATGAGGCGGTTGAGC
Oligo120	GAGAGGCGCCAGTAAAAGAGTCTGTCAAACTAGTC
Oligo121	ATGCGACAAAACACCGTAATCAGTACATAATC
Oligo122	AACGAACCTGTTTGATTCTGTAGCTCAACATGTAG
Oligo123	TTAAAGCCTCAAACAACGCCAACATATTACTACTA
Oligo124	CCACCCTGATAATCTAAACCTCAGAACCGCCAC
Oligo125	GGTTGCTCAGAATCCTGAGAAGCCAGCCCTC
Oligo126	AGAACCGCCACGTTTTGTCAAAAAAAAAGC

Oligo127	AATCAAGCAAATAAATCATCATTACTTGAAGCCTT
Oligo128	AGATAGCCGGAATAACAGTC
Oligo129	TGCAATTGCAACAGGAAAGGTACGCTTGACGA
Oligo130	AGAGAATTGATAAAACAAAGATACGCCAGCTGGCGGCGTAGA
Oligo131	AATCTGCCCCAGTCAAAGGGCGAAAAA
Oligo132	GCCGGAAGTGCCAGCTGCATTAAAATCCCACT
Oligo133	ACGACATTTTGCGGAACATTGCACGCGATTAAGTC
Oligo134	CCGGTAAAGCATAGCCCTAAA
Oligo135	GCTGAACCTAACAACTAATCCGCGGGCCTGAATTAAGTCAAT
Oligo136	AACTCCATCACCGGTTTGCGTATTGGAGTTGCGTT
Oligo137	GTGCTCATAACGGGGTCAGTATTAACAC
Oligo138	GAGGCATTTAGAATAACCCCGGTGATGTGCGATCGGTGTT
Oligo139	GCACGTAGCTTAATAAGGGACGGCTATTATCAAACCCT
Oligo140	CGCTCAACAGATTCTTAGTCTGGACGACGGCCTG
Oligo141	AGTTTCAGAATCTTTTGCGACAGTTACCAG
Oligo142	GCGTTCAATAGAAAATTCAAGGTGGTCCTTATTTAC
Oligo143	ATAATGAGAAAGGCCGCTATCAGCAGAGGTGCC
Oligo144	AGAAACAATATCCTAATCCAATCGTTATCAATTAACAATT
Oligo145	TGTGTGAGATTAGAGCCGTAAAAGT
Oligo146	AGGCCATTCAGCATCAGTAACACTATCATAACC
Oligo147	GTGAGGCTCATTGCAGGTGTTCATTCTTCGTTAGTAA
Oligo148	AGACCAACATACAGTTACGAATCTTACCAAGTACC
Oligo149	ATTAGAGCCATCGAAATGGGTAAAAGGGAGT
Oligo150	ACCGATATATCGCTTTTAGTTTCCAAAGATTTGA
Oligo151	CCGGAGCAAGCTATCAAGGGAGCCCCCGATTTCCT
Oligo152	AACACTCACAGCTCACAATTCC
Oligo153	TGCCAAGTATTCGAGAGGGTTGATATAAGTATTCAAC
Oligo154	TCTGAATGCTGAAAAACTTAAATACCGAC
Oligo155	ATGGAAGGCTCCAAAAGGCGTAACGAATTGTGGCA
Oligo156	GTGAGAAGTGTACTGGTAATACACCACCAGC
Oligo157	ACAGCCAATACATAATATGGTAATCAAGTTT
Oligo158	TAGCCATAAATCAATATATTCAGGCAACGCCACATA
Oligo159	GCACCATGTAGCGCGCCTACCGACAAAAGGTATGG
Oligo160	ATACGGCGGCCGCTGGCATTCGCCATGTGAGTCCTTGAAAA
Oligo161	AAATCTCCGTCTTTGATTTGTTTACCATCGGAAATTAT
Oligo162	AGGTTTAGTACTTAGTAATTTTTTCCCGTT
Oligo163	CGTGATAAAGTGTTTATCAGCATATTATTTATAGCCT
Oligo164	GCTTTAATTGAGCGCTAAAGCCCAAACTAACGATG
Oligo165	TGGGGTGGGAACAAACGGTGTTAAACCTGAGACCAGT
Oligo166	TTACAGAGAAACAAAGTACGCAGACCGGAAGTT

Table C.13: Staple sequences for folding the 24HB including the oligo number. Staple sequences that are to be taken out for handles are marked in red.

Oligo Number	Sequence (5' → 3')
Oligo1	AAACAATGGTCACAATTCTATCATAAATAGCGAGAGG
Oligo2	TTCAAAATTATAGTGAATTTTAACCTCCGGCTTAGGATTCACCA
Oligo3	GGCAATTGGTCAGTTCTAAAGCAATTTGATTTCTCACCTTGC
Oligo4	GCGGGAGTTAGAACATTGTATTTGTTAAAATCAAAAA
Oligo5	CTAGTACAGACCAGGACACTCCAACAGGTCATAAGGGAGAAC
Oligo6	GCATAACCGATATACACAGCTTGCTTTCGGCGACAG
Oligo7	TATCTGAATAAACCAATATAAATCCAGCTACAATTTTATC
Oligo8	GTAAAACTGATTGTACCTTGCTTTTTTAATGGAAA
Oligo9	TTTTGCGTTTAAAATAGAAGTATTAGACATAATACATTTGAGTACTATG
Oligo10	TTCTCACGGAGGAATTTGTGAGAGCAATCGGCGAAACG
Oligo11	GGGCGGCATCGTGGTTCTCTGTAAACGTGTTAAATCAGCTCACCG
Oligo12	ACGGTCAATCAGGATTAGAGAGTACCTTCGGATGGCTT
Oligo13	AGCCTAGCCTTACTCTCATAGTTAGACGTTAGATTTGT
Oligo14	TCCAAGCCCAATAGGAACCACCCTCCAACCATATTTCTTAGGA
Oligo15	CCAGTGAGGGAGTCGCTGCGGTATGTTAGCAATATAAAAGAAACCAAC
Oligo16	CTTAGAATCAGAACGCGAGGCGTTTTAGCTTAAATTGAAATAAAAC
Oligo17	GCAGAAGAGTGAGGCCATCAATTACAAAATCTTGAGAGGAAGCGC
Oligo18	CGGTTGAGCCGCAGAGCCGGGTCACTGCGCT
Oligo19	TCACCGTCACCGACTTGACCCGACTTGGAAATTATTCATTAAAGCGTCA
Oligo20	TTGGGCTTAAGAAGGAAGTTAAGTCAGAGAAAGCGCACAATAGAAATGCA
Oligo21	ATTCTACTTGAAAACAAATCATAGCAAATCAGATATTCCGGT
Oligo22	CTATTTTTGAATGGCTATACGTGGCACAGAC
Oligo23	AAATTTCATAGCTCGCACTCACGGCTGGGGTG
Oligo24	GGATTCAACGAGCAGCCCTCAGAGCATAACCTGTAAAGAGGTCCATGT
Oligo25	AATTCGGTTGGAATTAGCAATAAATAGACTGCCAGAG
Oligo26	GGTCAGAGGCTTCCATTAAACGCAACATCAACGTAACAGACGAG
Oligo27	CATTTTTACGTTGCGCCGACATGCGGGATCGTCACCTAAAAC
Oligo28	CCACCCTCAGAACCGCCCATGTACCGTAACACTGAGTTTGTGAATTA
Oligo29	AATCACCTAGCCGAACAAACACTATCTTGGAGGTTCAATAG
Oligo30	AATGAGAAGAGTCAATTTGCAC
Oligo31	TAAAAGGATACAATGCCTGAGTACCTCATTTTTTAACCGGCCT
Oligo32	GATTATTTAATTAGCGAACTCCTTTTGACATGTCAATCATAAAACA
Oligo33	TCTCCGGAATAGCTGGTTTAGGATTAGCGTTGATACCGATATTTT
Oligo34	GTACTCAGTCGAGAGCTCAGTGAGGCTGTTATTCTGAAACATTATA
Oligo35	AGGCCGGAATGAAACCATCGATAGCAGCACCGTAATCAGTAGATAA
Oligo36	TACCGCGTTTTTATCGGGTATCTGTCTTATCCCAT
Oligo37	AGCAAGGTCTGAGAGCTATCGAGAACAAGCAAGCCGCCCAAT
Oligo38	GTCACACGTTATTTACATTGGCAGTTGGGTTATATACAAGACA
Oligo39	GTCAAAATCATCAAATGGTCATAAATATTCAAAATGTTTCAT

Oligo40	GTGCCGGAGGTTTAGTACCGCCACCCTCACCATCCATTAGAACCG
Oligo41	TACAGCGCCATGAACTTTCAGAGGTGGACAGCATC
Oligo42	GAAAATAGACTTGAAGGGTGCTCATTTGCCAATCAGAAATATT
Oligo43	ATTTTTTAATATTAAGCAAAAGCC
Oligo44	TCAAGAAGCAAAGCGGATTGCATTCACGAGAATGACCAAAGCAA
Oligo45	AATCAAAGCCCCCTTATTAAGTATTAAACCAGGCGAGGTGACGCCCAC
Oligo46	TCGACTATATGTAAATGACTACCTTTTATCAATAGCGAATTTTCC
Oligo47	AAGAAATTAACAGAAATAAAGGATTTTCTAATGGTAATCA
Oligo48	AAACACGAATCCCCCGGTCTTTAGGCAAATATAGCAGAGGGCCAA
Oligo49	TTGCCCTAAGCTGCAGGAAGTTTTGAGGAGCGAAACGACCTGGCCTGAT
Oligo50	TCAAGAGAAGGAGAGATGGTTTATTTCGGAACCTAAGACTCC
Oligo51	ATCAGCGTTTTCATCGGCATTTTCGGTCATGTTTGCCGGA
Oligo52	TAATCGGTAAACCAGCTAATACCCAATAATAAGTAGAACCTACCA
Oligo53	CAATCGCGAGAAAACTTGACCTAAAACCGTAATTATTAGGT
Oligo54	CGACGGCCAGTGCCAAGCTGCACGCGCGGGAAGTTG
Oligo55	TCCTGTATCACGACGTGGATAACCAGCTTAATCCGCC
Oligo56	CGCGTCTAATAGGATTAAATGAAAATTTAAGCCTTACGGTAACTGGAGC
Oligo57	TAAATTGTTGTGAAAATGCCAAATGGGGCGCGAGCACCGAACTAAC
Oligo58	CAAAATCACCGGAAGAATGAACAAACATAAA
Oligo59	CCTAATTTACGAGCATGTAAGTTAATTTACCGAC
Oligo60	CTTTGATTAAAGAGTCTGTCCAACAGGAACGGTACGCGATTAA
Oligo61	GGTAACGCCAGGGTTTTCCCTGACCGTTCCCACGCAAATGT
Oligo62	CTTTCATCAACATTAAATGTGAATAATT
Oligo63	GTAATACTGTCCAACAGGAGCATTAACATCCAAAATTTAAA
Oligo64	AACTTTAATTTTTTTCAAACTAAACAGCGGATTTGCTAAACAACTACAAA
Oligo65	AACCGAATAACGCCTTATTACGCAAAAGCCAGAGCCGCCGCCAGCATTAA
Oligo66	CGTGTGATAAATAGTTTATCAATTAGACGATAG
Oligo67	CGATTGAGCAGCACCGTCGGTAGGTGTCGCCGCCACGGGAACTGTAAAA
Oligo68	TGGGAACAAACGGTGTAGATGGGCGACGACGACAGTAAGGGCGATCGG
Oligo69	AGTTTTGGATAGCGCGGAATCCTTTAAACAGTTCAGAAAAAAAGCGA
Oligo70	GGGGTAATAACCAAACCCTCGTTTCAACTCGTCAAAGGGCGAAA
Oligo71	GGCTCATACGTTAATAAAAGACGATAAAAGATTTTAAGAACT
Oligo72	GACGGTACTGGTAATAGCCCCCTGCCTAATACAAAGGC
Oligo73	TCAGACCAGAACCACCATAAGCGTCACAGTGCCGTG
Oligo74	CCACCCTCAGAACCGCCACCCTCTTAAGTCCAAATAATTCCTT
Oligo75	GAACGCGCTAAACAAAAAGTACTGTAATTTAGAGCTTGACGGGAGTT
Oligo76	ACACCGGTTGAAATCATCTTCTTTTCAAATATATTTTGAAACCAATCAA
Oligo77	TAATTACTAGTTTAGTAAAGCCAACGCTCGGAAGATGACGTCTTGTT
Oligo78	AACGTTAAAGTTAAGACGGGGAAGGTACCAGC
Oligo79	TCAGAGGGTATAACTGAACACCCTTTACATCGGGAGAAAGGTAAA
Oligo80	TGAGTACCGCCAGCCATTTAATATCATACTT
Oligo81	AGCGGTGTGCCGGTGAGGCGGCAGCTGATTAGCTGGCGAAAGTGCAAGG

Oligo82	TAAAGCTCTGAGAAAACCCGTCACCGTGCATAAAGA
Oligo83	CTTTTGCACTGCCAGTTTGAGGGGCATCGTAGGATTCTCCG
Oligo84	AAATCTTATACCATTAATCAGGCTTGAATAAGGC
Oligo85	ACCACAGGCCAGTAATAAGAGAGAGAATAACTGTAAATCC
Oligo86	GCGTTATACTCTGTCCAGACGACGACAACTAGGCGTTAAATAAGAATAA
Oligo87	AGGGATTTTAGCCTGAAAAAGTCACGCATGTAGCACAGAA
Oligo88	TGCGGTGCGCAACTTCTGGGATAGGGTTGAGTGCAGCCTCGTGG
Oligo89	GGAACAACATAAGAGGCCTACGAAGGCACCATTCAACTGTCAG
Oligo90	AAAAATGAAAGGAGAATATTGAGCAGTACCGCACTCGATGCAAATAAAG
Oligo91	TTCGCCAAATGCCAACGGCCCTGACGTGCCGGACT
Oligo92	GGAAGATCCGGTCAAATAAAAGGGATATATTACGCCATCGCATTAA
Oligo93	TAAGAGCAACACTACTAATAGTAGTCCTTTACATT
Oligo94	CATAACGCCAAATTAAAGAACGTGGTTGACCATTAGAAATATGCAAC
Oligo95	AAGATTCATCAGTTGAGATCTATCAGGGCGATGGCGCG
Oligo96	ATTAAAAAAGCGCAATCTCCAAAAACTAAAACGATATTACAGGGAAGAA
Oligo97	AATAAGTTTTTTGGGGTCGAGGTGCCTTGATATTCACACCGTTCCTAAT
Oligo98	GCTTAATTGAGAATCGATTCTTACCAGTATATCATAT
Oligo99	AGGCAAAGCCTAAATCAAAAGAATCCTCATA
Oligo100	AACCGTTTAGGAATACCACATTACCAGTGAAAAGGGGGTAA
Oligo101	ACGTGAACCATCACTACCCCCAGCGATTAATGAAT
Oligo102	GGAATGAGGCAGGTCAGACGATTGGCCGTAAAGCACTAAGGCA
Oligo103	GAGCCATTATTTATCCCCATTTGTCACAAACGAGCGTCTTCAGC
Oligo104	AAGCGACGAATTATTCATTTAATTACAT
Oligo105	AACAAGAGAGGGTATTCTAGCTGATAAAGGAGACAAGGCATAG
Oligo106	ACAGTGGCATATAACCTCGAGTAGCTGGAAGTTTCATTCCATATA
Oligo107	AATACGTTTACCTTATGCGTATTCAGAACGAGTAG
Oligo108	TCCAAAAAACAGCGGGTTTTGGGTTGATATAAGTATAGGTGCCACCCT
Oligo109	GCCAGTTAATAGTTTTAACGGGGTTACATGGGAATTTAAACA
Oligo110	AACAGGGGATAACCCCAAGAATTTCATCGTACCAAACGTCAGCCAGCAA
Oligo111	TTAAATATACTTTGAATACCAAGTATAATCCATTATCA
Oligo112	CCAAATGTGCGGGGATGGGATAGGTCACGTTGGCGGATAGGCCAG
Oligo113	GTAGGTAAAGATTCCACCATCAATATGTGATCGGCCTCA
Oligo114	GAAAGTCTCTCTTTTGATGATACAGGAGTTTGGAATGGGCCAGTAGA
Oligo115	AATGTATCGGTTTATATCCTAACATTGAGTCCC
Oligo116	GACTGAATACCAAACCGATTTAGCGTCAGACTGTAGCTTCAGTTACC
Oligo117	CAGTTTTTGTAAATAAATCCAGAGCCTAATTTGGAAACAAACATC
Oligo118	GCAGCAACGTCAGCCGGCCAGTTTTCGTC
Oligo119	TCGCAATTATGACAGCTAAAATCGCGTAGAGGAAGCCCGAATATA
Oligo120	ATTAAGAATACACCTCAGCACTAAAGGAAAGAGGAGTAA
Oligo121	ACTCATCTTTGAGACCGCTTTATGACAAAGAGCCATATCACC
Oligo122	AAATAAGGCAATAGAGAATTGATTAGAGGAATCAT
Oligo123	GATCCTTTACAGAATATCATGTTCAGCAGAGCC

Oligo124	TGTAGAACCGCAAGTTCAGGCGCCTCTTCGCTATTACGCCGCCCCGCCA
Oligo125	AAACTGATTCCCAATTCTGCGAAGTTTAGCTCGGAACACGG
Oligo126	AGTTTGGAATTGAGGCTTGCAGGGAGTTAAAGGAAGGAACCGTT
Oligo127	ACAACGTAGACCCTTTTAAGCAGAAGTAGCATAGCA
Oligo128	CATCCCGATTTAGGCAGAGGCATTTTCGAGTCCCTAAAGG
Oligo129	ACATTAACGTGTAGCAAGAAACAACAAGATTAGTTGCTAT
Oligo130	ATGATCCGAAAGCCTAACAACGCCAACACGAC
Oligo131	AGAGGAAGGAGCGGGCGCTAGGGCGCAGTTGAAGAAGGTTAGATGAT
Oligo132	ACGGACTTTCCGGCAAACGCGAAACGATTAAAAAATGTACATCAAACTT
Oligo133	TTTGAGGGTTGTTCCGCTTTCCGGCACCGCTGTTGGCTGGTCA
Oligo134	TAAAGTAGCTCAAATTTTTGTAATTGCCAGACCGGAAGCAATTCA
Oligo135	ACAGTAAAGTACAACGGAGTAATACCAAGCCCACT
Oligo136	TTTCTGTATGGGATGTGAGAACCAAATCAAATCCTC
Oligo137	AAGAAAACAAAATTCAATTACCTGAGCAATTCGCCATAC
Oligo138	TTAACAAATTACCTTCAGAGTAAAACTGTAAATCGTCGCTAGTGA
Oligo139	TGAACCTTGAAAAAATTAACAGAACGAACCACCA
Oligo140	GGTCAAATGCCGGAGTCCACTAAGGAATTAGCACTCCAGCCAAGTTTGG
Oligo141	AAATTGTGTTTGCTCTTAACGAAATCCGGACAGCATATATTTTC
Oligo142	ATCATCCTCCATGGGAACGATGACCAACTTCAGGGATAGCACAGAC
Oligo143	AGGGCGAGTTTTGTCGTCTTTCCAGCGTAACGATCTAAACATTC
Oligo144	GCCAAAGTTGCAAAGACACCACGGAATAAGTTTATTAAAGGTATC
Oligo145	AAAATTCATATGGTTTAAATATTGACGCGACCGAAGAAATACAGCA
Oligo146	CTGAATCTTACCAACGCTATTTGAAGCCGAACCTGCCAT
Oligo147	CAGTACATATGTGATTAATTATAGCTTAGATTAAGACG
Oligo148	AAAGTTGTCCGTTAGCACATAGCCCGATGCCGGAAACC
Oligo149	AAACAAGCTAGATCTACAAAGGCTATCA
Oligo150	TTTATTGCCTGAGAGTTCGTAAAACTAGTATACTTTT
Oligo151	AGAGGAATATAATGCTGTACGGTGTATTTAGTACTCCAAAATGCAGATA
Oligo152	AACCGATTACAAACTACAACGCCTGTAGCAT
Oligo153	TTTGCTGGAAGGCAAAACAATAACGGAAAGAAG
Oligo154	ATATTGGATTTGATTGCAGTAACAGTACCTTGAGCGTAAAATTACCCAA
Oligo155	GGCCTTTAATCGATGATATTTCATGGATATTCAACCGGCTATT
Oligo156	CCAATGTACCCCGGTTGATGCCAGCAGTTGGG
Oligo157	GCTGACCTTCATCAAGACAGATACCGAACGGCGCAG
Oligo158	TTACCCAACCTGACTATAGCGCATAGGCTG
Oligo159	CCCGGAAGCGTTTGCCATCTTTTCATAAT
Oligo160	TCATGTCATTCAACAAGAACCGGATATTCA
Oligo161	AGAAGGCAAAAGACCAGAGCCACCACCGG
Oligo162	GTAATAACCATATTGGCGAACGTGGCGAGAAAGGAAGGGAAGA
Oligo163	GTTGCTTGCGCCGCTACAGGGCGCAACAGTAGG
Oligo164	TGATTGACAGGCCTCAGAGCCGCCAGCCG
Oligo165	TGCACCGGTTGCGGTATCAGGC

Oligo166	TCGTCGAGAGTGATGAAGGGT
Oligo167	GATTATCATCTAAAATAT
Oligo168	TCCCTTACACTGGGGTCATTGCAGGTTGCCCTGCGGCTGGTAATGGGTAA
Oligo169	AAATACCCCGCCTG
Oligo170	CCTGTGTGAAATTGAAACAGCGGATCGACATAAAGGTACCGAGCTCGAAT
Oligo171	CTGACCTGAAAGCGTAAGAATTAGTCTTTAATGCGCGAACTG
Oligo172	AAGCATAAAGTGTTTTACCAGTCCCAAAAGAGACGCAGTTATCCGCTCAC
Oligo173	TCAATCGTCTGAAATGGAACCAGTAATAAAAGGGACATT
Oligo174	TTGCGTTGCGCTCAAGCCTGGGGTGCCT
Oligo175	AACTATCGGCCTTGCTGGGCAACAGGAAAAACGCTC
Oligo176	TAATGAATCGGCCACCGCTTTCCAGTCG
Oligo177	GCCACCGAGTAAGTAATAACAT
Oligo178	AGTGAGACGGGCAATTTGCGTATTGGGC
Oligo179	TGCCCGAACGTTATTAATGAACAAAGAAACCACCAGAAG
Oligo180	GGGAGCTAAACAGGAGGCCCAGAATCCTG
Oligo181	TCCACGCTGGTTTGCCTTCACCGCCTGG
Oligo182	ACACCCGCCGCGCTTAATTGACGAGCACGTATAACG
Oligo183	GGCAAAATCCCTTAAGCAGGCGAAAATC
Oligo184	CCTGCAGCCAGCGGTGTTCAGCAAATCG
Oligo185	GATTAGAGCCGTCAATAGTTTACAAACAA
Oligo186	TGTGCACTCTGTGGCCTGCATCAGACGA
Oligo187	GGCAAATCAACTGGCAAGTGTA
Oligo188	GGGGGTTTCTGCCGGCGGCCAGAATGCG
Oligo189	CAGCAAACAAATATCAAA
Oligo190	CAGTTGAGGATCCCCGAAAATCCCGGCTGATTGCCAGCACGCGTGCCTGT

Table C.14: Staple sequences for folding the 18HB including the oligo number. Middle staples that can be taken out for the dynamic DNA origami are marked in blue. Staple sequences that are to be taken out for handles are marked in red. They can be utilized independently from each other.

Oligon Number	Sequence
Oligo1	AAAGGGATGGATCAAACCAATCAATAAAGCCTTAAAT
Oligo2	ATCAGAGCGGGAGCTATCGAATTTCCTAATAAAAAGCGTCACCATGACA
Oligo3	TCCTCGTAGCTGTAACAAGAATGCGTTACCATTACAGAC
Oligo4	ACGAGCTGTTATCATCAACACAGTATAAAAATCACACAAAC
Oligo5	CAGGGCGCGTCACAACATAATGCACAGTAGGTCAGTTGTAAAG
Oligo6	CGCTTAATAAAGTACAATAACGCCATATATTACAAGTCT
Oligo7	GCGTAAGCCTAATAGTAATTCATGTAAAACGAACAGTAA
Oligo8	CAAGTGACATTAATAAAGTATTTTCGAAAGAAAATTGAT
Oligo9	GAGCGGCTGCCCGTACCAAAAACATAAAATGAAAAT
Oligo10	AGGAAGAACCTGTAGCATAAGAAGCCTCGATTTTCAACGGAGAT
Oligo11	GAAAAATAATGAAAATTAAGGGATAAAATCATTGCCTGA
Oligo12	CCATCACCTGAGTGCCGTTTTTTTAGTAGCCCCCCACCG
Oligo13	TGGACTGGGAGAGGGCAAGGTCATATAGATGGTTCCGCGACCT
Oligo14	AGAGTCGGGCGCCTAACATCCCTGAGTCGAGTAGTTAGC
Oligo15	GTGTTGTTTCACCTTCTACTGATTCAACCCTGACCGGTCA
Oligo16	AATAGCCAGCTGAGAGCTGACCGGAGATCATTCAAACTGA
Oligo17	AAATCCCTGGCCCCTATATTTTCATTTTGGAAGTTTC
Oligo18	TGATGGTGCAAGCGGAAT
Oligo19	CCACCGTATCGGCGCACTCAGACCTAATTCATCGAGCCGC
Oligo20	GTGTTTCCAGAACACGGGTAAATACCGAGCGTCACACCCT
Oligo21	GGTACGCCATTGCTCTTTCCAAGGCGTGACAGAACAGAGCCGCCAC
Oligo22	GAGAATTTTAGACAGGAAC
Oligo23	GGTCCTAGCTGAGAACCGCCAGGC
Oligo24	CAAGCGCAATATATTGACGGAAATTCATCGATATCATAAAGTC
Oligo25	ACCCAGCTACATATCCCACGTAATCCTCGCTACG
Oligo26	TATCCTGAATAGCAGATCCGACTTGAGCCATCACCATTATACAAACCTT
Oligo27	GCGTAAGCCCTTTAGAGCCAACCACATTCAACTAGCT
Oligo28	TGCCATAGCAATAATGCAGATACATAGATTCAGCTTAATGCCT
Oligo29	CCATATAAGAGAAAGGAATTACGAGACAACATTTTAACAATCA
Oligo30	AATCCAAATAGAATTGAAGAGCAACACTATTTAATAATTTAGGCTTTT
Oligo31	TTAAATATCAGCTCGTTTACCAGACCGTTGGGGCCAGTAATTT
Oligo32	AGCAGTCAGAGGAAAACCAAAATAGCGGCTCATATACTTTTTTT
Oligo33	AACATAACTGAATTTTGCAAAAGAAGCCTTATGTTATTTCTTTA
Oligo34	ATATACATAAATCACAATCAATAGACGGTCATTAATTTCTAAA
Oligo35	GTCATTAGCAATCGGCCATGAAGGTTT
Oligo36	TGCGGATGGCAGAGAGTTTTAGACTGGATAGGGCTTGATTTTAAAATCA
Oligo37	GAATAAAACTCCTACTGCGGAATCGTACCAGAAAATGTGTTCAT
Oligo38	ATGTAAAGCGAATTCATTGAATCCCCCTCAAATTAATTC
Oligo39	AAGTATCGCGTTTGCTTTAAA
Oligo40	ATTCAAGCCCGCGAGAATGA

Oligo41	CCAATGCATCAAATCAGGTCT
Oligo42	GCGTTTCGCATCCACGCAGTCTGAGC
Oligo43	GGTATTCTTAGCAAATATGGTTTACCAGCGCGCGTTATTTAATGTTG
Oligo44	CGTTTTAGCACTCCTTACAAAAGGGCGACATGCCTTTACCGTGTCCTT
Oligo45	GGAGAAAAGAAGATTGAGGGAGGGACAGTAGCTAAATAAAATC
Oligo46	GGAATACCCGTTTTGATCGGCTGAAAGTCACAG
Oligo47	CCGAGGAAAATTAGTTCATGTAGCCCGGGTTTATGGAGA
Oligo48	ACCAGAAAAAGGTGAATTATCCGGAAACCTGTTTATTAG
Oligo49	AGAAAAGTACTTACCAAGTCCTGTTCCTGTCGGGGATTT
Oligo50	TATAAATAGCACATCGTAAATAACAAGTCAC
Oligo51	ATCTTACCGCTTTCCACCTGTTTCGCTCACACATAACAA
Oligo52	AACAATGAAAGTTACAGTTCAGCTACGAGCTAGATGATT
Oligo53	AGCCCAATAATTATTTGACGACGGTAAAGCGCCCTCTCT
Oligo54	TAACCCACAAAGAAACAAGGTAAGAGTGAGAGTACGGTG
Oligo55	TGAGCGCTACGTCAAAGAGAATATTGCGTTCCGTGCAAA
Oligo56	TGAACAAAGCCTTTACTCGGTTGCTTTCCAATGTGCGAG
Oligo57	AATTAAAAACAGCCTCAGCGTGCCAAAGACAAAT
Oligo58	TAATTGCTCCTTTTATAGAGGGGGTAATAGAACTTTAAATTTTTGGAA
Oligo59	CAGGATTTTAGAGCTCATACAGCGGTTTGCGTATTCACTATTAAAGAACG
Oligo60	GAAGCTAATGCTGTAGCATAGGGTGGTAGATGAAG
Oligo61	GAGCTTCTTTAAATGCATCAAAGTGAGAGACATCACG
Oligo62	TCAAATACGGTGTCGGGGCGCTTGCCCTCCGGTGTCT
Oligo63	AAAATACATAGAAGGCCAAGCAAAGAAGAAATTTACATT
Oligo64	TAAGAGGCATATAATGTTTAGTGAGAGACGTTATCAA
Oligo65	GCAGTATGTAAGAACGAAGTACCCTTGCTGCTCAA
Oligo66	ATGATTAAGGAACCTCTCCAAGAAATATTAGGAA
Oligo67	CAGTTAAGCTGCCAGTCAACAAGAGAAAACATTGCT
Oligo68	CCATAATTACCCGATATTCTGCCTGAGCTGAAAGCAACG
Oligo69	TTACCTTGACAATAAATTCTACAAAAGGAGTTAGCGTATT
Oligo70	GGCTTGAAGGGTGATCGTAATATCTTAGCCATCCT
Oligo71	CAGAACCACCCGTAATAGGTAAAATAAC
Oligo72	AGCCGCCGTATAAGTTTAACAAATATCAATTGTTTG
Oligo73	GGAGGTTGAAAGTGCCCCTTTTTTCGGAAGGGTTAGAACC
Oligo74	GATTGGCCTTTTGCTCCATAAATACGCCTGCCAGGAG
Oligo75	AAATAAAAAGGATTGAATAACCGATCCGCAGTAAA
Oligo76	CCAGAATGGGAGGCTGGCCAGCTCACTCATGTGAGCG
Oligo77	CTGAATTTATCTGAAAATGTGAGGAACCACGCACTGC
Oligo78	GCGTCATACGCCTATTTCGGATTAGCAATACAGGCAA
Oligo79	CACTTATTAGTATTTTGGGTGGCAACA
Oligo80	GATACAGGATATAAACACGGCGGAGAAGAAGGATTTG
Oligo81	TAAGTTTTAACGGGTAAAGAACTGAGAGGCCACCC
Oligo82	TTGTCAAGCGCTGGGCGCTTAATGAATTGTGC
Oligo83	TAAATTGTGTTTGACCTCTGCCATATTAACGAACGGG
Oligo84	GAACCGCCTCACCCTCCGCGCAGGTACCTTGGAACAA
Oligo85	GCTCCGAATACACGACAGTATTCGCATACAT

Oligo86	CGGAACGAGCCTAAAAGATCGCACGGCCAGGAGAACG
Oligo87	ATCATAAGATGCCACCCGGCACAGTCACGACAGTAG
Oligo88	CCAACTTTATTAAACGAAACCAGGGTAACGAGCTTG
Oligo89	TGAACGGTCTTTTTCCGCCATTGTGCTGCAAACTCA
Oligo90	CACCCTCAAACCGCCTTTCAATTCAGATGGGAGCGG
Oligo91	CAGAGCCAGTTTAGTAAGATGACGTAGATTCCTGATTATC
Oligo92	TCCAGACGTTAGGGGTTGACCAGCATATGAAACATTCATTGGAAA
Oligo93	ATGGGGGCGGATGGCAGGTGCAAGGCACCGTCAAGCCGAACAAAGTT
Oligo94	CTAAACAACTTTCAAGCGGGGTTGATATTCCAGTAGTTGGGAATTTTA
Oligo95	GAGTGAGAATTCAAGAGTCCTCATAGATTTAGGAATGCAAGCCAATAAT
Oligo96	ACTAAAGGAAGTATTAAAAAGCGCGGTAGAAAACGCCACAAGA
Oligo97	AATTTTTTCACTATTATCCGTTCCTAACGGAGCATAGTAGTTA
Oligo98	TCCAAAAAAAGCCCCCTATGGCTTATCTACGCATAACCAGAGA
Oligo99	GGAGCCTTTAGTGCCCGGTGTACTGTCAGGAGACGATAGTAAT
Oligo100	TTATCAGCTTAGGTCAGTGCCTTGGATAGGTCATTGATTCAGCATCAG
Oligo101	TCTTAATTATACATCATCGTGAATTATTTTGCCTAGACGGGAG
Oligo102	CCGATAGTTACTCATCTCGAAATTAATTTCTAAAATGACCTT
Oligo103	TTTCGTCACCAGTACGAACCGCCCCTCAGGCATTTTAAATTCACGTAG
Oligo104	CAATGACAACAACCGGCAAAAATGTTACTAAATTGCGTCCAAAACAGGT
Oligo105	CATAACCGATAGCACCAAGCGCAGAGAGAAACCATAAATACCAGACCG
Oligo106	CGCTGAGGCTTGCATACGTAGGAACCGGTGAATAA
Oligo107	TAAAGGCCGCTTTTAGTTTCCGAAAGAGCGTAACACAGAAAAAAAGACT
Oligo108	CGTCACCCTCAGCACTAAAGAGTACAGAGATATTCAATCAAAAAAAGAT
Oligo109	CAACGCCTGTAGCATCCCTCAGGAACCGCGACTGTAGCCAAAGATTAC
Oligo110	GACAGCCCTCATAGTTCAGGAGCCACCCTTCAAGTTTTCAACCCTGGC
Oligo111	AACGATCTAAAGTTTGGAATAGGTGTATCAGAAAACAAAACAGAATT
Oligo112	ACTTCCGCAGGAAAAAAGTCTTTGGTCTGAAACATCAACCGTACTAGCGT
Oligo113	TGATATAGCCCTAGTGAATATTACATATAGCCCTGTCGTCTT
Oligo114	GCGGGAAAAATAAAGACGCTGAATTAGTCGAGATAAATGAATTTTCTGT
Oligo115	ATTTTAGCAGAAAACATAGAACAGTAAGTACCAATTTTG
Oligo116	TCCTCGAGGCGGTTTTCCCTGTGAGTAGGATTACAGTTTCAGCG
Oligo117	AAACCGCCTGCATGAATCGTCGCTATCGCTCAAGAACGCGGAGCCTAATT
Oligo118	GTACAAGAGCCAATAATTCACATTAACATGAAATTGCGAATAAT
Oligo119	GAAACTGATGTCCCAATAGCAACCCGTCGGAACCGTTGAAAATC
Oligo120	ATTATGCATCAATTAAATCGGAACAAAGTTAATAGGCTCCAAAA
Oligo121	AAATGGGTTTTGAAAATTCGTAATGGAGTAACAATTGTATCGGT
Oligo122	CCCCATGTGAAATGTAAACGTGTAGAGAAACAAGCTTTCGAGGTGAATT
Oligo123	GGCAGAGAACCCTGATGCAACAAAATAGAGCCAACTGAG
Oligo124	ATAAGGTCGTCTTGTATAACCGTGCACCCAGCGAACAGCTTGATA
Oligo125	GTATAGACCGTATACCCCG
Oligo126	AAGGTTGAGTATAACTAGCCAGCTTTTACGAAGTATTCGGT
Oligo127	TGTCTTTTACATATCGATGGGTGCCGGGGTAAAAGGGAGT
Oligo128	TGTTGCCGTTTAGAGTCTGCGCCATTATGAGGAGCGGGAT
Oligo129	AAAAACATTGCAGGCTATCCGCA

Oligo130	TCGTCTGAACGTAAGATATATAACTATATGATCTTCTTCGAGAATTATCC
Oligo131	ATACCTACATCAATATTAACCTCCGCAAAAGACCGCCATCCACA
Oligo132	TCTGAAGCCCCGGGACGACTAAAACGCGCCGA
Oligo133	GATATGCAGATTCACCGCCTTATAAATCAAAAG
Oligo134	GGGAAGTGCGCTAACGTTGT
Oligo135	AAGTCCGTAAAATCAAAGGCGA
Oligo136	GCTAAAGCGTGAGGGCGAAA
Oligo137	CATCAATATACAACTAAGAACTGAAATGC
Oligo138	GATTATAAAATATCCGCCATTTTTTGTTACCGAGCAACAGGAGGCCGATT
Oligo139	AATAATGGACTTGTGGGAATTGAACCACCATCTGAAATGGTCATTAGA
Oligo140	GATCTGGTTGGCAACAGAGGTGCACTCGGTGAAATACGTATAACGTGCTT
Oligo141	TAACATTATCTTAAATCCAGAGATATTCACCTCA
Oligo142	CAGAGAGCCTCAATTAACACCCAATATTAATTCCAACTATGGTTGCTTTG
Oligo143	AAATTAAGCTGAACCACGCTGAAACATACGGAAGCATGCGCCGCTA
Oligo144	GTGAAGCCAAAATCTAAAGCATCACCTTCTCTCAGCAGGCTATAT
Oligo145	TGCATGACAGGATGGGCATTCTATCACGCTAACTCTAGCGGTCACGCTGC
Oligo146	ACGCAGAGGGGTTGTGAGATCACTGATAGCGCTCAGCGCTAGGGCGCTGG
Oligo147	TGGTAACATCATTATAACGCTTTCTGCAGTCGGGAGGAAGAAAGCGAAAG
Oligo148	TGGAACTGACCCGTATTTCGCTCTAATGGCTGCATCCGTCTATCAGAGAA
Oligo149	AAAGAAACTGCGGCGATGCCATATTCCAACGCGCGCCAACGTCAAAGGGC
Oligo150	CAAACGCCGACTGGTGAGATGATGATATAGAGTCGGCATACAAAGAG
Oligo151	AGGATATACTCCTGATCGGGTGTTTATGTTTTTCTTTCCAGTTTGGAACA
Oligo152	GGAAACTGTTGTTCCTGTTTCCCATGCACGGGCAACCGAGATAGGGTTGA
Oligo153	AGAAACCCAAACAACTGAAAGATGGATTCTCAAACAGTAAAAGAGTCTGT
Oligo154	AAACAGCGAAGACGGAAACCAGTTTCTTGCGTGTTGCCAGGGTT
Oligo155	ACGAGCACTGGAAACGACATAGATTGGGGTTGCAGGTTCCGAAATCGGCA
Oligo156	AATTATCATTTAGAGCACAGATTTGACGGTAATATTTATAATCAGTGAGG
Oligo157	AGACAATAGAGGCTATTCGCTCATCCGCCAGCCAGAATCCTGAGAA
Oligo158	ACGTAAAATTATTATCAAGAATAAACACCGGAAGCAGCACACCAG
Oligo159	TACCTTTCATTTGAGAAGTTACTAGTTACGAGGCTATTTTGC
Oligo160	CAGGGTTGTAATGGACGATAGCGTATCATAAAATAAATTT
Oligo161	GAAGCAATATATTAGAATTTCTTACATAGATAACGCTAACGA
Oligo162	GTGGCTTGCTTCTGTATAAGACTCCAGAAAGGAACA
Oligo163	CTGCTTCATCAGCGTCTGTGAGAATACAACATAAATAAACAG
Oligo164	CGCCGCCTCGAGTAAGAACGCCACGCCAACTGTCCAATCCC
Oligo165	AGAACCAAGTTAATCCAAAAATATATTATTTTAGCAAATCAG
Oligo166	ACACCTCCGTGAGCTCATAGAGGCACCGACAAGATTTTTTGT
Oligo167	AAATATTGACCGCATTAAATTATGACCCTGTATATACCAGGTAA
Oligo168	ACATCACGTTGGTTAATATGCGGGAAGCTAAAAGAGAGAAT
Oligo169	GGGAATCGTAAGCAAATAAACGCAACAATAAAGGGAAGCGCGATAAGAG
Oligo170	CCTCATGCGGTTTGAGAAAAACAAGAACCCCAAAGAATTTT
Oligo171	CTTTATTATCGGCCTCAGGAACGAAAGAATCGCCCACG
Oligo172	AAAACGACTCCAGCATGTCAAAGGTAAAAATAGTAGTAGCTCAAC
Oligo173	TTCCCCGCTTCTAACGGTAAGAAAGGAAAGGTGATGCAACTA
Oligo174	TTAAGTTGGCAAAGGAGCAAAATCACCATCAATATAAATCAAGACAGA

Oligo175	GGGGGATCAGGCTGAGGTCATAACCGTTAATAACCCAGTTGATTC
Oligo176	AACAAGGCGAATTATTCAACCCTCAAAACTA
Oligo177	AGGTTTAACGTACCTGAGGCTTAGGGTTTGATTAAACCCGAGG
Oligo178	ATTGTGAAACAGAGACTAGATAAATTTATCATCCGACTTGCG
Oligo179	ATAAATGCGCTAGATTAGAGCCGTTGATGGCAAATAAAGAA
Oligo180	AATAAAACATTTTAGGAGCACTAAATCCTGAAATTATTTGC
Oligo181	ATTCCGAACGAGGAAGGTTATCTACTTCTG
Oligo182	GAAGATAAAAATCAACAGTTGAAACAAGTTGGTCGTT
Oligo183	TAATCAGTATCAATATCTGGTCAGAACTTATATAGATGAAC
Oligo184	TCCACAGTGCCTCAAATATCAAACGTTCGAATGTTGTGAGT
Oligo185	AAAGCAGCAAATGAATAGATACTTCTGGGGTCCACCACACCCGCCG
Oligo186	TAATGACGCTCAGGTGAGTATCTGGGCAGAGAAAATG
Oligo187	TTGAGGAGAGGAGGTCAATGGGTTCGACTGGTTACAGCGCA
Oligo188	GTTTAAAAGACGCATCGCTATTACCCTTTTCCATGAAT
Oligo189	AATATGCTGATAGTAACTATCGACACCATCGAAGATGGCAG
Oligo190	GATTCACAGCAGTTAATCGAACAAGCTGGATCAACAGTTCA
Oligo191	GAATAGTGTCACCTGGAAGAGTTTCCAGCAATTCAC
Oligo192	GTTGATATGCAATGCAATAAATTAATTGCT
Oligo193	TGCTTCTGACTTCGACAACTCGTAATTTTGCTTACATCGGG
Oligo194	ATGCTCAAACTTATCAAGCACTGCCGACCAGTGCCAAG
Oligo195	GGTATACGTGAGTATTAGACTTTAACCAGAAAATATACAGT
Oligo196	TTTTTTGAATTAATACATTTGAGGATCATATTTTC
Oligo197	GCAGGCGAAAATCCTGTT
Oligo198	TCTTTGATTAGTGGAATCATT
Oligo199	CTTGCGCAAATTAACCGTTGTAGCAATACT
Oligo200	TTGACCATTAGATACAAACGAGTAGATTTAGT
Oligo201	ACCGCGCCCAAAGAAACGCAA
Oligo202	AGTCAGAAGCAAAGCGGATTTCT
Oligo203	AGACACCACGGAATAAGTTCGTTTGCCTTTTTCTCGC
Oligo204	ATCAAGAGTAATCCTGACTATTAT
Oligo205	ATCAAAATCACCGGAACCACATTTTCTTGAATAACAATAATGAG
Oligo206	GCATAGGCAGAGGCTGTTGGGAGCCAGCTTATTACGAAGGTGTTATCT
Oligo207	AGCAACGGCTACTGGCTGACCTTC
Oligo208	CCCAATAGGAACCCATGTACCGTAACCCACCCTGAGC
Oligo209	ACGACCAGTAATA
Oligo210	TCAATGAGTTAGTGGTTTGCCCCA
Oligo211	AAAGGGACATTCACAAAGAAC
Oligo212	CGGATGGGAGTATATAAATGAGTA
Oligo213	ATTTTAAAAGTTCGGATTCGC
Oligo214	GCCTCTTCGCTATTACAGGGCGATCGGTGCGG
Oligo215	ACTTTGAGGAGCGAAAGACAGCATCGGAACGAGGGT
Oligo216	CTGATTGCTAGGGATAGCAAG
Oligo217	AAGTGGCCAACTTTGCCCGAACGTTATTA
Oligo218	GCTATTTTTGAGAGATAATGCCGGAGAGGGTA

Oligo219	GCGAGAAAACATCTTTTCATA

Table C.15: Staple sequences for folding the Cube including the oligo number and whether it is an endstaple. Three staple sequences that are to be taken out for handles (Handles 1-3) are marked in red. Sixteen staples are extended by four thymine to prevent stacking of single cube structures (blue).

Oligo Number	Sequence (5' → 3')
Oligo1	TTTTTACGTGAACCATCACCCAGCACTAAATCTTTATGG
Oligo2	CAAGACGAGGAAGGTTATTAATACATTAACGGAACTTTT
Oligo3	GCTTCCACCACCCTCATCTAGCCACCACCGGAAAC
Oligo4	ATACTGCCTTGAGTAAAAGACAGCACATGAGGAAA
Oligo5	ATTAAGAGGATATATTCGCAGCAGCAACTGACCAG
Oligo6	CCACAAACAGCAGCTTGCCAAAAAAATAATTTCAG
Oligo7	AGTGAAGAGAAGGTCATAGCCCCTCGCCGACAGAA
Oligo8	AGGGGAATTTCTTGCATAACATCTTGAGGCTGGCTAT
Oligo9	ACCGCCACCCTTAGCCCGCGTAATCAGTAGTTATGCAC
Oligo10	TCTCTTTCGAGCGAGAAAATTCAGTCCCTCAATTT
Oligo11	CCGCCCATGTACCGTACAACAGTTTTTTCACGCGA
Oligo12	CGTTGTCCTCGAGAAGTGTTTTTATAATCCACGCAATTT
Oligo13	CACACGAATCGTCTGAAAACATTCTGGCCAGCCAG
Oligo14	CAAAAGCCCAATAGGAACCACCCTCAAATCACC
Oligo15	TTTTGCGTAACGATCTAAAGTTAACAACTCAACATTACG
Oligo16	GTGAAATTGTTAACAGTTGAGGATCCCCGGGTTGT
Oligo17	TTTTTTCCACAACATGTGCCTAGCTCACTAGCTGCAGTT
Oligo18	TATTTCGGCCTTGCTGGTATAGCAATACTTCTTTG
Oligo19	CCAGAAATTTTGACGCTCGGGCCTCTTCAGAAACTTTT
Oligo20	TTTTGCGTCCGCACGGTCCGGCCAGGAT
Oligo21	CGGTGGGAAGTTCGCCAGCT
Oligo22	TAATTAACGGAAATCGCGTAATTTTATATGTGAAA
Oligo23	CCAGGGTGCCGAGCAAATAAACATCGTTGCCCCGG
Oligo24	AGTGTGGGTAAGGGATGTGCTGCAAGG
Oligo25	AGATAGAAGGCTATTAGTCTGGGAAACAATTG
Oligo26	GTTCGTGCCCCGCGTTGCATGAGTGAGCTAACGCT
Oligo27	TAACCGGGAACCAAGCTTCGGCGGAGATGGGCGC
Oligo28	CCCCGATTTAGGAAAGGAATATCAACAGCAGCATC
Oligo29	TTTTGGTTTATTAAACCGTCTATCAGGGCGATGGCCGAA
Oligo30	CGAAAGATAAAACAGACGGGATAGCCGAAACGCATAAC
Oligo31	TACAAGAGGCGTTAATGAATCGGCCATTAATTCTACAG
Oligo32	ATTAACACCCGCCGCGGCTTGAAAGGAGCGGGCGC
Oligo33	TTGCTCAGCGGAGCTTACGTCGGTGCCGCAAGCGG
Oligo34	GCGTGCGGCTTAGACTTTACCAGTCCTGTAGAACA
Oligo35	TCTAAAGCATGGCGGTTGACGGAAAATTTAATTTC

Oligo36	CACGCAACCGGTCATTTCATTTGCAGCGGAAAA
Oligo37	ACAGACCTCAAAGGGAAGAAAGCGATTAAGGGAGC
Oligo38	GTGCAATGCCAAGTCCACGAGTGTTGTTCCAGTGG
Oligo39	ACTTGTAGAACAGCCTCCTCCGTTTGAATCGAATA
Oligo40	AGTACAATAGACTAAAATATCGGAACCCTATGCAC
Oligo41	CAGAGCACATCCTCATTGTTGCCGTAACAACGCTC
Oligo42	GGCAAAAGTTACAGCACCGGCTGGATCCGAAAGGC
Oligo43	TGGTGGTCACCTTGCTGATTGAAAGGAATTGGAAC
Oligo44	GATGCATCGACAAAACACCGGAATCCCAGTATA
Oligo45	TTCTGAATATCTGATATTCCTGATTAAATGAAAGT
Oligo46	GAAACCGCCAGAATCCCGGAAGGGTAACGCGGGGC
Oligo47	AAGAATGCAAATAACCTCGCAAGCCGCCCAATACT
Oligo48	TAGATGGTCATGGAAGGGTTACAGCAGACTGATAGCTT
Oligo49	TTAATTTGAATCCCTTCTCGCCAGAATCCTACAAGAATTTT
Oligo50	TAAAATAGAGTCAATAGTGGTTGGGTTATATTAGC
Oligo51	ACGGGTTTTCCATCAGACAATGCGGATTCCACTGT
Oligo52	AGAAACAAAAAAGGGTGGATTAATTAAC
Oligo53	TCACATTACGCTTGTAAATCGTCGCAAGACGCT
Oligo54	CAGGCCAGTGCGGATAACCCATGTTTCTCCGTGCA
Oligo55	TAGGAACCACCACACCGCGAACCACGAACCTAATA
Oligo56	GAAAATCCTGTCCTTCACGCGGTGAGGCGGTCAAA
Oligo57	TTTTCATTTAACGATTCATTTCAATTACCTACCAA
Oligo58	CAGGCAAAGCGCCAGGCGATCCGAAAGGCGC
Oligo59	TTCCGGCACCGACGACAGGTGCATCTGGTGTATTG
Oligo60	TTCTGAAGTTTCACTAATTGCTGAATATAATGCTGTA
Oligo61	GACGCTTCTGGTGCCGATTTCATTTAACCTTGC
Oligo62	CAGTCAGCTGGGGTGCGGCCGTTTTTGAGCCTCCTCATAT
Oligo63	GAGAAGATGGTCAATATAACAAAGAAACGATTTTAAA
Oligo64	ACCGAGCGAGTCCAGCTTAATAGGATGTTAAATAA
Oligo65	CTTAGAATTTATACCTTTTACATCGTCTTTCAGGT
Oligo66	TATATGTAAATATATTTTAGTTTAAATCGCCA
Oligo67	CTGGCGGGCAACAGCTGACGCGGGGCTTTAATGCG
Oligo68	ATCTTAAATAAGAATAGCATTTTTATACCAAAATTTTA
Oligo69	TATTTCAGCTCAAGAGACGGTGAAGGGTCACTCCT
Oligo70	ATTGCAGGAAGGTCAATCTGAACGGCTATCAGGTC
Oligo71	ATTAGGAATTATCATCTACTTTTTAAAAGTTTTCA
Oligo72	GTATATAAAAACAGTTGGTCCAGCAGGTATGACGC
Oligo73	AAGCAAGGAGACACCTCATAAGAAAAGAACTGGCCAT
Oligo74	ATTGTATACAAGCTAATGTCCTGAAAGACTCCGGA
Oligo75	AACAGCAGAGGCAGATCTACAAAGGTAATCGTTCC
Oligo76	TTAGGTAGGGCGAACGTTATTAAGAAGGATTTAGATTTT
Oligo77	CACCACAACATATAAAAGTCATATGGTGATACATA
Oligo78	TGAGTGATATTAGGGTAGCTATTTTTGAGATTAAT
Oligo79	GAAAAATAAACGTACAACATGTTCAATTCTTAATA

Oligo80	TCAGTAATACATCGTCAAAACAGTTAACAAACGGA
Oligo81	GGCTTGGATATCCCATCCTAAAGGCGTTCTGACCTAC
Oligo82	TTCCTTATTTTTTCAAATGCTGAATTGCG
Oligo83	AAGCTTTAACCTCATCAATACAGCGCTCACCGTGT
Oligo84	ATAATGCCACAAGAATTGACCGAAGCCCTTCCGAA
Oligo85	CAAGTCAGAGCTGACCCTACGCAAGAATGCAAGGG
Oligo86	ATTACCTGTTTAAGCATTAGACGGGCAGAGAG
Oligo87	AAGGTTAGATTTATTAATCAGAGGCGAATTCTGACGGG
Oligo88	CCCGACGTCAACCATATTGAAC
Oligo89	CGGTTCCCAATGATACATTTTTCATCTACTAAAGG
Oligo90	AACGTTTTTTGAAGCCTTAGTGAATGAATTACTTAATTA
Oligo91	TCCTCGTTACGTTCTTAATGCGCCGCTACAGGTAA
Oligo92	TGCGAGTGAGACCCTGAGCCCAGCATCGGCAATAG
Oligo93	GCGTCCAATCCAAATACATTTGTATCCACACTAAA
Oligo94	GGATATTAGAGCGGAAGCACTTCAAAAAAGATGTC
Oligo95	ACCTCGAAACATGACCCCACCTAAAACGAAAGAAA
Oligo96	ATAATTGTTTAACTTGCGGGAGGCCATAGATATAG
Oligo97	CAGGGAAGCGCTCAATCAGCCTGATAATAAGCGTC
Oligo98	GAACAGAGAATACCGCCTCTCAGAGTTGATGACGC
Oligo99	ATTAAGCAAGCAAATCAAACCATCGAGAACAACGG
Oligo100	ATAACACTGACCTTGGAACCGGACAGTGCCCGTATAGTTTTT
Oligo101	TATATAAGAGGAGCTATATTCGCAAGTCACGTTGC
Oligo102	AGAATCAGGTCATGCTTTTAAATATGTAAAATAGA
Oligo103	ACCCATCATACTAGTAGTAAATGTGTAATGGGACG
Oligo104	AGAAAAGTAACGGAATACCCGGATTGTGAGCC
Oligo105	AACGTTAGCAAGCAGCACGAATAGGCAGGCGGATA
Oligo106	TCAGAGCGGGAGCTAAAACGGTAGACCTGACAG
Oligo107	AGTTCAAAATATCGTTTACAAAAGGAATTACGTAGTTTT
Oligo108	AAAGGTGGCGATAAAACGCCTTATGTTCCTCAGAA
Oligo109	ACACGTAGAAAATTATCAGCCAGCAAGAGCCAAGT
Oligo110	CGCACGACGACAATAACATTCGAGCCAGTAATAAT
Oligo111	TTTTACGCCCAGACGATCAATAAAAGGCCCTAGCATATT
Oligo112	ACTAATGCATTAACGGAATTACACTGAGTTTCTTA
Oligo113	GAAATTATTCTACCAGCGCCAAAGAAGAAAATAAA
Oligo114	TTAATAAAAACTTGCCAGTATTTTAGATAAAAAAA
Oligo115	AGTATAAACATTAAAGGTGAATACATAATGATTACAA
Oligo116	TTTTTTTAATCGGTAATATCATTGAAACATTAATA
Oligo117	CATTACCACAATAATAAGCAGACAATAATC
Oligo118	CAACAAGAACTAAAATCTATTACAGACCACATTCA
Oligo119	CTGAGTTTGATATAAGTACAGAACCGCCACGAAAA
Oligo120	CAGGACAGGAGGCACGTAGCGCGTATGCGCGTGCG
Oligo121	TCAACTATCTTAGTTAAGAAGTACCGCACTATGTGTCT
Oligo122	TAAGAAGAGTACGCTGAGACTCCTCCCGTCGAG
Oligo123	TTTCGGATTAGTTCTGAAACATGAAAAACAGTACC
Oligo124	GGAACCAGAAGCACTTATTAGCGTTCTAATATAGA

Oligo125	CTTTGCGCATACAAGAACGCTGCTCCACCAGATTT
Oligo126	ACGGCCGAAAGAAACTCCAGTTGATGTCTGGAGGG
Oligo127	TTGTACGGAGAGGTCAGGGGCTTAGAGCTTAACGA
Oligo128	CGCCACCAATTTATCCTTTCCAGAATCTTACC
Oligo129	ACACTCATCTTAAGTACAGTCGAAACGAGGCGCAA
Oligo130	AGTCTCTGAATACAAACAGGTCAGACGATTGGCAGAGC
Oligo131	TCCAGGTTTCCATTAGGCAAAAGAATTTGATATTCTTACCGT
Oligo132	CGGGACTTTTTTCGGAACTCACCCTGTCGCTGCGC
Endcap1	TTTTCGGATTTGCTATTGTCGTCTTTCCAGACGTTAGTAAATTTTTTTT
Endcap2	ATTACAAACTAACCGCCAGCCATTGCAACATTTT
Endcap3	ACATATGGAAATACCTGAAACAAAACTTTTTTAATGGAAACAGTTTTT
Endcap4	CAAAGAGTAACAAGGAGCCTAGAAAGATAAATATTTACGAGCATTTTT
Endcap5	GCACCACCAGATTATCATAAATCCTT CAAACAATTCGACTTTT
Endcap6	AGATTGGATTATAAATTTAGAAAACCATTCCAAGAACTTTT
Endcap7	TTTTCTGGGTGGCGAAGCTTGACCGTAAAAATCAAGTTTTTTGGGTTTT
Endcap8	ACCATCAATTTTGGGGCGCGAGCTGATTTT
Endcap9	TTTTACGCCATTAAAGCCGCAAAGATCAAAAAGCAAAGCGGTTTT
Endcap10	TGTATTCAAAATGCCTGAGTAATGTGTTTTT
Endcap11	ATTGGCCGGAGCAACCGTATAACCCGCGAGAGGCTTTT
Endcap12	TTCTTACCGCGTTTTTATTTTCATCGTTTT
Endcap13	TCAATTATCCTGAGCCTAATTTGCCAGTTATTTT
Endcap14	CGTGCCCTAAACAATATTCGTCAGATGAATTTTT
Endcap15	GAATGTAGAAAATGGGATGTGAGAATAGAAAGGAACATTTT
Endcap16	GGAAATTAGACCGTCACGAAGGTAGCGACATTCAACCGATTTTT
Endcap17	TTAAACGAGTAGTTTATCTTGATACCGATAGTTGCGCTTTT
Endcap18	TATCAACCATAGGCTTGCAGGGAGTTAAATTTT
Endcap19	GAATCCGCGAACTAAAGTAAAATACGTAATGCCACTTTTT
Endcap20	CACTGAGGCAAATAAATCCTCATTAAAGCTTTT
Endcap21	TTTTAAGTGTAAAGCCTGGGACGAGCCGGTGCTGATAC
Endcap22	TTTTTAATCATGGTCATAGCACCGAGCGTTCTTC
Endcap23	TTTTACTAATAGATTAGAGCCGTTTAGACTTTTGCCCTTA
Endcap24	TTTTATACAGTAACAGTCAAAATCGATAGCCTTATCCCCT
Endcap25	TTTTGTCCACGCTGGTTTGCAGAGTTGCCGG
Endcap26	TTTTATCGTAACCTATCGGCAACTAAAGTAGCTCTCATTTTTGCTTTT
Endcap27	TTTTGGTTTTTCTTTTCACCTATTGGGTCGTCATCGT
Endcap28	TTTTGTAGAAACCAATTAGCCGAGCAATAGGTTTGCCCAT
Endcap29	TTTTTTTAGTTTGACCATTATCTGCGAACCAGACAGT
Endcap30	TTTTGCACCCAGCTACAATTGATTAGTTAGCGAAGGTA
Endcap31	TTTTATTGCATCAATATCGCGCCG
Endcap32	TTTTGGAAACCTGTCGTGCCGCCCGCTAGCCAGCCGC
Endcap33	TTTTTTATTTTGTCACAATCAATCAAAAGGAATATTGGTA
Endcap34	TTTTCAGGACGTTGGGAAGAGGCTCATGCGAATAAAGGCTCCAAAAGGAGCCT
Endcap35	TTTTAGCGCGTTTTCATCGGTTTAGCGATCGATAGGCC
Endcap36	TTTTATAATCAAAATCTAATGCCTTTAACGGGGTCAGATG

Endcap37	TTTTGTCAAAGGGCGAAAAAGAACGTGGCAGCAAGTGCCATCCTTTT
Endcap38	TTTTGTCGAGGTGCGGGGAAAGTTTT
Endcap39	TTTTGAGGCTTTGAGGCCTGCTCCATTTT
Endcap40	TTTTCTGGTAATAAGTCCCTGCCTATTTTTTT
Endcap41	TTTTGGCCGCTTTTGCGACAGATGATTTT
Endcap42	TTTTCGGAACCTATTAGATTAGCGGGGTTTTT
Endcap43	TTTTCGACAATGACAATCATTACCCTTTT
Endcap44	TTTTTTTGCTCAGTACTGTATCACCGTATTTT
Endcap45	TTTTTTAATTGTATCGGTAAATTGGTTTT
Endcap46	TTTTCTCAGGAGGTTTCCACCCTCATTTTTTT
Endcap47	TTTTACTAAAGGAATTTATACCAGTTTTT
Endcap48	TTTTTCAGGGATAGCACTACAACGCCTGTTTT
Endcap49	TTTTAAAAGAGTCCATCACTTGTTTT
Endcap50	TTTTTGAATTTTCTGTGATTCATCATTTT
Endcap51	TTTTTAGCATTCCACAGACAGCCCTCATAGGTCACCAACGTTTT
Endcap52	TTTTCCTGAGTAGAAGAACTGTAATAATGTCCATAGTGAGGAGATTTT
Endcap53	TTTTGCACGCGTGCCTTCGAATTCGTTTT
Endcap54	TTTTGGAAAAACGCTCTGGCAGATTCACTTTT
Endcap55	TTTTTGTGCACTCTGTGGAAGCATATTTT
Endcap56	TTTTCAGTCACACGACAAGCGTAAGAATTTTT
Endcap57	TTTTCGGGTTACCTGCTTCCAGTCGTTTT
Endcap58	TTTTACGTGGCACAGAACATCGCCATTATTTT
Endcap59	TTTTAAAGAATAGCCCGAGAAATCCCTTATAAATCATTTT
Endcap60	TTTTAGGTTTCTTTGCCGCCAGGGTTTTT
Endcap61	TTTTAAAATACCGAACCTGCAACAGTGCTTTT
Endcap62	TTTTGCACTCAATCCGCAGCAAGCGTTTT
Endcap63	TTTTCACGCTGAGAGCACCCTCAATCAATTTT
Endcap64	TTTTTATCTGGTCAGTGGAGCACTAACATTTT
Endcap65	TTTTCTGGTCTGGTCAGACTCCAACTTTT
Endcap66	TTTTGTCGCTGGCGTCAGCGTGGTGTTTT
Endcap67	TTTTAACTCGTATTTTTGCGGATTTT
Endcap68	TTTTCCGGCGAACCAAGTGTAGTTTT
Endcap69	TTTTGGCGGCCTTTAGTGATTAAAAAACCAAAAATAAACGTTATTTTTT
Endcap70	TTTTACAAAGAAAATTCATCAATTTT
Endcap71	TTTTAATTTCTGCGCAGGCGCTTTCTTTT
Endcap72	TTTTTATAATCCTAAAATTATTTTTT
Endcap73	TTTTTGTGAGAGAGGTAATGGGTAATTTT
Endcap74	TTTTTGCACGTAAAACAGAACCATATCGATTGTTGATGTTTT
Endcap75	TTTTGAGCCGCCAGGCATCAGATGCTTTT
Endcap76	TTTTCGATTAAGTTCACTGCGCGCCTTTT
Endcap77	TTTTGAATACCAAAAGATGATGTTTT
Endcap78	TTTTCGCAACTGTGGGTTTCTGCCATTTT
Endcap79	TTTTAAACAAACATCAAGAAGCAAAAGGTTACAATTCGCCTGATTGCTTTTTTT
Endcap80	TTTTGCACTCCAGCCATTCAGGCTGTTTT
Endcap81	TTTTACATAAATCAATCCCTTAGAATCCTTTT

Endcap82	TTTTTTGAAAACATAGCATAGGTCTGAGTTTT
Endcap83	TTTTCGTGGGAACAAATCAGAGGTGTTTT
Endcap84	TTTTAGACTACCTTTTTCCAATCGCAAGTTTT
Endcap85	TTTTGCGTCTGGCCTTCCCGGAATTTTTT
Endcap86	TTTTACAAAGAACGCGAATGGTTTGAAATTTT
Endcap87	TTTTCGGTCACGCCTATGGTTGTTTT
Endcap88	TTTTAAAATTCGCATTTCAAACTTATTTT
Endcap89	TTTTTACCGACCGTGTAAGCCTGTTTAGTTTT
Endcap90	TTTTATCAGAAAAGCCAGCCGCACATTTT
Endcap91	TTTTTATCATATGCGTAGAATCGCCATATTTT
Endcap92	TTTTGAGCAAACAAGATTTCGTCTCTTTT
Endcap93	TTTTTTTAACAACGCCAACATGTAAGAGAAGTCCAGAAAGTTTT
Endcap94	TTTTTAAATTAATCCTGAGAGTCTGTTTT
Endcap95	TTTTAAGGTAAAGCGCCTGTTTTTTT
Endcap96	TTTTAGGTAAAGACCCCGGTTGATATTTT
Endcap97	TTTTATCAACAATAGATAAGCAGAACGTAATTCTTATAAAGTACCGACAATTTT
Endcap98	TTTTAGAAGCCTTTAATATTTTGTTTTTT
Endcap99	TTTTATTAAGCAACAAAAATAATTCTTTT
Endcap100	TTTTGGGTATTAAACCCCCAATATTGAGCGTGCCATCTTTTCTTTT
Endcap101	TTTTAAAGGTGGCCGTCGGATTCTCTTTT
Endcap102	TTTTTAGGAATCATAAGAACGCTTTT
Endcap103	TTTTGAGGCGTTTTGCTATTTTTTTT
Endcap104	TTTTTAAATATGCCTCAGGAAGATCTTTT
Endcap105	TTTTCTTTGACGAGCCGATTAATTTT
Endcap106	TTTTTTTGATAAGAGGAACATGTTTTTTT
Endcap107	TTTTCAAAATAAACAGAAATGAAAATAGTTTT
Endcap108	TTTTGCTTCAAAGCGAACGAGTAGATTTT
Endcap109	TTTTCAGCCTTTACAGACCCTGAACAAATTTT
Endcap110	TTTTGTCAGAGGGTAAATAAGAGCAAGATTTT
Endcap111	TTTTAATGACCATAAAATTAGCAAATTTT
Endcap112	TTTTAACAATGAAATAACAAAGTTACCATTTT
Endcap113	TTTTCAATACTGCGGATTTTGCGGGTTTT
Endcap114	TTTTGAAGGAAACCGATTATTACGCAGTTTTT
Endcap115	TTTTTTTTGCAAAGTTTAGAGGTTTTT
Endcap116	TTTTATGTTAGCAAACCACGGAATAAGTTTTT
Endcap117	TTTTAGCAACACTATCTCTAGCTGATTTT
Endcap118	TTTTGTTGAGATTAGGCATAGTAAGTTTT
Endcap119	TTTTTGAGGGAGGCGACTTGAGTTTT
Endcap120	TTTTCCATTTGGGAACGTCACCTTTT
Endcap121	TTTTGCTTGAGATCTGGATAGCGTCTTTT
Endcap122	TTTTAATGAAACCTCAGACTGTTTTT
Endcap123	TTTTAGGGATTTTCCACCGAGTTTTT
Endcap124	TTTTAAATCAACGTCAGAAAACGAGTTTT
Endcap125	TTTTACGGTGTACAGACCAGGAAAGAGGGGATCGGAGGGTAGCAACGGCTACATTTT

Endcap126	TTTTTGTTACTTAGTTTTAATTCGATTTT
Endcap127	TTTTCCTCAGAACGCCGCCGCCTTTT
Endcap128	TTTTTACCAAGCGTTAATTGCTCCTTTTT
Endcap129	TTTTAGCATTGACAGGAGGTCACCAGACGCCACCCCCTCAGAGCCGCCACTTTT
Endcap130	TTTTACGAAGGCACCACAGCGATTATTTT
Endcap131	TTTTCAGAATGGAAAGTACAGGAGTGTATTTT

Table C.16: Staple sequences for folding the 1LS including the oligo number. Blue staples denote biotinylated staples for surface immobilization. Red staples represent DNA-PAINT staple with a docking site of the concatenated 24 bp binding sequence (sequence A + B + C) on the 3'-end.

Oligo Number	Sequence (5' → 3')
Oligo1	TAAATGAATTTTCTGTATGGGATTAATTTCTT
Oligo2	TCTAAAGTTTTGTCGTCTTTCCAGCCGACAA
Oligo3	TCCACAGACAGCCCTCATAGTTAGCGTAACGA
Oligo4	TCACCAGTACAAACTACAACGCCTAGTACCAG
Oligo5	AGGAACCCATGTACCGTAACACTTGATATAA
Oligo6	CCACCCTCATTTTCAGGGATAGCAACCGTACT
Oligo7	AGAAAGGAACAACTAAAGGAATTCAAAAAAA
Oligo8	ACAACTTTCAACAGTTTCAGCGGATGTATCGG
Oligo9	TGACAACTCGCTGAGGCTTGCATTATACCAAGCGCGATGATAAA
Oligo10	TTAGGATTGGCTGAGACTCCTCAATAACCGAT
Oligo11	GCGGATAACCTATTATTCTGAAACAGACGATTGGCCTTGAAGAGCCAC
Oligo12	GTATAGCAAACAGTTAATGCCCAATCCTCA
Oligo13	CAGGAGGTGGGGTCAGTGCCTTGAGTCTCTGAATTTACCGGGAACCAG
Oligo14	AGGCTCCAGAGGCTTTGAGGACACGGGTAA
Oligo15	TTTATCAGGACAGCATCGGAACGACACCAACCTAAAACGAGGTCAATC
Oligo16	AAACAGCTTTTTGCGGGATCGTCAACACTAAA
Oligo17	TTGCTCCTTTCAAATATCGCGTTTGAGGGGGT
Oligo18	CCAACAGGAGCGAACCAGACCGGAGCCTTTAC
Oligo19	TTAACGTCTAACATAAAAACAGGTAACGGA
Oligo20	ATCCCAATGAGAATTAACTGAACAGTTACCAG
Oligo21	GCCAGTTAGAGGGTAATTGAGCGCTTTAAGAA
Oligo22	ACGCTAACACCCACAAGAATTGAAAATAGC
Oligo23	CTGTAGCTTGACTATTATAGTCAGTTCATTGA
Oligo24	GATGGCTTATCAAAAAGATTAAGAGCGTCC
Oligo25	TTTGGGGATAGTAGTAGCATTAAAAGGCCG
Oligo26	CCAATAGCTCATCGTAGGAATCATGGCATCAA
Oligo27	TATCCGGTCTCATCGAGAACAAGCGACAAAAG
Oligo28	GCGAACCTCCAAGAACGGGTATGACAATAA
Oligo29	GCCTTAAACCAATCAATAATCGGCACGCGCCT

Oligo30	AACAGTTTTGTACCAAAAACATTTTATTTC
Oligo31	GATTTAGTCAATAAAGCCTCAGAGAACCCTCA
Oligo32	AATGGTCAACAGGCAAGGCAAAGAGTAATGTG
Oligo33	TAAATCATATAACCTGTTTAGCTAACCTTTAA
Oligo34	TTCTACTACGCGAGCTGAAAAGGTTACCGCGC
Oligo35	TTTTATTTAAGCAAATCAGATATTTTTTGT
Oligo36	GTACCGCAATTCTAAGAACGCGAGTATTATTT
Oligo37	CTTATCATTCCCGACTTGCGGGAGCCTAATTT
Oligo38	TGTAGAAATCAAGATTAGTTGCTCTTACCA
Oligo39	TAAATCGGGATTCCCAATTCTGCGATATAATG
Oligo40	AAATTAAGTTGACCATTAGATACTTTTGCG
Oligo41	GAGACAGCTAGCTGATAAATTAATTTTTGT
Oligo42	GTAATAAGTTAGGCAGAGGCATTTATGATATT
Oligo43	GTAAAGTAATCGCCATATTTAACAAAACTTTT
Oligo44	ACAACATGCCAACGCTCAACAGTCTTCTGA
Oligo45	GTTTATCAATATGCGTTATACAAACCGACCGT
Oligo46	AACGCAAAATCGATGAACGGTACCGGTTGA
Oligo47	TATATTTTGTCATTGCCTGAGAGTGGAAGATT
Oligo48	TAGGTAAACTATTTTTGAGAGATCAAACGTTA
Oligo49	GAGGGTAGGATTCAAAAGGGTGAGACATCCAA
Oligo50	CAACCGTTTCAAATCACCATCAATTCGAGCCA
Oligo51	CATGTAATAGAATATAAAGTACCAAGCCGT
Oligo52	AATTGAGAATTCTGTCCAGACGACTAAACCAA
Oligo53	AGTATAAAGTTCAGCTAATGCAGATGTCTTTC
Oligo54	TTAGTATCACAATAGATAAGTCCACGAGCA
Oligo55	AACAAGAGGGATAAAAATTTTTAGCATAAAGC
Oligo56	GCTATCAGAAATGCAATGCCTGAATTAGCA
Oligo57	TAAATCAAAATAATTCGCGTCTCGGAAACCAGGCAAAGGGAAGG
Oligo58	ATCGCAAGTATGTAAATGCTGATGATAGGAAC
Oligo59	TCAAATATAACCTCCGGCTTAGGTAACAATTTCATTTGAAGGCGAATT
Oligo60	CCTAAATCAAAATCATAGGTCTAAACAGTA
Oligo61	GTGATAAAAAGACGCTGAGAAGAGATAACCTTGCTTCTGTTCGGGAGA
Oligo62	TAATCAGCGGATTGACCGTAATCGTAACCG
Oligo63	GTATAAGCCAACCCGTCGGATTCTGACGACAGTATCGGCCGCAAGGCG
Oligo64	ATATTTTGGCTTTCATCAACATTATCCAGCCA
Oligo65	TGTAGCCATTAAAATTCGCATTAAATGCCGGA
Oligo66	GCCATCAAGCTCATTTTTTAACCACAAATCCA
Oligo67	TATAACTAACAAAGAACGCGAGAACGCCAA
Oligo68	ACCTTTTTATTTTAGTTAATTTCATAGGGCTT
Oligo69	GAATTTATTTAATGGTTTGAAATATTCTTACC
Oligo70	CTTAGATTTAAGGCGTTAAATAAAGCCTGT
Oligo71	ACAAACGGAAAAGCCCCAAAAACACTGGAGCA

Oligo72	GCGAGTAAAAATATTTAAATTGTTACAAAG
Oligo73	AGAAAACAAAGAAGATGATGAAACAGGCTGCG
Oligo74	CATAAATCTTTGAATACCAAGTGTTAGAAC
Oligo75	TGCATCTTTCCCAGTCACGACGGCCTGCAG
Oligo76	GCTTTCCGATTACGCCAGCTGGCGGCTGTTTC
Oligo77	TCTTCGCTGCACCGCTTCTGGTGCGGCCTTCC
Oligo78	GCGATCGGCAATTCCACACAACAGGTGCCTAATGAGTG
Oligo79	CAACTGTTGCGCCATTCGCCATTCAAACATCA
Oligo80	CTGAGCAAAAATTAATTACATTTTGGGTTA
Oligo81	ATTCATTTTTGTTTGGATTATACTAAGAAACCACCAGAAG
Oligo82	CGCGCAGATTACCTTTTTTAATGGGAGAGACT
Oligo83	CCTGATTGCAATATATGTGAGTGATCAATAGT
Oligo84	AACAATAACGTAAAACAGAAATAAAAATCCTTTGCCCGAA
Oligo85	CTTTTACAAAATCGTCGCTATTAGCGATAG
Oligo86	CCAGGGTTGCCAGTTTGAGGGGACCCGTGGGA
Oligo87	ATTAAGTTTACCGAGCTCGAATTCGGGAAACCTGTCGTGC
Oligo88	GATGTGCTTCAGGAAGATCGCACAATGTGA
Oligo89	GCAATTCACATATTCCTGATTATCAAAGTGTA
Oligo90	CTACCATAGTTTGAGTAACATTTAAAATAT
Oligo91	GTCGACTTCGGCCAACGCGCGGGGTTTTTC
Oligo92	CTGTGTGATTGCGTTGCGCTCACTAGAGTTGC
Oligo93	AAGGCCGCTGATACCGATAGTTGCGACGTTAG
Oligo94	ATATTCGGAACCATCGCCCACGCAGAGAAGGA
Oligo95	TATTAAGAAGCGGGGTTTTGCTCGTAGCAT
Oligo96	TTTCGGAAGTGCCGTCGAGAGGGTGAGTTTCG
Oligo97	GCCCGTATCCGGAATAGGTGTATCAGCCCAAT
Oligo98	GTTTTAACTTAGTACCGCCACCCAGAGCCA
Oligo99	ACGGCTACAAAAGGAGCCTTTAATGTGAGAAT
Oligo100	CAGCGAAACTTGCTTTCGAGGTGTTGCTAA
Oligo101	CACATTAAAATTGTTATCCGCTCATGCGGGCC
Oligo102	AAGCCTGGTACGAGCCGGAAGCATAGATGATG
Oligo103	ATTATCATTCAATATAATCCTGACAATTAC
Oligo104	GCGGAACATCTGAATAATGGAAGGTACAAAAT
Oligo105	ATTTTAAAATCAAAATTATTTGCACGGATTCG
Oligo106	CTCGTATTAGAAATTGCGTAGATACAGTAC
Oligo107	TTAATGAACTAGAGGATCCCCGGGGGGTAACG
Oligo108	TTCCAGTCGTAATCATGGTCATAAAAGGGG
Oligo109	CCCAGCAGGCGAAAAATCCCTTATAAATCAAGCCGGCG
Oligo110	TCAATATCGAACCTCAAATATCAATTCCGAAA
Oligo111	TCAACAGTTGAAAGGAGCAAATGAAAAATCTAGAGATAGA
Oligo112	CTTTAGGGCCTGCAACAGTGCCAATACGTG
Oligo113	AGATTAGAGCCGTCAAAAAACAGAGGTGAGGCCTATTAGT

Oligo114	TTTTCACTCAAAGGGCGAAAAACCATCACC
Oligo115	AGCTGATTGCCCTTCAGAGTCCACTATTAAAGGGTGCCGT
Oligo116	AGCAAGCGTAGGGTTGAGTGTTGTAGGGAGCC
Oligo117	GCCCGAGAGTCCACGCTGGTTTGCAGCTAACT
Oligo118	TCGGCAAATCCTGTTTGATGGTGGACCCTCAA
Oligo119	ACCTTGCTTGGTCAGTTGGCAAAGAGCGGA
Oligo120	AGCCAGCAATTGAGGAAGGTTATCATCATTTT
Oligo121	TTAACACCAGCACTAACAACTAATCGTTATTA
Oligo122	CAGAAGATTAGATAATACATTTGTCGACAA
Oligo123	CTCCAACGCAGTGAGACGGGCAACCAGCTGCA
Oligo124	TGGAACAACCGCCTGGCCCTGAGGCCCGCT
Oligo125	AACGTGGCGAGAAAGGAAGGGAAACCAGTAA
Oligo126	TAAAAGGGACATTCTGGCCAACAAAGCATC
Oligo127	ACCCTTCTGACCTGAAAGCGTAAGACGCTGAG
Oligo128	GCACAGACAATATTTTTGAATGGGGTCAGTA
Oligo129	CTTTAATGCGCGAACTGATAGCCCCACCAG
Oligo130	CAAATCAAGTTTTTTGGGGTCGAAACGTGGA
Oligo131	AAAGCACTAAATCGGAACCCTAATCCAGTT
Oligo132	CCCGATTTAGAGCTTGACGGGGAAAAAGAATA
Oligo133	TTGACAGGCCACCACCAGAGCCGCGATTTGTA
Oligo134	TTAAAGCCAGAGCCGCCACCCTCGACAGAA
Oligo135	AATACGTTTGAAAGAGGACAGACTGACCTT
Oligo136	ACACTCATCCATGTTACTTAGCCGAAAGCTGC
Oligo137	GACCTGCTCTTTGACCCCCAGCGAGGGAGTTA
Oligo138	TTGTGTCGTGACGAGAAACACCAAATTTCAACTTTAAT
Oligo139	TCATCGCCAACAAAGTACAACGGACGCCAGCA
Oligo140	CACCAGAAAGGTTGAGGCAGGTCATGAAAG
Oligo141	CACCCTCAGAAACCATCGATAGCATTGAGCCATTTGGGAA
Oligo142	CCACCCTCTATTCACAAACAAATACCTGCCTA
Oligo143	GCCTCCCTCAGAATGGAAAGCGCAGTAACAGT
Oligo144	AGCCACCACTGTAGCGCGTTTTCAAGGGAGGGAAGGTAAA
Oligo145	AAATCACCTTCCAGTAAGCGTCAGTAATAA
Oligo146	GACCAACTAATGCCACTACGAAGGGGGTAGCA
Oligo147	ATAAGGGAACCGGATATTCATTACGTCAGGACGTTGGGAA
Oligo148	GCGCAGACAAGAGGCAAAAGAATCCCTCAG
Oligo149	GCAAGGCCTCACCAGTAGCACCATGGGCTTGA
Oligo150	TCAAGTTTCATTAAAGGTGAATATAAAAGA
Oligo151	CATCAAGTAAAACGAACTAACGAGTTGAGA
Oligo152	TCATTCAGATGCGATTTTAAGAACAGGCATAG
Oligo153	ATTACCTTTGAATAAGGCTTGCCCAAATCCGC
Oligo154	GATGGTTTGAACGAGTAGTAAATTTACCATTA
Oligo155	CAGCAAAAGGAAACGTCACCAATGAGCCGC

Oligo156	TCACCGACGCACCGTAATCAGTAGCAGAACCG
Oligo157	GAAATTATTGCCTTTAGCGTCAGACCGGAACC
Oligo158	ACCGATTGTCGGCATTTTCGGTCATAATCA
Oligo159	TACGTTAAAGTAATCTTGACAAGAACCGAACT
Oligo160	TTATACCACCAAATCAACGTAACGAACGAG
Oligo161	CGTTTACCAGACGACAAAGAAGTTTTGCCATAATTCGA
Oligo162	TTATTACGAAGAACTGGCATGATTGCGAGAGG
Oligo163	CGTAGAAAATACATACCGAGGAAACGCAATAAGAAGCGCA
Oligo164	AACGCAAAGATAGCCGAACAAACCCTGAAC
Oligo165	GTTTATTTTGTCACAATCTTACCGAAGCCCTTTAATATCA
Oligo166	TTTAGGACAAATGCTTTAAACAATCAGGTC
Oligo167	ATGCAGATACATAACGGGAATCGTCATAAATAAAGCAAAG
Oligo168	TAAGAGCAAATGTTTAGACTGGATAGGAAGCC
Oligo169	AATAGTAAACACTATCATAACCCTCATTGTGA
Oligo170	CTTTTGCAGATAAAAACCAAAATAAAGACTCC
Oligo171	ATACCCAACAGTATGTTAGCAAATTAGAGC
Oligo172	AAGGAAACATAAAGGTGGCAACATTATCACCG
Oligo173	AAGTAAGCAGACACCACGGAATAATATTGACG
Oligo174	AATAGCTATCAATAGAAAATTCAACATTCA
Oligo175	ATCCCCCTATACCACATTCAACTAGAAAAATC
Oligo176	AATACTGCCCAAAAGGAATTACGTGGCTCA
Oligo177	GCTTCAATCAGGATTAGAGAGTTATTTTCA
Oligo178	AGAGAGAAAAAAATGAAAATAGCAAGCAAACT
Oligo179	TTAGACGGCCAAATAAGAAACGATAGAAGGCT
Oligo180	AAAGTCACAAAATAAACAGCCAGCGTTTTA
Oligo181	GAGAGATAGAGCGTCTTTCCAGAGGTTTTGAA
Oligo182	TTTACCCCAACATGTTTTAAATTTCCATAT
Oligo183	CGGATTGCAGAGCTTAATTGCTGAAACGAGTA
Oligo184	CGAAAGACTTTGATAAGAGGTCATATTTCGCA

Table C.17: Staple sequences for folding the 12HB including the oligo number. 3×6 12HB and 3×1 12HB (marked with a *) staple sequences that are to be taken out for handles are marked in red. Similarly sequences that are taken out for biotinylated strands are marked in blue.

Oligo Number	Sequence (5' → 3')
Oligo1	CGAGTAACAACCGTTTACCAGTC
Oligo2	CATCAGCGTCTGGCCTTCCACAGGAACCTGGGG
Oligo3	GATAAAAATTTTTAGCCAGCTTT
Oligo4	GCCTTATACCCTGTAATACCAATTCTTGCGCTC
Oligo5	GACCGGAAGCAATTGCGGGAGAA
Oligo6	CGAGCACAGACTTCAAATACCTCAAAAGCTGCA
Oligo7	AAAAATCTACGTGCGTTTTAATT
Oligo8	CAGTCTTGATTTTAAGAACTCAACGTTGCGTAT
Oligo9	AAAACGAAAGAGGCTCATTATAC
Oligo10	ACTACCTTTAAACGGGTAACAGGGAGACGGGCA
Oligo11	TTGTCGTCTTTCTACGTAATGCC
Oligo12	AGCGTATCATTCCACAGACCCGCCACAGTTGCAGCAAGCG
Oligo13	GCGTCATACATGCCCTCATAGTT
Oligo14	GAATTGTAGCCAGAATGGATCAGAGCAAATCCT
Oligo15	TCACCGTCACCGGCGCAGTCTCT
Oligo16	ATTCAAGGGGAAGGTAAATGTGGCAAATAAATC
Oligo17	AGACGGGAGAATTGACGGAAATT
Oligo18	AAAAAAGGCAGCCTTTACAATCTTACCAGTTTG
Oligo19	TCCCATCCTAATGAGAATAACAT
Oligo20	CTGAAAACCTGTTTATCAAACATGTAACGTCAA
Oligo21	CGGTAGTACTCAATCCGCTGCTGGTCATGGTC
Oligo22	TTAGGTTGGGTTATAGATAAGTC
Oligo23	TACCTAATATCAAAATCATTCAATATTACGTGA
Oligo24	TAGAACCTACCAGTCTGAGAGAC
Oligo25	TTCTGGAATAATCCTGATTTTGCCCGGCCGTAA
Oligo26	AAGATAAAACAGTTGGATTATAC
Oligo27	CCGAACCCCCTAAAACATCGACCAGTTTAGAGC
Oligo28	GATTTTAGACAGGCATTAAAAATA
Oligo29	GACTTTCTCCGTGGCGCGGTTG
Oligo30	CCGGAAGACGTACAGCGCCGCGATTACAATTCC
Oligo31	GGGCCGGAAGCATAAAGTG
Oligo32	TCAGCTAACTCACATTAAT
Oligo33	AGCAGTCGGGAAACCTGTC
Oligo34	AATAACGCGCGGGGAGAGG
Oligo35	GATGTTTTTCTTTTCACCA
Oligo36	TCGTTCACCGCCTGGCCCT
Oligo37	CCTCCGAAATCGGCAAAAT
Oligo38	AAAAGATAGGGTTGAGTGT
Oligo39	CTATATTAAAGAACGTGGA
Oligo40	CATTCTATCAGGGCGATGG

Oligo41	TGGCAAGTTTTTTGGGGTC
Oligo42	AGACGGCGAACGTGGCGAG
Oligo43	ACACAACATACGAGGGATGTGGCTATTAATCGGCC
Oligo44	TAAAGGATTGTATAAGCGCACAAACGACATTAAATGTGAG
Oligo45	TGCCTAATGAGTGAGAAAAGCTCATATGTAGCTGA
Oligo46	TGCGTACTAATAGTAGTTGAAATGCATATTTCAACGCAAG
Oligo47	ACTGCCCGCTTTCCTGAAAAGCTATATTTTAAATA
Oligo48	GTGCCTGCTTTAAACAGGGAGAGAGTTTCAAAGCGAACCA
Oligo49	TTAATGAATCGGCCATTCATTCCAATACGCATAGT
Oligo50	CGGTTAACAAAGCTGCTGTAACAACAAGGACGTTGGGAAG
Oligo51	TGGGCGCCAGGGTGATTCATTAGAGTAACCTGCTC
Oligo52	GTGAGTTAAAGGCCGCTGACACTCATGAAGGCACCAACCT
Oligo53	ACAGCTGATTGCCCGTCGCTGCGCCCACACGTTGA
Oligo54	GAGAGCCTCAGAACCGCATTTTCTGTAACGATCTAAAGTT
Oligo55	GTCCACGCGCCACCTCACCGTTGAAACA
Oligo56	GGCGACACCACCCTCAGGTTGTACTGTACCGTTCCAGTAA
Oligo57	GTTTGATGGTGGTTCAGAACCCCGCCTCACAGAAT
Oligo58	CCCTTCATATAAAAGAACGTAGAGCCTTAAAGGTGAATTA
Oligo59	AAAAGAATAGCCCGATACATACGCAGTAAGCTATC
Oligo60	TGTTCCAACGCTAACGAACAAGTCAGCAGGGAAGCGCATT
Oligo61	GAACAAGAGTCCACCAATTTTTTAGTTGTCGTAGG
Oligo62	CTCCAATTTAGGCAGAGACAATCAATCAAGAAAAATAATA
Oligo63	AGGGCGAAAAACCGATTTAACGTAGGGCAAATACC
Oligo64	CCCACATGTGAGTGAATAACTGATGCTTTTAACCTCCGGC
Oligo65	ACCATCACCCAAATAAACAGTTCATTTGATTCGCC
Oligo66	GAGGTAACGTTATTAATTTTAAAACAAATAATGGAAGGGT
Oligo67	AGCACTAAATCGGATCGTATTTAGACTTATATCTG
Oligo68	ATAGCTGTTTCCTGGAACGTCCATAACGCCGTAAA
Oligo69	CCGATAATAAAAGGGACTTAACACCGCGAACCACCAGCAG
Oligo70	TTGACGGGGAAAGCTTCACCAGAAATGGCATCACT
Oligo71	AAAGGGCGCTGGCAAGTATTGGC
Oligo72	GCTCAAGTTGGGTAACGGGCGGAAAAATTTGTGAGAGATA
Oligo73	TTCGCGGATTGATTGCTCATTTTTTAAC
Oligo74	TTATGGCCTGAGCACCTCAGAGCATAAA
Oligo75	CCGAACTTTAATAAAAGCAAAGCGGATT
Oligo76	TATGCATTACAGAGGATGGTTTAATTTC
Oligo77	TTCCATTGACCCAAAGAGGCTTTGAGGA
Oligo78	TGTAGGGGATTTAGTAACACTGAGTTTC
Oligo79	ATTAAAATAAGTGCGACGATTGGCCTTG
Oligo80	AGGGACAAAATCTTCCAGCGCCAAAGAC
Oligo81	AAATAGGTAATTTACAAATAAGAAACGA
Oligo82	ACGCGTCGGCTGTAAGACGACGACAATA
Oligo83	TTCGCCATAAACTCTGGAGGTGTCCAGC
Oligo84	GAATTATCCAATAACGATAGCTTAGATT
Oligo85	TCAATAATAAAGTGTATCATCATATTCC

Oligo86	GATAGTGCAACATGATATTTTTGAATGG
Oligo87	GCGAAAGACGCAAAGCCGCCACGGGAAC
Oligo88	AATCAGTTAAAACGTGGGAGAAA
Oligo89	CAATAGGAACGCAAATTAAGCAA
Oligo90	TAAAGAGGCAAAATATTTTATAA
Oligo91	GCTAAATCGGTTTGACTATTATA
Oligo92	GTCAGAATCAGGCAGGATTCGCG
Oligo93	GCATCAAAAAGAAGTAAATTGGG
Oligo94	CTTGAAAACACCCTAACGGCATA
Oligo95	AACTTTAATCATGGGTAGCAACG
Oligo96	GCTACGACAGCAACTAAAAACCG
Oligo97	CTAAAGACTTTTAGGAACCCATG
Oligo98	TACCGGGATAGCAATGAATATAT
Oligo99	GTCACCAGTACAAGGTTGAGGCA
Oligo100	GGTCACGCCAGCACAGGAGTTAG
Oligo101	ATATTCACAAACAAATTCATATG
Oligo102	GTTTATGTCACATGGGAATCCAC
Oligo103	AAAAGGGCGACAATTATTTATCC
Oligo104	CAATCCAAAATACTGAACAGTAG
Oligo105	TTTTTTGTTTAATAAAGTAATTC
Oligo106	TGTCCAAGTACCAGAAACCCCAG
Oligo107	AACAACATGTTCATCCTTGAAAA
Oligo108	CATAGTTAATTTGTAAATGTCGC
Oligo109	ATCAGCGGGGTCAGCTTTCAGAG
Oligo110	AAGACGCTGAGACCAGAAGGAGC
Oligo111	GGAATCGGAACATTGCACGTTAA
Oligo112	TGATTATCAGATATACGTGGCAC
Oligo113	AGACAACCTGAACAGTATTCGAC
Oligo114	CTATTAGTCTTTCGCCGCTACAG
Oligo115	GGCGCCCCGCCGAATCCTGAGAAGTGAGGCCGATTAAAGG
Oligo116	GTGGAACGACGGGCTCTCAACTT
Oligo117	GGATAACCTCACAATTTTTGTTA
Oligo118	CCAGCCAAACTTCTGATTGCCGTTTTGGGTAAAGTTAAAC
Oligo119	GTTTGAGGGGACCTCATTTGCCG
Oligo120	CGTAAAGGTCACGAAACCAGGCAATAGCACCGCTTCTGGT
Oligo121	CAATATGATATTGATGGGCGCAT
Oligo122	GAGACAAAGATTATCAGGTCATTGACGAGAGATCTACAAA
Oligo123	AATGCTGTAGCTGAGAAAGGCCG
Oligo124	GAGCTTAAGAGGTCCCAATTCTGCAATTCCATATAACAGT
Oligo125	TCAACATCAGTTAAATAGCGAGAGTGAGACGACGATAAAA
Oligo126	AAATTGTGTCGAGAATACCACAT
Oligo127	ATTTGCCAAGCGGAACTGACCAACGAGTCAATCATAAGGG
Oligo128	ATTGCGAATAATGTACAACGGAG
Oligo129	GAAAGTTCAACAATCAGCTTGCTTAGCTTTAATTGTATCG

Oligo130	CTATTTCGGAACGAGTGAGAATA
Oligo131	AACAGAGTGCCTGGGGTTTTGCTCACAGAAGGATTAGGAT
Oligo132	GCAGCACCGTAAGTGCCCGTATA
Oligo133	ACCAAATTACCAGGTCATAGCCCCGAGTTTTCATCGGCAT
Oligo134	TAAGCCAGAGAGCCAGAAGGAAACTCGATAGCCGAACAAA
Oligo135	AGCAAGCCGTTTAAGAATTGAGT
Oligo136	ACCGCATTCCAACGGTATTCTAAGCGAGATATAGAAGGCT
Oligo137	TGACCTAAATTTTTAAACCAAGT
Oligo138	TTTAGAACGCGAATTACTAGAAAACTATAAACACCGGAAT
Oligo139	CATCGGGAGAAATTCAAATATAT
Oligo140	TCAGAGGTGTGTCGGCCAGAATGAGTGCACTCTGTGGT
Oligo141	ACAGTTTTTCAGATTTCAATTACCGTCGCAGAGGCGAATT
Oligo142	CAAATATCAAACCAGATGAATAT
Oligo143	GCATCGAGCCAGATATCTTTAGGACCTGAGGAAGGTTATC
Oligo144	TACTTCTTTGATAAAAATCTAAA
Oligo145	CATAATATTCCGTAATGGGATCCGTGCATCTGCCA
Oligo146	GTATACAGGTAATGTGTAGGTAGTCAAATCACCAT
Oligo147	TGTAAATCATGCTCCTTTTGATAATTGCTGAATAT
Oligo148	CGCCTGACGGTAGAAAGATTCTAATGCAGATACAT
Oligo149	GCGCAGCGACCAGCGATTATATATCATCGCCTGAT
Oligo150	TTCATTTTCTGCTAAACAACTGAACAACTAAAGGA
Oligo151	ATCAGAGCCTTTAACGGGGTCTTAATGCCCCCTGC
Oligo152	AGAGTTTATACCAGTAGCACCTGAAACCATCGATA
Oligo153	CATGCCAGTGAGCGCTAATATCCAATAATAAGAGC
Oligo154	TTGAGAATATCTTTCCTTATCACTCATCGAGAACA
Oligo155	TTCGCTATTCGCAAGACAAAGTTAATTTCATCTTC
Oligo156	ACATCATTTAAATTGCGTAGAAACAGTACCTTTTA
Oligo157	ATACCCTTCGTGCCACGCTGAACCTTGCTGAACCT
Oligo158	AACGTTGTAGAAACAGCGGATAGTTGGGCGGTTGT
Oligo159	TCAGGTGAAATTTCTACGGAAACAATCG
Oligo160	TAAATCGGTTGGTGCACATCAAAAATAA
Oligo161	TGCAACTCAAAAGGCCGTACCAAAAACA
Oligo162	AAGAGATTCATTTTGTTTAAGAGGAAGC
Oligo163	CATGTCAGAGATTTGATGTGAATTACCT
Oligo164	AAATCCCCGAAACAATTCATGAGGAAGT
Oligo165	TGAAATTGTTTCAGGGAACTACAACGCC
Oligo166	CAAGTGCTGAGTAAGAAAATAAATCCTC
Oligo167	TTACCTCTTAGCAAATTTCAACCGATTG
Oligo168	AATCATAATAACCCGGCGTCAAAAATGA
Oligo169	GACCGTCGAACGGGGAAGCTAATGCAGA
Oligo170	TGATTTAGAAAACTCAAGAGTCAATAGT
Oligo171	GTCAGTCGTTTAACGAGATGGCAATTCA
Oligo172	TGCCTGAACAGCAAATGAATGCGCGAACT
Oligo173	AAAAGTGTCAGCAACAATTGCAGGCGCT
Oligo174	GAAAGATCGCACTCCAGCCAGCT

Oligo175	TTCCGAATTGTAAACGTGTCGCCAGCATCGGTGCGGGCCT
Oligo176	GCTAATGCCGGAGAGGGTAGCTA
Oligo177	TTTTTATCCAATAAATCTCTACCCCGGTAAAACTAGCATG
Oligo178	GGCTAAAGTACGGTGTCTGGAAG
Oligo179	TTTCACGAGAATGACCATTTTCATTTGGTCAATAACCTGT
Oligo180	TGCAACACTATCATAACCCTCGT
Oligo181	TTACCAATAAGGCTTGCAGTGCGGAAGTTTAGACTGGATA
Oligo182	ACTACTTAGCCGGAACGAGGCGC
Oligo183	AGACGTCGTCACCCTCAGATCTTGACGCTGGCTGACCTTC
Oligo184	AATCCAAAAAAAAGGCTCCAAAA
Oligo185	GGAGCAGCCACCACCCTTCGCATAACGACAATGACAACAA
Oligo186	GTGTATTAAGAGGCTGAGACTCC
Oligo187	TCAAGCAGAACCACCACTCACTCAGGTAGCCCGGAATAGG
Oligo188	TATTGCCTTTAGCGTCAGACTGT
Oligo189	AGCGCCACCACGGAATACGCCTCAGACCAGAGCCACCACC
Oligo190	TTGAAGCCCTTTTTAAGAAAAGT
Oligo191	AAGCACAGAGCCTAATTATTGTTAGCGATTAAGACTCCTT
Oligo192	GTTTACCGCGCCCAATAGCAAGC
Oligo193	AAATCAGCCAGTAATAACACTATTTTTGAAGCCTTAAATC
Oligo194	TATGTGATAAATAAGGCGTTAAA
Oligo195	TAAGATCTGTAAATCGTTGTTAATTGTAAAGCCAACGCTC
Oligo196	CAGCTTTGAATACCAAGTTACAA
Oligo197	AATCGTTGAGTAACATTGGAATTACCTAATTACATTTAAC
Oligo198	ATTTGGCAAATCAACAGTTGAAA
Oligo199	GCCCGCACAGGCGGCCTTTAGTG
Oligo200	GGAATAACAGAGATAGACATACAAACTTGAGGATTTAGAA
Oligo201	TAAGTAGAAGAACTCAAACTATCG
Oligo202	GCCTTACGCTGCGCGTAAAATTATTTTTTGACGCTCAATC
Oligo203	ATGAATCCCAGTCACGATCGAACGTGCCGGCCAGAGCACA
Oligo204	CTTTTTTTCGTCTCGTCGCTGGC
Oligo205	GGGCGTGAAATATTAGCGCCATTCGC
Oligo206	TCAGGCTGCGCAACTGTTGGGAA
Oligo207	TAATCGTAGCATTACCTGAGAGTCTG
Oligo208	TTAACAAGAGAATCGATGAACGG
Oligo209	CAAATGGTTCAGAAGAACGAGTAGAT
Oligo210	GCTTGACCATTAGATACATTTCG
Oligo211	AAAATTCCATTCAGGCTTTTGCAAAA
Oligo212	ATTTTGCCAGAGGGGGTAATAGT
Oligo213	CATAGAATTTGCGGTTTGAAAGAGGA
Oligo214	CCGAACGGTGTACAGACCAGGCG
Oligo215	GCGCCCGCACCCTCTCGAGGTGAATT
Oligo216	TGAACAGCTTGATACCGATAGTT
Oligo217	AAGTAAGAGCCGCCAGTACCAGGCGG
Oligo218	GGTGCCGTCGAGAGGGTTGATAT

Oligo219	CGGAAGCACGCAAACTTATTAGCGTT
Oligo220	ATTCTTTTCATAATCAAAATCAC
Oligo221	CAGCATCAACCGCACGGCGGGCCGTT
Oligo222	GGCATAAGCGTCTTCGAGGAAACGCA
Oligo223	AAAACGGAATACCCAAAAGAACT
Oligo224	GGTTTGCGCATTTTAACGCGAGGCGT
Oligo225	AACGAACCTCCCGACTTGCGGGA
Oligo226	CAGTAAGAACCTTGAGCCTGTTTAGT
Oligo227	AAATGCGTTATACAAATTCTTAC
Oligo228	AAAATTTTTTAAAATGAGCAAAAGAA
Oligo229	GTTGAAACAAACATCAAGAAAAC
Oligo230	TACATAAATTCTGGGCACTAACAACT
Oligo231	GTATTAGAGCCGTCAATAGATAA
Oligo232	TCGGTCATACCGGGGGTTTCTGC
Oligo233	AGCCTCCCCAGGGTCCGGCAAACGCG
Oligo234	GTCCGTCCTGCAAGATCGTCGGATTCTCTTCGCATTGGACGA
Oligo235	CATTCAACCCAAAATGTAGAACCCTCATGAATTAGTACAACC
Oligo236	GAGCAAGGTGGCATTTACTCCAACAGGTTCTTTACGTCAACA
Oligo237	TTAGTGTGAATCCCTCTAATAAAACGAAAGAACGATGAATTA
Oligo238	GAAGTCAACCCAAATGGCAAAAGAATACTCGGAACAGAATCC
Oligo239	CAGATATAGGCTTGAACAGACGTTAGTAAAGCCCAAAAATTT
Oligo240	TCTTATACTCAGAAAGGCTTTTGATGATATTGACACGCTATT
Oligo241	ATAAGAAGCCACCCAAACTTGAGCCATTATCAATACATCAGT
Oligo242	TGCCATACATAAAGATTAACTGAACACCAACAGCCGGAATAG
Oligo243	ATAATGAATCCTGAGATTACGAGCATGTGACAAAAACTTATT
Oligo244	TTTAGCAAACGCCACAATATAACTATATTCCCTTATAAATGG
Oligo245	ATCATTTACATAAAAGTATCAAAATTATAAGAAACTTCAATA
Oligo246	GATGAATAAATCCTGTAGGTGAGGCGGTAGCGTAAGTCCTCA
Oligo247	TTCACCTAGCGTGGCGGGTGAAGGGATACCAGTGCATAAAAA
Oligo248	AATAGCTGTCACACGCAACGGTACGCCAGCGCTTAATGTAGTA
Oligo249	CGGGAGCTAAACAGGTTGTTAGAATCAGAG
Oligo250	TGGTAATGGGTAACCATCCCAC
Oligo251	GCAGCACTTTGCTCTGAGCCGGGTCACTGTTGCCCTGCGGC
Oligo252	AGGAGCGGGCGCTAGGAAGGGAAGAAAGCGAA
Oligo253	CCGGGTACCGAGCTCGAATTCGTAATCTGGTCA
Oligo254	TATAACGTGCTTTCCTCTTTATAACAGTACTAT
Oligo255	GCAACCAGCTTACGGCGGTGGTGAGGTTTCAGTTGAGGATCC?
Oligo256	GGTTGCTTTGACGAGCACG?
Oligo257	GGGTTACCTGCAGCCAGCGGTG?
Oligo258	GTCCATCACGCAAATTCCGAGTAAAAGAGTCT
Oligo259	CCGGTGCAGCACCGATCCCTTACACTTGCC
Oligo260	AACAATATTACCGTCGCTGGTAATATCCAG?
Oligo261	ATCCAGCGCAGTGTCACTGC
Oligo262	GCGCCTGAATGCCAACGGCCCAGCCTCCCGCGTGCCTGTTCTTC
Oligo263	CCTACATACGTAGCGGCCAGCCATTGCAACAGG

Oligo264	AAAAACGCTCATGGAAATA
Oligo265	GCGTCCGTGCCTGCATCAGACG
Oligo266	TACCTGGTTTGCCCCAGCA*
Oligo267	AACACCCTAAAGGGAGCCC*
Oligo268	GTATGTGAAATTGTTATCC*
Oligo269	AACGCCAAAAGGCGGATGGCTTA
Oligo270	AAGAAACAATGACCGGAAACGTC
Oligo271	GTACATCGACATCGTTAACGGCA
Oligo272	ATACCACCATCAGTGAGGCCAAACCGTTGTAGCAA

C.10.2 Handle Sequences

Table C.18: 4LB handle sequences and additions. Handle sequences added to standard oligos are marked in red. Additional Staples are needed, because the staples have been restructured to be short enough for synthesis.

Oligo Name	Sequence (5' → 3')
4LB poly A Handle 1	TACCGTGTTTTGTGAGACGGACTATGGTTAAAAAAAAAAAAAAA
4LB poly A Handle 2	GCTGAGATCTCGTCTTTAGTGCACCAGAAAAAAAAAAAAAAA
4LB poly A Handle 3	GCAAGGCGACAGGAAGTGAGAAGCCTTTTTAAAAAAAAAAAAAAA
4LB poly A Handle 4	AACATAGATTGTAACGTAAAAGAAAAAAAAAAAAAAAAAAA
4LB poly A Handle 5	TTGGCGAGCTTTAGCGAACAGATATAAAAAAAAAAAAAAA
4LB poly A Handle 6	TTTGGAAGAAAAATAGCAATAGCTACTGAAAAAAAAAAAAAAA
4LB poly A Handle 7	TGTGGCAAAATGAATTATCAAAAAAAAAAAAAA
4LB poly A Handle 8	TGGCCTTGATGAATTTAACGTTGAAAAAAAAAAAAAAA
4LB Random Handle 1	TACCGTGTTTTGTGAGACGGACTATGGTTCTTGAGGACTTAAAA
4LB Random Handle 2	GCTGAGATCTCGTCTTTAGTGCACCAGCTTGAGGACTTAAAA
4LB Random Handle 3	GCAAGGCGACAGGAAGTGAGAAGCCTTTTTCTTGAGGACTTAAAA
4LB Random Handle 4	AACATAGATTGTAACGTAAAAGAAAACTTGAGGACTTAAAA
4LB Random Handle 5	TTGGCGAGCTTTAGCGAACAGATATACTTGAGGACTTAAAA
4LB Random Handle 6	TTTGGAAGAAAAATAGCAATAGCTACTGCTTGAGGACTTAAAA
4LB Random Handle 7	TGTGGCAAAATGAATTATCCTTGAGGACTTAAAA
4LB Random Handle 8	TGGCCTTGATGAATTTAACGTTGACTTGAGGACTTAAAA
4LB Addition 1	GCTCAGAATCCTGAGAAGCCAGCCCTC
4LB Addition 2	AAGGAGCGAACCTACGGGTTTTCGG
4LB Addition 3	ACCTAACCACCGTGCCAC
4LB Addition 4	TAATGGAGAAGGGCTGCAAGGTAAA
4LB Addition 5	GAGCAAGATTTTTCATCGTAGGAATACAG
4LB Addition 6	CATCCTGGCTCGAATTACTTAA
4LB Addition 7	GCCTGTTTCATATTTGAGCATATTCAGAATTTAATTGCT
4LB Addition 8	TGAGATATTGATAGCAAGGCCGGAACAAAGTACGAAAGACGAT
4LB Addition 9	ATACGGCGGCCGCTGGCATTCGCCATGTGAGTCCTTGAA
4LB Addition 10	GAAGGCTCAATTCATCGGTTTAATTGAGAATCGCAGTATCACGA
4LB Addition 11	AACATGACCAGCAATAACATCCAATATTTAACGA
4LB Addition 12	ATAATAAATGAATTCGCGAAAACGTCACGGGAGGGAAGGTAAATGG
4LB Addition 13	ACCGTCCCTGACGATTATTACAAG
4LB Addition 14	ATGGAAGGCTCCAAAAGGCGTAACGAAT
4LB Addition 15	AAATCTCCGTCTTTGATTTGTTTACCATCGGAAATTAT

Table C 19: 24HB handle sequences. Handle sequences added to standard oligos are marked in red. Additional Staples are needed, because the staples have been restructured to be short enough for synthesis.

Oligo Name	Sequence (5' → 3')
24HB poly A Handle 1	CCTTTTATCAATAGCGAATTTTCCCAAAAAAAAAAAAAAA
24HB poly A Handle 2	TTTATGACAAAGAGCCATATCACCAAAAAAAAAAAAAAA
24HB poly A Handle 3	AATTCCTTATCAGCGTTTTCAAAAAAAAAAAAAAA
24HB poly A Handle 4	CTTTCATCAACATTAAATGTGAATAATTCAAAAAAAAAAAAAAA
24HB poly A Handle 5	GGCACCATTCAACTGTCAGGAAAAAAAAAAAAAAA
24HB poly A Handle 6	TTAAACAAATAAGTTTTTTGGGGTAAAAAAAAAAAAAAA
24HB poly A Handle 7	ACGTGGTTGACCATTAGAAATATGCAAAAAAAAAAAAAAA
24HB poly A Handle 8	GCCAAAGTTGCAAAGACACCAAAAAAAAAAAAAAA
24HB Random Handle 1	TAATGCCCAAAAGAATCCTATTTCACTTGAGGACTTAAAA
24HB Random Handle 2	CGGTTGCGTCAGCGTGCAAACAAGACTTGAGGACTTAAAA
24HB Random Handle 3	GCAACTCTCTACGTTAATAAACTTGAGGACTTAAAA
24HB Random Handle 4	GCTTGCACCCTCAGTTAGTACCACTTGAGGACTTAAAA
24HB Random Handle 5	TACTACAAATTCTTGAGGCGAAACTTGAGGACTTAAAA
24HB Random Handle 6	CAGTATCGATTAGAGAATTTACTTGAGGACTTAAAA
24HB Random Handle 7	TACAAACAAGACAAAATAAAACTTGAGGACTTAAAA
24HB Random Handle 8	CGCAATCAATAGATTTAAGAAAACTTGAGGACTTAAAA
24HB Addition 1	CTAAAGTAGCTCAAATTTTTGTAATTGCCAGACCGGAAGCAATTCA
24HB Addition 2	CATAACGCCAAATTAAAGA
24HB Addition 3	CGGAATAAGTTTATTAAAGGTATC
24HB Addition 4	TCGACTATATGTAAATGACTA
24HB Addition 5	TTAGAATCAGAACGCGAGGCGTTTTAGCTTAAATTGAAATAAAAC
24HB Addition 6	ACTCATCTTTGAGACCGC
24HB Addition 7	TCGGCATTTTCGGTCATGTTTGCCGGA
24HB Addition 8	GCGTCTAATAGGATTAAATGAAAATTTAAGCCTTACGGTAACTGGAGC
24HB Addition 9	CCACCCTCAGAACCGCCACCCTCTTAAGTCCAAAT
24HB Addition 10	GGAACAACATAAGAGGCCTACGAA
24HB Addition 11	GCCAGTTAATAGTTTTAACGGGGTTACATGGGAAT
24HB Addition 12	CGAGGTGCCTTGATATTCACACCGTTCCTAAT

Table C.20: 18HB handle sequences. Handle sequences added to standard oligos are marked in red.

Oligo Name	Sequence (5' → 3')
18HB poly A Handle 1	AAGTATCGCGTTTGCTTTAAAAAAAAAAAAAAAA
18HB poly A Handle 2	GGCTTGAAGGGTGATCGTAATATCTTAGCCATCCTAAAAAAAAAAAAAAA
18HB poly A Handle 3	GATTGGCCTTTTGCTCCATAAATACGCCTGCCAGGAGAAAAAAAAAAAAAAA
18HB poly A Handle 4	CAATGACAACAACCGGCAAAAATGTTACTAAATTGCGTCCAAAACAGGTAAAAAAAAAAAAAAA
18HB poly A Handle 5	CATCAATATACAACTAAGAACTGAAATGCAAAAAAAAAAAAAAA
18HB poly A Handle 6	AGAAACCCAAACAACTGAAAGATGGATTCTCAAACAGTAAAAGAGTCTGTAAAAAAAAAAAAAAA
18HB poly A Handle 7	AAACAGCGAAGACGGAAACCAGTTTCTTGCGTGTTGCCAGGGTTAAAAAAAAAAAAAAA
18HB poly A Handle 8	ACGTAAAATTATTATCAAGAATAAACACCGGAAGCAGCACACCAGAAAAAAAAAAAAAAA
18HB poly A Handle 9	GGGAATCGTAAGCAAATAAACGCAACAATAAAGGGAAGCGCGATAAGAGAAAAAAAAAAAAAAA

Table C.21: Cube handle sequences. Handle sequences added to standard oligos are marked in red.

Oligo Name	Sequence (5' → 3')
Cube Random Handle 1	CGCACGACGACAATAACATTCGAGCCAGTAATAATCTTGAGGACTT
Cube Random Handle 2	CAGGACAGGAGGCACGTAGCGCGTATGCGCGTGCGCTTGAGGACTT
Cube Random Handle 3	TTGTACGGAGAGGTCAGGGGCTTAGAGCTTAACGACTTGAGGACTT

Table C.22: 1LS handle sequences. Handle sequences added to standard oligos are marked in red or in blue.

Oligo Name	Sequence (5' → 3')
1LS ABC	TTCTACTACGCGAGCTGAAAAGGTTACCGCGC-AATGCCCG-TCCTCCTC-TCCTCTAG
1LS ext_1	ACACTCATCCATGTTACTTAGCCGAAAGCTGCTTCCTCTACCACCTACATCAC
1LS ext_2	TAAATGAATTTTCTGTATGGGATTAATTTCTTTTCCTCTACCACCTACATCAC
1LS ext_3	AAACAGCTTTTTGCGGGATCGTCAACACTAAATTCCTCTACCACCTACATCAC

Table C.23: 3×6 12HB handle sequences. 3×1 12HB handle sequences are marked with a *. The handle sequences that are added to the standard oligos are marked in red.

Oligo Name	Sequence (5' → 3')
12HB Spot 1_1	GCGAAAGACGCAAAGCCGCCACGGGAACAACATTCC
12HB Spot 1_2	CCGGAAGACGTACAGCGCCGCGATTACAATTCCAACATTCC
12HB Spot 1_3	GTATGTGAAATTGTTATCCAACATTCC*
12HB Spot 1_4	GCCCGCACAGGCGGCCTTTAGTGAACATTCC
12HB Spot 1_5	CTTTTTTTCGTCTCGTCGCTGGCAACATTCC
12HB Spot 1_6	CGAGTAACAACCGTTTACCAGTCAACATTCC
12HB Spot 2_1	GAATTGTAGCCAGAATGGATCAGAGCAAATCCTAACATTCC
12HB Spot 2_2	GTGTATTAAGAGGCTGAGACTCCAACATTCC
12HB Spot 2_3	TCACCGTCACCGGCGCAGTCTCTAACATTCC
12HB Spot 2_4	GGTGCCGTCGAGAGGGTTGATATAACATTCC
12HB Spot 2_5	TACCTGGTTTGCCCCAGCAAACATTCC*
12HB Spot 2_6	ATTAAAATAAGTGCGACGATTGGCCTTGAACATTCC
12HB Spot 3_1	ATTTGGCAAATCAACAGTTGAAAAACATTCC
12HB Spot 3_2	CCGAACCCCCTAAAACATCGACCAGTTTAGAGCAACATTCC
12HB Spot 3_3	GATTTTAGACAGGCATTAAAAATAAACATTCC
12HB Spot 3_4	GATAGTGCAACATGATATTTTTGAATGGAACATTCC
12HB Spot 3_5	AACACCCTAAAGGGAGCCCAACATTCC*
12HB Spot 3_6	GTATTAGAGCCGTCAATAGATAAAACATTCC
12HB Biotin 1	GTACATCGACATCGTTAACGGCA-Biotin
12HB Biotin 2	AACGCCAAAAGGCGGATGGCTTA-Biotin
12HB Biotin 3	AAGAAACAATGACCGGAAACGTC-Biotin
12HB Biotin 4	ATACCACCATCAGTGAGGCCAAACCGTTGTAGCAA-Biotin

Table C.24: Octahedron Sticky Endstaples. Spacer sequence added to the standard oligos is marked in blue, handle sequences added to the standard oligos are marked in red.

Oligo Name	Sequence (5' → 3')
Octahedrons Endstaple A 1	CGTTTTAGCCTTGAGATGGTTTAATTTCAATGTGAATTACCTTTTTTTTTTTTTTTTTTTTTTATCCGTTA
Octahedrons Endstaple A 2	AAAGAATAGATGGTTGCTTTGACGAGCACCTTTCCTCGTTATTTTTTTTTTTTTTTTTTTTTTATCCGTTA
Octahedrons Endstaple A 3	AGCCGGCGATGTCCAGACGACGACAATAAAAGCTAATGCAGATTTTTTTTTTTTTTTTTTTTTTTATCCGTTA
Octahedrons Endstaple A 4	GTCAGGACGTCAAAAATCAGGTCTTTACCTAGTCAGAAGCATTTTTTTTTTTTTTTTTTTTTTTATCCGTTA
Octahedrons Endstaple A 5	TGAATTTATAAAAGGGCGACATTCAACCGGGAAGGTAAATATTTTTTTTTTTTTTTTTTTTTTTATCCGTTA
Octahedrons Endstaple A 6	ACCGGAATCCATGTAATTTAGGCAGAGGCATTCCAACGTCAAATTTTTTTTTTTTTTTTTTTTTTTATCCGTTA
Octahedrons Endstaple A 7	TAAAGGGATGAAAGCGTAAGAATACGTGGATTTTTGAATGGTTTTTTTTTTTTTTTTTTTTTTTATCCGTTA
Octahedrons Endstaple A 8	AAAACGCTCTATTAATTAATTTTCCCTTAGAACATAGCGATATTTTTTTTTTTTTTTTTTTTTTTATCCGTTA
Octahedrons Endstaple A 9	ATCATATTCTCTGAATTTACCGTTCCAGTACCTCATAGTTAGTTTTTTTTTTTTTTTTTTTTTTATCCGTTA
Octahedrons Endstaple A 10	TGCTTTGAAAATTACCTTTTTTAATGGAAACTAAAAGAGTCTGTTTTTTTTTTTTTTTTTTTTTTATCCGTTA
Octahedrons Endstaple A 11	TAAAACATCCTTTTCACCAGTGAGACGGGCATTCATCAGTTGTTTTTTTTTTTTTTTTTTTTTTATCCGTTA
Octahedrons Endstaple A 12	AAAATATCTGTTATTAATTTTAAAAGTTTGTCATTTTGCGGATTTTTTTTTTTTTTTTTTTTTTTATCCGTTA
Octahedrons Endstaple A 13	CCCGAAAGACCTCAGCAGCGAAAGACAGCGGGTAGCAACGGTTTTTTTTTTTTTTTTTTTTTTTATCCGTTA

Octahedrons Endstaple A 14	ATAACAGTTAATTCTACTAATAGTAGTAGCAAACACCGCCTGCTTTTTTTTTTTTTTTTTTTTTTATCCGTTA
Octahedrons Endstaple A 15	AAAGAAGTTCACGCTGGTTTGCCCCAGCAGTGTTTGATGGTGTTTTTTTTTTTTTTTTTTTTTTTATCCGTTA
Octahedrons Endstaple A 16	GAACCCATGGCCTTGAGTAACAGTGCCCGTGGCCGGAAACGTTTTTTTTTTTTTTTTTTTTTTTTATCCGTTA
Octahedrons Endstaple A 17	TTTTTTCACACAACAACCATCGCCCACGCATGTCAGGATTAGATTTTTTTTTTTTTTTTTTTTTTTTATCCGTTA
Octahedrons Endstaple A 18	ATGAGGAAGAACGTAACAAAGCTGCTCATTTATCATTCCAAGTTTTTTTTTTTTTTTTTTTTTTTTATCCGTTA
Octahedrons Endstaple A 19	ACGGTCAATCCTCAGAACCGCCACCCTCAGCTCAGAGCCACCTTTTTTTTTTTTTTTTTTTTTTTTATCCGTTA
Octahedrons Endstaple A 20	AAAATAGCATAAAAGAAACGCAAAGACACCATGTAAATGCTGTTTTTTTTTTTTTTTTTTTTTTTTATCCGTTA
Octahedrons Endstaple A 21	CGAACAAAGTGCCGTCGAGAGGGTTGATATACAAAAGAATACATTTTTTTTTTTTTTTTTTTTTTTTTATCCGTTA
Octahedrons Endstaple A 22	CACCGTCACAGGAGGTTGAGGCAGGTCAGAAATGGAAGGGTTTTTTTTTTTTTTTTTTTTTTTTTATCCGTTA
Octahedrons Endstaple A 23	ATCAAAATCAAGTATTAAGAGGCTGAGACTCCCCTGAACAAAGTTTTTTTTTTTTTTTTTTTTTTTTATCCGTTA
Octahedrons Endstaple A 24	GAACAAGAAAGTTACAAAATAAACAGCCACCCAATCCAAATTTTTTTTTTTTTTTTTTTTTTTTTATCCGTTA
Octahedrons Endstaple B 1	CGTTTTAGCCTTGAGATGGTTTAATTTCAATGTGAATTACCTTTTTTTTTTTTTTTTTTTTTTTTTAACGGAT
Octahedrons Endstaple B 2	AAAGAATAGATGGTTGCTTTGACGAGCACCTTTCCTCGTTATTTTTTTTTTTTTTTTTTTTTTTTTAACGGAT
Octahedrons Endstaple B 3	AGCCGGCGATGTCCAGACGACGACAATAAAAGCTAATGCAGATTTTTTTTTTTTTTTTTTTTTTTTTAACGGAT
Octahedrons Endstaple B 4	GTCAGGACGTCAAAAATCAGGTCTTTACCTAGTCAGAAGCATTTTTTTTTTTTTTTTTTTTTTTTTAACGGAT
Octahedrons Endstaple B 5	TGAATTTATAAAAGGGCGACATTCAACCGGGAAGGTAAATATTTTTTTTTTTTTTTTTTTTTTTTTAACGGAT
Octahedrons Endstaple B 6	ACCGGAATCCATGTAATTTAGGCAGAGGCATTCCAACGTCAAATTTTTTTTTTTTTTTTTTTTTTTTTAACGGAT
Octahedrons Endstaple B 7	TAAAGGGATGAAAGCGTAAGAATACGTGGATTTTTGAATGGTTTTTTTTTTTTTTTTTTTTTTTTTAACGGAT
Octahedrons Endstaple B 8	AAAACGCTCTATTAATTAATTTTCCCTTAGAACATAGCGATATTTTTTTTTTTTTTTTTTTTTTTTTAACGGAT
Octahedrons Endstaple B 9	ATCATATTCTCTGAATTTACCGTTCCAGTACCTCATAGTTAGTTTTTTTTTTTTTTTTTTTTTTTTAACGGAT
Octahedrons Endstaple B 10	TGCTTTGAAAATTACCTTTTTTAATGGAAACTAAAAGAGTCTGTTTTTTTTTTTTTTTTTTTTTTTTAACGGAT
Octahedrons Endstaple B 11	TAAAACATCCTTTTCACCAGTGAGACGGGCATTCATCAGTTGTTTTTTTTTTTTTTTTTTTTTTTTAACGGAT
Octahedrons Endstaple B 12	AAAATATCTGTTATTAATTTTAAAAGTTTGTCATTTTGCGGATTTTTTTTTTTTTTTTTTTTTTTTTAACGGAT
Octahedrons Endstaple B 13	CCCGAAAGACCTCAGCAGCGAAAGACAGCGGGTAGCAACGGTTTTTTTTTTTTTTTTTTTTTTTTTAACGGAT
Octahedrons Endstaple B 14	ATAACAGTTAATTCTACTAATAGTAGTAGCAAACACCGCCTGCTTTTTTTTTTTTTTTTTTTTTTTTTAACGGAT
Octahedrons Endstaple B 15	AAAGAAGTTCACGCTGGTTTGCCCCAGCAGTGTTTGATGGTGTTTTTTTTTTTTTTTTTTTTTTTTTAACGGAT
Octahedrons Endstaple B 16	GAACCCATGGCCTTGAGTAACAGTGCCCGTGGCCGGAAACGTTTTTTTTTTTTTTTTTTTTTTTTTAACGGAT
Octahedrons Endstaple B 17	TTTTTTCACACAACAACCATCGCCCACGCATGTCAGGATTAGATTTTTTTTTTTTTTTTTTTTTTTTTAACGGAT
Octahedrons Endstaple B 18	ATGAGGAAGAACGTAACAAAGCTGCTCATTTATCATTCCAAGTTTTTTTTTTTTTTTTTTTTTTTTTAACGGAT
Octahedrons Endstaple B 19	ACGGTCAATCCTCAGAACCGCCACCCTCAGCTCAGAGCCACCTTTTTTTTTTTTTTTTTTTTTTTTTAACGGAT
Octahedrons Endstaple B 20	AAAATAGCATAAAAGAAACGCAAAGACACCATGTAAATGCTGTTTTTTTTTTTTTTTTTTTTTTTTTAACGGAT
Octahedrons Endstaple B 21	CGAACAAAGTGCCGTCGAGAGGGTTGATATACAAAAGAATACATTTTTTTTTTTTTTTTTTTTTTTTTTAACGGAT
Octahedrons Endstaple B 22	CACCGTCACAGGAGGTTGAGGCAGGTCAGAAATGGAAGGGTTTTTTTTTTTTTTTTTTTTTTTTTTAACGGAT
Octahedrons Endstaple B 23	ATCAAAATCAAGTATTAAGAGGCTGAGACTCCCCTGAACAAAGTTTTTTTTTTTTTTTTTTTTTTTTTAACGGAT
Octahedrons Endstaple B 24	GAACAAGAAAGTTACAAAATAAACAGCCACCCAATCCAAATTTTTTTTTTTTTTTTTTTTTTTTTTAACGGAT

C.10.3 Fluorescently modified sequences

C.10.3.1 External (Handles)

Table C.25: Handle sequence for attaching Cy5 to DNA nanostructures including the oligo name.

Oligo Name	Sequence (5' → 3')
Cy5 Poly T Antihandle 5'	Cy5-TTTTTTTTTTTTTTTTT
Cy5 Poly T Antihandle 3'	TTTTTTTTTTTTTTTTT-Cy5
Cy5 Random Antihandle 5'	Cy5-TTTTAAGTCCTCAAG
Cy5 Random Antihandle 3'	TTTTAAGTCCTCAAG-Cy5
1LS DNA-PAINT Imager A	CTAGAGGA-Atto655
1LS DNA-PAINT Imager B	GAGGAGGA-Atto655
1LS DNA-PAINT Imager C	CGGGCATT-Atto655
1LS External Label Strand	GTGATGTAGGTGGTAGAGGAAT-Atto542
12HB DNA-PAINT Imager Sequence	GGAATGTT-Atto655
Cy5 6bp Hairpin Antihandle 5'	Cy5- CCTCATTCTTTCGAGG
Cy5 6bp Hairpin Antihandle 3'	CCTCATTCTTTCGAGG -Cy5
Cy5 8bp Hairpin Antihandle 5'	Cy5-CTCCTCATTCTTTCGAGGAG
Cy5 8bp Hairpin Antihandle 3'	CTCCTCATTCTTTCGAGGAG-Cy5

C.10.3.2 Internal

Table C.26: Internal Fluorescent Staples with Cy5.

Oligo Name	Sequence (5' → 3')
24HB Internal Cy5 Staple 1	Cy5-TCAGAGGGTATAACTGAACACCCTTTACATCGGGAGAAAGGTAAA
24HB Internal Cy5 Staple 2	Cy5-TAAAGCTCTGAGAAAACCCGTCACCGTGCATAAAGA
24HB Internal Cy5 Staple 3	Cy5-ACTCATCTTTGAGACCGC
4LB Internal Cy5 Staple 1	Cy5-GTTTCATATTTGAGCATATTCAGAATTTAATTGCT
4LB Internal Cy5 Staple 2	Cy5-AAAATTGACAACTTAGCCCGGAATAGGTGTATCACTGG
4LB Internal Cy5 Staple 3	Cy5- CGGCGTAAAGTGGTCCGTCTGTTGGAACAGTATTAGA
Cube Internal Cy5 Staple 1	Cy5-TAGATGGTCATGGAAGGGTTACAGCAGACTGATAGCTT
Cube Internal Cy5 Staple 2	Cy5-ATTGCAGGAAGGTCAATCTGAACGGCTATCAGGTC
Cube Internal Cy5 Staple 3	Cy5-ATAACACTGACCTTGGAACCGGACAGTGCCCGTATAGT

C.10.4 Modifications for Dynamic DNA Origami

Table C.27: 18HB middle bent: sequences that are taken out

Oligo Name	Sequence (5' → 3')
18HB Middle 1	GCGTAAGCCTAATAGTAATTCATGTAAAACGAACAGTAA
18HB Middle 2	AGCCCAATAATTATTTGACGACGGTAAAGCGCCCTCTCT
18HB Middle 3	ATTATGCATCAATTAAATCGGAACAAAGTTAATAGGCTCCAAAA
18HB Middle 4	GCGTCATACGCCTATTTCGGATTAGCAATACAGGCAA
18HB Middle 5	CGCTTAATAAAGTACAATAACGCCATATATTACAAGTCT
18HB Middle 6	TAACCCACAAAGAAACAAGGTAAGAGTGAGAGTACGGTG
18HB Middle 7	TAATGACGCTCAGGTGAGTATCTGGGCAGAGAAAATG
18HB Middle 8	CCATATAAGAGAAAGGAATTACGAGACAACATTTTAACAATCA
18HB Middle 9	GTGAAGCCAAAATCTAAAGCATCACCTTCTCTCAGCAGGCTATAT
18HB Middle 10	GAAACTGATGTCCCAATAGCAACCCGTCGGAACCGTTGAAAATC
18HB Middle 11	TTGAGGAGAGGAGGTCAATGGGTTCGACTGGTTACAGCGCA
18HB Middle 12	TTAAATATCAGCTCGTTTACCAGACCGTTGGGGCCAGTAATTT
18HB Middle 13	AAATTAAGCTGAACCACGCTGAAACATACGGAAGCATGCGCCGCTA
18HB Middle 14	CAAGTGACATTAATAAAGTATTTTCGAAAGAAAATTGAT
18HB Middle 15	CTGCTTCATCAGCGTCTGTGAGAATACAACATAAATAAACAG
18HB Middle 16	AAAGCAGCAAATGAATAGATACTTCTGGGGTCCACCACACCCGCCG
18HB Middle 17	CTGAATTTATCTGAAAATGTGAGGAACCACGCACTGC
18HB Middle 18	ACACCTCCGTGAGCTCATAGAGGCACCGACAAGATTTTTTGT
18HB Middle 19	AATTTTTTCACTATTATCCGTTCCTAACGGAGCATAGTAGTTA
18HB Middle 20	TCCAAAAAAAGCCCCCTATGGCTTATCTACGCATAACCAGAGA
18HB Middle 21	TGCATGACAGGATGGGCATTCTATCACGCTAACTCTAGCGGTCACGCTGC
18HB Middle 22	CGCCGCCTCGAGTAAGAACGCCACGCCAACTGTCCAATCCC
18HB Middle 23	AATCCAAATAGAATTGAAGAGCAACACTATTTAATAATTTAGGCTTTT
18HB Middle 24	GTACAAGAGCCAATAATTCACATTAACATGAAATTGCGAATAAT
18HB Middle 25	ACTAAAGGAAGTATTAAAAAGCGCGGTAGAAAACGCCACAAGA

C.10.5 Staple Design for Silicification and Handle Clustering Test

Table C.28: 24HB Random Placement Handles for Silicification Clustering Test. These are handles that have been added randomly all over the 24HB. Handle sequences added to the standard oligos are marked in red. Additional staples are needed, because the staples have been restructured to be short enough for synthesis.

Oligo Name	Sequence (5' → 3')
24HB Random Handle 1 Poly T	CCTTTTATCAATAGCGAATTTTCCCAAAAAAAAAAAAAAA
24HB Random Handle 2 Poly T	TTTATGACAAAGAGCCATATCACCAAAAAAAAAAAAAAA
24HB Random Handle 3 Poly T	AATTCCTTATCAGCGTTTTCAAAAAAAAAAAAAAA
24HB Random Handle 4 Poly T	CTTTCATCAACATTAAATGTGAATAATTCAAAAAAAAAAAAAAA
24HB Random Handle 5 Poly T	GGCACCATTCAACTGTCAGGAAAAAAAAAAAAAAA
24HB Random Handle 6 Poly T	TTAAACAAATAAGTTTTTTGGGGTAAAAAAAAAAAAAAA
24HB Random Handle 7 Poly T	ACGTGGTTGACCATTAGAAATATGCAAAAAAAAAAAAAAA
24HB Random Handle 8 Poly T	GCCAAAGTTGCAAAGACACCAAAAAAAAAAAAAAA
24HB Random Handle 1 Random	CCTTTTATCAATAGCGAATTTTCCCACTTGAGGACTTAAAA
24HB Random Handle 2 Random	TTTATGACAAAGAGCCATATCACCACTTGAGGACTTAAAA
24HB Random Handle 3 Random	AATTCCTTATCAGCGTTTTCACTTGAGGACTTAAAA
24HB Random Handle 4 Random	CTTTCATCAACATTAAATGTGAATAATTCACTTGAGGACTTAAAA
24HB Random Handle 5 Random	GGCACCATTCAACTGTCAGGACTTGAGGACTTAAAA
24HB Random Handle 6 Random	TTAAACAAATAAGTTTTTTGGGGTACTTGAGGACTTAAAA
24HB Random Handle 7 Random	ACGTGGTTGACCATTAGAAATATGCACTTGAGGACTTAAAA
24HB Random Handle 8 Random	GCCAAAGTTGCAAAGACACCACTTGAGGACTTAAAA
24HB Random Handle 1 Hairpin 6bp	CCTTTTATCAATAGCGAATTTTCCCACTCCTCGAAAGAATGAGGAG
24HB Random Handle 2 Hairpin 6bp	TTTATGACAAAGAGCCATATCACCACTCCTCGAAAGAATGAGGAG
24HB Random Handle 3 Hairpin 6bp	AATTCCTTATCAGCGTTTTCACTCCTCGAAAGAATGAGGAG
24HB Random Handle 4 Hairpin 6bp	CTTTCATCAACATTAAATGTGAATAATTCACTCCTCGAAAGAATGAGGAG
24HB Random Handle 5 Hairpin 6bp	GGCACCATTCAACTGTCAGGACTCCTCGAAAGAATGAGGAG
24HB Random Handle 6 Hairpin 6bp	TTAAACAAATAAGTTTTTTGGGGTACTCCTCGAAAGAATGAGGAG
24HB Random Handle 7 Hairpin 6bp	ACGTGGTTGACCATTAGAAATATGCACTCCTCGAAAGAATGAGGAG
24HB Random Handle 8 Hairpin 6bp	GCCAAAGTTGCAAAGACACC ACTCCTCGAAAGAATGAGGAG
24HB Random Handle 1 Hairpin 8bp	CCTTTTATCAATAGCGAATTTTCCCACCCTCCTCGAAAGAATGAGGAGGG
24HB Random Handle 2 Hairpin 8bp	TTTATGACAAAGAGCCATATCACCACCCTCCTCGAAAGAATGAGGAGGG
24HB Random Handle 3 Hairpin 8bp	AATTCCTTATCAGCGTTTTCACCCTCCTCGAAAGAATGAGGAGGG
24HB Random Handle 4 Hairpin 8bp	CTTTCATCAACATTAAATGTGAATAATTCACCCTCCTCGAAAGAATGAGGAGGG
24HB Random Handle 5 Hairpin 8bp	GGCACCATTCAACTGTCAGGACCCTCCTCGAAAGAATGAGGAGGGA
24HB Random Handle 6 Hairpin 8bp	TTAAACAAATAAGTTTTTTGGGGTACCCTCCTCGAAAGAATGAGGAGGG
24HB Random Handle 7 Hairpin 8bp	ACGTGGTTGACCATTAGAAATATGCACCCTCCTCGAAAGAATGAGGAGGG
24HB Random Handle 8 Hairpin 8bp	GCCAAAGTTGCAAAGACACCACCCTCCTCGAAAGAATGAGGAGGG
24HB Random Addition Handle 1	CTAAAGTAGCTCAAATTTTTGTAATTGCCAGACCGGAAGCAATTCA
24HB Random Addition Handle 2	CATAACGCCAAATTAAAGA
24HB Random Addition Handle 3	CGGAATAAGTTTATTAAAGGTATC
24HB Random Addition Handle 4	TCGACTATATGTAAATGACTA

24HB Random Addition Handle 5	TTAGAATCAGAACGCGAGGCGTTTTAGCTTAAATTGAAATAAAAC
24HB Random Addition Handle 6	ACTCATCTTTGAGACCGC
24HB Random Addition Handle 7	TCGGCATTTTCGGTCATGTTTGCCGGA
24HB Random Addition Handle 8	GCGTCTAATAGGATTAAATGAAAATTTAAGCCTTACGGTAACTGGAGC
24HB Random Addition Handle 9	CCACCCTCAGAACCGCCACCCTCTTAAGTCCAAAT
24HB Random Addition Handle 10	GGAACAACATAAGAGGCCTACGAA
24HB Random Addition Handle 11	GCCAGTTAATAGTTTTAACGGGGTTACATGGGAAT
24HB Random Addition Handle 12	CGAGGTGCCTTGATATTCACACCGTTCCTAAT

Table C.29: 24HB Cluster Placement Handles for Silicification Clustering Test. Two clusters: One on the right side of the design with 6 handles and one on the left hand with 4 handles. To make tight clusters, some handles are on the 5' end instead of the 3' end. Handle sequences added to the standard oligos are marked in red. Additional staples are needed, because the staples have been restructured to be short enough for synthesis.

Oligo Name	**Sequence (5' → 3')**
24HB Cluster Right Handle 1 Poly T	CATAACCTGTAAAGAGGTCCATGTTTTATTGCCTGAAAAAAAAAAAAAAA
24HB Cluster Right Handle 2 Poly T	TTTAAGCCTTACGGTAACTGGAGCAAAAAAAAAAAAAAA
24HB Cluster Right Handle 3 Poly T	AAAAAAAAAAAAAAAGGTCAAATGCCGGAGTCCACTAAGGAAT
24HB Cluster Right Handle 4 Poly T	CTACAAAGGCTATCAAAAAAAAAAAAAAA
24HB Cluster Right Handle 5 Poly T	AAAAAAAAAAAAAAAAAACAAGCTAGATCT
24HB Cluster Right Handle 6 Poly T	AAAAAAAAAAAAAAAAGAGTTCGTAAAACTAGTATACTTTT
24HB Cluster Right Handle 1 Random	CATAACCTGTAAAGAGGTCCATGTTTTATTGCCTGACTTGAGGACTTAAAA
24HB Cluster Right Handle 2 Random	TTTAAGCCTTACGGTAACTGGAGCACTTGAGGACTTAAAA
24HB Cluster Right Handle 3 Random	CTTGAGGACTTAAAAAGGTCAAATGCCGGAGTCCACTAAGGAAT
24HB Cluster Right Handle 4 Random	CTACAAAGGCTATCAACTTGAGGACTTAAAA
24HB Cluster Right Handle 5 Random	CTTGAGGACTTAAAAAAAACAAGCTAGATCT
24HB Cluster Right Handle 6 Random	CTTGAGGACTTAAAAAAGAGTTCGTAAAACTAGTATACTTTT
24HB Cluster Right Handle 1 Hairpin 6bp	CATAACCTGTAAAGAGGTCCATGTTTTATTGCCTGACTCCTCGAAAGAATGAGGAG
24HB Cluster Right Handle 2 Hairpin 6bp	TTTAAGCCTTACGGTAACTGGAGCACTCCTCGAAAGAATGAGGAG
24HB Cluster Right Handle 3 Hairpin 6bp	CTCCTCGAAAGAATGAGGAGAGGTCAAATGCCGGAGTCCACTAAGGAAT
24HB Cluster Right Handle 4 Hairpin 6bp	CTACAAAGGCTATCAACTCCTCGAAAGAATGAGGAG
24HB Cluster Right Handle 5 Hairpin 6bp	CTCCTCGAAAGAATGAGGAGAAAACAAGCTAGATCT
24HB Cluster Right Handle 6 Hairpin 6bp	CTCCTCGAAAGAATGAGGAGAAGAGTTCGTAAAACTAGTATACTTTT
24HB Cluster Right Handle 1 Hairpin 8bp	CATAACCTGTAAAGAGGTCCATGTTTTATTGCCTGACCCTCCTCGAAAGAATGAGGAGGG
24HB Cluster Right Handle 2 Hairpin 8bp	TTTAAGCCTTACGGTAACTGGAGCACCCTCCTCGAAAGAATGAGGAGGG
24HB Cluster Right Handle 3 Hairpin 8bp	CCCTCCTCGAAAGAATGAGGAGGGAGGTCAAATGCCGGAGTCCACTAAGGAAT
24HB Cluster Right Handle 4 Hairpin 8bp	CTACAAAGGCTATCAACCCTCCTCGAAAGAATGAGGAGGG
24HB Cluster Right Handle 5 Hairpin 8bp	CCCTCCTCGAAAGAATGAGGAGGGAAAACAAGCTAGATCT
24HB Cluster Right Handle 6 Hairpin 8bp	CCCTCCTCGAAAGAATGAGGAGGGAAGAGTTCGTAAAACTAGTATACTTTT
24HB Cluster Right Addition Handle 1	GGATTCAACGAGCAGCCCTCAGAG
24HB Cluster Right Addition Handle 2	CGCGTCTAATAGGATTAAATGAAAA
24HB Cluster Right Addition Handle 3	TAGCACTCCAGCCAAGTTTGG
24HB Cluster Right Addition Handle 4	AAACAAGCTAGAT

24HB Cluster Right Addition Handle 5	CTACAAAGGCTATCA
24HB Cluster Left Handle 1 Poly T	TATCTGTCTTATCCCATCCTAATTAAAAAAAAAAAAAAA
24HB Cluster Left Handle 2 Poly T	AAAAAAAAAAAAAAATAATCGGTAAACCAGCTA
24HB Cluster Left Handle 3 Poly T	AAAAAAAAAAAAAAATACGAGCATGTAAGTTAATTTACCGAC
24HB Cluster Left Handle 4 Poly T	TTCTTTTCAAATATATTTTGAAACCAATCAAAAAAAAAAAAAAAA
24HB Cluster Left Handle 1 Random	TATCTGTCTTATCCCATCCTAATTACTTGAGGACTTAAAA
24HB Cluster Left Handle 2 Random	CTTGAGGACTTAAAAATAATCGGTAAACCAGCTA
24HB Cluster Left Handle 3 Random	CTTGAGGACTTAAAAATACGAGCATGTAAGTTAATTTACCGAC
24HB Cluster Left Handle 4 Random	TTCTTTTCAAATATATTTTGAAACCAATCAAACTTGAGGACTTAAAA
24HB Cluster Left Handle 1 Hairpin 6bp	TATCTGTCTTATCCCATCCTAATTACTCCTCGAAAGAATGAGGAG
24HB Cluster Left Handle 2 Hairpin 6bp	CTCCTCGAAAGAATGAGGAGATAATCGGTAAACCAGCTA
24HB Cluster Left Handle 3 Hairpin 6bp	CTCCTCGAAAGAATGAGGAGATACGAGCATGTAAGTTAATTTACCGAC
24HB Cluster Left Handle 4 Hairpin 6bp	TTCTTTTCAAATATATTTTGAAACCAATCAAACTCCTCGAAAGAATGAGGAG
24HB Cluster Left Handle 1 Hairpin 8bp	TATCTGTCTTATCCCATCCTAATTACCCTCCTCGAAAGAATGAGGAGGG
24HB Cluster Left Handle 2 Hairpin 8bp	CCCTCCTCGAAAGAATGAGGAGGGATAATCGGTAAACCAGCTA
24HB Cluster Left Handle 3 Hairpin 8bp	CCCTCCTCGAAAGAATGAGGAGGGATACGAGCATGTAAGTTAATTTACCGAC
24HB Cluster Left Handle 4 Hairpin 8bp	TTCTTTTCAAATATATTTTGAAACCAATCAACCCTCCTCGAAAGAATGAGGAGGG
24HB Cluster Left Addition Handle 1	TACCGCGTTTTTATCGGG
24HB Cluster Left Addition Handle 2	ATACCCAATAATAAGTAGAACCTACCA
24HB Cluster Left Addition Handle 4	ACACCGGTTGAAATCATC

Table C.30: 24HB Elongated Endstaple Handles for Silicification Clustering Test. These are endstaples that have been elongated with the handle sequences. Handle sequences added to the standard oligos are marked in red. Additional staples are needed, because the staples have been restructured to be short enough for synthesis.

Oligo Name	**Sequence (5' → 3')**
24HB Elongated Endcap Handle 1 Poly T	TTGCGTTGCGCTCAAGCCTGGGGTGCCTAAAAAAAAAAAAAAA
24HB Elongated Endcap Handle 2 Poly T	TAATGAATCGGCCACCGCTTTCCAGTCGAAAAAAAAAAAAAAA
24HB Elongated Endcap Handle 3 Poly T	AGTGAGACGGGCAATTTGCGTATTGGGCAAAAAAAAAAAAAAA
24HB Elongated Endcap Handle 4 Poly T	TCCACGCTGGTTTGCCTTCACCGCCTGGAAAAAAAAAAAAAAA
24HB Elongated Endcap Handle 5 Poly T	GGCAAAATCCCTTAAGCAGGCGAAAATCAAAAAAAAAAAAAAA
24HB Elongated Endcap Handle 6 Poly T	CCTGCAGCCAGCGGTGTTCAGCAAATCGAAAAAAAAAAAAAAA
24HB Elongated Endcap Handle 7 Poly T	TGTGCACTCTGTGGCCTGCATCAGACGAAAAAAAAAAAAAAA
24HB Elongated Endcap Handle 8 Poly T	GGGGGTTTCTGCCGGCGGCCAGAATGCGAAAAAAAAAAAAAAA
24HB Elongated Endcap Handle 1 Random	TTGCGTTGCGCTCAAGCCTGGGGTGCCTACTTGAGGACTTAAAA
24HB Elongated Endcap Handle 2 Random	TAATGAATCGGCCACCGCTTTCCAGTCGACTTGAGGACTTAAAA
24HB Elongated Endcap Handle 3 Random	AGTGAGACGGGCAATTTGCGTATTGGGCACTTGAGGACTTAAAA
24HB Elongated Endcap Handle 4 Random	TCCACGCTGGTTTGCCTTCACCGCCTGGACTTGAGGACTTAAAA
24HB Elongated Endcap Handle 5 Random	GGCAAAATCCCTTAAGCAGGCGAAAATCACTTGAGGACTTAAAA
24HB Elongated Endcap Handle 6 Random	CCTGCAGCCAGCGGTGTTCAGCAAATCGACTTGAGGACTTAAAA
24HB Elongated Endcap Handle 7 Random	TGTGCACTCTGTGGCCTGCATCAGACGAACTTGAGGACTTAAAA
24HB Elongated Endcap Handle 8 Random	GGGGGTTTCTGCCGGCGGCCAGAATGCGACTTGAGGACTTAAAA

24HB Elongated Endcap Handle 1 6bp Hairpin	TTGCGTTGCGCTCAAGCCTGGGGTGCCTACTCCTCGAAAGAATGAGGAG
24HB Elongated Endcap Handle 2 6bp Hairpin	TAATGAATCGGCCACCGCTTTCCAGTCGACTCCTCGAAAGAATGAGGAG
24HB Elongated Endcap Handle 3 6bp Hairpin	AGTGAGACGGGCAATTTGCGTATTGGGCACTCCTCGAAAGAATGAGGAG
24HB Elongated Endcap Handle 4 6bp Hairpin	TCCACGCTGGTTTGCCTTCACCGCCTGGACTCCTCGAAAGAATGAGGAG
24HB Elongated Endcap Handle 5 6bp Hairpin	GGCAAAATCCCTTAAGCAGGCGAAAATCACTCCTCGAAAGAATGAGGAG
24HB Elongated Endcap Handle 6 6bp Hairpin	CCTGCAGCCAGCGGTGTTCAGCAAATCGACTCCTCGAAAGAATGAGGAG
24HB Elongated Endcap Handle 7 6bp Hairpin	TGTGCACTCTGTGGCCTGCATCAGACGAACTCCTCGAAAGAATGAGGAG
24HB Elongated Endcap Handle 8 6bp Hairpin	GGGGGTTTCTGCCGGCGGCCAGAATGCGACTCCTCGAAAGAATGAGGAG
24HB Elongated Endcap Handle 1 8bp Hairpin	TTGCGTTGCGCTCAAGCCTGGGGTGCCTACCCTCCTCGAAAGAATGAGGAGGG
24HB Elongated Endcap Handle 2 8bp Hairpin	TAATGAATCGGCCACCGCTTTCCAGTCGACCCTCCTCGAAAGAATGAGGAGGG
24HB Elongated Endcap Handle 3 8bp Hairpin	AGTGAGACGGGCAATTTGCGTATTGGGCACCCTCCTCGAAAGAATGAGGAGGG
24HB Elongated Endcap Handle 4 8bp Hairpin	TCCACGCTGGTTTGCCTTCACCGCCTGGACCCTCCTCGAAAGAATGAGGAGGG
24HB Elongated Endcap Handle 5 8bp Hairpin	GGCAAAATCCCTTAAGCAGGCGAAAATCACCCTCCTCGAAAGAATGAGGAGGG
24HB Elongated Endcap Handle 6 8bp Hairpin	CCTGCAGCCAGCGGTGTTCAGCAAATCGACCCTCCTCGAAAGAATGAGGAGGG
24HB Elongated Endcap Handle 7 8bp Hairpin	TGTGCACTCTGTGGCCTGCATCAGACGAACCCTCCTCGAAAGAATGAGGAGGG
24HB Elongated Endcap Handle 8 8bp Hairpin	GGGGGTTTCTGCCGGCGGCCAGAATGCGACCCTCCTCGAAAGAATGAGGAGGG

Table C.31: 24HB Row Placement Handles for Silicification Clustering Test. There are three rows, that can be used alone or in tandem. They are spaced such, that they make an equilateral triangle, when all are used. Two rows with 10 handles each and one row with 9 handles. Handle sequences added to the standard oligos are marked in red. Additional staples are needed, because the staples have been restructured to be short enough for synthesis.

Oligo Name	**Sequence (5' → 3')**
24HB Row 1 Handle 1 Poly T	AATTCGGTTGGAATTAGCAATAAATAGACTGCCAGAGAAAAAAAAAAAAAAA
24HB Row 1 Handle 2 Poly T	AAGAAATTAACAGAAATAAAGGATTTTCTAATGGTAATCAAAAAAAAAAAAAAA
24HB Row 1 Handle 3 Poly T	CTGTTATTCTGAAACATTATAAAAAAAAAAAAAAA
24HB Row 1 Handle 4 Poly T	CGACGGCCAGTGCCAAGCTGCACGCGCGGGAAGTTGAAAAAAAAAAAAAAA
24HB Row 1 Handle 5 Poly T	AGAAAGCGCACAATAGAAATGCAAAAAAAAAAAAAAA
24HB Row 1 Handle 6 Poly T	TGAGTACCGCCAGCCATTTAATATCATACTTAAAAAAAAAAAAAAA
24HB Row 1 Handle 7 Poly T	TAAAGCTCTGAGAAAACCCGTCACCGTGCATAAAGAAAAAAAAAAAAAAA
24HB Row 1 Handle 8 Poly T	CTTTTGCACTGCCAGTTTGAGGGGCATCGTAGGATTCTCCGAAAAAAAAAAAAAAA
24HB Row 1 Handle 9 Poly T	AAGACGATAAAAGATTTTAAGAACTAAAAAAAAAAAAAAA
24HB Row 1 Handle 10 Poly T	TGATTGACAGGCCTCAGAGCCGCCAGCCGAAAAAAAAAAAAAAA
24HB Row 1 Handle 1 Random	AATTCGGTTGGAATTAGCAATAAATAGACTGCCAGAGACTTGAGGACTTAAAA
24HB Row 1 Handle 2 Random	AAGAAATTAACAGAAATAAAGGATTTTCTAATGGTAATCAACTTGAGGACTTAAAA
24HB Row 1 Handle 3 Random	CTGTTATTCTGAAACATTATAACTTGAGGACTTAAAA
24HB Row 1 Handle 4 Random	CGACGGCCAGTGCCAAGCTGCACGCGCGGGAAGTTGACTTGAGGACTTAAAA
24HB Row 1 Handle 5 Random	AGAAAGCGCACAATAGAAATGCAACTTGAGGACTTAAAA
24HB Row 1 Handle 6 Random	TGAGTACCGCCAGCCATTTAATATCATACTTACTTGAGGACTTAAAA
24HB Row 1 Handle 7 Random	TAAAGCTCTGAGAAAACCCGTCACCGTGCATAAAGAACTTGAGGACTTAAAA
24HB Row 1 Handle 8 Random	CTTTTGCACTGCCAGTTTGAGGGGCATCGTAGGATTCTCCGACTTGAGGACTTAAAA
24HB Row 1 Handle 9 Random	AAGACGATAAAAGATTTTAAGAACTACTTGAGGACTTAAAA

24HB Row 1 Handle 10 Random	TGATTGACAGGCCTCAGAGCCGCCAGCCGACTTGAGGACTTAAAA
24HB Row 1 Handle 1 Hairpin 6bp	AATTCGGTTGGAATTAGCAATAAATAGACTGCCAGAGACTCCTCGAAAGAATGAGGAG
24HB Row 1 Handle 2 Hairpin 6bp	AAGAAATTAACAGAAATAAAGGATTTTCTAATGGTAATCAACTCCTCGAAAGAATGAGGAG
24HB Row 1 Handle 3 Hairpin 6bp	CTGTTATTCTGAAACATTATAACTCCTCGAAAGAATGAGGAG
24HB Row 1 Handle 4 Hairpin 6bp	CGACGGCCAGTGCCAAGCTGCACGCGCGGGAAGTTGACTCCTCGAAAGAATGAGGAG
24HB Row 1 Handle 5 Hairpin 6bp	AGAAAGCGCACAATAGAAATGCAACTCCTCGAAAGAATGAGGAG
24HB Row 1 Handle 6 Hairpin 6bp	TGAGTACCGCCAGCCATTTAATATCATACTTACTCCTCGAAAGAATGAGGAG
24HB Row 1 Handle 7 Hairpin 6bp	TAAAGCTCTGAGAAAACCCGTCACCGTGCATAAAGAACTCCTCGAAAGAATGAGGAG
24HB Row 1 Handle 8 Hairpin 6bp	CTTTTGCACTGCCAGTTTGAGGGGCATCGTAGGATTCTCCGACTCCTCGAAAGAATGAGGAG
24HB Row 1 Handle 9 Hairpin 6bp	AAGACGATAAAAGATTTTAAGAACTACTCCTCGAAAGAATGAGGAG
24HB Row 1 Handle 10 Hairpin 6bp	TGATTGACAGGCCTCAGAGCCGCCAGCCGACTCCTCGAAAGAATGAGGAG
24HB Row 1 Handle 1 Hairpin 8bp	AATTCGGTTGGAATTAGCAATAAATAGACTGCCAGAGACCCTCCTCGAAAGAATGAGGAGGG
24HB Row 1 Handle 2 Hairpin 8bp	AAGAAATTAACAGAAATAAAGGATTTTCTAATGGTAATCAACCCTCCTCGAAAGAATGAGGAGGG
24HB Row 1 Handle 3 Hairpin 8bp	CTGTTATTCTGAAACATTATAACCCTCCTCGAAAGAATGAGGAGGG
24HB Row 1 Handle 4 Hairpin 8bp	CGACGGCCAGTGCCAAGCTGCACGCGCGGGAAGTTGACCCTCCTCGAAAGAATGAGGAGGG
24HB Row 1 Handle 5 Hairpin 8bp	AGAAAGCGCACAATAGAAATGCAACCCTCCTCGAAAGAATGAGGAGGG
24HB Row 1 Handle 6 Hairpin 8bp	TGAGTACCGCCAGCCATTTAATATCATACTTACCCTCCTCGAAAGAATGAGGAGGG
24HB Row 1 Handle 7 Hairpin 8bp	TAAAGCTCTGAGAAAACCCGTCACCGTGCATAAAGAACCCTCCTCGAAAGAATGAGGAGGG
24HB Row 1 Handle 8 Hairpin 8bp	CTTTTGCACTGCCAGTTTGAGGGGCATCGTAGGATTCTCCGACCCTCCTCGAAAGAATGAGGAGGG
24HB Row 1 Handle 9 Hairpin 8bp	AAGACGATAAAAGATTTTAAGAACTACCCTCCTCGAAAGAATGAGGAGGG
24HB Row 1 Handle 10 Hairpin 8bp	TGATTGACAGGCCTCAGAGCCGCCAGCCGACCCTCCTCGAAAGAATGAGGAGGG
24HB Row 1 Addition Handle 3	GTACTCAGTCGAGAGCTCAGTGAGG
24HB Row 1 Addition Handle 5	TTGGGCTTAAGAAGGAAGTTAAGTCAG
24HB Row 1 Addition Handle 9	GGCTCATACGTTAATAA
24HB Row 2 Handle 1 Poly T	TTTATGACAAAGAGCCATATCACCAAAAAAAAAAAAAAA
24HB Row 2 Handle 2 Poly T	GCGGGAGTTAGAACATTGTATTTGTTAAAATCAAAAAAAAAAAAAAAA
24HB Row 2 Handle 3 Poly T	CTATTTTTGAATGGCTATACGTGGCACAGACAAAAAAAAAAAAAAA
24HB Row 2 Handle 4 Poly T	GCCACCCTCACCATCCATTAGAACAAAAAAAAAAAAAAA
24HB Row 2 Handle 5 Poly T	TTACCCAACCTGACTATAGCGCATAGGCTGAAAAAAAAAAAAAAA
24HB Row 2 Handle 6 Poly T	GAACAAGCAAGCCGCCCAATAAAAAAAAAAAAAAA
24HB Row 2 Handle 7 Poly T	ATTTTTTAATATTAAGCAAAAGCCAAAAAAAAAAAAAAA
24HB Row 2 Handle 8 Poly T	ATTAAGAATACACCTCAGCACTAAAGGAAAGAGGAGTAAAAAAAAAAAAAAAA
24HB Row 2 Handle 9 Poly T	AAATAAGGCAATAGAGAATTGATTAGAGGAATCATAAAAAAAAAAAAAAA
24HB Row 2 Handle 10 Poly T	AAATGTACATCAAACTTAAAAAAAAAAAAAAA
24HB Row 2 Handle 1 Random	TTTATGACAAAGAGCCATATCACCACTTGAGGACTTAAAA
24HB Row 2 Handle 2 Random	GCGGGAGTTAGAACATTGTATTTGTTAAAATCAAAAAACTTGAGGACTTAAAA
24HB Row 2 Handle 3 Random	CTATTTTTGAATGGCTATACGTGGCACAGACACTTGAGGACTTAAAA
24HB Row 2 Handle 4 Random	GCCACCCTCACCATCCATTAGAACACTTGAGGACTTAAAA
24HB Row 2 Handle 5 Random	TTACCCAACCTGACTATAGCGCATAGGCTGACTTGAGGACTTAAAA
24HB Row 2 Handle 6 Random	GAACAAGCAAGCCGCCCAATACTTGAGGACTTAAAA
24HB Row 2 Handle 7 Random	ATTTTTTAATATTAAGCAAAAGCCACTTGAGGACTTAAAA
24HB Row 2 Handle 8 Random	ATTAAGAATACACCTCAGCACTAAAGGAAAGAGGAGTAACTTGAGGACTTAAAA

24HB Row 2 Handle 9 Random	AAATAAGGCAATAGAGAATTGATTAGAGGAATCATACTTGAGGACTTAAAA
24HB Row 2 Handle 10 Random	AAATGTACATCAAACTTACTTGAGGACTTAAAA
24HB Row 2 Handle 1 Hairpin 6bp	TTTATGACAAAGAGCCATATCACCACTCCTCGAAAGAATGAGGAG
24HB Row 2 Handle 2 Hairpin 6bp	GCGGGAGTTAGAACATTGTATTTGTTAAAATCAAAAAACTCCTCGAAAGAATGAGGAG
24HB Row 2 Handle 3 Hairpin 6bp	CTATTTTTGAATGGCTATACGTGGCACAGACACTCCTCGAAAGAATGAGGAG
24HB Row 2 Handle 4 Hairpin 6bp	GCCACCCTCACCATCCATTAGAACACTCCTCGAAAGAATGAGGAG
24HB Row 2 Handle 5 Hairpin 6bp	TTACCCAACCTGACTATAGCGCATAGGCTGACTCCTCGAAAGAATGAGGAG
24HB Row 2 Handle 6 Hairpin 6bp	GAACAAGCAAGCCGCCCAATACTCCTCGAAAGAATGAGGAG
24HB Row 2 Handle 7 Hairpin 6bp	ATTTTTTAATATTAAGCAAAAGCCACTCCTCGAAAGAATGAGGAG
24HB Row 2 Handle 8 Hairpin 6bp	ATTAAGAATACACCTCAGCACTAAAGGAAAGAGGAGTAAACTCCTCGAAAGAATGAGGAG
24HB Row 2 Handle 9 Hairpin 6bp	AAATAAGGCAATAGAGAATTGATTAGAGGAATCATACTCCTCGAAAGAATGAGGAG
24HB Row 2 Handle 10 Hairpin 6bp	AAATGTACATCAAACTTACTCCTCGAAAGAATGAGGAG
24HB Row 2 Handle 1 Hairpin 8bp	TTTATGACAAAGAGCCATATCACCACCCTCCTCGAAAGAATGAGGAGGG
24HB Row 2 Handle 2 Hairpin 8bp	GCGGGAGTTAGAACATTGTATTTGTTAAAATCAAAAAACCCTCCTCGAAAGAATGAGGAGGG
24HB Row 2 Handle 3 Hairpin 8bp	CTATTTTTGAATGGCTATACGTGGCACAGACACCCTCCTCGAAAGAATGAGGAGGG
24HB Row 2 Handle 4 Hairpin 8bp	GCCACCCTCACCATCCATTAGAACACCCTCCTCGAAAGAATGAGGAGGG
24HB Row 2 Handle 5 Hairpin 8bp	TTACCCAACCTGACTATAGCGCATAGGCTGACCCTCCTCGAAAGAATGAGGAGGG
24HB Row 2 Handle 6 Hairpin 8bp	GAACAAGCAAGCCGCCCAATACCCTCCTCGAAAGAATGAGGAGGG
24HB Row 2 Handle 7 Hairpin 8bp	ATTTTTTAATATTAAGCAAAAGCCACCCTCCTCGAAAGAATGAGGAGGG
24HB Row 2 Handle 8 Hairpin 8bp	ATTAAGAATACACCTCAGCACTAAAGGAAAGAGGAGTAACCCTCCTCGAAAGAATGAGGAGGG
24HB Row 2 Handle 9 Hairpin 8bp	AAATAAGGCAATAGAGAATTGATTAGAGGAATCATACCCTCCTCGAAAGAATGAGGAGGG
24HB Row 2 Handle 10 Hairpin 8bp	AAATGTACATCAAACTTACCCTCCTCGAAAGAATGAGGAGGG
24HB Row 2 Addition Handle 1	ACTCATCTTTGAGACCGC
24HB Row 2 Addition Handle 4	GTGCCGGAGGTTTAGTACC
24HB Row 2 Addition Handle 6	AGCAAGGTCTGAGAGCTATCGA
24HB Row 2 Addition Handle 10	ACGGACTTTCCGGCAAACGCGAAACGATTAAA
24HB Row 3 Handle 1 Poly T	CGTTTCAACTCGTCAAAGGGCGAAAAAAAAAAAAAAAA
24HB Row 3 Handle 2 Poly T	TACTGTAATTTAGAGCTTGACGGGAGTTAAAAAAAAAAAAAA
24HB Row 3 Handle 3 Poly T	AGCACTCCAGCCAAGTTTGGAAAAAAAAAAAAAA
24HB Row 3 Handle 4 Poly T	ACGTGAACCATCACTACCCCCAGCGATTAATGAATAAAAAAAAAAAAAA
24HB Row 3 Handle 5 Poly T	TGGCGAGAAAGGAAGGGAAGAAAAAAAAAAAAAAA
24HB Row 3 Handle 6 Poly T	GCAGCAACGTCAGCCGGCCAGTTTTCGTCAAAAAAAAAAAAAA
24HB Row 3 Handle 7 Poly T	TTAGCAATATAAAAGAAACCAACAAAAAAAAAAAAAAA
24HB Row 3 Handle 8 Poly T	GGAATAAGTTTATTAAAGGTATCAAAAAAAAAAAAAA
24HB Row 3 Handle 9 Poly T	AATTTGATTTCTCACCTTGCAAAAAAAAAAAAAA
24HB Row 3 Handle 1 Random	CGTTTCAACTCGTCAAAGGGCGAAAACTTGAGGACTTAAAA
24HB Row 3 Handle 2 Random	TACTGTAATTTAGAGCTTGACGGGAGTTACTTGAGGACTTAAAA
24HB Row 3 Handle 3 Random	AGCACTCCAGCCAAGTTTGGACTTGAGGACTTAAAA
24HB Row 3 Handle 4 Random	ACGTGAACCATCACTACCCCCAGCGATTAATGAATACTTGAGGACTTAAAA
24HB Row 3 Handle 5 Random	TGGCGAGAAAGGAAGGGAAGAACTTGAGGACTTAAAA
24HB Row 3 Handle 6 Random	GCAGCAACGTCAGCCGGCCAGTTTTCGTCACTTGAGGACTTAAAA
24HB Row 3 Handle 7 Random	TTAGCAATATAAAAGAAACCAACACTTGAGGACTTAAAA

24HB Row 3 Handle 8 Random	GGAATAAGTTTATTAAAGGTATCACTTGAGGACTTAAAA
24HB Row 3 Handle 9 Random	AATTTGATTTCTCACCTTGCACTTGAGGACTTAAAA
24HB Row 3 Handle 1 Hairpin 6bp	CGTTTCAACTCGTCAAAGGGCGAAAACTCCTCGAAAGAATGAGGAG
24HB Row 3 Handle 2 Hairpin 6bp	TACTGTAATTTAGAGCTTGACGGGAGTTACTCCTCGAAAGAATGAGGAG
24HB Row 3 Handle 3 Hairpin 6bp	AGCACTCCAGCCAAGTTTGGACTCCTCGAAAGAATGAGGAG
24HB Row 3 Handle 4 Hairpin 6bp	ACGTGAACCATCACTACCCCCAGCGATTAATGAATACTCCTCGAAAGAATGAGGAG
24HB Row 3 Handle 5 Hairpin 6bp	TGGCGAGAAAGGAAGGGAAGAACTCCTCGAAAGAATGAGGAG
24HB Row 3 Handle 6 Hairpin 6bp	GCAGCAACGTCAGCCGGCCAGTTTTCGTCACTCCTCGAAAGAATGAGGAG
24HB Row 3 Handle 7 Hairpin 6bp	TTAGCAATATAAAAGAAACCAACACTCCTCGAAAGAATGAGGAG
24HB Row 3 Handle 8 Hairpin 6bp	GGAATAAGTTTATTAAAGGTATCACTCCTCGAAAGAATGAGGAG
24HB Row 3 Handle 9 Hairpin 6bp	AATTTGATTTCTCACCTTGCACTCCTCGAAAGAATGAGGAG
24HB Row 3 Handle 1 Hairpin 8bp	CGTTTCAACTCGTCAAAGGGCGAAAACCCTCCTCGAAAGAATGAGGAGGG
24HB Row 3 Handle 2 Hairpin 8bp	TACTGTAATTTAGAGCTTGACGGGAGTTACCCTCCTCGAAAGAATGAGGAGGG
24HB Row 3 Handle 3 Hairpin 8bp	AGCACTCCAGCCAAGTTTGGACCCTCCTCGAAAGAATGAGGAGGG
24HB Row 3 Handle 4 Hairpin 8bp	ACGTGAACCATCACTACCCCCAGCGATTAATGAATACCCTCCTCGAAAGAATGAGGAGGG
24HB Row 3 Handle 5 Hairpin 8bp	TGGCGAGAAAGGAAGGGAAGAACCCTCCTCGAAAGAATGAGGAGGG
24HB Row 3 Handle 6 Hairpin 8bp	GCAGCAACGTCAGCCGGCCAGTTTTCGTCACCCTCCTCGAAAGAATGAGGAGGG
24HB Row 3 Handle 7 Hairpin 8bp	TTAGCAATATAAAAGAAACCAACACCCTCCTCGAAAGAATGAGGAGGG
24HB Row 3 Handle 8 Hairpin 8bp	GGAATAAGTTTATTAAAGGTATCACCCTCCTCGAAAGAATGAGGAGGG
24HB Row 3 Handle 9 Hairpin 8bp	AATTTGATTTCTCACCTTGCACCCTCCTCGAAAGAATGAGGAGGG
24HB Row 3 Addition Handle 1	GGGGTAATAACCAAACCCT
24HB Row 3 Addition Handle 2	GAACGCGCTAAACAAAAAG
24HB Row 3 Addition Handle 4	GGTCAAATGCCGGAGTCCACTAAGGAATT
24HB Row 3 Addition Handle 5	GTAATAACCATATTGGCGAACG
24HB Row 3 Addition Handle 7	CCAGTGAGGGAGTCGCTGCGGTATG
24HB Row 3 Addition Handle 8	GCCAAAGTTGCAAAGACACCAC
24HB Row 3 Addition Handle 9	GGCAATTGGTCAGTTCTAAAGC

C.10.6 Scaffolds

C.10.6.1 p8064

GGCAATGACCTGATAGCCTTTGTAGATCTCTCAAAAATAGCTACCCTCTCCGGCATTAATTTATCAGCTAGAACGGTTGAATATCATATTGATGTGATTT
GACTGTCTCCGGCCTTTCTCACCCTTTTGAATCTTTACCTACACATTACTCAGGCATTGCATTTAAAATATATGAGGGTTCTAAAAATTTTTATCCTTGCGT
TGAAATAAAGGCTTCTCCCGCAAAAGTATTACAGGGTCATAATGTTTTTGGTACAACCGATTTAGCTTTATGCTCTGAGGCTTTATTGCTTAATTTTGCTA
ATTCTTTGCCTTGCCTGTATGATTTATTGGATGTTAATGCTACTACTATTAGTAGAATTGATGCCACCTTTTCAGCTCGCGCCCCAAATGAAAATATAGCT
AAACAGGTTATTGACCATTTGCGAAATGTATCTAATGGTCAAACTAAATCTACTCGTTCGCAGAATTGGGAATCAACTGTTATATGGAATGAAACTTCC
AGACACCGTACTTTAGTTGCATATTTAAAACATGTTGAGCTACAGCATTATATTCAGCAATTAAGCTCTAAGCCATCCGCAAAAATGACCTCTTATCAAA
AGGAGCAATTAAAGGTACTCTCTAATCCTGACCTGTTGGAGTTTGCTTCCGGTCTGGTTCGCTTTGAAGCTCGAATTAAAACGCGATATTTGAAGTCTTT
CGGGCTTCCTCTTAATCTTTTTGATGCAATCCGCTTTGCTTCTGACTATAATAGTCAGGGTAAAGACCTGATTTTTGATTTATGGTCATTCTCGTTTTCTGA
ACTGTTTAAAGCATTTGAGGGGGATTCAATGAATATTTATGACGATTCCGCAGTATTGGACGCTATCCAGTCTAAACATTTTACTATTACCCCCTCTGGC
AAAACTTCTTTTGCAAAAGCCTCTCGCTATTTTGGTTTTTATCGTCGTCTGGTAAACGAGGGTTATGATAGTGTTGCTCTTACTATGCCTCGTAATTCCTTT
TGGCGTTATGTATCTGCATTAGTTGAATGTGGTATTCCTAAATCTCAACTGATGAATCTTTCTACCTGTAATAATGTTGTTCCGTTAGTTCGTTTTATTAAC
GTAGATTTTTCTTCCCAACGTCCTGACTGGTATAATGAGCCAGTTCTTAAAATCGCATAAGGTAATTCACAATGATTAAAGTTGAAATTAAACCATCTCA
AGCCCAATTTACTACTCGTTCTGGTGTTTCTCGTCAGGGCAAGCCTTATTCACTGAATGAGCAGCTTTGTTACGTTGATTTGGGTAATGAATATCCGGTT
CTTGTCAAGATTACTCTTGATGAAGGTCAGCCAGCCTATGCGCCTGGTCTGTACACCGTTCATCTGTCCTCTTTCAAAGTTGGTCAGTTCGGTTCCCTTAT
GATTGACCGTCTGCGCCTCGTTCCGGCTAAGTAACATGGAGCAGGTCGCGGATTTCGACACAATTTATCAGGCGATGATACAAATCTCCGTTGTACTTT
GTTTCGCGCTTGGTATAATCGCTGGGGGTCAAAGATGAGTGTTTTAGTGTATTCTTTTGCCTCTTTCGTTTTAGGTTGGTGCCTTCGTAGTGGCATTACG
TATTTTACCCGTTTAATGGAAACTTCCTCATGAAAAAGTCTTTAGTCCTCAAAGCCTCTGTAGCCGTTGCTACCCTCGTTCCGATGCTGTCTTTCGCTGCT
GAGGGTGACGATCCCGCAAAAGCGGCCTTTAACTCCCTGCAAGCCTCAGCGACCGAATATATCGGTTATGCGTGGGCGATGGTTGTTGTCATTGTCGG
CGCAACTATCGGTATCAAGCTGTTTAAGAAATTCACCTCGAAAGCAAGCTGATAAACCGATACAATTAAAGGCTCCTTTTGGAGCCTTTTTTTTGGAGAT
TTTCAACGTGAAAAAATTATTATTCGCAATTCCTTTAGTTGTTCCTTTCTATTCTCACTCCGCTGAAACTGTTGAAAGTTGTTTAGCAAAATCCCATACAGA
AAATTCATTTACTAACGTCTGGAAAGACGACAAAACTTTAGATCGTTACGCTAACTATGAGGGCTGTCTGTGGAATGCTACAGGCGTTGTAGTTTGTAC
TGGTGACGAAACTCAGTGTTACGGTACATGGGTTCCTATTGGGCTTGCTATCCCTGAAAATGAGGGTGGTGGCTCTGAGGGTGGCGGTTCTGAGGGT
GGCGGTTCTGAGGGTGGCGGTACTAAACCTCCTGAGTACGGTGATACACCTATTCCGGGCTATACTTATATCAACCCTCTCGACGGCACTTATCCGCCT
GGTACTGAGCAAAACCCCGCTAATCCTAATCCTTCTCTTGAGGAGTCTCAGCCTCTTAATACTTTCATGTTTCAGAATAATAGGTTCCGAAATAGGCAGG
GGGCATTAACTGTTTATACGGGCACTGTTACTCAAGGCACTGACCCCGTTAAAACTTATTACCAGTACACTCCTGTATCATCAAAAGCCATGTATGACGC
TTACTGGAACGGTAAATTCAGAGACTGCGCTTTCCATTCTGGCTTTAATGAGGATTTATTTGTTTGTGAATATCAAGGCCAATCGTCTGACCTGCCTCAA
CCTCCTGTCAATGCTGGCGGCGGCTCTGGTGGTGGTTCTGGTGGCGGCTCTGAGGGTGGTGGCTCTGAGGGTGGCGGTTCTGAGGGTGGCGGCTCTG
AGGGAGGCGGTTCCGGTGGTGGCTCTGGTTCCGGTGATTTTGATTATGAAAAGATGGCAAACGCTAATAAGGGGGCTATGACCGAAAATGCCGATGA
AAACGCGCTACAGTCTGACGCTAAAGGCAAACTTGATTCTGTCGCTACTGATTACGGTGCTGCTATCGATGGTTTCATTGGTGACGTTTCCGGCCTTGCT
AATGGTAATGGTGCTACTGGTGATTTTGCTGGCTCTAATTCCCAAATGGCTCAAGTCGGTGACGGTGATAATTCACCTTTAATGAATAATTTCCGTCAAT
ATTTACCTTCCCTCCCTCAATCGGTTGAATGTCGCCCTTTTGTCTTTGGCGCTGGTAAACCATATGAATTTTCTATTGATTGTGACAAAATAAACTTATTCC
GTGGTGTCTTTGCGTTTCTTTTATATGTTGCCACCTTTATGTATGTATTTTCTACGTTTGCTAACATACTGCGTAATAAGGAGTCTTAATCATGCCAGTTCT
TTTGGGTATTCCGTTATTATTGCGTTTCCTCGGTTTCCTTCTGGTAACTTTGTTCGGCTATCTGCTTACTTTTCTTAAAAAGGGCTTCGGTAAGATAGCTAT
TGCTATTTCATTGTTTCTTGCTCTTATTATTGGGCTTAACTCAATTCTTGTGGGTTATCTCTCTGATATTAGCGCTCAATTACCCTCTGACTTTGTTCAGGG
TGTTCAGTTAATTCTCCCGTCTAATGCGCTTCCCTGTTTTTATGTTATTCTCTCTGTAAAGGCTGCTATTTTCATTTTTGACGTTAAACAAAAAATCGTTTCT
TATTTGGATTGGGATAAATAATATGGCTGTTTATTTTGTAACTGGCAAATTAGGCTCTGGAAAGACGCTCGTTAGCGTTGGTAAGATTCAGGATAAAAT
TGTAGCTGGGTGCAAAATAGCAACTAATCTTGATTTAAGGCTTCAAAACCTCCCGCAAGTCGGGAGGTTCGCTAAAACGCCTCGCGTTCTTAGAATACC
GGATAAGCCTTCTATATCTGATTTGCTTGCTATTGGGCGCGGTAATGATTCCTACGATGAAAATAAAAACGGCTTGCTTGTTCTCGATGAGTGCGGTAC
TTGGTTTAATACCCGTTCTTGGAATGATAAGGAAAGACAGCCGATTATTGATTGGTTTCTACATGCTCGTAAATTAGGATGGGATATTATTTTTCTTGTT
CAGGACTTATCTATTGTTGATAAACAGGCGCGTTCTGCATTAGCTGAACATGTTGTTTATTGTCGTCGTCTGGACAGAATTACTTTACCTTTTGTCGGTAC
TTTATATTCTCTTATTACTGGCTCGAAAATGCCTCTGCCTAAATTACATGTTGGCGTTGTTAAATATGGCGATTCTCAATTAAGCCCTACTGTTGAGCGTT
GGCTTTATACTGGTAAGAATTTGTATAACGCATATGATACTAAACAGGCTTTTTCTAGTAATTATGATTCCGGTGTTTATTCTTATTTAACGCCTTATTTAT
CACACGGTCGGTATTTCAAACCATTAAATTTAGGTCAGAAGATGAAATTAACTAAAATATATTTGAAAAAGTTTTCTCGCGTTCTTTGTCTTGCGATTGG
ATTTGCATCAGCATTTACATATAGTTATATAACCCAACCTAAGCCGGAGGTTAAAAAGGTAGTCTCTCAGACCTATGATTTTGATAAATTCACTATTGAC
TCTTCTCAGCGTCTTAATCTAAGCTATCGCTATGTTTTCAAGGATTCTAAGGGAAAATTAATTAATAGCGACGATTTACAGAAGCAAGGTTATTCACTCA
CATATATTGATTTATGTACTGTTTCCATTAAAAAAGGTAATTCAAATGAAATTGTTAAATGTAATTAATTTTGTTTTCTTGATGTTTGTTTCATCATCTTCTT
TTGCTCAGGTAATTGAAATGAATAATTCGCCTCTGCGCGATTTTGTAACTTGGTATTCAAAGCAATCAGGCGAATCCGTTATTGTTTCTCCCGATGTAAA
AGGTACTGTTACTGTATATTCATCTGACGTTAAACCTGAAAATCTACGCAATTTCTTTATTTCTGTTTTACGTGCAAATAATTTTGATATGGTAGGTTCTA
ACCCTTCCATTATTCAGAAGTATAATCCAAACAATCAGGATTATATTGATGAATTGCCATCATCTGATAATCAGGAATATGATGATAATTCCGCTCCTTCT
GGTGGTTTCTTTGTTCCGCAAAATGATAATGTTACTCAAACTTTTAAAATTAATAACGTTCGGGCAAAGGATTTAATACGAGTTGTCGAATTGTTTGTAA
AGTCTAATACTTCTAAATCCTCAAATGTATTATCTATTGACGGCTCTAATCTATTAGTTGTTAGTGCTCCTAAAGATATTTTAGATAACCTTCCTCAATTCC
TTTCAACTGTTGATTTGCCAACTGACCAGATATTGATTGAGGGTTTGATATTTGAGGTTCAGCAAGGTGATGCTTTAGATTTTTCATTTGCTGCTGGCTCT
CAGCGTGGCACTGTTGCAGGCGGTGTTAATACTGACCGCCTCACCTCTGTTTTATCTTCTGCTGGTGGTTCGTTCGGTATTTTTAATGGCGATGTTTTAG
GGCTATCAGTTCGCGCATTAAAGACTAATAGCCATTCAAAAATATTGTCTGTGCCACGTATTCTTACGCTTTCAGGTCAGAAGGGTTCTATCTCTGTTGG
CCAGAATGTCCCTTTTATTACTGGTCGTGTGACTGGTGAATCTGCCAATGTAAATAATCCATTTCAGACGATTGAGCGTCAAAATGTAGGTATTTCCATG
AGCGTTTTTCCTGTTGCAATGGCTGGCGGTAATATTGTTCTGGATATTACCAGCAAGGCCGATAGTTTGAGTTCTTCTACTCAGGCAAGTGATGTTATTA
CTAATCAAAGAAGTATTGCTACAACGGTTAATTTGCGTGATGGACAGACTCTTTTACTCGGTGGCCTCACTGATTATAAAAACACTTCTCAGGATTCTGG
CGTACCGTTCCTGTCTAAAATCCCTTTAATCGGCCTCCTGTTTAGCTCCCGCTCTGATTCTAACGAGGAAAGCACGTTATACGTGCTCGTCAAAGCAACC
ATAGTACGCGCCCTGTAGCGGCGCATTAAGCGCGGCGGGTGTGGTGGTTACGCGCAGCGTGACCGCTACACTTGCCAGCGCCCTAGCGCCCGCTCCTT
TCGCTTTCTTCCCTTCCTTTCTCGCCACGTTCGCCGGCTTTCCCCGTCAAGCTCTAAATCGGGGGCTCCCTTTAGGGTTCCGATTTAGTGCTTTACGGCAC
CTCGACCCCAAAAAACTTGATTTGGGTGATGGTTCACGTAGTGGGCCATCGCCCTGATAGACGGTTTTTCGCCCTTTGACGTTGGAGTCCACGTTCTTTA
ATAGTGGACTCTTGTTCCAAACTGGAACAACACTCAACCCTATCTCGGGCTATTCTTTTGATTTATAAGGGATTTTGCCGATTTCGGAACCACCATCAAA
CAGGATTTTCGCCTGCTGGGGCAAACCAGCGTGGACCGCTTGCTGCAACTCTCTCAGGGCCAGGCGGTGAAGGGCAATCAGCTGTTGCCCGTCTCACT
GGTGAAAAGAAAAACCACCCTGGCGCCCAATACGCAAACCGCCTCTCCCCGCGCGTTGGCCGATTCATTAATGCAGCTGGCACGACAGGTTTCCCGAC

TGGAAAGCGGGCAGTGAGCGCAACGCAATTAATGTGAGTTAGCTCACTCATTAGGCACCCCAGGCTTTACACTTTATGCTTCCGGCTCGTATGTTGTGT
GGAATTGTGAGCGGATAACAATTTCACACAGGAAACAGCTATGACCATGATTACGAATTCGAGCTCGGTACCCGGGGATCCTCAACTGTGAGGAGGCT
CACGGACGCGAAGAACAGGCACGCGTGCTGGCAGAAACCCCCGGTATGACCGTGAAAACGGCCCGCCGCATTCTGGCCGCAGCACCACAGAGTGCAC
AGGCGCGCAGTGACACTGCGCTGGATCGTCTGATGCAGGGGGCACCGGCACCGCTGGCTGCAGGTAACCCGGCATCTGATGCCGTTAACGATTTGCT
GAACACACCAGTGTAAGGGATGTTTATGACGAGCAAAGAAACCTTTACCCATTACCAGCCGCAGGGCAACAGTGACCCGGCTCATACCGCAACCGCGC
CCGGCGGATTGAGTGCGAAAGCGCCTGCAATGACCCCGCTGATGCTGGACACCTCCAGCCGTAAGCTGGTTGCGTGGGATGGCACCACCGACGGTGC
TGCCGTTGGCATTCTTGCGGTTGCTGCTGACCAGACCAGCACCACGCTGACGTTCTACAAGTCCGGCACGTTCCGTTATGAGGATGTGCTCTGGCCGGA
GGCTGCCAGCGACGAGACGAAAAAACGGACCGCGTTTGCCGGAACGGCAATCAGCATCGTTTAACTTTACCCTTCATCACTAAAGGCCGCCTGTGCGG
CTTTTTTTACGGGATTTTTTTTATGTCGATGTACACAACCGCCCAACTGCTGGCGGCAAATGAGCAGAAATTTAAGTTTGATCCGCTGTTTCTGCGTCTCTT
TTTCCGTGAGAGCTATCCCTTCACCACGGAGAAAGTCTATCTCTCACAAATTCCGGGACTGGTAAACATGGCGCTGTACGTTTCGCCGATTGTTTCCGGT
GAGGTTATCCGTTCCCGTGGCGGCTCCACCTCTGAAAGCTTGGCACTGGCCGTCGTTTTACAACGTCGTGACTGGGAAAACCCTGGCGTTACCCAACTT
AATCGCCTTGCAGCACATCCCCCTTTCGCCAGCTGGCGTAATAGCGAAGAGGCCCGCACCGATCGCCCTTCCCAACAGTTGCGCAGCCTGAATGGCGA
ATGGCGCTTTGCCTGGTTTCCGGCACCAGAAGCGGTGCCGGAAAGCTGGCTGGAGTGCGATCTTCCTGAGGCCGATACTGTCGTCGTCCCCTCAAACT
GGCAGATGCACGGTTACGATGCGCCCATCTACACCAACGTGACCTATCCCATTACGGTCAATCCGCCGTTTGTTCCCACGGAGAATCCGACGGGTTGTT
ACTCGCTCACATTTAATGTTGATGAAAGCTGGCTACAGGAAGGCCAGACGCGAATTATTTTTGATGGCGTTCCTATTGGTTAAAAAATGAGCTGATTTA
ACAAAAATTTAATGCGAATTTTAACAAAATATTAACGTTTACAATTTAAATATTTGCTTATACAATCTTCCTGTTTTTGGGGCTTTTCTGATTATCAACCGG
GGTACATATGATTGACATGCTAGTTTTACGATTACCGTTCATCGATTCTCTTGTTTGCTCCAGACTCTCA

C.10.6.2 p8634

TGATAGACGGTTTTTCGCCCTTTGACGTTGGAGTCCACGTTCTTTAATAGTGGACTCTTGTTCCAAACTGGAACAACACTCAACCCTATCTCGGGCTATT
CTTTTGATTTATAAGGGATTTTGCCGATTTCGGAACCACCATCAAACAGGATTTTCGCCTGCTGGGGCAAACCAGCGTGGACCGCTTGCTGCAACTCTCT
CAGGGCCAGGCGGTGAAGGGCAATCAGCTGTTGCCCGTCTCACTGGTGAAAAGAAAAACCACCCTGGCGCCCAATACGCAAACCGCCTCTCCCCGCG
CGTTGGCCGATTCATTAATGCAGCTGGCACGACAGGTTTCCCGACTGGAAAGCGGGCAGTGAGCGCAACGCAATTAATGTGAGTTAGCTCACTCATTA
GGCACCCCAGGCTTTACACTTTATGCTTCCGGCTCGTATGTTGTGTGGAATTGTGAGCGGATAACAATTTCACACAGGAAACAGCTATGACCATGATTA
CGAATTCGAGCTCGGTACCCGGGGATCCTCAACTGTGAGGAGGCTCACGGACGCGAAGAACAGGCACGCGTGCTGGCAGAAACCCCCGGTATGACC
GTGAAAACGGCCCGCCGCATTCTGGCCGCAGCACCACAGAGTGCACAGGCGCGCAGTGACACTGCGCTGGATCGTCTGATGCAGGGGGCACCGGCA
CCGCTGGCTGCAGGTAACCCGGCATCTGATGCCGTTAACGATTTGCTGAACACACCAGTGTAAGGGATGTTTATGACGAGCAAAGAAACCTTTACCCA
TTACCAGCCGCAGGGCAACAGTGACCCGGCTCATACCGCAACCGCGCCCGGCGGATTGAGTGCGAAAGCGCCTGCAATGACCCCGCTGATGCTGGAC
ACCTCCAGCCGTAAGCTGGTTGCGTGGGATGGCACCACCGACGGTGCTGCCGTTGGCATTCTTGCGGTTGCTGCTGACCAGACCAGCACCACGCTGAC
GTTCTACAAGTCCGGCACGTTCCGTTATGAGGATGTGCTCTGGCCGGAGGCTGCCAGCGACGAGACGAAAAAACGGACCGCGTTTGCCGGAACGGCA
ATCAGCATCGTTTAACTTTACCCTTCATCACTAAAGGCCGCCTGTGCGGCTTTTTTTACGGGATTTTTTTATGTCGATGTACACAACCGCCCAACTGCTGG
CGGCAAATGAGCAGAAATTTAAGTTTGATCCGCTGTTTCTGCGTCTCTTTTTCCGTGAGAGCTATCCCTTCACCACGGAGAAAGTCTATCTCTCACAAAT
TCCGGGACTGGTAAACATGGCGCTGTACGTTTCGCCGATTGTTTCCGGTGAGGTTATCCGTTCCCGTGGCGGCTCCACCTCTGAAAGCTTGGCACTGGC
CGTCGTTTTACAACGTCGTGACTGGGAAAACCCTGGCGTTACCCAACTTAATCGCCTTGCAGCACATCCCCCTTTCGCCAGCTGGCGTAATAGCGAAGA
GGCCCGCACCGATCGCCCTTCCCAACAGTTGCGCAGCCTGAATGGCGAATGGCGCTTTGCCTGGTTTCCGGCACCAGAAGCGGTGCCGGAAAGCTGGC
TGGAGTGCGATCTTCCTGAGGCCGATACTGTCGTCGTCCCCTCAAACTGGCAGATGCACGGTTACGATGCGCCCATCTACACCAACGTGACCTATCCCA
TTACGGTCAATCCGCCGTTTGTTCCCACGGAGAATCCGACGGGTTGTTACTCGCTCACATTTAATGTTGATGAAAGCTGGCTACAGGAAGGCCAGACGC
GAATTATTTTTGATGGCGTTCCTATTGGTTAAAAAATGAGCTGATTTAACAAAAATTTAATGCGAATTTTAACAAAATATTAACGTTTACAATTTAAATAT
TTGCTTATACAATCTTCCTGTTTTTGGGGCTTTTCTGATTATCAACCGGGGTACATATGATTGACATGCTAGTTTTACGATTACCGTTCATCGATTCTCTTG
TTTGCTCCAGACTCTCAGGCAATGACCTGATAGCCTTTGTAGATCTCTCAAAAATAGCTACCCTCTCCGGCATTAATTTATCAGCTAGAACGGTTGAATA
TCATATTGATGGTGATTTGACTGTCTCCGGCCTTTCTCACCCTTTTGAATCTTTACCTACACATTACTCAGGCATTGCATTTAAAATATATGAGGGTTCTA
AAAATTTTTATCCTTGCGTTGAAATAAAGGCTTCTCCCGCAAAAGTATTACAGGGTCATAATGTTTTTGGTACAACCGATTTAGCTTTATGCTCTGAGGC
TTTATTGCTTAATTTTGCTAATTCTTTGCCTTGCCTGTATGATTTATTGGATGTTAATGCTACTACTATTAGTAGAATTGATGCCACCTTTTCAGCTCGCGC
CCCAAATGAAAATATAGCTAAACAGGTTATTGACCATTTGCGAAATGTATCTAATGGTCAAACTAAATCTACTCGTTCGCAGAATTGGGAATCAACTGT
TATATGGAATGAAACTTCCAGACACCGTACTTTAGTTGCATATTTAAAACATGTTGAGCTACAGCATTATATTCAGCAATTAAGCTCTAAGCCATCCGCA
AAAATGACCTCTTATCAAAAGGAGCAATTAAAGGTACTCTCTAATCCTGACCTGTTGGAGTTTGCTTCCGGTCTGGTTCGCTTTGAAGCTCGAATTAAAA
CGCGATATTTGAAGTCTTTCGGGCTTCCTCTTAATCTTTTTGATGCAATCCGCTTTGCTTCTGACTATAATAGTCAGGGTAAAGACCTGATTTTTGATTTA
TGGTCATTCTCGTTTTCTGAACTGTTTAAAGCATTTGAGGGGGATTCAATGAATATTTATGACGATTCCGCAGTATTGGACGCTATCCAGTCTAAACATT
TTACTATTACCCCCTCTGGCAAAACTTCTTTTGCAAAAGCCTCTCGCTATTTTGGTTTTTATCGTCGTCTGGTAAACGAGGGTTATGATAGTGTTGCTCTT
ACTATGCCTCGTAATTCCTTTTGGCGTTATGTATCTGCATTAGTTGAATGTGGTATTCCTAAATCTCAACTGATGAATCTTTCTACCTGTAATAATGTTGTT
CCGTTAGTTCGTTTTATTAACGTAGATTTTTCTTCCCAACGTCCTGACTGGTATAATGAGCCAGTTCTTAAAATCGCATAAGGTAATTCACAATGATTAAA
GTTGAAATTAAACCATCTCAAGCCCAATTTACTACTCGTTCTGGTGTTTCTCGTCAGGGCAAGCCTTATTCACTGAATGAGCAGCTTTGTTACGTTGATTT
GGGTAATGAATATCCGGTTCTTGTCAAGATTACTCTTGATGAAGGTCAGCCAGCCTATGCGCCTGGTCTGTACACCGTTCATCTGTCCTCTTTCAAAGTT
GGTCAGTTCGGTTCCCTTATGATTGACCGTCTGCGCCTCGTTCCGGCTAAGTAACATGGAGCAGGTCGCGGATTTCGACACAATTTATCAGGCGATGAT
ACAAATCTCCGTTGTACTTTGTTTCGCGCTTGGTATAATCGCTGGGGGTCAAAGATGAGTGTTTTAGTGTATTCTTTTGCCTCTTTCGTTTTAGGTTGGTG
CCTTCGTAGTGGCATTACGTATTTTACCCGTTTAATGGAAACTTCCTCATGAAAAAGTCTTTAGTCCTCAAAGCCTCTGTAGCCGTTGCTACCCTCGTTCC
GATGCTGTCTTTCGCTGCTGAGGGTGACGATCCCGCAAAAGCGGCCTTTAACTCCCTGCAAGCCTCAGCGACCGAATATATCGGTTATGCGTGGGCGA
TGGTTGTTGTCATTGTCGGCGCAACTATCGGTATCAAGCTGTTTAAGAAATTCACCTCGAAAGCAAGCTGATAAACCGATACAATTAAAGGCTCCTTTT
GGAGCCTTTTTTTTGGAGATTTTCAACGTGAAAAAATTATTATTCGCAATTCCTTTAGTTGTTCCTTTCTATTCTCACTCCGCTGAAACTGTTGAAAGTTGT
TTAGCAAAATCCCATACAGAAAATTCATTTACTAACGTCTGGAAAGACGACAAAACTTTAGATCGTTACGCTAACTATGAGGGCTGTCTGTGGAATGCT
ACAGGCGTTGTAGTTTGTACTGGTGACGAAACTCAGTGTTACGGTACATGGGTTCCTATTGGGCTTGCTATCCCTGAAAATGAGGGT
GGTGGCTCTGAGGGTGGCGGTTCTGAGGGTGGCGGTTCTGAGGGTGGCGGTACTAAACCTCCTGAGTACGGTGATACACCTATTCCGGGCTATACTT
ATATCAACCCTCTCGACGGCACTTATCCGCCTGGTACTGAGCAAAACCCCGCTAATCCTAATCCTTCTCTTGAGGAGTCTCAGCCTCTTAATACTTTCATG
TTTCAGAATAATAGGTTCCGAAATAGGCAGGGGGCATTAACTGTTTATACGGGCACTGTTACTCAAGGCACTGACCCCGTTAAAACTTATTACCAGTAC
ACTCCTGTATCATCAAAAGCCATGTATGACGCTTACTGGAACGGTAAATTCAGAGACTGCGCTTTCCATTCTGGCTTTAATGAGGATTTATTTGTTTGTG
AATATCAAGGCCAATCGTCTGACCTGCCTCAACCTCCTGTCAATGCTGGCGGCGGCTCTGGTGGTGGTTCTGGTGGCGGCTCTGAGGGTGGTGGCTCT
GAGGGTGGCGGTTCTGAGGGTGGCGGCTCTGAGGGAGGCGGTTCCGGTGGTGGCTCTGGTTCCGGTGATTTTGATTATGAAAAGATGGCAAACGCT
AATAAGGGGGCTATGACCGAAAATGCCGATGAAAACGCGCTACAGTCTGACGCTAAAGGCAAACTTGATTCTGTCGCTACTGATTACGGTGCTGCTAT

CGATGGTTTCATTGGTGACGTTTCCGGCCTTGCTAATGGTAATGGTGCTACTGGTGATTTTGCTGGCTCTAATTCCCAAATGGCTCAAGTCGGTGACGG
TGATAATTCACCTTTAATGAATAATTTCCGTCAATATTTACCTTCCCTCCCTCAATCGGTTGAATGTCGCCCTTTTGTCTTTGGCGCTGGTAAACCATATGA
ATTTTCTATTGATTGTGACAAAATAAACTTATTCCGTGGTGTCTTTGCGTTTCTTTTATATGTTGCCACCTTTATGTATGTATTTTCTACGTTTGCTAACATA
CTGCGTAATAAGGAGTCTTAATCATGCCAGTTCTTTTGGGTATTCCGTTATTATTGCGTTTCCTCGGTTTCCTTCTGGTAACTTTGTTCGGCTATCTGCTTA
CTTTTCTTAAAAAGGGCTTCGGTAAGATAGCTATTGCTATTTCATTGTTTCTTGCTCTTATTATTGGGCTTAACTCAATTCTTGTGGGTTATCTCTCTGATA
TTAGCGCTCAATTACCCTCTGACTTTGTTCAGGGTGTTCAGTTAATTCTCCCGTCTAATGCGCTTCCCTGTTTTTATGTTATTCTCTCTGTAAAGGCTGCTA
TTTTCATTTTTGACGTTAAACAAAAAATCGTTTCTTATTTGGATTGGGATAAATAATATGGCTGTTTATTTTGTAACTGGCAAATTAGGCTCTGGAAAGA
CGCTCGTTAGCGTTGGTAAGATTCAGGATAAAATTGTAGCTGGGTGCAAAATAGCAACTAATCTTGATTTAAGGCTTCAAAACCTCCCGCAAGTCGGG
AGGTTCGCTAAAACGCCTCGCGTTCTTAGAATACCGGATAAGCCTTCTATATCTGATTTGCTTGCTATTGGGCGCGGTAATGATTCCTACGATGAAAATA
AAAACGGCTTGCTTGTTCTCGATGAGTGCGGTACTTGGTTTAATACCCGTTCTTGGAATGATAAGGAAAGACAGCCGATTATTGATTGGTTTCTACATG
CTCGTAAATTAGGATGGGATATTATTTTTCTTGTTCAGGACTTATCTATTGTTGATAAACAGGCGCGTTCTGCATTAGCTGAACATGTTGTTTATTGTCGT
CGTCTGGACAGAATTACTTTACCTTTTGTCGGTACTTTATATTCTCTTATTACTGGCTCGAAAATGCCTCTGCCTAAATTACATGTTGGCGTTGTTAAATAT
GGCGATTCTCAATTAAGCCCTACTGTTGAGCGTTGGCTTTATACTGGTAAGAATTTGTATAACGCATATGATACTAAACAGGCTTTTTCTAGTAATTATG
ATTCCGGTGTTTATTCTTATTTAACGCCTTATTTATCACACGGTCGGTATTTCAAACCATTAAATTTAGGTCAGAAGATGAAATTAACTAAAATATATTTG
AAAAAGTTTTCTCGCGTTCTTTGTCTTGCGATTGGATTTGCATCAGCATTTACATATAGTTATATAACCCAACCTAAGCCGGAGGTTAAAAAGGTAGTCT
CTCAGACCTATGATTTTGATAAATTCACTATTGACTCTTCTCAGCGTCTTAATCTAAGCTATCGCTATGTTTTCAAGGATTCTAAGGGAAAATTAATTAAT
AGCGACGATTTACAGAAGCAAGGTTATTCACTCACATATATTGATTTATGTACTGTTTCCATTAAAAAAGGTAATTCAAATGAAATTGTTAAATGTAATT
AATTTTGTTTTCTTGATGTTTGTTTCATCATCTTCTTTTGCTCAGGTAATTGAAATGAATAATTCGCCTCTGCGCGATTTTGTAACTTGGTATTCAAAGCAA
TCAGGCGAATCCGTTATTGTTTCTCCCGATGTAAAAGGTACTGTTACTGTATATTCATCTGACGTTAAACCTGAAAATCTACGCAATTTCTTTATTTCTGT
TTTACGTGCAAATAATTTTGATATGGTAGGTTCTAACCCTTCCATTATTCAGAAGTATAATCCAAACAATCAGGATTATATTGATGAATTGCCATCATCTG
ATAATCAGGAATATGATGATAATTCCGCTCCTTCTGGTGGTTTCTTTGTTCCGCAAAATGATAATGTTACTCAAACTTTTAAAATTAATAACGTTCGGGCA
AAGGATTTAATACGAGTTGTCGAATTGTTTGTAAAGTCTAATACTTCTAAATCCTCAAATGTATTATCTATTGACGGCTCTAATCTATTAGTTGTTAGTGC
TCCTAAAGATATTTTAGATAACCTTCCTCAATTCCTTTCAACTGTTGATTTGCCAACTGACCAGATATTGATTGAGGGTTTGATATTTGAGGTTCAGCAAG
GTGATGCTTTAGATTTTTCATTTGCTGCTGGCTCTCAGCGTGGCACTGTTGCAGGCGGTGTTAATACTGACCGCCTCACCTCTGTTTTATCTTCTGCTGGT
GGTTCGTTCGGTATTTTTAATGGCGATGTTTTAGGGCTATCAGTTCGCGCATTAAAGACTAATAGCCATTCAAAAATATTGTCTGTGCCACGTATTCTTA
CGCTTTCAGGTCAGAAGGGTTCTATCTCTGTTGGCCAGAATGTCCCTTTTATTACTGGTCGTGTGACTGGTGAATCTGCCAATGTAAATAATCCATTTCA
GACGATTGAGCGTCAAAATGTAGGTATTTCCATGAGCGTTTTTCCTGTTGCAATGGCTGGCGGTAATATTGTTCTGGATATTACCAGCAAGGCCGATAG
TTTGAGTTCTTCTACTCAGGCAAGTGATGTTATTACTAATCAAAGAAGTATTGCTACAACGGTTAATTTGCGTGATGGACAGACTCTTTTACTCGGTGGC
CTCACTGATTATAAAAACACTTCTCAGGATTCTGGCGTACCGTTCCTGTCTAAAATCCCTTTAATCGGCCTCCTGTTTAGCTCCCGCTCTGATTCTAACGA
GGAAAGCACGTTATACGTGCTCGTCAAAGCAACCATAGTACGCGCCCTGTAGCGGCGCATTAAGCGCGGCGGGTGTGGTGGTTACGCGCAGCGTGAC
CGCTACACTTGCCAGCGCCCTAGCGCCCGCTCCTTTCGCTTTCTTCCCTTCCTTTCTCGCCACGTTCGCCGGCTTTCCCCGTCAAGCTCTAAATCGGGGGC
TCCCTTTAGGGTTCCGATTTAGTGCTTTACGGCACCTCGACCCCAAAAAACTTGATTTGGGTGATGGTTCACGTAGTGGGCCATCGCCC

C.10.6.3 p7249

AATGCTACTACTATTAGTAGAATTGATGCCACCTTTTCAGCTCGCGCCCCAAATGAAAATATAGCTAAACAGGTTATTGACCATTTGCGAAATGTATCTA
ATGGTCAAACTAAATCTACTCGTTCGCAGAATTGGGAATCAACTGTTATATGGAATGAAACTTCCAGACACCGTACTTTAGTTGCATATTTAAAACATGT
TGAGCTACAGCATTATATTCAGCAATTAAGCTCTAAGCCATCCGCAAAAATGACCTCTTATCAAAAGGAGCAATTAAAGGTACTCTCTAATCCTGACCTG
TTGGAGTTTGCTTCCGGTCTGGTTCGCTTTGAAGCTCGAATTAAAACGCGATATTTGAAGTCTTTCGGGCTTCCTCTTAATCTTTTTGATGCAATCCGCTT
TGCTTCTGACTATAATAGTCAGGGTAAAGACCTGATTTTTGATTTATGGTCATTCTCGTTTTCTGAACTGTTTAAAGCATTTGAGGGGGATTCAATGAAT
ATTTATGACGATTCCGCAGTATTGGACGCTATCCAGTCTAAACATTTTACTATTACCCCCTCTGGCAAAACTTCTTTTGCAAAAGCCTCTCGCTATTTTGG
TTTTTATCGTCGTCTGGTAAACGAGGGTTATGATAGTGTTGCTCTTACTATGCCTCGTAATTCCTTTTGGCGTTATGTATCTGCATTAGTTGAATGTGGTA
TTCCTAAATCTCAACTGATGAATCTTTCTACCTGTAATAATGTTGTTCCGTTAGTTCGTTTTATTAACGTAGATTTTTCTTCCCAACGTCCTGACTGGTATA
ATGAGCCAGTTCTTAAAATCGCATAAGGTAATTCACAATGATTAAAGTTGAAATTAAACCATCTCAAGCCCAATTTACTACTCGTTCTGGTGTTTCTCGTC
AGGGCAAGCCTTATTCACTGAATGAGCAGCTTTGTTACGTTGATTTGGGTAATGAATATCCGGTTCTTGTCAAGATTACTCTTGATGAAGGTCAGCCAG
CCTATGCGCCTGGTCTGTACACCGTTCATCTGTCCTCTTTCAAAGTTGGTCAGTTCGGTTCCCTTATGATTGACCGTCTGCGCCTCGTTCCGGCTAAGTAA
CATGGAGCAGGTCGCGGATTTCGACACAATTTATCAGGCGATGATACAAATCTCCGTTGTACTTTGTTTCGCGCTTGGTATAATCGCTGGGGGTCAAAG
ATGAGTGTTTTAGTGTATTCTTTTGCCTCTTTCGTTTTAGGTTGGTGCCTTCGTAGTGGCATTACGTATTTTACCCGTTTAATGGAAACTTCCTCATGAAA
AAGTCTTTAGTCCTCAAAGCCTCTGTAGCCGTTGCTACCCTCGTTCCGATGCTGTCTTTCGCTGCTGAGGGTGACGATCCCGCAAAAGCGGCCTTTAACT
CCCTGCAAGCCTCAGCGACCGAATATATCGGTTATGCGTGGGCGATGGTTGTTGTCATTGTCGGCGCAACTATCGGTATCAAGCTGTTTAAGAAATTCA
CCTCGAAAGCAAGCTGATAAACCGATACAATTAAAGGCTCCTTTTGGAGCCTTTTTTTTGGAGATTTTCAACGTGAAAAAATTATTATTCGCAATTCCTTT
AGTTGTTCCTTTCTATTCTCACTCCGCTGAAACTGTTGAAAGTTGTTTAGCAAAATCCCATACAGAAAATTCATTTACTAACGTCTGGAAAGACGACAAA
ACTTTAGATCGTTACGCTAACTATGAGGGCTGTCTGTGGAATGCTACAGGCGTTGTAGTTTGTACTGGTGACGAAACTCAGTGTTACGGTACATGGGTT
CCTATTGGGCTTGCTATCCCTGAAAATGAGGGTGGTGGCTCTGAGGGTGGCGGTTCTGAGGGTGGCGGTTCTGAGGGTGGCGGTACTAAACCTCCTG
AGTACGGTGATACACCTATTCCGGGCTATACTTATATCAACCCTCTCGACGGCACTTATCCGCCTGGTACTGAGCAAAACCCCGCTAATCCTAATCCTTC
TCTTGAGGAGTCTCAGCCTCTTAATACTTTCATGTTTCAGAATAATAGGTTCCGAAATAGGCAGGGGGCATTAACTGTTTATACGGGCACTGTTACTCAA
GGCACTGACCCCGTTAAAACTTATTACCAGTACACTCCTGTATCATCAAAAGCCATGTATGACGCTTACTGGAACGGTAAATTCAGAGACTGCGCTTTCC
ATTCTGGCTTTAATGAGGATTTATTTGTTTGTGAATATCAAGGCCAATCGTCTGACCTGCCTCAACCTCCTGTCAATGCTGGCGGCGGCTCTGGTGGTGG
TTCTGGTGGCGGCTCTGAGGGTGGTGGCTCTGAGGGTGGCGGTTCTGAGGGTGGCGGCTCTGAGGGAGGCGGTTCCGGTGGTGGCTCTGGTTCCGG
TGATTTTGATTATGAAAAGATGGCAAACGCTAATAAGGGGGCTATGACCGAAAATGCCGATGAAAACGCGCTACAGTCTGACGCTAAAGGCAAACTT
GATTCTGTCGCTACTGATTACGGTGCTGCTATCGATGGTTTCATTGGTGACGTTTCCGGCCTTGCTAATGGTAATGGTGCTACTGGTGATTTTGCTGGCT
CTAATTCCCAAATGGCTCAAGTCGGTGACGGTGATAATTCACCTTTAATGAATAATTTCCGTCAATATTTACCTTCCCTCCCTCAATCGGTTGAATGTCGC
CCTTTTGTCTTTGGCGCTGGTAAACCATATGAATTTTCTATTGATTGTGACAAAATAAACTTATTCCGTGGTGTCTTTGCGTTTCTTTTATATGTTGCCACC
TTTATGTATGTATTTTCTACGTTTGCTAACATACTGCGTAATAAGGAGTCTTAATCATGCCAGTTCTTTTGGGTATTCCGTTATTATTGCGTTTCCTCGGTT
TCCTTCTGGTAACTTTGTTCGGCTATCTGCTTACTTTTCTTAAAAAGGGCTTCGGTAAGATAGCTATTGCTATTTCATTGTTTCTTGCTCTTATTATTGGGC
TTAACTCAATTCTTGTGGGTTATCTCTCTGATATTAGCGCTCAATTACCCTCTGACTTTGTTCAGGGTGTTCAGTTAATTCTCCCGTCTAATGCGCTTCCCT
GTTTTTATGTTATTCTCTCTGTAAAGGCTGCTATTTTCATTTTTGACGTTAAACAAAAAATCGTTTCTTATTTGGATTGGGATAAATAATATGGCTGTTTAT
TTTGTAACTGGCAAATTAGGCTCTGGAAAGACGCTCGTTAGCGTTGGTAAGATTCAGGATAAAATTGTAGCTGGGTGCAAAATAGCAACTAATCTTGA
TTTAAGGCTTCAAAACCTCCCGCAAGTCGGGAGGTTCGCTAAAACGCCTCGCGTTCTTAGAATACCGGATAAGCCTTCTATATCTGATTTGCTTGCTATT
GGGCGCGGTAATGATTCCTACGATGAAAATAAAAACGGCTTGCTTGTTCTCGATGAGTGCGGTACTTGGTTTAATACCCGTTCTTGGAATGATAAGGA

AAGACAGCCGATTATTGATTGGTTTCTACATGCTCGTAAATTAGGATGGGATATTATTTTTCTTGTTCAGGACTTATCTATTGTTGATAAACAGGCGCGT
TCTGCATTAGCTGAACATGTTGTTTATTGTCGTCGTCTGGACAGAATTACTTTACCTTTTGTCGGTACTTTATATTCTCTTATTACTGGCTCGAAAATGCCT
CTGCCTAAATTACATGTTGGCGTTGTTAAATATGGCGATTCTCAATTAAGCCCTACTGTTGAGCGTTGGCTTTATACTGGTAAGAATTTGTATAACGCAT
ATGATACTAAACAGGCTTTTTCTAGTAATTATGATTCCGGTGTTTATTCTTATTTAACGCCTTATTTATCACACGGTCGGTATTTCAAACCATTAAATTTAG
GTCAGAAGATGAAATTAACTAAAATATATTTGAAAAAGTTTTCTCGCGTTCTTTGTCTTGCGATTGGATTTGCATCAGCATTTACATATAGTTATATAACC
CAACCTAAGCCGGAGGTTAAAAAGGTAGTCTCTCAGACCTATGATTTTGATAAATTCACTATTGACTCTTCTCAGCGTCTTAATCTAAGCTATCGCTATG
TTTTCAAGGATTCTAAGGGAAAATTAATTAATAGCGACGATTTACAGAAGCAAGGTTATTCACTCACATATATTGATTTATGTACTGTTTCCATTAAAAA
AGGTAATTCAAATGAAATTGTTAAATGTAATTAATTTTGTTTTCTTGATGTTTGTTTCATCATCTTCTTTTGCTCAGGTAATTGAAATGAATAATTCGCCTC
TGCGCGATTTTGTAACTTGGTATTCAAAGCAATCAGGCGAATCCGTTATTGTTTCTCCCGATGTAAAAGGTACTGTTACTGTATATTCATCTGACGTTAA
ACCTGAAAATCTACGCAATTTCTTTATTTCTGTTTTACGTGCAAATAATTTTGATATGGTAGGTTCTAACCCTTCCATTATTCAGAAGTATAATCCAAACA
ATCAGGATTATATTGATGAATTGCCATCATCTGATAATCAGGAATATGATGATAATTCCGCTCCTTCTGGTGGTTTCTTTGTTCCGCAAAATGATAATGTT
ACTCAAACTTTTAAAATTAATAACGTTCGGGCAAAGGATTTAATACGAGTTGTCGAATTGTTTGTAAAGTCTAATACTTCTAAATCCTCAAATGTATTATC
TATTGACGGCTCTAATCTATTAGTTGTTAGTGCTCCTAAAGATATTTTAGATAACCTTCCTCAATTCCTTTCAACTGTTGATTTGCCAACTGACCAGATATT
GATTGAGGGTTTGATATTTGAGGTTCAGCAAGGTGATGCTTTAGATTTTTCATTTGCTGCTGGCTCTCAGCGTGGCACTGTTGCAGGCGGTGTTAATAC
TGACCGCCTCACCTCTGTTTTATCTTCTGCTGGTGGTTCGTTCGGTATTTTTAATGGCGATGTTTTAGGGCTATCAGTTCGCGCATTAAAGACTAATAGCC
ATTCAAAAATATTGTCTGTGCCACGTATTCTTACGCTTTCAGGTCAGAAGGGTTCTATCTCTGTTGGCCAGAATGTCCCTTTTATTACTGGTCGTGTGACT
GGTGAATCTGCCAATGTAAATAATCCATTTCAGACGATTGAGCGTCAAAATGTAGGTATTTCCATGAGCGTTTTTCCTGTTGCAATGGCTGGCGGTAAT
ATTGTTCTGGATATTACCAGCAAGGCCGATAGTTTGAGTTCTTCTACTCAGGCAAGTGATGTTATTACTAATCAAAGAAGTATTGCTACAACGGTTAATT
TGCGTGATGGACAGACTCTTTTACTCGGTGGCCTCACTGATTATAAAAACACTTCTCAGGATTCTGGCGTACCGTTCCTGTCTAAAATCCCTTTAATCGG
CCTCCTGTTTAGCTCCCGCTCTGATTCTAACGAGGAAAGCACGTTATACGTGCTCGTCAAAGCAACCATAGTACGCGCCCTGTAGCGGCGCATTAAGCG
CGGCGGGTGTGGTGGTTACGCGCAGCGTGACCGCTACACTTGCCAGCGCCCTAGCGCCCGCTCCTTTCGCTTTCTTCCCTTCCTTTCTCGCCACGTTCGC
CGGCTTTCCCCGTCAAGCTCTAAATCGGGGGCTCCCTTTAGGGTTCCGATTTAGTGCTTTACGGCACCTCGACCCCAAAAAACTTGATTTGGGTGATGG
TTCACGTAGTGGGCCATCGCCCTGATAGACGGTTTTTCGCCCTTTGACGTTGGAGTCCACGTTCTTTAATAGTGGACTCTTGTTCCAAACTGGAACAACA
CTCAACCCTATCTCGGGCTATTCTTTTGATTTATAAGGGATTTTGCCGATTTCGGAACCACCATCAAACAGGATTTTCGCCTGCTGGGGCAAACCAGCGT
GGACCGCTTGCTGCAACTCTCTCAGGGCCAGGCGGTGAAGGGCAATCAGCTGTTGCCCGTCTCACTGGTGAAAAGAAAAACCACCCTGGCGCCCAATA
CGCAAACCGCCTCTCCCCGCGCGTTGGCCGATTCATTAATGCAGCTGGCACGACAGGTTTCCCGACTGGAAAGCGGGCAGTGAGCGCAACGCAATTAA
TGTGAGTTAGCTCACTCATTAGGCACCCCAGGCTTTACACTTTATGCTTCCGGCTCGTATGTTGTGTGGAATTGTGAGCGGATAACAATTTCACACAGG
AAACAGCTATGACCATGATTACGAATTCGAGCTCGGTACCCGGGGATCCTCTAGAGTCGACCTGCAGGCATGCAAGCTTGGCACTGGCCGTCGTTTTA
CAACGTCGTGACTGGGAAAACCCTGGCGTTACCCAACTTAATCGCCTTGCAGCACATCCCCCTTTCGCCAGCTGGCGTAATAGCGAAGAGGCCCGCACC
GATCGCCCTTCCCAACAGTTGCGCAGCCTGAATGGCGAATGGCGCTTTGCCTGGTTTCCGGCACCAGAAGCGGTGCCGGAAAGCTGGCTGGAGTGCG
ATCTTCCTGAGGCCGATACTGTCGTCGTCCCCTCAAACTGGCAGATGCACGGTTACGATGCGCCCATCTACACCAACGTGACCTATCCCATTACGGTCAA
TCCGCCGTTTGTTCCCACGGAGAATCCGACGGGTTGTTACTCGCTCACATTTAATGTTGATGAAAGCTGGCTACAGGAAGGCCAGACGCGAATTATTTT
TGATGGCGTTCCTATTGGTTAAAAAATGAGCTGATTTAACAAAAATTTAATGCGAATTTTAACAAAATATTAACGTTTACAATTTAAATATTTGCTTATAC
AATCTTCCTGTTTTTGGGGCTTTTCTGATTATCAACCGGGGTACATATGATTGACATGCTAGTTTTACGATTACCGTTCATCGATTCTCTTGTTTGCTCCAG
ACTCTCAGGCAATGACCTGATAGCCTTTGTAGATCTCTCAAAAATAGCTACCCTCTCCGGCATTAATTTATCAGCTAGAACGGTTGAATATCATATTGAT
GGTGATTTGACTGTCTCCGGCCTTTCTCACCCTTTTGAATCTTTACCTACACATTACTCAGGCATTGCATTTAAAATATATGAGGGTTCTAAAAATTTTTAT
CCTTGCGTTGAAATAAAGGCTTCTCCCGCAAAAGTATTACAGGGTCATAATGTTTTTGGTACAACCGATTTAGCTTTATGCTCTGAGGCTTTATTGCTTA
ATTTTGCTAATTCTTTGCCTTGCCTGTATGATTTATTGGATGTT

Appendix D – In-work References

D.1 List of Figures

D.2 List of Tables

References

1. Whitesides, G.M., *The 'right' size in nanobiotechnology.* Nat Biotechnol, 2003. **21**(10): p. 1161-5.
2. Nie, S., et al., *Nanotechnology applications in cancer.* Annu Rev Biomed Eng, 2007. **9**: p. 257-88.
3. Jain, P.K., et al., *Calculated Absorption and Scattering Properties of Gold Nanoparticles of Different Size, Shape, and Composition: Applications in Biological Imaging and Biomedicine.* The Journal of Physical Chemistry B, 2006. **110**(14): p. 7238-7248.
4. Rosi, N.L. and C.A. Mirkin, *Nanostructures in biodiagnostics.* Chem Rev, 2005. **105**(4): p. 1547-62.
5. Erathodiyil, N. and J.Y. Ying, *Functionalization of Inorganic Nanoparticles for Bioimaging Applications.* Accounts of Chemical Research, 2011. **44**(10): p. 925-935.
6. Seeman, N.C., *Structural DNA nanotechnology: growing along with Nano Letters.* Nano Lett, 2010. **10**(6): p. 1971-8.
7. Rothemund, P.W., *Folding DNA to create nanoscale shapes and patterns.* Nature, 2006. **440**(7082): p. 297-302.
8. Zhang, Q., et al., *DNA origami as an in vivo drug delivery vehicle for cancer therapy.* ACS Nano, 2014. **8**(7): p. 6633-43.
9. Nguyen, L., et al., *DNA-Origami-Templated Silica Growth by Sol-Gel Chemistry.* Angew Chem Int Ed Engl, 2019. **58**(3): p. 912-916.
10. Berg, J.M., J.L. Tymoczko, and L. Stryer, *Biochemistry, Fifth Edition*. 2002: W. H. Freeman.
11. Watson, J.D. and F.H. Crick, *Molecular structure of nucleic acids; a structure for deoxyribose nucleic acid.* Nature, 1953. **171**(4356): p. 737-8.
12. Franklin, R.E. and R.G. Gosling, *The structure of sodium thymonucleate fibres. I. The influence of water content.* Acta Crystallographica, 1953. **6**(8-9): p. 673-677.
13. Orgogozo, V., A.E. Peluffo, and B. Morizot, *The "Mendelian Gene" and the "Molecular Gene": Two Relevant Concepts of Genetic Units.* Curr Top Dev Biol, 2016. **119**: p. 1-26.
14. Bruce Alberts, et al., *Molecular Biology of the Cell*. 4 ed. 2002, New York: Garland Science.
15. Norrgard, K. *Forensics, DNA Fingerprinting, and CODIS*. 2008 [cited 2024 20.10.]; Available from: https://www.nature.com/scitable/topicpage/forensics-dna-fingerprinting-and-codis-736/.
16. McPherson, E., *Genetic diagnosis and testing in clinical practice.* Clin Med Res, 2006. **4**(2): p. 123-9.
17. National Research Council Committee on, I. and H. Assessing Unintended Effects of Genetically Engineered Foods on Human, in *Safety of Genetically Engineered Foods: Approaches to Assessing Unintended Health Effects*. 2004, National Academies Press (US), Copyright 2004 by the National Academy of Sciences. All rights reserved.: Washington (DC).

18. Rizzi, E., et al., *Ancient DNA studies: new perspectives on old samples.* Genetics Selection Evolution, 2012. **44**(1): p. 21.
19. O'Donnell, M., L. Langston, and B. Stillman, *Principles and concepts of DNA replication in bacteria, archaea, and eukarya.* Cold Spring Harb Perspect Biol, 2013. **5**(7).
20. Beaucage, S.L. and R.P. Iyer, *Advances in the Synthesis of Oligonucleotides by the Phosphoramidite Approach.* Tetrahedron, 1992. **48**(12): p. 2223-2311.
21. Pérez-Rentero, S., et al., *Synthesis of oligonucleotides carrying thiol groups using a simple reagent derived from threoninol.* Molecules, 2012. **17**(9): p. 10026-45.
22. Chollet, A. and E.H. Kawashima, *Biotin-labeled synthetic oligodeoxyribonucleotides: chemical synthesis and uses as hybridization probes.* Nucleic Acids Res, 1985. **13**(5): p. 1529-41.
23. Jahnke, K., et al., *Choice of fluorophore affects dynamic DNA nanostructures.* Nucleic Acids Res, 2021. **49**(7): p. 4186-4195.
24. Zhang, X., M.R. Servos, and J. Liu, *Instantaneous and quantitative functionalization of gold nanoparticles with thiolated DNA using a pH-assisted and surfactant-free route.* J Am Chem Soc, 2012. **134**(17): p. 7266-9.
25. Beaucage, S.L. and R.P. Iyer, *The synthesis of modified oligonucleotides by the phosphoramidite approach and their applications.* Tetrahedron, 1993. **49**(28): p. 6123-6194.
26. Brown, T.A., *Genomes 3*. 2006, New York: Garland Science.
27. Herdewijn, P.L., Mahesh K. , *Modified Nucleosides: in Biochemistry, Biotechnology and Medicine*. 2008: Wiley-VCH Verlag GmbH & Co. KGaA.
28. Pellestor, F. and P. Paulasova, *The peptide nucleic acids (PNAs), powerful tools for molecular genetics and cytogenetics.* Eur J Hum Genet, 2004. **12**(9): p. 694-700.
29. Maurya, R., et al., *Chapter 25 - Recent development and applications of xeno nucleic acids*, in *New Frontiers and Applications of Synthetic Biology*, V. Singh, Editor. 2022, Academic Press. p. 415-422.
30. Nielsen, P.E., et al., *Sequence-selective recognition of DNA by strand displacement with a thymine-substituted polyamide.* Science, 1991. **254**(5037): p. 1497-500.
31. Pinheiro, V.B. and P. Holliger, *The XNA world: progress towards replication and evolution of synthetic genetic polymers.* Curr Opin Chem Biol, 2012. **16**(3-4): p. 245-52.
32. Seeman, N.C., *Nucleic acid junctions and lattices.* J Theor Biol, 1982. **99**(2): p. 237-47.
33. Douglas, S.M., et al., *Self-assembly of DNA into nanoscale three-dimensional shapes.* Nature, 2009. **459**(7245): p. 414-8.
34. He, Y., et al., *Self-Assembly of Hexagonal DNA Two-Dimensional (2D) Arrays.* Journal of the American Chemical Society, 2005. **127**(35): p. 12202-12203.
35. Wang, P., et al., *Practical aspects of structural and dynamic DNA nanotechnology.* MRS Bulletin, 2017. **42**(12): p. 889-896.
36. Ke, Y., et al., *Three-dimensional structures self-assembled from DNA bricks.* Science, 2012. **338**(6111): p. 1177-83.
37. Wei, B., M. Dai, and P. Yin, *Complex shapes self-assembled from single-stranded DNA tiles.* Nature, 2012. **485**(7400): p. 623-6.

38. Castro, C.E., et al., *A primer to scaffolded DNA origami.* Nat Methods, 2011. **8**(3): p. 221-9.
39. Zhang, H., et al., *Folding super-sized DNA origami with scaffold strands from long-range PCR.* Chemical Communications, 2012. **48**(51): p. 6405-6407.
40. Bush, J., et al., *Synthesis of DNA Origami Scaffolds: Current and Emerging Strategies.* Molecules, 2020. **25**(15).
41. Engelhardt, F.A.S., et al., *Custom-Size, Functional, and Durable DNA Origami with Design-Specific Scaffolds.* ACS Nano, 2019. **13**(5): p. 5015-5027.
42. Kozyra, J., et al., *Designing Uniquely Addressable Bio-orthogonal Synthetic Scaffolds for DNA and RNA Origami.* ACS Synth Biol, 2017. **6**(7): p. 1140-1149.
43. Veneziano, R., et al., *Designer nanoscale DNA assemblies programmed from the top down.* Science, 2016. **352**(6293): p. 1534.
44. Dey, S., et al., *DNA origami.* Nature Reviews Methods Primers, 2021. **1**(1): p. 13.
45. Zhou, Y., J. Dong, and Q. Wang, *Fabricating higher-order functional DNA origami structures to reveal biological processes at multiple scales.* NPG Asia Materials, 2023. **15**(1): p. 25.
46. Douglas, S.M., et al., *Rapid prototyping of 3D DNA-origami shapes with caDNAno.* Nucleic Acids Res, 2009. **37**(15): p. 5001-6.
47. Doty, D., B.L. Lee, and T. Stérin *scadnano: A browser-based, scriptable tool for designing DNA nanostructures*. 2020. arXiv:2005.11841 DOI: 10.48550/arXiv.2005.11841.
48. Kim, D.N., et al., *Quantitative prediction of 3D solution shape and flexibility of nucleic acid nanostructures.* Nucleic Acids Res, 2012. **40**(7): p. 2862-8.
49. Šulc, P., et al., *Sequence-dependent thermodynamics of a coarse-grained DNA model.* J Chem Phys, 2012. **137**(13): p. 135101.
50. Poppleton, E., et al., *OxDNA.org: a public webserver for coarse-grained simulations of DNA and RNA nanostructures.* Nucleic Acids Res, 2021. **49**(W1): p. W491-w498.
51. Fornace ME, H.J., Newman CT, Porubsky NJ, Pierce MB, Pierce NA, *NUPACK: Analysis and Design of Nucleic Acid Structures, Devices, and Systems.* ChemRxiv, 2022.
52. Zadeh, J.N., et al., *NUPACK: Analysis and design of nucleic acid systems.* J Comput Chem, 2011. **32**(1): p. 170-3.
53. Williams, S., et al. *Tiamat: A Three-Dimensional Editing Tool for Complex DNA Structures*. 2009. Berlin, Heidelberg: Springer Berlin Heidelberg.
54. Benson, E., et al., *DNA rendering of polyhedral meshes at the nanoscale.* Nature, 2015. **523**(7561): p. 441-444.
55. Rossi-Gendron, C., et al., *Isothermal self-assembly of multicomponent and evolutive DNA nanostructures.* Nature Nanotechnology, 2023. **18**(11): p. 1311-1318.
56. Kopielski, A., et al., *Isothermal DNA origami folding: avoiding denaturing conditions for one-pot, hybrid-component annealing.* Nanoscale, 2015. **7**(5): p. 2102-2106.
57. Roodhuizen, J.A.L., et al., *Counterion-Dependent Mechanisms of DNA Origami Nanostructure Stabilization Revealed by Atomistic Molecular Simulation.* ACS Nano, 2019. **13**(9): p. 10798-10809.
58. Loretan, M., et al., *DNA Origami as Emerging Technology for the Engineering of Fluorescent and Plasmonic-Based Biosensors.* Materials (Basel), 2020. **13**(9).
59. Johnson, J.A., et al., *The path towards functional nanoparticle-DNA origami composites.* Materials Science and Engineering: R: Reports, 2019. **138**: p. 153-209.

60. Stephanopoulos, N. and P. Šulc, *DNA Nanodevices as Mechanical Probes of Protein Structure and Function.* Applied Sciences, 2021. **11**(6): p. 2802.
61. Hermanson, G.T., *Bioconjugate Techniques*. 3 ed. 2013: Elsevier Inc.
62. Fantoni, N.Z., A.H. El-Sagheer, and T. Brown, *A Hitchhiker's Guide to Click-Chemistry with Nucleic Acids.* Chem Rev, 2021. **121**(12): p. 7122-7154.
63. Niemeyer, C.M., *Nanoparticles, Proteins, and Nucleic Acids: Biotechnology Meets Materials Science.* Angew Chem Int Ed Engl, 2001. **40**(22): p. 4128-4158.
64. Ramakrishnan, S., et al., *Structural stability of DNA origami nanostructures under application-specific conditions.* Comput Struct Biotechnol J, 2018. **16**: p. 342-349.
65. Agarwal, N.P., et al., *Block Copolymer Micellization of DNA Origami Promotes Solubility in Organic Solvents.* Langmuir, 2022. **38**(38): p. 11650-11657.
66. Agarwal, N.P., et al., *Block Copolymer Micellization as a Protection Strategy for DNA Origami.* Angew Chem Int Ed Engl, 2017. **56**(20): p. 5460-5464.
67. Gerling, T., et al., *Sequence-programmable covalent bonding of designed DNA assemblies.* Sci Adv, 2018. **4**(8): p. eaau1157.
68. Müller, W.E., et al., *Sponge spicules as blueprints for the biofabrication of inorganic-organic composites and biomaterials.* Appl Microbiol Biotechnol, 2009. **83**(3): p. 397-413.
69. Kröger, N.S., Manfred, *Biomineralization: From Biology to Biotechnology and Medical Application*, P.e.D.E. Bäuerlein, Editor. 2004, Wiley-VCH Verlag GmbH & Co. KGaA
70. Massey, F.P., A.R. Ennos, and S.E. Hartley, *Silica in grasses as a defence against insect herbivores: contrasting effects on folivores and a phloem feeder.* J Anim Ecol, 2006. **75**(2): p. 595-603.
71. Paunescu, D., et al., *Reversible DNA encapsulation in silica to produce ROS-resistant and heat-resistant synthetic DNA 'fossils'.* Nat Protoc, 2013. **8**(12): p. 2440-8.
72. Liu, X., et al., *Complex silica composite nanomaterials templated with DNA origami.* Nature, 2018. **559**(7715): p. 593-598.
73. Numata, M., et al., *Sol-gel reaction using DNA as a template: an attempt toward transcription of DNA into inorganic materials.* Angew Chem Int Ed Engl, 2004. **43**(25): p. 3279-83.
74. Jing, X., et al., *Solidifying framework nucleic acids with silica.* Nat Protoc, 2019. **14**(8): p. 2416-2436.
75. Wassermann, L.M., et al., *Full Site-Specific Addressability in DNA Origami-Templated Silica Nanostructures.* Adv Mater, 2023. **35**(23): p. e2212024.
76. Kielar, C., et al., *On the Stability of DNA Origami Nanostructures in Low-Magnesium Buffers.* Angew Chem Int Ed Engl, 2018. **57**(30): p. 9470-9474.
77. Stöber, W., A. Fink, and E. Bohn, *Controlled growth of monodisperse silica spheres in the micron size range.* Journal of Colloid and Interface Science, 1968. **26**(1): p. 62-69.
78. Ober, M.F., et al., *In situ small-angle X-ray scattering reveals strong condensation of DNA origami during silicification.* Nature Communications, 2022. **13**(1): p. 5668.
79. Nguyen, M.-K., et al., *Ultrathin Silica Coating of DNA Origami Nanostructures.* Chemistry of Materials, 2020. **32**(15): p. 6657-6665.
80. Shang, Y., et al., *Site-Specific Synthesis of Silica Nanostructures on DNA Origami Templates.* Adv Mater, 2020. **32**(21): p. e2000294.

81. Agarwal, N.P. and A. Gopinath, *DNA origami 2.0.* bioRxiv, 2022: p. 2022.12.29.522100.
82. Xinxin Jing, et al., *Molecular tuning of DNA framework-programmed silicification by cationic silica cluster attachment.* arxiv, 2024.
83. Wang, S., et al., *Controlling Silicification on DNA Origami with Polynucleotide Brushes.* Journal of the American Chemical Society, 2024. **146**(1): p. 358-367.
84. Carter, D. *George Gabriel Stokes and the phenomenon of fluorescence*. 2023 [cited 2024 20.10.2024]; Available from: https://www.mindat.org/article.php/4143/George+Gabriel+Stokes+and+the+phenomenon+of+fluorescence+.
85. Von Baeyer, A., *Ueber eine neue Klasse von Farbstoffen.* Berichte der deutschen chemischen Gesellschaft, 1871. **4**.
86. Yousheng, D., et al., *Recent Progress on Synthesis of Fluorescein Probes.* Mini-Reviews in Organic Chemistry, 2009. **6**(1): p. 35-43.
87. Karstens, T. and K. Kobs, *Rhodamine B and rhodamine 101 as reference substances for fluorescence quantum yield measurements.* The Journal of Physical Chemistry, 1980. **84**(14): p. 1871-1872.
88. Juan Carlos Stockert and A. Blázquez-Castro, *Fluorescence Microscopy in Life Sciences*. 2017: Bentham Science.
89. Jablonski, A., *Efficiency of Anti-Stokes Fluorescence in Dyes.* Nature, 1933. **131**(3319): p. 839-840.
90. *Jablonski diagram*. 2019, International Union of Pure and Applied Chemistry (IUPAC).
91. Schlichthaerle, T., et al., *DNA nanotechnology and fluorescence applications.* Curr Opin Biotechnol, 2016. **39**: p. 41-47.
92. Adamczyk, A.K., et al., *DNA Self-Assembly of Single Molecules with Deterministic Position and Orientation.* ACS Nano, 2022. **16**(10): p. 16924-16931.
93. Büber, E., et al., *DNA Origami Vesicle Sensors with Triggered Single-Molecule Cargo Transfer.* Angew Chem Int Ed Engl, 2024: p. e202408295.
94. Cole, F., et al., *Controlled mechanochemical coupling of anti-junctions in DNA origami arrays.* Nature Communications, 2024. **15**(1): p. 7894.
95. Patino, T., *Imaging DNA origami by fluorescence in situ hybridization.* Nat Nanotechnol, 2024. **19**(1): p. 1-2.
96. Pal, S. and T. Rakshit, *Folate-Functionalized DNA Origami for Targeted Delivery of Doxorubicin to Triple-Negative Breast Cancer.* Front Chem, 2021. **9**: p. 721105.
97. Kessler, L.F., et al., *Self-quenched Fluorophore Dimers for DNA-PAINT and STED Microscopy.* Angewandte Chemie International Edition, 2023. **62**(39): p. e202307538.
98. Beater, S., et al., *Choosing dyes for cw-STED nanoscopy using self-assembled nanorulers.* Phys Chem Chem Phys, 2014. **16**(15): p. 6990-6.
99. Deen, J., et al., *A general strategy for direct, enzyme-catalyzed conjugation of functional compounds to DNA.* Nucleic Acids Res, 2018. **46**(11): p. e64.
100. Ranasinghe, R.T. and T. Brown, *Ultrasensitive fluorescence-based methods for nucleic acid detection: towards amplification-free genetic analysis.* Chem Commun (Camb), 2011. **47**(13): p. 3717-35.

101. Thompson, I.A.P., et al., *An antibody-based molecular switch for continuous small-molecule biosensing.* Sci Adv, 2023. **9**(38): p. eadh4978.
102. Pfeiffer, M., et al., *Single antibody detection in a DNA origami nanoantenna.* iScience, 2021. **24**(9): p. 103072.
103. Fish, K.N., *Total internal reflection fluorescence (TIRF) microscopy.* Curr Protoc Cytom, 2009. **Chapter 12**: p. Unit12.18.
104. Lelek, M., et al., *Single-molecule localization microscopy.* Nat Rev Methods Primers, 2021. **1**.
105. Schnitzbauer, J., et al., *Super-resolution microscopy with DNA-PAINT.* Nature Protocols, 2017. **12**(6): p. 1198-1228.
106. Fluorofinder. *Families of Different Fluorophore Chemistry*. [cited 2024 20.10.2024]; Available from: https://fluorofinder.com/fluorophore-families/.
107. Labster. *Fluorophores*. [cited 2024 20.10.2024]; Available from: https://theory.labster.com/fluorophores/.
108. Knoll, M. and E. Ruska, *Das Elektronenmikroskop.* Zeitschrift für Physik, 1932. **78**(5): p. 318-339.
109. Ruska, E., *The early development of electron lenses and electron microscopy.* Microsc Acta Suppl, 1980(Suppl 5): p. 1-140.
110. Egerton, R.F., *Physical Principles of Electron Microscopy - An Introduction to TEM, SEM, and AEM*. 1 ed. 2005: Springer New York, NY.
111. Thomson, G. and A. Reid, *Diffraction of Cathode Rays by a Thin Film.* Nature, 1927. **119**: p. 890-890.
112. Rose, H.H., *Optics of high-performance electron microscopes.* Sci Technol Adv Mater, 2008. **9**(1): p. 014107.
113. Fultz, B.H.J.M., *Transmission Electron Microscopy and Diffractometry of Materials*. 3 ed. 2007: Springer Berlin, Heidelberg. 758.
114. Michler, G.H. *Transmissionselektronenmikroskopie*. [cited 2024 20.10.2024]; Available from: https://wiki.polymerservice-merseburg.de/index.php/Transmissionselektronenmikroskopie.
115. Carroni, M. and H.R. Saibil, *Cryo electron microscopy to determine the structure of macromolecular complexes.* Methods, 2016. **95**: p. 78-85.
116. Adrian, M., et al., *Cryo-electron microscopy of viruses.* Nature, 1984. **308**(5954): p. 32-36.
117. Benjin, X. and L. Ling, *Developments, applications, and prospects of cryo-electron microscopy.* Protein Sci, 2020. **29**(4): p. 872-882.
118. Hiramano92. *Cryogenic electron microscopy workflow*. 2023 [cited 2024 20.10.2024]; Available from: https://commons.wikimedia.org/wiki/File:Cryogenic_electron_microscopy_workflow.svg.
119. Vahabi, S., B. Nazemi Salman, and A. Javanmard, *Atomic force microscopy application in biological research: a review study.* Iran J Med Sci, 2013. **38**(2): p. 76-83.
120. Xia, F. and K. Youcef-Toumi, *Review: Advanced Atomic Force Microscopy Modes for Biomedical Research.* Biosensors (Basel), 2022. **12**(12).

121. Müller, D.J., et al., *Atomic Force Microscopy-Based Force Spectroscopy and Multiparametric Imaging of Biomolecular and Cellular Systems.* Chemical Reviews, 2021. **121**(19): p. 11701-11725.
122. Vista, M. *An Introduction to AFM-IR*. 2022 [cited 2024 20.10.2024]; Available from: https://molecularvista.com/blog/afm-ir-overview/.
123. Jungmann, R., et al., *Single-molecule kinetics and super-resolution microscopy by fluorescence imaging of transient binding on DNA origami.* Nano Lett, 2010. **10**(11): p. 4756-61.
124. Sharonov, A. and R.M. Hochstrasser, *Wide-field subdiffraction imaging by accumulated binding of diffusing probes.* Proc Natl Acad Sci U S A, 2006. **103**(50): p. 18911-6.
125. Nieves, D.J., K. Gaus, and M.A.B. Baker, *DNA-Based Super-Resolution Microscopy: DNA-PAINT.* Genes (Basel), 2018. **9**(12).
126. Axelrod, D., *Total internal reflection fluorescence microscopy in cell biology.* Traffic, 2001. **2**(11): p. 764-74.
127. Oleksiievets, N., et al., *Fluorescence lifetime DNA-PAINT for multiplexed super-resolution imaging of cells.* Communications Biology, 2022. **5**(1): p. 38.
128. Strauss, M.T., et al., *Quantifying absolute addressability in DNA origami with molecular resolution.* Nature Communications, 2018. **9**(1): p. 1600.
129. Pilz, I., O. Glatter, and O. Kratky, *[11] Small-angle x-ray scattering*, in *Methods in Enzymology*. 1979, Academic Press. p. 148-249.
130. Svergun, D.I. and M.H.J. Koch, *Small-angle scattering studies of biological macromolecules in solution.* Reports on Progress in Physics, 2003. **66**(10): p. 1735.
131. Huber, K., *Basic X-ray Scattering Applied to Soft Matter. By Wim H. de Jeu.* Angewandte Chemie International Edition, 2016. **55**(44): p. 13645-13645.
132. Sivia, D.S., *Elementary Scattering Theory: For X-ray and Neutron Users*. 2011: Oxford University Press.
133. Kikhney, A.G. and D.I. Svergun, *A practical guide to small angle X-ray scattering (SAXS) of flexible and intrinsically disordered proteins.* FEBS Lett, 2015. **589**(19 Pt A): p. 2570-7.
134. Pollack, L., *SAXS studies of ion-nucleic acid interactions.* Annu Rev Biophys, 2011. **40**: p. 225-42.
135. Caselli, L., et al., *Small-angle X-ray and neutron scattering applied to lipid-based nanoparticles: Recent advancements across different length scales.* Adv Colloid Interface Sci, 2024. **327**: p. 103156.
136. Meisburger, S.P., et al., *X-ray Scattering Studies of Protein Structural Dynamics.* Chem Rev, 2017. **117**(12): p. 7615-7672.
137. Das, R. and S. Doniach, *Structural Studies of Proteins and Nucleic Acids in Solution Using Small Angle X-Ray Scattering (SAXS)*, in *Soft Matter Characterization*, R. Borsali and R. Pecora, Editors. 2008, Springer Netherlands: Dordrecht. p. 1083-1108.
138. Kawamukai, H., et al., *Conformational Distribution of a Multidomain Protein Measured by Single-Pair Small-Angle X-ray Scattering.* J Phys Chem Lett, 2024. **15**(3): p. 744-750.
139. Lo, Y.H., M.C. Pillon, and R.E. Stanley, *Combining X-Ray Crystallography with Small Angle X-Ray Scattering to Model Unstructured Regions of Nsa1 from S. Cerevisiae.* J Vis Exp, 2018(131).

140. Mertens, H.D.T. and D.I. Svergun, *Combining NMR and small angle X-ray scattering for the study of biomolecular structure and dynamics.* Arch Biochem Biophys, 2017. **628**: p. 33-41.
141. McGuire, S.C., Y. Zhang, and S.S. Wong, *A combined TEM and SAXS study of the growth and self-assembly of ultrathin Pt nanowires.* Nanotechnology, 2022. **33**(47).
142. Da Vela, S. and D.I. Svergun, *Methods, development and applications of small-angle X-ray scattering to characterize biological macromolecules in solution.* Curr Res Struct Biol, 2020. **2**: p. 164-170.
143. 22412:2017, I., *Particle size analysis — Dynamic light scattering (DLS)*. 2 ed. 2017.
144. Gottlieb, M.A. and R. Pfeiffer. *The Brownian Movemnt*. The Feynman Lectures 2013 [cited 2024 20.10.2024]; Available from: https://www.feynmanlectures.caltech.edu/I_41.html.
145. Newell, D.B. and E. Tiesinga, *The International System of Units (SI).* National Institute of Standards and Technology, 2019.
146. Hunter, R.J., *Zeta Potential in Colloid Science - Principles and Applications*. 1 ed. 1988: Academic Press.
147. Panalytical, M. *Zetasizer Nano Range - Simple and versatile light scattering systems*. [cited 2024 23.10.]; Available from: https://www.malvernpanalytical.com/en/support/product-support/zetasizer-range/zetasizer-nano-range.
148. Sambrook, J.R., D.W., *Molecular Cloning: A Laboratory Manual*. 3 ed. Vol. 1. 2001, New York: Cold Spring Harbor Laboratory Press.
149. Stellwagen, N.C., *Electrophoresis of DNA in agarose gels, polyacrylamide gels and in free solution.* Electrophoresis, 2009. **30 Suppl 1**(Suppl 1): p. S188-95.
150. Seeman, N.C., *DNA in a material world.* Nature, 2003. **421**(6921): p. 427-31.
151. Hartl, C., et al., *Position Accuracy of Gold Nanoparticles on DNA Origami Structures Studied with Small-Angle X-ray Scattering.* Nano Lett, 2018. **18**(4): p. 2609-2615.
152. Yan, H., et al., *DNA-templated self-assembly of protein arrays and highly conductive nanowires.* Science, 2003. **301**(5641): p. 1882-4.
153. Mann, S., *Biomimetic Materials Chemistry*. 1997, US: Wiley VCH Publishers Inc. 400.
154. Sigel, A., H. Sigel, and R.K.O. Sigel, *Biomineralization: From Nature to Application*. 1 ed. Metal Ions in Life Sciences. . Vol. 4. 2008: John Wiley & Sons. 700.
155. Athanasiadou, D. and K.M.M. Carneiro, *DNA nanostructures as templates for biomineralization.* Nat Rev Chem, 2021. **5**(2): p. 93-108.
156. Majikes, J.M. and J.A. Liddle, *DNA Origami Design: A How-To Tutorial.* J Res Natl Inst Stand Technol, 2021. **126**: p. 126001.
157. Zhang, J.Z., et al., *The Persistence Length of Semiflexible Polymers in Lattice Monte Carlo Simulations.* Polymers (Basel), 2019. **11**(2).
158. Roth, E., et al., *Measuring the Conformation and Persistence Length of Single-Stranded DNA Using a DNA Origami Structure.* Nano Letters, 2018. **18**(11): p. 6703-6709.
159. Xin, Y., et al., *Environment-Dependent Stability and Mechanical Properties of DNA Origami Six-Helix Bundles with Different Crossover Spacings.* Small, 2022. **18**(18): p. e2107393.

160. Roth Weizman, E., A. Glick Azaria, and Y. Garini, *Conformation of ring single-stranded DNA measured by DNA origami structures.* Biophysical Journal, 2022. **121**(11): p. 2127-2134.
161. Castro, C.E., et al., *Mechanical design of DNA nanostructures.* Nanoscale, 2015. **7**(14): p. 5913-5921.
162. Bruetzel, L.K., et al., *A Mo-anode-based in-house source for small-angle X-ray scattering measurements of biological macromolecules.* Rev Sci Instrum, 2016. **87**(2): p. 025103.
163. Ober, M.F., et al., *SAXS measurements of azobenzene lipid vesicles reveal buffer-dependent photoswitching and quantitative Z→E isomerisation by X-rays.* Nanophotonics, 2022. **11**(10): p. 2361-2368.
164. Wang, Y., et al., *DNA origami single crystals with Wulff shapes.* Nat Commun, 2021. **12**(1): p. 3011.
165. Yi, Z., et al., *A New Insight into Growth Mechanism and Kinetics of Mesoporous Silica Nanoparticles by in Situ Small Angle X-ray Scattering.* Langmuir, 2015. **31**(30): p. 8478-87.
166. Xin, Y., et al., *Cryopreservation of DNA Origami Nanostructures.* Small, 2020. **16**(13): p. e1905959.
167. Fazel, M., et al., *High-precision estimation of emitter positions using Bayesian grouping of localizations.* Nature Communications, 2022. **13**(1): p. 7152.
168. Jensen, K.K., et al., *Kinetics for hybridization of peptide nucleic acids (PNA) with DNA and RNA studied with the BIAcore technique.* Biochemistry, 1997. **36**(16): p. 5072-7.
169. Abels, J.A., et al., *Single-Molecule Measurements of the Persistence Length of Double-Stranded RNA.* Biophysical Journal, 2005. **88**(4): p. 2737-2744.
170. Schmied, J.J., et al., *DNA origami-based standards for quantitative fluorescence microscopy.* Nat Protoc, 2014. **9**(6): p. 1367-91.
171. Scheckenbach, M., et al., *Self-Regeneration and Self-Healing in DNA Origami Nanostructures.* Angewandte Chemie International Edition, 2021. **60**(9): p. 4931-4938.
172. Linko, V., et al., *One-step large-scale deposition of salt-free DNA origami nanostructures.* Scientific Reports, 2015. **5**(1): p. 15634.
173. Wang, X., et al., *Biomineralization of DNA Nanoframeworks for Intracellular Delivery, On-Demand Diagnosis, and Synergistic Cancer Treatments.* Anal Chem, 2022. **94**(48): p. 16803-16812.
174. Zeng, K., et al., *Biodegradable nano-organosilica gene carrier for high-efficiency gene transfection.* J Mater Chem B, 2020. **8**(12): p. 2483-2494.
175. Wang, L., et al., *A series of silane-modified rhodamine dyes for near-IR biological fluorescence imaging of Hela cells and A549 lung cancer cells: Synthesis and sensing behavior towards ions, amino acids and hypocholorous acid.* Dyes and Pigments, 2022. **207**: p. 110742.
176. Traverso, N., et al., *Role of glutathione in cancer progression and chemoresistance.* Oxid Med Cell Longev, 2013. **2013**: p. 972913.
177. Gamcsik, M.P., et al., *Glutathione levels in human tumors.* Biomarkers, 2012. **17**(8): p. 671-91.
178. Liu, J.Y. and C.M. Sayes, *A toxicological profile of silica nanoparticles.* Toxicology Research, 2022. **11**(4): p. 565-582.

179. Chen, L., et al., *The toxicity of silica nanoparticles to the immune system.* Nanomedicine (Lond), 2018. **13**(15): p. 1939-1962.
180. Göldel, L., *Investigation of the cellular uptake mechanism and cellular distribution of silicified and calcified DNA-origami hybrid nanostructures*, in *Chemistry*. 2021, TUM: Munich, DE. p. 78.
181. Lacroix, A., et al., *Uptake and Fate of Fluorescently Labeled DNA Nanostructures in Cellular Environments: A Cautionary Tale.* ACS Cent Sci, 2019. **5**(5): p. 882-891.
182. Sun, W.-C., et al., *Synthesis of Fluorinated Fluoresceins.* The Journal of Organic Chemistry, 1997. **62**(19): p. 6469-6475.
183. Zhang, X.F., J. Zhang, and L. Liu, *Fluorescence properties of twenty fluorescein derivatives: lifetime, quantum yield, absorption and emission spectra.* J Fluoresc, 2014. **24**(3): p. 819-26.
184. Blackholm, M., *In-vitro investigation of fluorescent silica nanostructures templated by DNA origami*, in *Biochemistry*. 2023, Ludwig-Maximilians-Universität München. p. 96.
185. Yao, R.W. and M.K. Rosen, *Advanced Surface Passivation for High-Sensitivity Studies of Biomolecular Condensates.* bioRxiv, 2024.
186. Inc., A.B. *Spectrum [Rhodamine B]*. 2024 2024-10-23; Available from: https://www.aatbio.com/fluorescence-excitation-emission-spectrum-graph-viewer/rhodamine_b.
187. Nickels, P.C., et al., *Molecular force spectroscopy with a DNA origami–based nanoscopic force clamp.* Science, 2016. **354**(6310): p. 305-307.
188. Schindelin, J., et al., *Fiji: an open-source platform for biological-image analysis.* Nature Methods, 2012. **9**(7): p. 676-682.
189. Chandrasekaran, A.R. and K. Halvorsen, *Nuclease Degradation Analysis of DNA Nanostructures Using Gel Electrophoresis.* Curr Protoc Nucleic Acid Chem, 2020. **82**(1): p. e115.
190. Wagenbauer, K.F., et al., *How We Make DNA Origami.* ChemBioChem, 2017. **18**(19): p. 1873-1885.
191. Lambert, T.J., *FPbase: a community-editable fluorescent protein database.* Nat Methods, 2019. **16**(4): p. 277-278.
192. Scheres, S.H., *RELION: implementation of a Bayesian approach to cryo-EM structure determination.* J Struct Biol, 2012. **180**(3): p. 519-30.
193. Mastronarde, D.N., *Automated electron microscope tomography using robust prediction of specimen movements.* J Struct Biol, 2005. **152**(1): p. 36-51.
194. Pettersen, E.F., et al., *UCSF ChimeraX: Structure visualization for researchers, educators, and developers.* Protein Sci, 2021. **30**(1): p. 70-82.
195. Pettersen, E.F., et al., *UCSF Chimera--a visualization system for exploratory research and analysis.* J Comput Chem, 2004. **25**(13): p. 1605-12.
196. Panalytical, M. *Dynamic Light Scattering (DLS) - Dynamic Light Scattering for size characterization of proteins, nanoparticles, polymers and colloidal dispersions*. [cited 2024 23.10.]; Available from: https://www.malvernpanalytical.com/en/products/technology/light-scattering/dynamic-light-scattering.
197. Derr, N.D., et al., *Tug-of-war in motor protein ensembles revealed with a programmable DNA origami scaffold.* Science, 2012. **338**(6107): p. 662-5.

198. Jun, H., et al., *Automated Sequence Design of 3D Polyhedral Wireframe DNA Origami with Honeycomb Edges.* ACS Nano, 2019. **13**(2): p. 2083-2093.

Declaration of Authorship

I hereby declare that this thesis is my own work, and that I have not used any sources and aids other than those stated in the thesis.

Erklärung

Hiermit erkläre ich, die vorliegende Arbeit selbstständig verfasst zu haben und keine anderen als die in der Arbeit angegebenen Quellen und Hilfsmittel benutzt zu haben.

München, February 19, 2025 …….

Lea Marie Wassermann